Effect of Anthranilic Acid Insertion in β-Sheet Breaker Hybrid Peptidomimetics (BSBHps) on hIAPP Aggregation

A Dissertation Submitted to the
Indian Institute of Technology Guwahati
as Partial Fulfillment for the Degree of
Doctor of Philosophy in Chemistry

Submitted by

Sourav Kalita

Roll No: 146122023

Department of Chemistry

Indian Institute of Technology Guwahati

Guwahati, Assam-781039

India

Dedicated

to

My Family

Indian Institute of Technology Guwahati

Department of Chemistry

STATEMENT

I do hereby declare that the matter embodied in this thesis is the result of investigations carried out by me in the Department of Chemistry, Indian Institute of Technology Guwahati, India, under the supervision of Prof. Bhubaneswar Mandal.

In keeping with the general practice of reporting scientific observations, due acknowledgements have been made wherever the work described is based on the findings of other investigators.

26th July, 2021

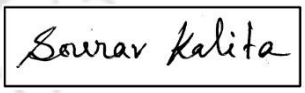

Sourav Kalita

Department of Chemistry

Indian Institute of Technology Guwahati

Certificate

Indian Institute of Technology Guwahati

Department of Chemistry

CERTIFICATE

This is to certify that **Mr. Sourav Kalita** has been working under my supervision since July 2014 as a registered Ph. D. student. I am forwarding his thesis entitled "**Effect of Anthranilic Acid Insertion in β-Sheet Breaker Hybrid Peptidomimetics (BSBHps) on hIAPP Aggregation**" for being submitted for the Ph. D. (Science) degree from this institute. I certify that he has fulfilled all the requirements according to the rules of this institute regarding the investigations embodied in his thesis and this work has not been submitted elsewhere for a degree.

26th July, 2021

Prof. Bhubaneswar Mandal

Thesis Supervisor

Department of Chemistry

Indian Institute of Technology Guwahati

Synopsis:

This thesis entitled, "Effect of Anthranilic Acid Insertion in β-Sheet Breaker Hybrid Peptidomimetics on hIAPP Aggregation," has been divided into five main chapters, including the experimental sections and the future perspectives. The abstracts of the main chapters are described below-

Chapter 1: Introduction and objectives

Protein misfolding and its subsequent aggregation into amyloids in the biological system cause numerous human diseases, including Alzheimer's disease (AD), Type II Diabetes (T2D), and Parkinson's disease, out of which T2D is one of the fastest-growing health challenges of the 21st century. The growing evidence suggests that T2D is developed by the deposition of amyloid plaques in the pancreatic cells, caused by the accumulation of the aggregating IAPP (Islet Amyloid Polypeptide). The mechanism of human IAPP (hIAPP) aggregation is not fully understood yet. However, research over the past few years suggests that monomeric hIAPP misfolds into a β-sheet structure by an unknown pathway, which leads to aggregation, forming toxic oligomers, and amyloid deposits. hIAPP aggregates initially into oligomers, primarily responsible for the dysfunction of pancreatic β-cell and glucagon, leading to T2D. Hence, preventing the amyloidogenic peptide from acquiring a β-sheet rich conformation may arise as a therapeutic strategy for inhibiting the amyloid formation and uprooting amyloidogenic diseases. Although there is no cure for T2D, further research will undoubtedly lead to developing proper therapeutics against T2D.

In the past two decades, various strategies, including small organic molecules, insulin therapy and β-sheet breaker peptides, have been developed to modulate the aggregation of hIAPP. However none of them has yet achieved a suitable platform for therapeutic applications.

Peptide-based molecules are excellent drug candidates due to their therapeutic superiority over the small molecules in target specificity, binding affinity, and low toxicity. However, the peptide-based strategy also suffers from several drawbacks, including peptide solubility, ineffective against cytotoxicity, proteolytic stability, restricting their use as drugs.

Our main objective is to develop modified β-sheet breaker hybrid peptides to fight against T2D using conformationally restricted peptides. For this purpose, we have selected various isomers of aminobenzoic acid (especially 2-aminobenzoic acid) as a β-breaker element. 2-aminobenzoic acid or anthranilic acid (Ant) is an exciting component for peptidomimetics due to the conformational restriction imposed by its structure. In the structure of Ant, both the amine group and the carboxyl group are directly connected to the aromatic moiety, constituting a planar structure with a fixed dihedral angle, $\Phi = 0^{\circ}$. Therefore, the peptide sequence containing Ant in its backbone exhibits enhanced conformational rigidity due to the π-stacking ability of the aromatic moiety. Due to its higher structural rigidity, we planned to insert Ant as a β-breaker element into the peptide backbone within the central hydrophobic region of the hIAPP peptide.

Furthermore, the Ant moiety favours the formation of either a turn or a helical conformation when incorporated into the peptide sequence. Moreover, Ant is found in many biologically active naturally occurring peptides (e.g., psychrophilin, cycloaspeptide, asperterrestide), and it is the precursor for the biosynthesis of tryptophan. Most importantly, it is a β-amino acid; hence its presence in peptidomimetics can enhance their proteolytic stabilities over the α-amino acid.

Therefore, in the various chapters of the thesis, we have reported on developing different Ant-containing *β*-sheet breaker hybrid peptides for inhibiting hIAPP aggregation and disruption of preformed amyloid at physiological conditions.

Chapter 2: Introduction of β, γ, and δ aminobenzoic acid as β-sheet breaker hybrid peptides and their applications in the inhibition of hIAPP aggregation

Initially, Westermark *et al*. pointed out that a limited segment of hIAPP has an intrinsic tendency to form amyloid, which might be responsible for T2D. The small peptide fragments of hIAPP, such as FGAIL ($hIAPP_{23-27}$), NFGAIL ($hIAPP_{22-27}$), SNNFGAIL ($hIAPP_{20-27}$) and SNNFGAILSS ($hIAPP_{20-29}$) are sufficient for the formation of amyloid *in vitro*. Hence, if one focuses on these peptide sequences and plans for a small peptide-based inhibitor constituting a breaker element inside the recognition sequence, it would be considered as a promising therapeutic strategy against the formation of amyloid and its disruption. Soto *et al.* initiated the concept of β-sheet breaker peptides (BSBPs) *via* incorporating proline residue into the recognition motif of Aβ peptide, which emerged to be a great discovery in the field of amyloid disruption. In line with this, various small peptide-based inhibitors containing different breaker elements have already been reported, including *N*-methylated amino acids, α-aminoisobutyric acids (Aib), α, β-dehydrophenylalanine, and aspartic acid derivatives. However, one of the major drawbacks of these breaker elements is proteolytic instability, as they contain α-amino acids and degrade quickly in the presence of proteolytic enzymes.

On the contrary, 2-amino benzoic acid (Ant) is a β-amino acid with higher structural rigidity, and its insertion in a peptide sequence induces a turn or helical conformation. Hence, we believed that the insertion of β, γ, and δ aminobenzoic acid in a small recognising peptide sequence would increase proteolytic stability and emerge as a better candidate as peptide-based inhibitor against hIAPP amyloid aggregation. These peptides are termed as β-sheet breaker hybrid peptides (BSBHps), as they are formed by combining α- and β-amino acids.

To achieve our goal, we synthesized three BSBHps by inserting various isomers of aminobenzoic acid (2, 3, and 4-amino benzoic acid) separately as breaker components in the

peptide $hIAPP_{22-27}$ at I26 position. After that, we investigated the inhibition and disruption efficiencies of the resulting peptidomimetics against amyloid aggregation of hIAPP. Along with these, we synthesized one control breaker peptide *via* incorporating α-aminoisobutyric acid (Aib) in the peptide sequence to compare the results.

From the results, we have outlined an innovative strategy of β-sheet breaker hybrid peptidomimetics (BSBHps) as impressive inhibitors of hIAPP amyloid fibril formation and its disruption. We demonstrated that BSBHps containing ortho (2-Abz) and meta (3-Abz) isomer were highly effective inhibitors against hIAPP amyloid formation. On the other hand, the para (4-Abz) isomer could hardly inhibit hIAPP aggregation; rather, it enhances the aggregation process, which might be due to its structural lack of kink formation efficiency. Moreover, we also expressed that these BSBHps containing the ortho and para isomers effectively disrupt the preformed amyloid of hIAPP into non-toxic fragments as confirmed by membrane leakage assay. Peptides containing β and γ-amino acids are proteolytically more stable than standard α-analogs. BSBHps having ortho- and meta- isomers of aminobenzoic acid exhibited superior inhibitory and disruption efficiencies than control breaker peptides containing α-amino isobutyric acid (Aib). Hence, these peptidomimetics may emerge as a better candidate for developing an efficient therapeutic tool against hIAPP-based amyloidogenesis.

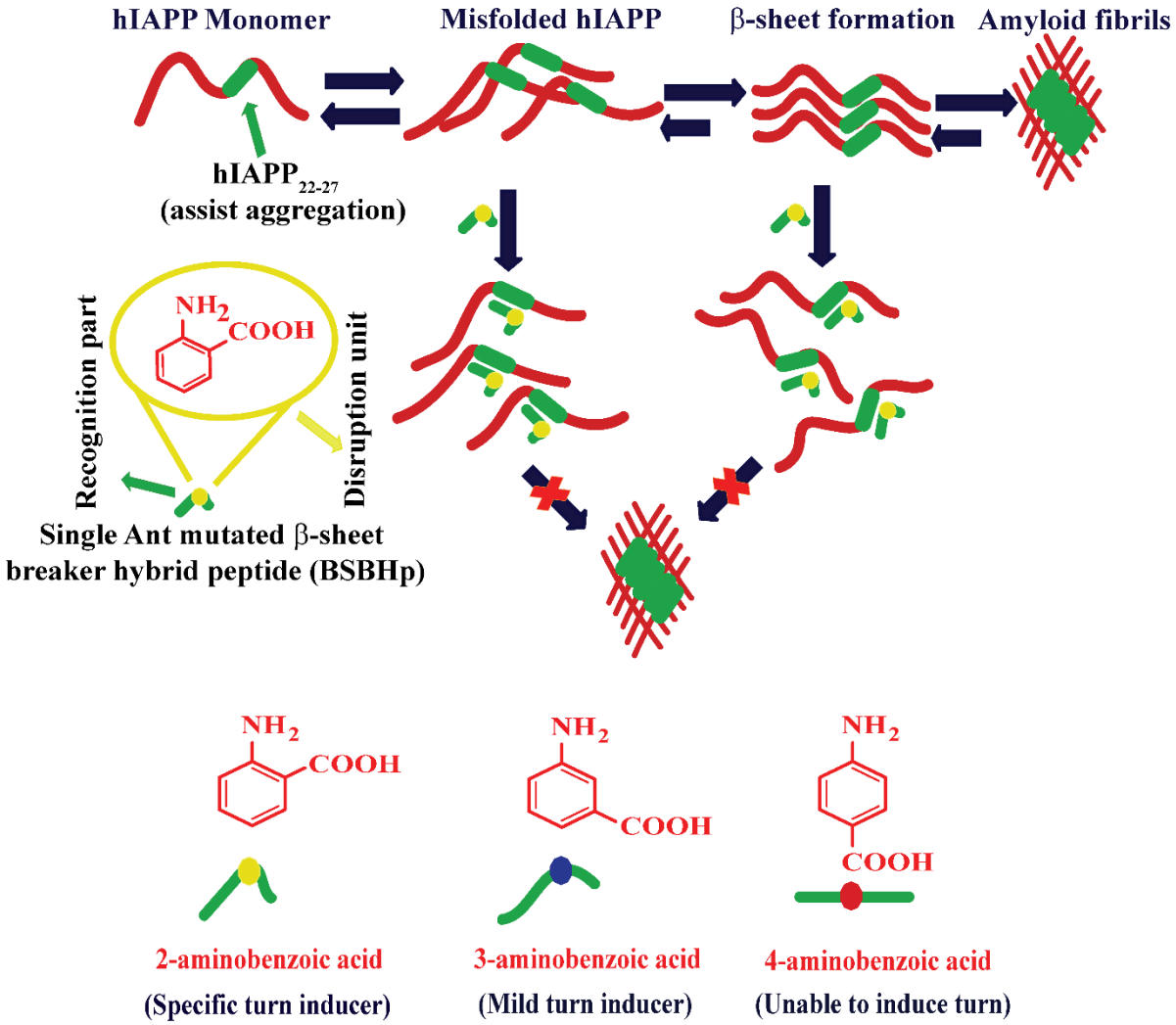

Figure 1: Schematic representation of hIAPP aggregation and proposed hypothesis for the inhibition process of amyloid formation by single mutant BSBHp

Chapter 3: Application of double breaker unit *via* incorporating isomers of aminobenzoic acid as β-sheet breaker hybrid peptides in the anti-amyloidogenic activity of hIAPP

From our previous studies, we found that single breaker peptidomimetics were active as efficient breaker peptides. However, to gain better efficiency in arresting the amyloid aggregation of hIAPP, we planned to insert the breaker elements simultaneously at two different positions of $hIAPP_{22\text{-}27}$. After that, we wished to investigate their inhibition and disruption efficiencies over the aggregation of wild-type hIAPP and anticipated that these might be more effective than the single-site mutated peptidomimetics in fighting against amyloidosis.

To test our hypothesis, we have incorporated the three isomers of aminobenzoic acid individually as breaker elements at two different positions, i.e., at G24 and I26 positions of $hIAPP_{22\text{-}27}$. Further, we also synthesized one control breaker peptide by incorporating α-aminoisobutyric acid (Aib) at the same positions of the peptide to compare the results.

From the investigations, we observed that double mutant ortho (2-Abz) and meta (3-Abz) isomer containing BSBHps were more effective inhibitors against the amyloid formation of hIAPP than the single mutant peptidomimetics. However, the para (4-Abz) isomer does not act as an inhibitor; instead, it enhances the aggregation process similarly to its single mutant analog. We have also discussed that these double breaker containing BSBHps disrupts the preformed amyloid of hIAPP efficiently into non-toxic fragments as confirmed from membrane leakage assay. Further, the double breaker comprising BSBHps were observed to be highly stable in the presence of proteolytic enzymes. Hence, these results can be used as a scaffold for drug designing against T2D and other amyloid-related diseases.

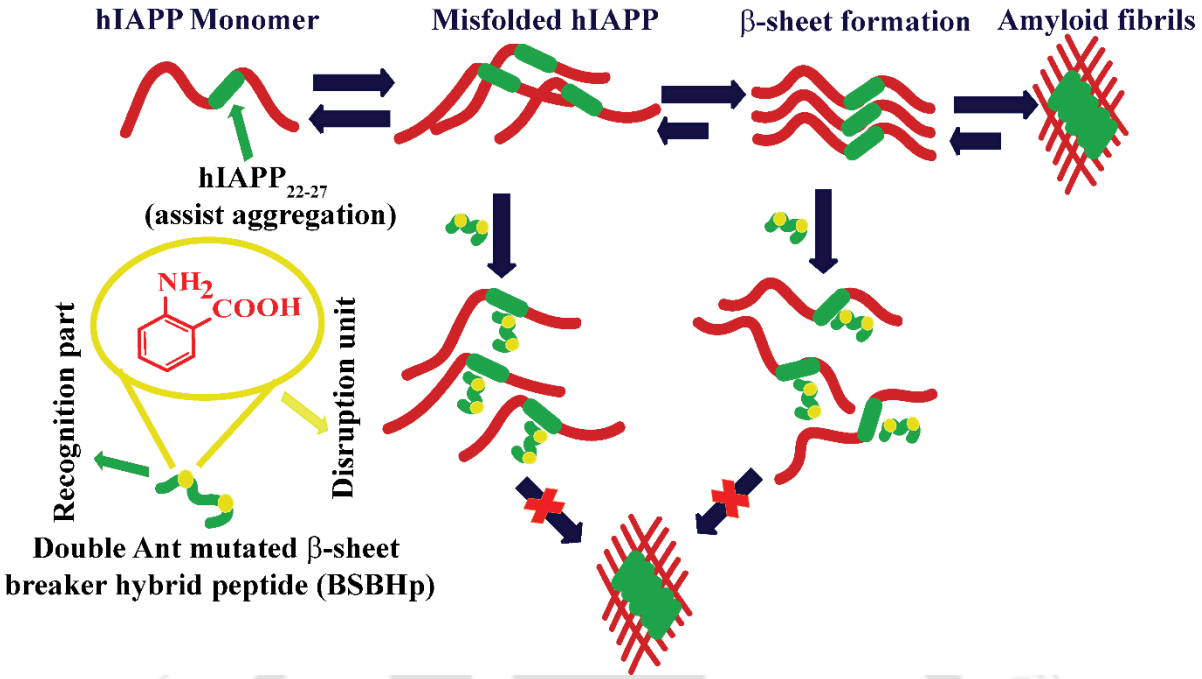

Figure 2: Schematic representation of hIAPP aggregation and proposed hypothesis for the inhibition process of amyloid formation by double mutant BSBHp

Chapter 4: Investigation of anti-amyloid activity of peptidomimetics designed by single point mutation by rigid β-amino acid in hIAPP$_{8-37}$ at different positions

Our earlier chapters demonstrated that the BSBHps designed by incorporating different isomers of aminobenzoic acid in the core hydrophobic region of hIAPP$_{22-27}$ exhibited satisfactory results in inhibiting hIAPP aggregation. However, among the different isomers, 2-aminobenzoic acid or Anthranilic acid (Ant) was the best breaker element, but 4-aminobenzoic acid did not exhibit any inhibition behaviour; instead, it enhanced the aggregation process. This effect might be due to the favourable kink formation ability of 2-aminobenzoic acid (Ant) in the sequence. As the conformational rigidity is higher in the peptidomimetics containing anthranilic acid (Ant) due to the fixed dihedral angle, we selected Ant as the β-breaker element inside the peptide backbone.

In a report of Raleigh *et al*., it was investigated that insertion of a single proline moiety in the hydrophobic region of hIAPP emerges the designed peptidomimetic as a highly efficient inhibitor. Further, Pramlintide (PM), containing three proline residues in the sequence of hIAPP has been accepted for clinical trials; however, it possesses several drawbacks, including poor solubility, which prevents itself co-formulation with insulin, especially at physiological pH. Moreover, one of the significant drawbacks of peptides-based therapeutics is that they are highly susceptible to degradation in the presence of proteolytic enzymes. However, inserting β-amino acids over the α-amino acids into the peptide sequence increases the stability of the peptides towards proteolytic degradation.

We, therefore, targeted the hydrophobic core region of hIAPP and designed two peptidomimetics by a single point mutation with Ant at two sites (i.e., G24Ant and I26Ant) for the two different peptidomimetics within full-length hIAPP$_{8-37}$. Moreover, we also designed a control peptidomimetic inserting the same breaker element in the hIAPP$_{22-27}$

smaller sequence. In our earlier chapters, we have described that the Ant containing small BSBHps could inhibit the aggregation of hIAPP and disrupted its preformed fibrillar structures at comparatively high doses (10-fold molar ratios). Moreover, due to the presence of non-coded β-amino acid, Ant, they were found to be proteolytically stable. However, due to the smaller size and lack of residual interaction, these BSBHps may not be efficient in binding with the aggregating hIAPP, explaining why their use in a higher dose for the inhibition or disruption of hIAPP aggregation.

Through our experimental findings, we have demonstrated the superior effect of a single point Ant mutated $hIAPP_{8-37}$ (longer peptidomimetic) over its smaller Ant mutant variant in $hIAPP_{22-27}$ (smaller peptidomimetic) in modulating aggregation caused by hIAPP. Experimental data supports that long peptidomimetics were potent inhibitors of amyloid formation at a significantly lower concentration than the smaller one. On the other hand, differences in the mutant position at G24X and I26X, (X=Ant) did not show any significant difference in their abilities to inhibit the amyloid formation of hIAPP.

Furthermore, we demonstrated the effect of peptidomimetics in terms of disruption of the preformed amyloid of hIAPP. Both the breaker peptides could disrupt the preformed amyloid into non-toxic species, as evident from LUV studies. Furthermore, in methodical DLS and TEM experiments, it was observed that the long peptidomimetics were able to alter the aggregation pathway of hIAPP and the soluble oligomers thus generated were found to rupture the lipid membrane slightly. The improved efficacies of the long peptidomimetics may be attributed to their better sequence recognition and packed binding to the fibrillar assembly generated by hIAPP over the smaller one. Moreover, MTT assay revealed that Ant-containing peptidomimetics are non-toxic to RIN-5F cells and rescue from hIAPP mediated toxicity. Hence, a single point anthranilic acid mutant of full-length $hIAPP_{8-37}$ at G24X or

I26X (X=Ant) enhances significantly anti-amyloidogenic activity associated with hIAPP. Finally, it can be concluded that these peptidomimetics are highly efficient inhibitors of hIAPP induced aggregation as well as disruptors of the preformed amyloids at low molar ratios. These peptidomimetics can be lead scaffolds for therapeutic design towards T2D and other amyloid-related diseases.

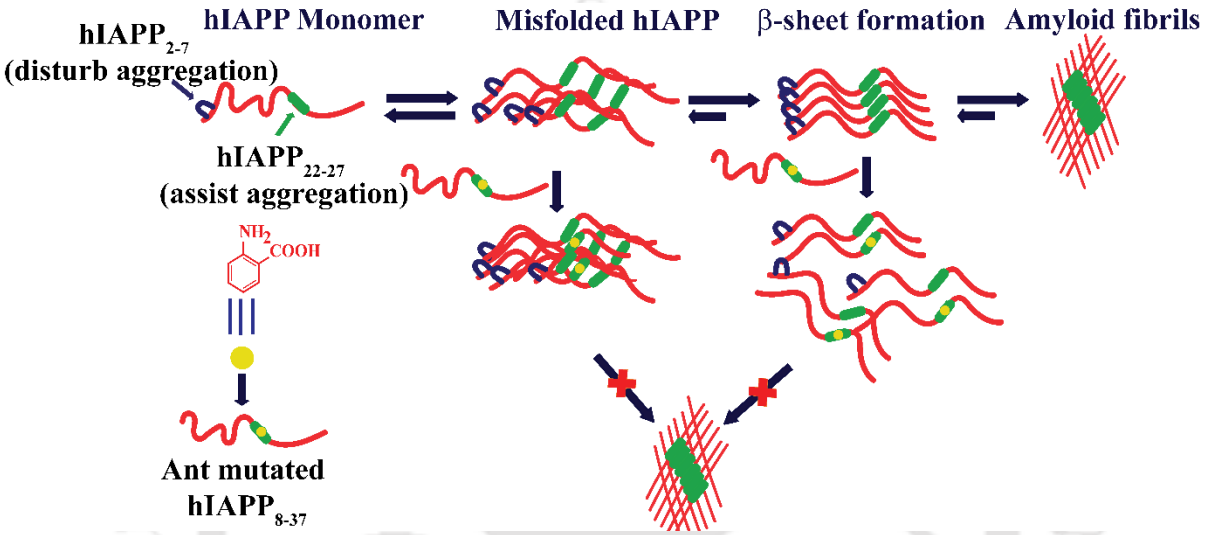

Figure 3: Schematic representation of hIAPP aggregation and proposed hypothesis for the inhibition process of amyloid formation by single point mutated $hIAPP_{8-37}$

Chapter 5: Disruption of hIAPP aggregates into non-toxic species by side-chain to tail stapled peptides

Despite tremendous research and scientific development on protein misfolding and amyloids, no complete cure for amyloidogenic diseases has been established to date. In recent years, stapled peptides have emerged as one of the most efficient drug candidates for various biological dysfunctions due to their various structural advantages. The stapling technique has been rapidly developed as one of the most accepted strategies for inhibiting protein-protein interactions (PPI) in the living system. Peptidomimetics made by one-component stapled peptides have also been investigated recently to inhibit amyloid fibrillogenesis. Looking into these enormous advantages and clinical activities, the stapled peptide approach can pave some new possibilities as critical therapeutics for targeting some incurable diseases like T2D.

Herein, we have designed two side-chain to tail stapled peptides in the absence and presence of a turn-inducing moiety, anthranilic acid (Ant) incorporated into the highly aggregating fragment of $hIAPP_{22-27}$. Further, we have also synthesized two linear control peptides, one without the anthranilic moiety and another containing the turn-inducing element maintaining the sequence homology with the hIAPP for proper recognition and binding with the same. The anthranilic moiety was introduced in both the stapled and linear one in I26 position of $hIAPP_{22-27}$, i.e., the NFGAIL sequence. Besides this, one glutamic acid (E) and one arginine (R) moieties were introduced at the C-terminus of the designed stapled peptides. The stapling process was carried out between the side chain of glutamic acid and the tail of the backbone, i.e., the N-terminus of asparagine. The arginine group was inserted to increase the aqueous solubility of the peptides.

From the systematic studies, it is clear that both the stapled peptides (SPs) are potent inhibitors of the highly aggregated amyloid fibrils generated from hIAPP, with a 2-fold molar

excess of them showing the most efficient inhibition abilities. Further, these two SPs can potentially disrupt the preformed amyloid fibrils of hIAPP into non-toxic species, as confirmed by the dye leakage assay. The structural rigidity of the SPs contributes to their efficiencies as better inhibitors only in two-fold molar excess in contrast to other breaker strategies. Further, these two SPs showed far better efficiencies towards inhibition and disruption than their linear analogs. Further, the potential of the SPs towards suppressing the hIAPP induced aggregation was independent of the turn-inducing moiety (Ant), which indicated the factor of 'peptide stapling' in terms of conformational restriction plays a vital role in arresting the amyloids formed.

Moreover, the systematic analyses *via* DLS and TEM established that SPs altered the native aggregation pathway of hIAPP into off-pathway aggregation, and the generated species were found to be non-toxic as revealed by LUVs dye leakage assay. After that, we demonstrated that the SPs were relatively stable than their linear analogs in the presence of proteolytic enzymes. The enzymatic stability enhancement of the SPs was supposed to be due to the conformational strain imposed by the stapling. Hence, with more fruitful analysis and survey in this direction, the staple peptides may emerge as a new therapeutic implementation towards the society to challenge against T2D or related diseases shortly.

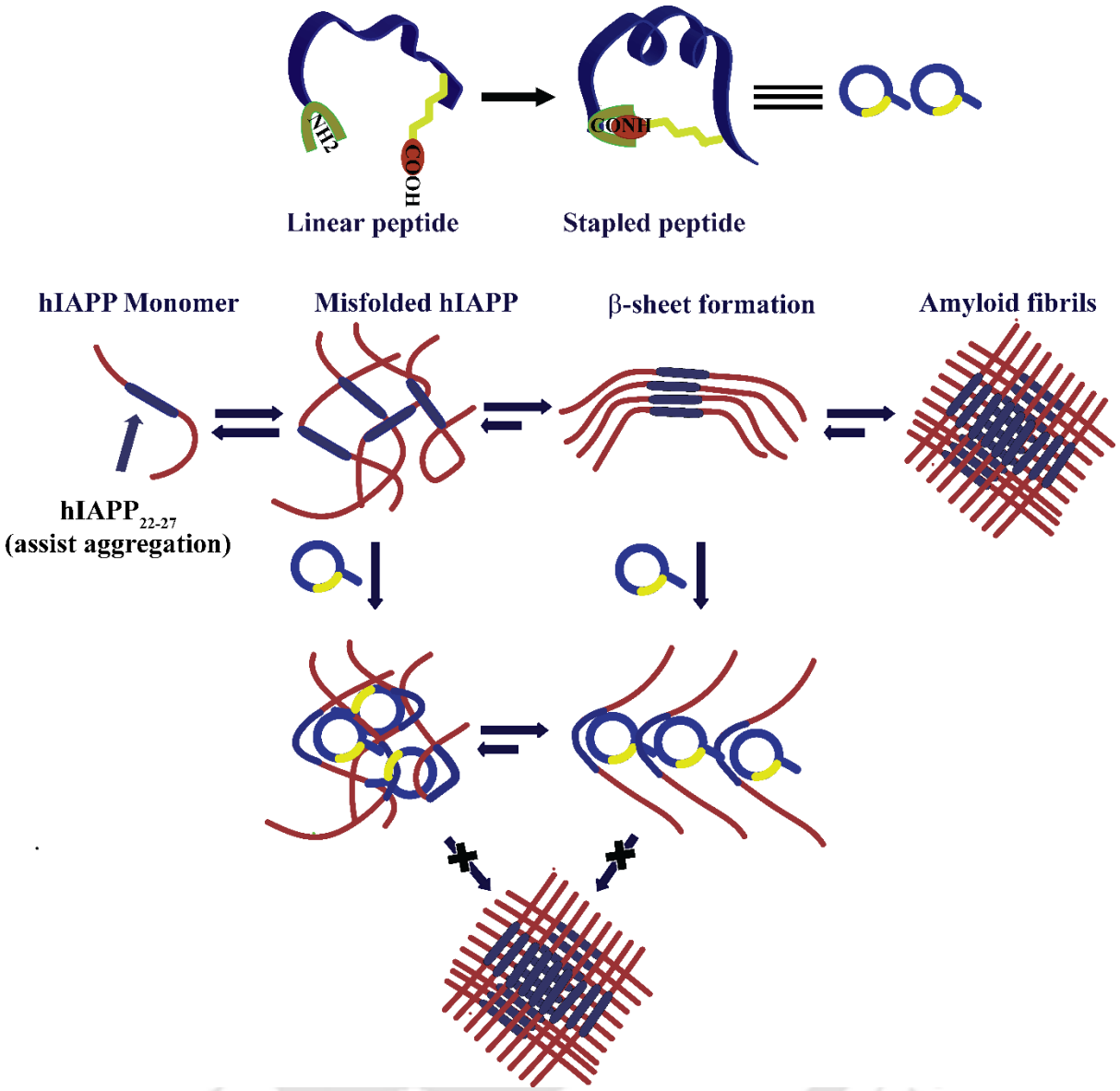

Figure 4: Schematic representation of hIAPP aggregation and proposed hypothesis for the inhibition process of amyloid formation by the stapled peptide.

Overall, in this thesis, we have demonstrated four different strategies for designing peptide-based molecules, their potentials in inhibiting the amyloid formation and disrupting preformed fibrillar networks under physiological conditions. We have also investigated the inhibitory action of the designed peptides upon amyloid aggregation using different biophysical tools. Such strategies may hold a promising approach for developing therapeutic agents for combating Type II diabetes and other amyloidoses.

Table of contents

Chapter 2: Introduction of β, γ and δ aminobenzoic acid as β-sheet breaker hybrid peptides and their applications in the inhibition of hIAPP aggregation

Chapter 3: Application of double breaker unit via incorporating isomers of aminobenzoic acid as β-sheet breaker hybrid peptides in the anti-amyloidogenic activity of hIAPP

Acknowledgements

At the very outset, with a deepest sense of gratitude, I would like to express my sincere thanks to my supervisor, Prof. Bhubaneswar Mandal, for his invaluable guidance, encouragement, inspiration and moral support, which helped me to enhance my knowledge and inspired me to take right decisions at crucial moments. I am very much thankful to him for giving me freedom to pursue my own interests in his laboratory. Moreover, I am fortunate enough to have availed his supervision, which have helped me to overcome my struggling and challenging phase of life.

I would like to acknowledge my doctoral committee members, Prof. Anil Kumar Saikia, Prof. Debapratim Das and Dr. Kalyan Raidongia for their valuable advice and suggestions. I would like to thank specially Prof. Debapratim Das for providing me the facility of lyophilizer. I would also like to express my sincere thanks to Prof. Sachin Kumar (faculty member of Department of Bioscience and Bioengineering, IIT Guwahati), Prof. Anirban Bhunia (faculty member of Department of Biophysics, Bose Institute, Kolkata) and Dr. Atin Kumar Mandal (faculty member of Division of Molecular Medicine, Bose Institute, Kolkata) for collaboration works. In addition, I am equally thankful to all the faculty members of the Department of Chemistry for their constant help and encouragement.

I would like to thank IIT Guwahati for all the facilities and hospitality provided during my stay in the campus. I am thankful to Dr. Babulal Das (for all kinds of instrumental help) Mr. Aniruddha Gogoi and Mr. Imdadul Islam (for HRMS) from the Department of Chemistry, Dr. Dolly Gogoi (for MALDI-TOF), and Mr. Sujit Kumar Deb (for TEM) from Central Instruments Facility, IIT Guwahati. I am equally thankful to all the non-teaching staff of Department of Chemistry for their help during my Ph.D. tenure.

I must thank my lab seniors, colleagues and juniors, Dr. N. K. Chaitanya, Dr. Nani Babu Palakurthy, Dr. Thalluri Kishore, Dr. Abhijit Saha, Dr. Ashim Paul (special thanks), Dr. Dharm Dev, Dr. Tanmay Mondal, Dr. Srinivasa Rao Manne, Dr. Jyoti Chandra, Dr. Rajat Subhra Giri, Dr. Sujan Kalita (special thanks), Ms. Tapasi Kalita, Mr. Govinda Doloi, Mr. Sandip Mandal, Mr. Sayanta Roy, Mr. Altaf Hussain Kawa and Mr. Sukesh Shill for the constant cooperation, support and creating the humorous and pleasant environment in the

laboratory. I am also thankful to Ms. Manisha Shah from the Department of Bioscience and Bioengineering for her help in performing the cell based experiments. I also would like to thank all of my Ph.D. batch mates (July, 2014) and all of my friends at IIT Guwahati with whom I spent time and shared many joyful moments during festivals and picnics.

I extend my sincere thanks to all the teachers, who always encourage me since my childhood to university life, especially Mr. Munin Goswami sir, Mr. Chiku Jain sir, Dr. B. C. Das Purakayastha sir, Dr. Diganta Choudhury sir via their invaluable motivation, suggestions and advice for academic as well as for progress of life. I also would like to thank my school and college friends for their constant support, encouragement and all the help they extended from time to time whenever required. Further, I would like also thank my ONGC colleagues, seniors and juniors for their constant support to me during my working days.

Most importantly, I express my sincere thanks to my grandfather, grandmother, father, mother, sister, uncles, aunties and all of my cousins for their endless moral support and motivation especially at difficult times. My Ph.D. endeavours would not have been completed without their blessings. They are the main soul and inspiration for each and every step that I achieve in my life. I express my sincere gratitude to them. I would like to thank all others who are associated with my work directly or indirectly at IIT Guwahati for their help.

Abbreviations:

Aβ	Amyloid beta
2-Abz	2-Aminobenzoic acid (Anthranilic acid)
3-Abz	3-Aminobenzoic acid
4-Abz	4-Aminobenzoic acid
Ac	Acetylated
Ac_2O	Acetic anhydride
AD	Alzheimer's disease
Aib	α-aminoisobutyric acid
Ant	Anthranilic acid
AU	Arbitrary unit
Boc	tert-butyloxycarbonyl
BOP	Benzotriazol-1-yloxy tris(dimethylamino) phosphonium hexafluorophosphate
BSBHp	β-sheet breaker hybrid peptide
CD	Circular dichroism
CF	5(6)-Carboxyfluorescein
CHCA	α-Cyano-hydroxy-cinnamic acid
DCM	Dichloromethane
DIPEA	Diisopropylethyl amine
DLS	Dynamic light scattering
DMF	N, N-dimethyl formamide
DMSO	Dimethyl sulfoxide
DPPC	1,2-Dipalmitoylphosphatidylcholine

EGCG	Epigallocatechin-3-gallate
ESI-MS	Electrospray ionization mass spectrometry
ESR	Electron spin resonance
Et_2O	Diethyl ether
FESEM	Field emission scanning electron microscopy
$FeSO_4$	Ferrous sulphate
FITC	Fluorescein Isothiocyanate
Fmoc	9-Fluorenylmethoxycarbonyl
FTIR	Fourier transform infrared spectroscopy
GM1	Monosialotetrahexosylganglioside
HEPES	N-2-hydroxyethyl piperazine-N-2-ethane sulphonic acid
HFIP	1,1,1,3,3,3-hexafluoro-iso-propanol
hIAPP	Human islet amyloid polypeptide
HOBt	1-hydroxy benzotriazole
HPLC	High pressure liquid chromatography
HRMS	High resolution mass spectrometry
KBr	Potassium bromide
LP	Linear peptide
LUV	Large unilamellar vesicles
MALDI	Matrix-assisted laser desorption ionization
MBHA	Methyl-benzhydryl-amine
mL	milli litre
mM	milli molar
μL	micro litre

μM	micro molar
μm	micro meter
MW	Molecular weight
nm	Nanometre
N-Me	N-methylated
NMI	N-methyl imidazole
OtBu	*tert*-butyl ester
Oxyma	Ethyl-hydroxyiminocyanoacetate
Pbf	2,2,4,6,7-pentamethyldihydrobenzofuran-5-sulfonyl
PD	Parkinson's disease
PBS	Phosphate-buffered saline
PyBOP	Benzotriazole-1-yl-oxy-tris-pyrolidine-phosphonium hexafluorophosphate
RP	Reverse phase
SPPS	Solid phase peptide synthesis
SP	Stapled peptide
tBu	*tert*-butyl
TEM	Transmission electron microscopy
TFA	Trifluoroacetic acid
THF	Tetrahydrofuran
ThT	Thioflavin T
TOF	Time-of-flight
T2D	Type II diabetes
$ZnBr_2$	Zinc bromide
$ZnCl_2$	Zinc chloride

Amino acids:

Ala	A	Alanine
Arg	R	Arginine
Asn	N	Asparagine
Asp	D	Aspartic acid
Cys	C	Cysteine
Gln	Q	Glutamine
Glu	E	Glutamic acid
Gly	G	Glycine
His	H	Histidine
Ile	I	Isoleucine
Leu	L	Leucine
Lys	K	Lysine
Met	M	Methionine
Phe	F	Phenylalanine
Pro	P	Proline
Ser	S	Serine
Thr	T	Threonine
Trp	W	Tryptophan
Tyr	Y	Tyrosine
Val	V	Valine

Chapter 1: Introduction and objectives

1.1. Introduction:

This thesis demonstrates a detailed study of type-2 diabetes (T2D), one of the growing world wide health problems, its causes, pathogenic consequences, and relation with human islet amylin polypeptide (hIAPP). This thesis primarily focuses on establishing the rational design of peptide-based molecules as drug candidates against T2D and their various chemical modifications to enhance therapeutic values.

1.2. Peptides and proteins:

Peptides and proteins are essential biological macromolecules, which play vital roles in our living system, including muscle movement, metabolic action, and immune protection. Proteins consist of polypeptide chains, consisting of usually 50 or more amino acids, where an amino group of one amino acid couples with the carboxyl group of the second amino acid.[1-3] The amino acid consists of an amine, a carboxylic acid, and an R (side chain) group at its α-carbon (Figure 1.1).[2] There are 20 different naturally occurring amino acids, which are the fundamental building block of all the peptides and proteins. The different R groups make a diverse family of proteins, which differ in charge, size, solubility, H-bonding capacity, and chemical reactivity. The size of the proteins may vary from one hundred to several kilo Daltons.

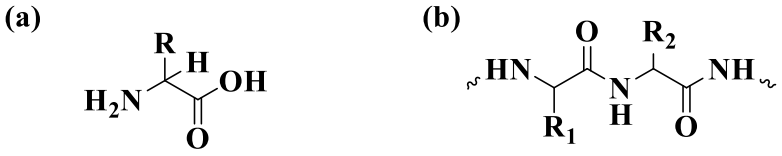

Figure 1.1: General structure of (a) an amino acid and (b) a peptide bond in a protein sequence

Generally, protein molecules adopt specific three-dimensional arrangements to perform various biological functions associated with the living system. There are different structural architectures for proteins, such as primary, secondary, tertiary, and quaternary structures.[4,5] The sequence of amino acids connected linearly with one amino acid to another constitutes the primary structure of a polypeptide chain. The secondary structure refers to the local folded structure that forms within a polypeptide due to interactions between the backbone atoms. The short-range structure of protein stabilized through the hydrogen bonding between the amide (-NHCO-) moieties of the protein backbone is observed in the secondary structure. The most common secondary structures are α-helix, β-sheet, and β-turn, which play significant roles in developing the structure, functionality, and stability of proteins. An amalgamation of β-sheet may lead to several amyloidogenic human diseases by forming protein aggregates and insoluble fibrillar assembly.[6,7] However, in rare cases, α-helix is also found to form amyloid by self-aggregation.[8] Further arrangements of the secondary structure to provide the next level of comprehensive three-dimensional protein structure is known as the tertiary structure. This structure is stabilized by the interactions between the R-groups of the constituted amino acids in the protein. Interactions that contribute to the tertiary structure include hydrogen bonding, ionic bonding, dipole-dipole interactions, and disulfide bond, which results in covalent bonding between the cysteine amino acids. Many proteins are made up of a single polypeptide chain and have only three levels of structure, i.e., primary, secondary, and tertiary structures. However, some proteins are made up of multiple

polypeptide chains, known as a subunit. When these subunits assemble in three-dimensional complexes, they constitute the quaternary structure of a protein, for example, hemoglobin.[4,5]

1.3. Protein folding and misfolding:

Protein folding, misfolding and unfolding are widespread processes in biological systems. These processes are crucial for synchronizing biological activity and directing the protein into its different cellular positions. The phenomenon by which a protein molecule undergoes conformational changes to achieve its compact three-dimensional structure for performing normal biological functions in the living body is known as protein folding.[9,10] The mechanism of protein folding is still a matter of debate; however, the driving force for the process is thought to attain the lowest possible energy. The protein folding depends on the R groups of the amino acids present in the sequence as the process depends on some coherent factors like H-bonds, hydrophobic effect, electrostatic, and Van der Walls interactions.[2] Another critical factor for the folding process is the secondary structure, as H-bonding assists the α-helix within the same strand between the CO and NH groups. However, the H-bonding of the β-strand is stabilized by the next neighbouring strand. Higher-order structures like β-hairpin and β-sheets are based on these secondary structures.

A protein remains folded in its native state, which is functionally active, and in this state, they are both thermodynamically and kinetically stable. Proteins are involved in all stages of neuronal activities and biological activities in the folded form only. However, sometimes during folding, proteins fail to fold into their desired functional conformations. Instead, it transforms into another structure, which differs from its native state, or remains partially unfolded. This wrongly folded or unfolded process is referred to as protein misfolding, which leads to the onset of various diseases, commonly known as protein misfolding diseases (Figure 1.2).[6] Although the exact cause of protein misfolding is uncertain; however, it is

thought that some standard parameters are associated, including pH, temperature, ionic factors, genetic, and mutations. Protein misfolding is a pathological state in which the native protein drops down from its standard functional form, leading to amyloidogenic diseases.[11,12]

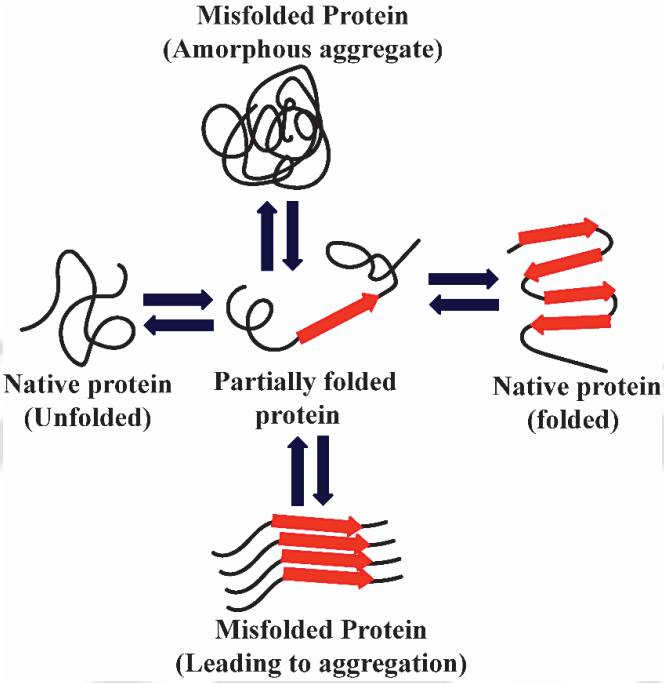

Figure 1.2: Protein folding and misfolding

1.4. Amyloids:

For some unknown reason, numerous unfolded, misfolded proteins or peptides accumulate together and deposit in the biological system as insoluble material by undergoing transitions from their native conformational structure (random coil) into ordered β-sheet conformations. These insoluble extracellular protein aggregates are known as amyloids.[3] Although different amyloidogenic proteins may generate amyloid fibrils, they all show similar properties, including morphology and insolubility. Amyloids get organized in a stacked cross-β sheet conformation and are usually seen as long filaments with a diameter of 3-10 nm and indefinite length, characterized by TEM and X-ray diffraction patterns.[13-18] In the amyloid

fibrils, proteins are arranged in β-sheets perpendicular to the fibrillar axis, while amyloids exist as cross-β structures bound to each other mainly by H-bonds.

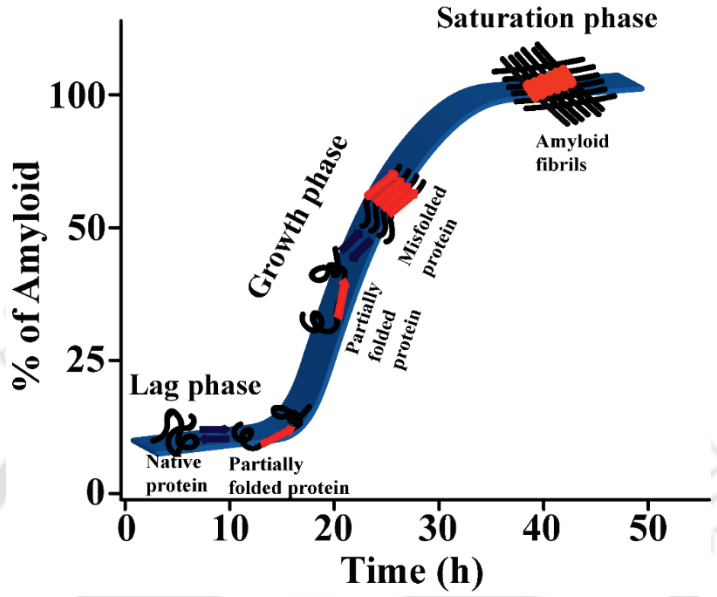

Figure 1.3: The process of amyloid formation characterized by a slow lag phase, followed by a growth phase and finally a saturation phase

The formation of amyloid fibrils is a nucleation-dependent process.[19,20] The amyloid formation process obeys the sigmoidal profile, where three phases are observed, a) nucleation or lag phase, b) elongation or growth phase, and c) saturation phase (Figure 1.3).[20] In the process of amyloid formation, initially protein monomers come closer to form the nuclei, i.e., the formation of soluble oligomers in the nucleation phase, followed by elongation with other monomers to form the protofibrils in the growth phase, which later convert to mature insoluble fibrils in the saturation phase. The time-dependent kinetics of amyloid formation is typically monitored by the Thioflavin T (ThT) based fluorescence technique, where the sigmoidal curve is observed for amyloid formation after a lag period, depending on the concentration of the aggregating protein.[21-23]

Many amyloid-related human diseases originating from amyloid toxicity have been identified. More than 30 proteins or peptides are known to form amyloids in various human-related diseases.[24, 25] Some amyloid-forming proteins or peptides and their respective diseases, commonly known as protein conformational disorders (PCD), are shown in Table 1.1.

Disease	Protein involved	No. of residue
Type II Diabetes	**Amylin or IAPP**	**37**
Alzheimer disease	Amyloid β	40 or 42
Parkinson disease	α-Synuclein	140
Huntington's disease	Huntingtin with polyQ expansion	3144
Sickle cell anaemia	Hemoglobin	141 or 146
Creutzfeldt-Jacob disease	Prion protein (PrP)	253
Spinocerebellar ataxius	Ataxin with polyQ expansion	816
Cystic Fibrosis	CFTR protein	67
Cataract	γ- Crystallins	Variable

Table 1.1: List of some protein misfolding diseases and the proteins involved.[25]

1.5. Diabetes:

Diabetes is considered a persistent metabolic disorder, which prevails either when the pancreas cannot generate a sufficient amount of insulin or when the body system is no longer capable of using the secreted insulin, finally leading to an increased glucose level in the blood.[26] Insulin is a hormone that originates from pancreatic β-cell, which act as a key to let glucose from the bloodstream into the cells in the body for energy production.[27] Ineffectiveness of insulin may lead to secondary complications in the body systems, which includes nerve and kidney failures, vulnerability to develop heart diseases, weakening of blood vessels and eyesight.[28]

Human beings require nutrition to prompt energy for normal growth and metabolic activities. The carbohydrates being consumed daily are broken down into glucose in due course and proceeds into the bloodstream. For the produced glucose to be utilized by body cells, the effectiveness of insulin hormone is required. However, for persons with diabetes, the outcome is an elevation of glucose level in the bloodstream, which eventually streams into the urine. This increased blood glucose is the "culprit" for numerous health-related issues associated with diabetes (Figure 1.4).[28] Until date, no such remedy has been approved for the chronic disorder; however, therapeutics comprises recasting way of life, fatness modification, and oral medications, including insulin administration for controlling the disease, which is still recommended as first-line medication.[29]

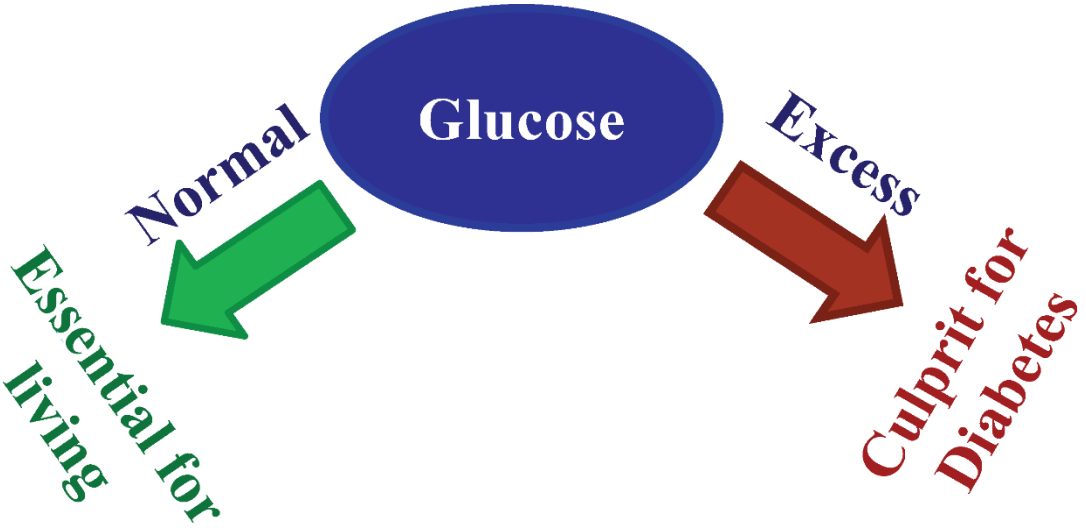

Figure 1.4: Glucose Homeostasis

1.5.1. Diabetes prevalence:

Diabetes is one of the fastest-growing health challenges of the 21st century. The prevalence of diabetes is continuously propagating worldwide. Fast urbanization is giving rise to various lifestyle changes, which adversely affect the metabolic processes, leading to an epidemic of diseases associated with such lifestyle changes. In the present global scenario, 463 million people are suffering from the disease, out of which in India, the figure comes out to be 77 million.[30] According to IDF (International Diabetes Forum), the prevalence of diabetes may rise to 578 million by 2030 and 700 million by 2045. About 4.2 million people passed away worldwide due to diabetes and its complexities in 2019, which is equivalent to one death in every eight seconds, despite approximately 760 billion U.S. dollars was spent on diabetes in that same year (IDF 2019). Globally 11.3% of deaths occurred due to diabetes, out of which almost half of this death occurred under 60 years of age. Diabetes is speculated to be the 7th leading cause of death globally by 2030. It imposes a significant economic impact on countries, as it is considered that the "indirect costs" of diabetes account for over 35% of

annual global health disbursement.[30,31] Considering these data, prevention of diabetes could be improved with a robust health system, fruitful policy and informed public.

1.5.2. Types of Diabetes:

Mainly three forms of diabetes exist (1) Type-1 diabetes (T1D), which is also recognised as insulin-dependent diabetes mellitus (IDDM), where the pancreas secrets a little or no insulin. (2) Type-2 diabetes (T2D), which is also recognised as non-insulin-dependent diabetes mellitus (NIDDM), where persons suffering from this type of diabetes have a combination of either resisting insulin from its specific assignment or limitation in producing insulin. (3) Gestational diabetes, which only affects pregnant women, and normally cures, as the pregnancy is over.[27]

1.5.2.1. Type 1 Diabetes (T1D):

Type 1 diabetes (formerly recognised as insulin-dependent, juvenile, or childhood-onset) is characterized by the destruction of pancreatic β-cells, which leads to insufficient production of insulin and needs imposition of external insulin on a daily basis to control the blood glucose level. The exact reason for the destruction of β-cell is unrevealed; however, genetic and environmental factors may stimulate type 1 diabetes.[32] Insulin triggers the conversion of blood glucose into energy to carry out body functions by the cells. In the absence of sufficient insulin hormone, the body's glucose intake persists in the bloodstream, and the body system will enter into a state of elevated glucose level, called hyperglycemia.[33] Therefore, all T1D are accounted as insulin-dependent, as the body cannot produce enough insulin for proper functioning , so people suffering from T1D must boost the insulin in their body systems. T1D accounts for 5-10% of the people who suffer from diabetes, in which symptoms include excessive excretion of urine (polyuria), thirst (polydipsia), unexpected weight loss, continual

hunger, change in vision and tiredness.[34] These symptoms may occur suddenly and person bearing such symptoms are advised to check their glucose levels intermittently.

1.5.2.2. Type 2 Diabetes (T2D):

Type 2 diabetes (formerly recognised as non-insulin-dependent or adult-onset) is the most common form of diabetes associated with the body's ineffective insulin use. T2D accounts for approximately 90-95% of all the diabetic patients and is the significant consequence of excessive body weight and physical inactivity.[27] Type 2 diabetes differs in presentation from type 1 in that T1D typically occurs in the early stage of life, whereas T2D appears mostly in older adults from about 40-45 age onwards. However, in recent years, the drastic increase in childhood obesity accompanies the higher rates of prediabetes and T2D in people under twenty.[27] Prediabetes is one of the forms before developing full-fledged diabetes, in which the glucose level is at an elevated point from 100-126 mg/dL, which is marginally upright than the recommended 80-100 mg/dL. According to the American Diabetes Association, to be recognized as T2D, the value of blood-glucose level has to exceed 126 mg/dL. To be diagnosed adequately from the disease, the identification of prediabetes stage has become extremely important for the physician, as the treatment at this condition may lead to the safeguard from a more pathetic situation.[35]

With an increase of glucose level in the bloodstream, the body system may be badly affected, and all cellular activities undergo obstruction in smooth functioning as cells lack the requisite energy that they would get from the glucose conversion. In normal conditions, the insulin hormone is secreted from the pancreas in small quantities to control glucose transported to cells for energy. However, as the number of glucose increases in the bloodstream, the pancreas prompted more insulin amounts to make up and impel the increased glucose into the cells. In T2D, the pancreas produces insulin, unlike in T1D; however, the pancreas cannot

produce a sufficient amount of insulin, or the body may not correctly utilize the produced insulin, which leads to elevated glucose levels in the bloodstream.[35] The symptoms of T1D and T2D are similar but ignored most of the time by individuals. As a result, the disease remains undiagnosed for up to several years.

1.5.2.3. Gestational Diabetes:

Gestational diabetes is hyperglycaemia with blood glucose values above normal but below those diagnosed with diabetes occurring during pregnancy. This type of diabetes may affect about 5% of all pregnant women. Women suffering from gestational diabetes are at an elevated risk of obstacles during the periods of pregnancy and delivery. Moreover, women experiencing gestational diabetes have a considerable possibility of developing T2D later in life.[36]

Out of three types of diabetes, T2D affects around 90-95% of all world cases. T2D generally develops after the age of 45, and the possibility of its effect increases with age. However, nowadays, T2D is increasing rapidly in the case of children too. One of the most critical activities to initiate efficient diabetes therapy is understanding the molecular mechanism that causes the disease.[35]

1.5.3. Diabetes risk factors:

Diverse risk factors are associated with diabetes. If a person is affected by T2D, it could be a consequence of numerous risk factors, including obesity or family history. The genetic effect, lifestyle modification, and environmental changes can dominate the risk factor for developing T2D. The fast-growing prevalence of T2D may be due to the increasing aging population due to medical science development. However, another factor, which includes an increasing number of obese people, like obesity, coupled with lack of exercise, can lead to T2D because

it can cause insulin resistance to the body.[37] Moreover, if family members have a history of diabetes, the risk increases 2-6 times than those without a family history.[38]

1.5.4. Popular methods for diagnosis of Diabetes:

The diagnosis of diabetes is usually carried out by symptom management. Persons bearing any symptoms of diabetes are advised for screening test for diagnosis of diabetes and prediabetes, which includes Fasting Plasma Glucose Test (FPGT), Oral Glucose Tolerance Test (OGTT), Glycated Haemoglobin Test (GHT, shows average plasma glucose concentration) and Random Blood Glucose Test (RBGT). Among the tests, the FPGT is the most widespread, as it is appropriate and cheaper. To measure blood glucose levels by the FPGT, the most convenient results are obtained when the test is carried out in the morning after fasting for at least 8 hours. If the fasting glucose level is obtained 100-125 mg/dL, it is considered prediabetes. If it exceeds 126 mg/dL, the physician proceeds for further tests to confirm the disease. Further blood glucose level is monitored by OGTT after 2 hours of taking normal food (which contains 75 g of glucose in water) and if the value lies between 140-199 mg/dL or greater than 200 mg/dL, it is considered as prediabetes and diabetes respectively. The GHT also gives an effective route for monitoring prediabetes and T2D, as the value lies between 42-47 mmol/mol indicates the prediabetic stage; however, a value above the range indicates the diabetic stage.

Moreover, RBGT is carried out to detect diabetes during a normal health assessment procedure, where a value of above 200 mg/dL with any symptoms is considered for a further test of diabetes. Furthermore, the presence of a higher amount of glucose in urine also gives indications for diabetes. However, other diagnostic procedures are used to identify T1D or T2D, including ketone tests, C-peptide tests, and glutamic acid decarboxylase autoantibody tests (Diabetes UK, 2016, NIDDK, 2014).

1.5.5. Secondary consequences of Diabetes:

Diabetes may influence several secondary complications, including kidney failure, heart problems, blindness, nerve blockage etc. Diabetes multiplies the chances of heart disease; as from an international survey, it was observed that 50% of people with diabetes expired due to cardiovascular diseases.[39] Furthermore, reduced blood flow and neuropathy in the feet enhances the risk of foot ulcers and finally requires limb amputation in people with diabetes. Moreover, blindness may occur due to diabetic retinopathy caused by the damage of the retina's small blood vessels in the tissue, where 1% of worldwide blindness may be attributed to diabetes. Further, in the overall risk of dying, persons suffering from diabetes are at least double the risk than a healthy non-diabetic individual. As there is no complete cure for the disease, therefore for controlling diabetes and its complications, the necessary and essential part is to maintain a healthy diet, weight regulation, retaining activeness with regular exercise and medication, including insulin therapy and other medications.[40,41]

The future options for the therapeutics of T2D are being investigated continuously from various aspects. The existing therapy for the disease depends on symptoms of the individuals. In future, people are looking for a complete cure for the disease, through either genetics management, new therapeutic agents, or a biochemical approach. During the investigations, one very encouraging lead appeared, which constitutes a particular polypeptide, **Amylin or IAPP**, and its prospective effects towards the deadly disease faced worldwide.[42, 43]

1.6. Amylin or IAPP:

Amylin or hIAPP (human Islet Amyloid Polypeptide) is a 37 amino acid residue long peptide hormone, co-stored and co-secreted from the pancreatic-β cells with insulin hormone at a constant molar ratio of 1:100 (amylin: insulin).[43] Mature IAPP contains an amidated C-

terminus and there is a disulfide linkage between Cys-2 and Cys-7 residues. The physiological role of soluble IAPP is still not understood to date; however, it is believed to complement insulin by suppressing postprandial glucagon secretion and regulating the rate of gastric emptying and maintaining glucose homeostasis. [44,45] Moreover, it is reported that IAPP takes a role in regulating body weight and it may cause apoptosis in isolated human islets.

1.6.1. Processing of IAPP:

IAPP is translated from an 89 amino acid residual prepropeptide containing 22 amino acids of signal peptide. The 37 residual IAPP is flanked by two short peptides, one at N-terminal (11 residual amino acid) and another at C-terminal (19 residual amino acid). The 22 amino acid residue signal peptide is cleaved by a signal peptidase to form a 67 amino acid propeptide IAPP (proIAPP).[46,47] Further, proIAPP undergoes processing in the Golgi complex and insulin secretory granule. The N- and C-terminals of proIAPP are cleaved by two enzymes, prohormone convertase PC1/3 and PC2, at the two dibasic sites (lysine and arginine).[46] Additional processing of human pro-IAPP at C-terminus by carboxypeptidase E and a glycine residue at the start of the C-terminal propeptide serves as the nitrogen donor for amidation by the peptidyl amidating mono-oxygenase complex (PAM). Finally, the polypeptide experiences post-translational tempering, forming a disulfide bond between Cys-2 and Cys-7 residues to form mature IAPP (Figure 1.5). IAPP is deposited along with the insulin in secretory granules and co-secreted from pancreatic β-cells as required.[47]

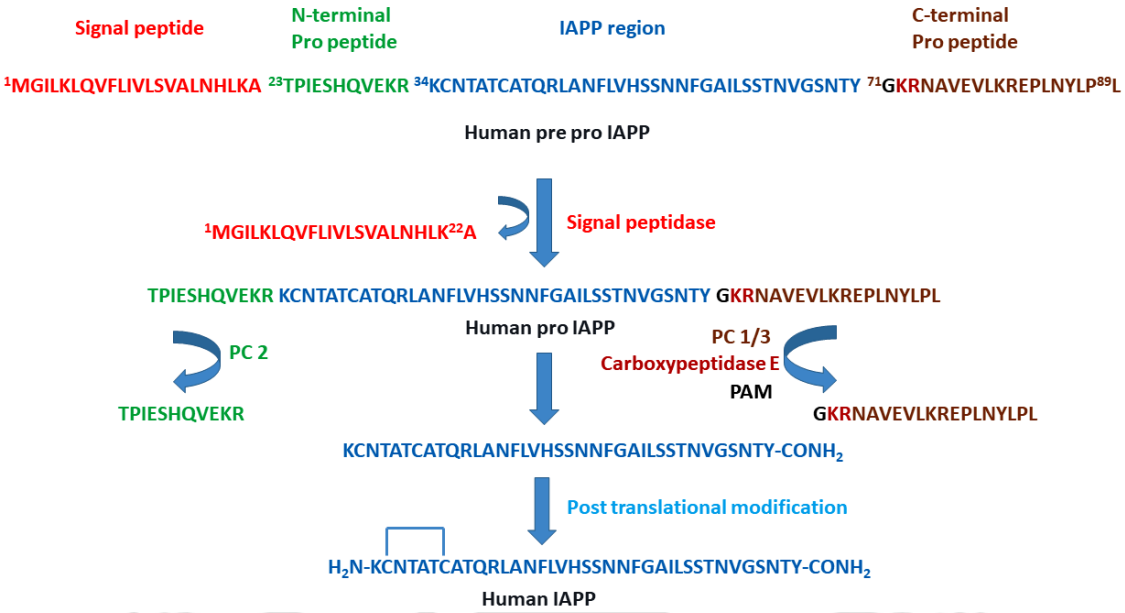

Figure 1.5: Processing of 89-residual human preproIAPP to form a mature native IAPP through various translational modifications.

Although the concentration of IAPP in the secretory granule is approximately 1-2% of that of insulin, the same is more than sufficient to promote fast amyloid formation *in vitro*. Therefore, there should be some criteria, which prevent premature and irreversible aggregation inside the granule.[48,49] As the formation of IAPP amyloid is pH-dependent, the lower pH environment of the granule may take part in decreasing the aggregation rate. Moreover, soluble insulin may also control the inhibition process of amyloid formation inside the granule.[50,51]

1.6.2. Sequence of IAPP and its relation with T2D:

IAPP belongs to the calcitonin-related peptide family, consisting of CGRP (α and β calcitonin gene-related peptide), adrenomedullin, and intermedin. However, it is most similar to CGRP with 37 amino acid residues (Figure 1.6).[52] They both accommodate a 2-7 residual disulfide bond, containing an amidated aromatic residue at the C-terminus along with their monomeric state; both have a propensity to form a transient helical structure. Various studies revealed that amylin or IAPP at physiological conditions misfolds its native structure and causes

amyloid fibres *in vitro*, but CGRP does not.[53] Both the peptides have reasonable similarities in sequence, especially in N- and C-terminal regions; however, they differ substantially in the mid-region, i.e., 20-29 positions. This observation guided the research community to propose that sequence within the 20-29 region of IAPP plays a significant role in forming amyloid fibrils.[54]

Moreover, IAPP exists in the pancreatic-β cells of all mammals, birds, and teleostean fishes.[55] However, earlier issues in considering the function of IAPP derived amyloid in the pathogenesis of T2D might have appeared from the fact that some mammalian species, such as rats and mice, neither form amyloid of IAPP nor develop diabetes.[56] The rat or mice IAPP has variations to human (hIAPP) at only six positions, apparently at 20-29 positions, accounting for five out of the six alterations. The rat IAPP (rIAPP) contains three proline residues at 25, 28 and 29 positions, while no proline is present in hIAPP. Proline is a significant secondary structure disruptor, and its presence makes the sequence energetically unfavourable for β-sheet formation, due to which it is attributed to the inability of amyloid formation by rIAPP.[57] These studies explain the importance of the $IAPP_{20\text{-}29}$ in the formation of amyloid. However, multiple proline substitution outside the specific region as Asn-14 or Asn-21 was found to help in abolishing IAPP amyloid formation.[58,59]

Human IAPP: ^{1}KCNTATCATQRLANFLV**H**SSNN**F**G**AI**L**SS**TNVGSNT^{37}Y-(NH_2)

Rat IAPP: ^{1}KCNTATCATQRLANFLV**R**SSNN**L**G**PV**L**PP**TNVGSNT^{37}Y-(NH_2)

(Disulphide linkage between 2 & 7 cysteine residue in both the case)

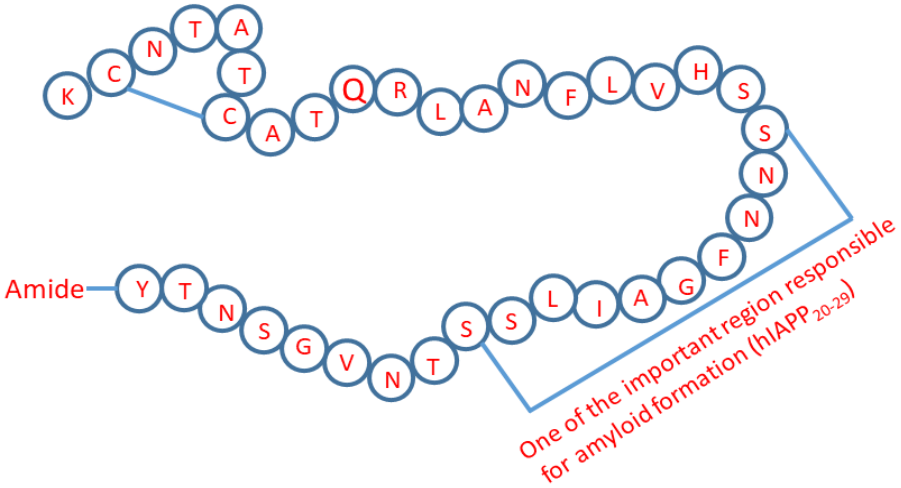

Figure 1.6: Structure of hIAPP

hIAPP misfolds and causes amyloid formation resulting in shrinkage of β-cell mass in the pancreatic islets of Langerhans *via* an unrevealed mechanism. hIAPP aggregates *in vitro,* and it is one of the most aggregation-prone naturally occurring peptides.[60] hIAPP itself is not the cause of T2D, but it leads to β-cell dysfunction and cell death, characteristic of the reduced mass of islet β-cell.[61] Amyloid formation occurs only in T2D; as in T1D, the hIAPP source is removed due to the destruction of the β-cells. Hence, to elucidate possible amyloidogenic and cell membrane interacting species, various investigations were carried out using different fragments of hIAPP through biophysical experiments. Current investigations revealed that the formation of amyloid and membrane disruption processes proceed via non-identical pathways restrained in two specific regions of hIAPP. The structural study suggested that $hIAPP_{1-19}$ is primarily accountable for the interaction with the membrane, whereas, from the theoretical prediction, $hIAPP_{1-8}$ is the only region unable to form amyloid as the amino acid residue of this region contains a disulfide bridge.[62,63] However, further studies revealed that other regions of the polypeptide such as $hIAPP_{8-20}$ and $hIAPP_{30-37}$ also play a significant role in fibrillogenesis, which implies that $hIAPP_{1-8}$ has exclusive membrane interacting ability; but, $hIAPP_{8-20}$ and $hIAPP_{30-37}$ are responsible for membrane insertion.[64,65]

Moreover, hIAPP involves six Asn residues in the sequence, and Asn deamidation is one of the most familiar post-translational processes, which involves amyloid formation by other amyloidogenic peptides. A neutral amino acid residue is put back by a negatively charged one in the deamidation process, which reduces the net charge of hIAPP and solubility. Hence, Asn deamidation leads to the acceleration of hIAPP amyloid formation, followed by a morphological change.[65] Furthermore, aromatic-aromatic and aromatic-hydrophobic interactions are thought to play a crucial role in hIAPP amyloid formation. However, studies revealed that aromatic residues are not necessary for the amyloid formation, although aromatic-aromatic interaction may interfere in the kinetics of fibril formation and dominate the amyloid fibril structure. Replacement of two phenylalanine and one tyrosine moiety in hIAPP by leucine reduced amyloid formations by five-fold than unsubstituted hIAPP, indicating alteration of the rate of self-assembly. Therefore, it could be proposed that hydrophobic and aromatic residues might be necessary for assisting protein-protein interaction leading to acceleration of fibrillization, however not that much necessary for the nucleation process.[66,67]

One of the most exciting factors in the sequence of hIAPP is the Cys-2 and Cys-7 bridging disulfide bond at the N-terminal. The bridge does not significantly impact the amyloid core structure due to conformational restriction imposed by the disulfide bond, but disruption of this disulfide bond effectively reduces the amyloid fibril formation. Moreover, a change in pH could cause a crucial change in the conformational and aggregation profile of the polypeptide, as switching from acidic to basic accelerates the aggregation process. Hence, structural ordering by disulfide bridge or by a change in pH, the fibrillization process of the polypeptide may be facilitated.[68]

Several factors recommend an intimate association between insulin and IAPP. The pathogenesis of T2D is characterized by systematic insulin resistance, which might be overcome by triggering the higher secretion of insulin. However, elevated secretion of insulin will lead to higher secretion of IAPP as well. The toxicity arising from a higher concentration of IAPP will result in a gradual reduction of β-cell mass, which has to be present to meet the increased demand for insulin.[69] Moreover, in healthy adults, IAPP to insulin molar ratio of secretion is about 1:100; but, the ratio converts to 1:20 for T2D affected adults resulting in higher concentration of IAPP.[70] Nevertheless, the relationship between IAPP and insulin sensitivity is still questionable, as secretion of IAPP from the pancreatic β-cell may not be modulated by insulin sensitivity.[69,71] Furthermore, from different studies, it is observed that in healthy people, insulin could perform a contrasting role in IAPP aggregation by inhibiting the aggregation, triggering IAPP aggregation during the T2D pathogenesis. Due to these conflicting consequences of insulin, it might not be useful as an inhibitor of IAPP aggregation.[72] Hence, further investigations are necessary to monitor the interactions of insulin and IAPP in both healthy and T2D suffering individuals. However, IAPP is considered as a crucial component in the transformation and pathology from the early phases to the later phases of the T2D disease.

1.6.3. Conformation of monomeric IAPP:

Amyloid-forming proteins may be divided into two categories, one that folds to a globular structure in their native state, such as β2-microglobulin, another, which is natively unfolded like Aβ and IAPP. Although the monomeric IAPP cannot fold into a globular structure, it does not belong to the classic random coil.[73] Theoretical studies predict one α-helical region at $hIAPP_{8-14}$ and three β-strand regions at $hIAPP_{18-23}$, $hIAPP_{24-29}$, and $hIAPP_{32-37}$, one β-turn at Asn31 position.[70,73] From the secondary structure estimation by CD measurement, hIAPP

contains 10% α-helical content in solution, which complements that monomeric hIAPP is a predominantly random coil or unstructured in solution.

1.6.4. Structure of IAPP induced amyloid fibril:

The unstructured and monomeric IAPP experiences aggregation at physiological conditions leading to the development of amyloid fibril *via* toxic soluble oligomers, which are primarily responsible for the onset of T2D by depositing them as pancreatic amyloid.[74] The fundamental observation during the pathogenesis of T2D in the islet β-cells is detecting amyloid fibrils of IAPP. In the structural modification of IAPP amyloid, fibrils acquire a cross-β orientation where the β-strand moves perpendicularly to the fibrillar axis with interstrand hydrogen bonds oriented parallel to the axis. However, the strands may be either parallel or antiparallel for other amyloidogenic proteins. Two atomic-level models have been suggested for the fibrillar structure of hIAPP; the first model is acquired from solid-state NMR, while the second is from structural and morphological studies of hIAPP fragments. Both the models proposed that the fibrillar assembly contained a parallel β-strand, while the protofibrils adopting a U-shaped structure, made up of two columns of hIAPP monomers. However, due to the rapid aggregation propensity to form amyloid fibre and non-crystalline or insolubility issues of IAPP, it is highly challenging to determine a detailed molecular structure from NMR and X-ray crystallography.[75] Studies with electron microscopy revealed that amyloid fibrils are relatively straight, having a diameter around 10 nm range. The same study observed that the monomeric IAPP, which experiences aggregation, leading to the formation of an oligomer having a diameter 2.7-4.0 nm which further aggregates to form a non-spherical filamentous structure known as protofibrils, having a width of approximately 5 nm.[76] The fibrillar structure developed from IAPP was similar to that of Aβ peptides, responsible for Alzheimer's disease. Recent evidence proposed that amyloid-forming proteins

or peptides might be different in their sequences; however, the amyloid fibrils generated from these proteins may show common structural characteristics such as folding/misfolding process containing predominantly cross β-sheet structures.[76]

1.6.5. Mechanism of IAPP aggregation:

In solution, IAPP exists as a natively unstructured protein, however on incubation at physiological conditions or in the presence of model membrane, hIAPP has been observed to change its conformation from random coil to characteristic β-sheet, leading to amyloid formation. Despite multiple investigations on IAPP, very little is known about the mechanism of IAPP aggregation. Based on this, the process may be divided into the following essential steps:

a) The native soluble monomer of hIAPP is transmuted into a long-lived partially folded intermediate. Thus, the intrinsically folded polypeptide of hIAPP exposes the C-terminal residues (20-37) by hydrophobic region, out of which $hIAPP_{20-29}$ exists the key region for fibril formation. This exposure results in a flanking hydrophobic surface, which interacts with each other forming "aggregation-prone" partially folded conformers. The partially folded intermediates associate in a specific manner to form oligomers or "nuclei". The nucleation phase is kinetically disfavoured and considered the rate-limiting phase of aggregation; however, no fibril is formed in this step, instead only lateral growth of oligomers occurs. The duration of this phase may vary from a few minutes to a lifetime, subject to different conditions, such as concentration and temperature.[76,77]

b) The second phase is known as the elongation phase, where the necessary amount of nucleation occurs and then quickly propagates fibril formation. This phase is much faster than

the lag phase, which rapidly increases the aggregation rate. Therefore, this phase is a procedure of longitudinal growth into mature amyloid fibril formation.[78-80]

c) In the third phase, fibrillization is considered a steady-state, and the fibrillar population is stable, known as the plateau phase. The process of amyloid formation is spontaneous, where after initiating the process, it will continue if there are a sufficient concentration and environment of the amyloidogenic peptide. The formed amyloid fibrils are neutralized by accessory cellular molecules and deposited within the extracellular matrix, capable of driving severe diseases. The exciting revelation about amyloid formation is that the mature fibril does not contain significant cell toxicity, whereas the oligomeric transition state is the main culprit for the cytotoxicity of cells.[78-80]

1.6.6. hIAPP induced toxicity:

From various investigations about the role of protein in T2D, it was elucidated that the toxicity of hIAPP to islet cells evolved through triggering membrane destruction and apoptosis. Earlier it was considered that the toxic form of these aggregating peptides for the membrane damage process was the amyloid fibrils themselves. However, from recent studies, it is evident that the soluble oligomers are highly prone to the cytotoxicity of the biomolecules, whereas the mature fibrils remain relatively inactive during the process. Nevertheless, membrane disruption and amyloid fibril formation are two distinctly different processes centered in two discrete regions of hIAPP. It has been proposed that N-terminal $hIAPP_{1-19}$ is mainly accountable for the interaction of the peptide with a membrane, whereas region $hIAPP_{20-29}$ is responsible for amyloid growth.[81]

The role of hIAPP-induced cytotoxicity is of great concern in the pathogenesis of T2D due to the ill-defined nature of the oligomers. However, they have been exclusively studied *in vitro*,

suggesting that they are inserted into cell membranes. The first identified toxicity process is the destruction of the lipid membrane, resulting in a severe effect on cellular homeostasis. The cytotoxicity of hIAPP is correlated with the pore-formation capability, where they can form channel-like pores by the oligomeric intermediates.[82,83]

The key to connecting the role of amyloid fibril formation and T2D lies in understanding the mechanism behind the cytotoxicity of the intermediates. If the mechanism of cytotoxicity can be determined, whether it be through damaging the membrane or some other form, then it gives a pivotal point to determine how to prevent the damage causing the cell toxicity. hIAPP toxicity has also been suggested by its ability to perturb the membrane, and this process depends on the peptide to lipid ratio, pH, ionic strength, and lipid composition.[84] *In vitro*, IAPP induced toxicity towards membrane disruption is initiated by a two-step process, which involves biphasic kinetics. Initially, the cytotoxicity occurs *via* ion-selective channel-like pore formation in the lipid layer, causing membrane destruction followed by cellular homeostasis. The pores formed are unstable and merge into larger aggregates in anionic lipid membranes, leading to detachment from the membrane. In the next phase, metal ion dyshomeostasis (Ca^{2+} ions) and the incitement of various stress signalling pathways adjoin cell death.

Moreover, hIAPP is pushed into the lipid membrane, resulting in disruption of the cell membrane. Furthermore, several investigations revealed that the rapid aggregation of hIAPP results in reactive oxygen species (ROS), leading to cell death. In some cases, the process of fibril formation at the membrane surfaces is responsible for membrane disruption; however, other investigations provided the information of non-requirement of β-structure to disrupt the membrane. Although the pathological role of hIAPP oligomer intermediate is still in an argument, the role of mature fibrils should not be eliminated for the disruption of β-cell in

T2D. However, investigations, which could lead to an appropriate clarification of β-cell toxicity, would also open the door for the modified prospect of therapeutics against T2D.[85]

1.7. Existing therapeutics against Diabetes:

For curing any disease, its diagnosis is crucial and should be done as soon as possible. T1D is relatively uncomplicated as our body is unable to generate insulin required for body functions and hence it must be compensated by administering insulin from outsourcing. However, T2D is too complicated; hence, different techniques are deployed for the treatment. Analysis target for T2D may differ in many ways, starting with modulation in lifestyle adaptation such as healthy diet and regular exercise, oral medications including insulin penetration for the intense cases where lack of insulin occurs.[86] Mainly, there are three types of insulin, i) synthetically produced human insulin, ii) animal insulin, and iii) insulin analogous. Among the three, in the third category, the chemical structure of human insulin is modified, due to which it may contribute rapid and long-lasting effects against the disease (Diabetes UK, 2016). Although the most commonly used technique for T2D is insulin therapy, despite several modifications in insulin medications over the last few years, a complete cure has not been accomplished until now. Other treatments for T2D are available as some commercial drugs, including Metformin, Januvia, Janumet, Avandia, Avandamet, Symlimpen60, Symlinpen120, DPP-4 inhibitors (gliptins), thiazolidinediones (glitazones), an alpha-glucosidase inhibitor, etc. All these medications can only provide temporary relief against diabetes but cannot stop the growth of secondary complications that may arise due to the severity of the disease (Diabetes UK, 2016). Although there is no complete cure for T2D, extensive research is in progress to develop proper therapeutics, and there lies a ray of hope for a complete cure of the dreadful disease. Recently, an analog of hIAPP called Pramlintide, containing three proline moieties in its peptide backbone, has a lower propensity to aggregate

and has received FDA approval for clinical implementation; however, it also suffers from several drawbacks.[87] In recent investigations, it has been observed that medications like Lixisenatide used for treating T2D exhibited a neuroprotective effect, which applies to Alzheimer's disease (AD).[88] Further, it has also been reported that a diabetic person with very high blood glucose levels may experience a higher possibility of developing Alzheimer's disease, which suggests a strong correlation between T2D and AD. Although this relationship is not fully understood, both diseases are characterized by the accumulation of insoluble amyloid resulting from the aggregating polypeptide. As there is no complete cure for AD too, from the above observation, it is suggested that developing a cure for diabetes may find better curative for AD and other amyloidogenic diseases. Moreover, Glucagon like peptide-1 (GLP-1) agonists are considered as novel anti-diabetic therapeutics, which can improve the glycaemic control and induce weight loss. In clinical practices, few GLP-1 agonists have been approved as 2nd or 3rd line agents after the failure of the commonly used anti-diabetic drugs. However, their optimal role in the clinical management of T2D has not been accomplished yet.[89]

Considering all these into account, inhibition of amyloid fibril formation or the ability to disrupt the preformed amyloid of hIAPP *via* resulting in non-toxic aggregates might lead to developing potential therapeutics against T2D. As the oligomers are considered toxic, such inhibitors or disruptors affect only the mature fibrils, but not the oligomeric species may not be specifically applicable as a therapeutic agent. Several modulators comprising small molecules, nanomaterials, composite materials, and natural products have been recognized as potential therapeutic agents for treating T2D.[90-92] Further, another inhibitor, Epigallocatechin 3-Gallate (EGCG), a biologically active flavanol in green tea, containing polyphenol moiety, was investigated for inhibition of aggregation that interacts with the monomer or early-formed oligomers in a process that might be able to restrict the accumulation of the

destructive species of hIAPP. It has been observed that EGCG can entrap the monomeric polypeptides and alter the route for the formation of hIAPP aggregation *via* oligomers, which suggests that EGCG may inhibit hIAPP amyloid fibril formation along with restricting hIAPP induced toxicity.[93] However, many factors, including inadequacy in specificity, cytotoxicity, quick metabolism, and most importantly, inefficiency in blocking extensive protein-protein interactions, suppressed the clinical application of small molecule-based modulators against hIAPP aggregation.

Further investigation leads to the development of peptide-based inhibitors, which provide effective alternatives against aggregation of hIAPP due to their viability in synthesis and modification, biocompatibility, and faint immunogenicity. Further, the peptides and peptidomimetics inhibitors synthesized through slight modification of the aggregating peptide exhibited significant importance due to the large surface area of the protein-protein interphase for drug design against T2D. Moreover, peptides may be an excellent drug candidate due to their therapeutic superiority over the small molecules in target specificity, binding affinity, and low toxicity. However, due to awful membrane permeability, low solubility and proteolytic instability restrict peptides from being readily used as a drug.[94] Systematic research and modification over the drawback of the peptide-based drug are being investigated, and the community is waiting for significant results against the deadly disease T2D or other amyloidogenic diseases.

1.8. Peptide-based inhibitors against hIAPP aggregation:

Since it has been believed that T2D is a protein aggregation disease, the peptide-based inhibitor is thought to be one of the most exciting and practical therapeutic approaches against the disease. In the past two decades, several peptide-based inhibitors have been evaluated against hIAPP aggregation, which can be divided into two major categories and several subcategories, such as:

1) Peptide inhibitors with natural amino acid
    a) Peptides derived from hIAPP sequence
    b) Peptides non-derived from hIAPP sequence
2) Peptide inhibitors with the chemical transformation
    a) Containing N-alkylated peptides
    b) Involving D-amino acids
    c) Incorporating non-natural amino acids
    d) Cyclic and conjugated peptides

1.8.1. Peptide inhibitors with natural amino acid:

Various studies explored the involvement of several segments of the amyloidogenic hIAPP sequence and their role in developing amyloid fibrils. Nevertheless, the small peptide fragments of hIAPP, FGAIL ($hIAPP_{23-27}$), NFGAIL ($hIAPP_{22-27}$), SNNFGAIL ($hIAPP_{20-27}$), and SNNFGAILSS ($hIAPP_{20-29}$) are known to form amyloid fibril similar to that of full-length hIAPP; however, no amyloidogenicity was observed for the sequence GAIL ($hIAPP_{24-27}$).[57,95] Furthermore, another region involving TNVGSNTY ($hIAPP_{30-37}$) at C-terminal and ATQRLANFLVHSS ($hIAPP_{8-20}$) undergoes self-association leading to the formation of amyloid *in vivo*, although $hIAPP_{20-29}$ was considered as the key region for fibril formation.[61,64,95] Thus, targeting this small peptide fragment and designing a small peptide-

based inhibitor incorporating breaker element into a recognizing moiety was accepted as bright therapeutic tools against the formation of hIAPP amyloid and its disruption.

Scrocchi *et al*. investigated and observed that (SNNFGA) $hIAPP_{20-25}$ and (GAILSS) $hIAPP_{24-29}$ emerged as potent inhibitors when co-incubated with hIAPP and found to be efficient in inhibiting hIAPP mediated cell death.[96] Further, Porat *et al*. observed that incorporating tyrosine in place of phenylalanine in the sequence of N**F**GAILSS ($hIAPP_{22-29}$) found to be efficient in the inhibition of hIAPP aggregation. However, this modified peptide NYGAILSS failed in the cytotoxic assay to BTC-tet cell and reduced β-cell viability.[97] Later in an investigation, Abedini *et al*. demonstrated the effect of proline insertion in the central hydrophobic region (I26P) on the full-length of hIAPP and observed that the I26P mutant accelerated the lag time of hIAPP aggregation by 20 times.[98] However, in a different study, Cao *et al*. observed that rIAPP might be a highly effective inhibitor against hIAPP aggregation as rIAPP does not form any amyloid *in vitro* and *in vivo*, probably due to the presence of three proline residues in the $rIAPP_{20-29.}$ This strategy also increases the lag time of hIAPP aggregation by tenfold in 1:5 and 22 fold in 1:10 (hIAPP: rIAPP) ratio.[99] Keeping these ideas, Wang *et al*. designed an analogous hIAPP by incorporating proline and some other amino acids in different residues to improve the solubility by increasing the net charge in the analogous. The quadruple mutant (H18R, A25P, S28P, S29P) and triple mutant (H18R, G24P, I26P) of hIAPP were observed to be non-amyloidogenic, non-toxic, and most interestingly displayed higher solubility than hIAPP and pramlintide at neutral pH.[100] However, in further investigation, Pramlintide (PM) showed higher inhibitory efficiency than rIAPP and the other mutant of pramlintide (H18R PM and F23L PM). Although PM has attractive efficiency in inhibiting the amyloid aggregation; however, it also undergoes lower solubility issues at physiological pH, proteolytic stability, and difficulty in synthesis, which diverted the researchers' attention into the small peptide sequence.[87] In a later experiment

performed by Khemtemourian *et al*. identified that hIAPP analogous (H18R, H18K, H18A, and H18E) displayed little fibril formation tendency in contrast to native hIAPP at physiological pH. Further, H18R-hIAPP pointed out to be a potent inhibitor, non-cytotoxic against hIAPP aggregation, which highlighted the significant influence of His-18, a residue positioned outside the key amyloidogenic $hIAPP_{20-29}$ region.[101]

In addition to the peptide-based inhibitor, which is derived from the amyloidogenic region of hIAPP, some other peptides, which lack that amyloidogenic region, have also been an effective inhibitor of amyloid aggregation. This group of peptide-based inhibitors includes β-cell granule peptide, insulin β-chain sequence, polyethylene glycol-modified on EALYLV peptide sequence, TK9 (TVYVYSRV(-NH_2) derived from extra membrane C-terminal tail of SARS coronavirus envelop, etc., which were able to inhibit the uncontrolled hIAPP aggregation by an unknown mechanism.[102-104] In the recent modification of Shi. *et al.*, a novel polypeptide FLPNF evaluated its inhibitory efficacy against hIAPP aggregation in a 1:10 molar ratio via π-π stacking interactions of phe5 residue with phe15 of hIAPP. Further, Xuan *et al*. designed a solution-phase bio panning technique to identify *de novo* peptide LTPHKHHKHLHA (LA12), which binds specifically to the core region of the hIAPP monomer and able to arrest its aggregation and lowered hIAPP induced cytotoxicity.[105]

1.8.2. Peptide inhibitors with chemical transformation:

Over and above the techniques, several modified peptide-based inhibitors were investigated with various chemical transformations with the aggregating peptide sequence. N-methylation at the native peptide sequence diminished NH groups' H-bonding ability and contributed conformational restriction to the peptide backbone. Further, the N-methylation techniques provided higher stability of the peptides against the proteolytic enzyme, which furnished additional superiority for the *in vivo* application of this technique over protein aggregating diseases. Kapurniotu *et al*. demonstrated the non-amyloidogenic behaviour of selective N-

methylated derivative on the amyloidogenic sequence of hIAPP. Double N-methylated derivatives such as F(N-Me)GA(N-Me)IL, NF(N-Me)GA(N-Me)IL, SNNF(N-Me)GA(N-Me)IL found not only lack of amyloid-forming tendency, it also observed to be an effective inhibitor against the amyloid formation and diminishing cytotoxicity of hIAPP induced β-cell death. [106] Later, Yan *et al*. reported a double N-methylated hIAPP analog as hIAPP-GI [G24(N-Me), I26(N-Me)] gained a highly potential inhibitive nature against amyloid via strong binding affinity with hIAPP in contrast to the double N-methylated $hIAPP_{20-27}$ version.[107]

Furthermore, several peptide-based inhibitors have been reported as effective against amyloidosis with the involvement of D-amino acid. Increased bioavailability, less immunogenic nature and higher proteolytic stability over their L-amino acid counterparts made the D-amino acid-containing peptides a promising technique against T2D. Wang *et al*. demonstrated that all D-amino acid-containing **D**-NFGAIL could inhibit aggregation effectively and rescuing the cell from hIAPP induced toxicity.[108] Moreover, Huggins *et al*. described that hairpin peptides containing D-proline inside cross-strand Trp-Trp (WW) and Tyr-Tyr (YY) pairs able to modulate aggregation caused by hIAPP. The hairpin peptides WW2 (KKLTVW-IpGK-WITVSA), YY2 ((KKLTVY-IpGK-YITVSA) and WW4 (KKLWVS-IpGK-KIWVSA) were able to increase the lag time of hIAPP aggregation more effectively than the rIAPP, including suppression of toxicity imposed by hIAPP. Further, these peptides were proposed to bear an exposed hydrophobic site, which interacts with the amyloidogenic region of hIAPP to block the peptides self-assembly process.[109]

In addition to these techniques, incorporating non-natural amino acids into the parent sequence has emerged as a positive strategy to terminate the amyloid formation. Peptides containing modified or non-coded amino acids have far better proteolytic resistance and higher bioavailability, facilitating the non-natural consisting peptides as an encouraging

therapeutic agent against challenging bio-molecular targets, including hIAPP aggregation. Gilead *et al*. reported that incorporation of α-aminoisobutyric acid (Aib) in $hIAPP_{13-20}$ sequence increases significant inhibition properties with a higher association for binding with hIAPP.[110] Andreasen *et al*. demonstrated that single site backbone modification at $hIAPP_{20-29}$ or $hIAPP_{22-27}$ by hydroxyethylene, ketomethylene or peptoid formation effectively modulates hIAPP aggregation.[111] Later, Mishra *et al*. investigated the incorporation of ΔF (non-natural amino acid and analog of phenylalanine with a double bond between C_α and C_β atoms) at I26 position of $hIAPP_{23-27}$.[112] From the investigation, it was observed that the modified inhibitor was able to inhibit hIAPP aggregation exclusively and it does not contain any cytotoxic effect on cultured pancreatic rat insulinoma (RIN 5fm) cells.

One more technique involving cyclic and conjugated peptides, which displayed better activity compared to their linear analogs due to the conformational rigidity, has emerged. These peptides have emerged as a promising medicinal activity due to their biochemical stability, structural rigidity, selectivity, and membrane permeability. Sivanesam *et al*. demonstrated two sequences, β-cap-WW2 (AcW-KKLTVW-IpGK-WITV-SAWTG-NH_2) and cyclo-WW2 [cyclo-(GKWITVS-IpPKKLTVWIp)], possessing rigid and more stable β-hairpin conformation, which showed effective inhibition against the amyloid formation; however, the cyclo-WW2 acted as more potent inhibitors at sub-stoichiometric too.[113] Moreover, Profit *et al*. engineered an octa-peptide NFGAILSS by conjugating substitution benzene carboxylic acid, distinguishingly at the N-terminal of the peptides. Among various conjugates, the substitution of 2,4,5-tricarboxylic benzoic acid at the N-terminal (C1) showed effective abolishment of amyloid fibril of hIAPP, which blocked the conformational transition to the aggregation-prone β-sheet structure. From the mechanistic angle, the electrostatic repulsion between hIAPP and C1 might able to prevent the oligomerization by stabilizing off-pathway helical intermediates and finally could restrict the amyloid formation.[114]

1.9. Objective of the thesis:

Over the past two decades, extensive research has been carried out for drug development against T2D; however, a complete cure is yet to achieve. Although the exact cause of the disease is still under lively debate, IAPP amyloid deposition via aggregation associated with reduced β-cell mass is believed to contribute to the progress of T2D significantly. Numerous strategies have been taken care of against the disease, including small molecule-based inhibitors and peptide-based therapeutic agents. However, several factors, including lack of specificity, minimal protein interaction tendency, and cytotoxicity, restrained small molecule-based inhibitors as promising pharmacological agents against amyloid aggregation. Further, peptide-based inhibitors significantly affected hIAPP aggregation and its induced cytotoxicity; still, the effective therapeutic agent is yet to deliver to society due to several obstacles that interrupted the development of a proper drug. These obstacles include understanding the hIAPP aggregation mechanism *in vitro* and *in vivo*, the difficulty of targeting initiation sites of islet amyloid formation, elucidation of the behaviour of toxic species, and the mechanism of cell death induced by hIAPP. Although Pramlintide, marketed as Symlin, received FDA approval for clinical application, it possesses several drawbacks, including less solubility at physiological pH, less stability against proteolytic degradation, and antagonistic solubility, which restrict the co-formulation with insulin. Moreover, most reported β-sheet breaker peptides are unstable against proteolytic degradation, ineffective against cytotoxicity, poor membrane permeability, including higher doses of inhibitors. Hence, developing a promising therapeutic agent with minimal side effects with lower doses against T2D will be achieved by elucidating the proper mechanism of hIAPP aggregation.[115]

Keeping in mind the drawbacks of peptide-based inhibitors, our main objective is to develop modified β-sheet breaker hybrid peptides to fight against T2D using conformationally restricted peptides. For this purpose, we have selected various isomers of aminobenzoic acid

(especially 2-aminobenzoic acid) as a β-breaker element. 2-aminobenzoic acid or anthranilic acid (Ant) is an interesting component of peptidomimetics due to the conformational restriction imposed by its structure. In the structure of Ant, both the amine group and the carboxyl group are directly connected to the aromatic moiety, constituting a planar structure with a fixed dihedral angel, Φ = 0°.[116] Therefore, in the peptide sequence containing Ant in the backbone, conformational rigidity was enhanced due to the π-stacking ability of the aromatic moiety.[117,118]. Due to its higher structural rigidity, we planned to incorporate Ant as a β-breaker element into the peptide backbone within the central hydrophobic region of hIAPP peptide. Furthermore, the Ant moiety favours the formation of either a turn or a helical conformation while inserted into the peptide sequence. [119]. Moreover, anthranilic acid is found in many biologically active naturally occurring peptides (e.g. psychrophilin, cycloaspeptide, asperterrestide, etc.), and it is the precursor for the biosynthesis of tryptophan.[120]. Most importantly, it is a β-amino acid, which can improve the proteolytic stability in enzymes over the α-amino acids.[121]

The objectives of the thesis are:

1. To introduce β, γ and δ aminobenzoic acids as modulators of β-sheet breaker hybrid peptides (BSBHps) and investigation of their effects on hIAPP fibrillogenesis.
2. To develop BSBHps incorporating various isomers of aminobenzoic acid as a double mutant to arrest hIAPP aggregation.
3. To investigate the anti-amyloid activity of single point mutation by rigid β-amino acid in $hIAPP_{8-37}$ at different positions.
4. To develop a novel side chain to tail stapled peptides and apply their anti-amyloidogenic efficacy in inhibiting hIAPP amyloid and disrupting the preformed hIAPP amyloid.

Chapter 2: Introduction of β, γ, and δ aminobenzoic acid as β-sheet breaker hybrid peptides and their applications in the inhibition of hIAPP aggregation

2.1. β-sheet breaker hybrid peptides:

Initially, Westermark *et al.* pointed out that a limited segment of hIAPP has an intrinsic tendency to form amyloid, which might be responsible for T2D. The small peptide fragments of hIAPP, such as FGAIL ($hIAPP_{23-27}$), NFGAIL ($hIAPP_{22-27}$), SNNFGAIL ($hIAPP_{20-27}$), and SNNFGAILSS ($hIAPP_{20-29}$) are sufficient for the formation of amyloid *in vitro* in a similar fashion as $hIAPP_{1-37.}$ [60,105] Hence, if one focuses on these peptide sequences and plan for a small peptide-based inhibitor constituting a breaker element inside the recognition sequence, it may lead to a promising strategy against the formation of amyloid and its disruption. Soto *et al.* introduced the concept of β-sheet breaker peptides (BSBPs), which emerged out to be a great discovery in the field of amyloid disruption.[122] They incorporated proline residue as a breaker element into the recognition motif of the Aβ peptide and illustrated its efficiency to disrupt the amyloid by generating a kink in the sequence. In line with this, various small peptide-based inhibitors containing different breaker elements are already described, including *N*-methylated amino acids,[106] α-aminoisobutyric acids (Aib),[110] α,β-dehydrophenylalanine,[112] and aspartic acid derivatives.[123] However, one of the major drawbacks of these breaker elements is proteolytic instability, as they contain α-amino acids and degrade quickly in presence of proteolytic enzymes. On the contrary, 2-aminobenzoic acid is a β-amino acid, which possesses higher structural rigidity. Its insertion in a peptide sequence prefers the development of turn or helical conformation.[118,119] Furthermore, 2-

aminobenzoic acid derivatives have been reported as transthyretin amyloid fibril and Aβ peptide aggregation inhibitors.[124,125] Hence, we assumed that the insertion of β, γ, and δ aminobenzoic acids in a small recognising peptide sequence would increase proteolytic stability and be a better peptide-based inhibitor against hIAPP amyloid aggregation.[121]

Here, we have inserted three conformationally restricted aromatic amino acids, such as β (2-aminobenzoic acid or 2-Abz), γ (3-aminobenzoic acid or 3-Abz), and δ (4-aminobenzoic acid or 4-Abz) individually in the $hIAPP_{22-27}$ sequence and synthesized α/β, α/γ, and α/δ hybrid peptidomimetics, which were collectively termed as β-sheet breaker hybrid peptides (BSBHps). Then, we wished to demonstrate their effects of inhibition on the aggregation of $hIAPP_{1-37}$. Further, we wished to explore the efficiency of the synthesized BSBHps to disrupt $hIAPP_{1-37}$ amyloids and investigate the extent of toxicity of the disrupted species.

2.2. Proposed hypothesis:

Various strategies have been adopted to fight against amyloid-related diseases, but no complete cure has been established yet. However, peptides are believed to be highly selective, safe, and efficient; thus, they have been categorized as a better approach to challenge amyloidogenesis.[126] Hence, our prime motive is to develop a suitable peptide-based strategy to inhibit the amyloid or disrupt the preformed amyloid of the aggregating peptide. We proceeded with this inspiration for some β-breaker peptides containing different aminobenzoic acid isomers and expected that these might act effectively against hIAPP amyloid (Scheme 2.1).

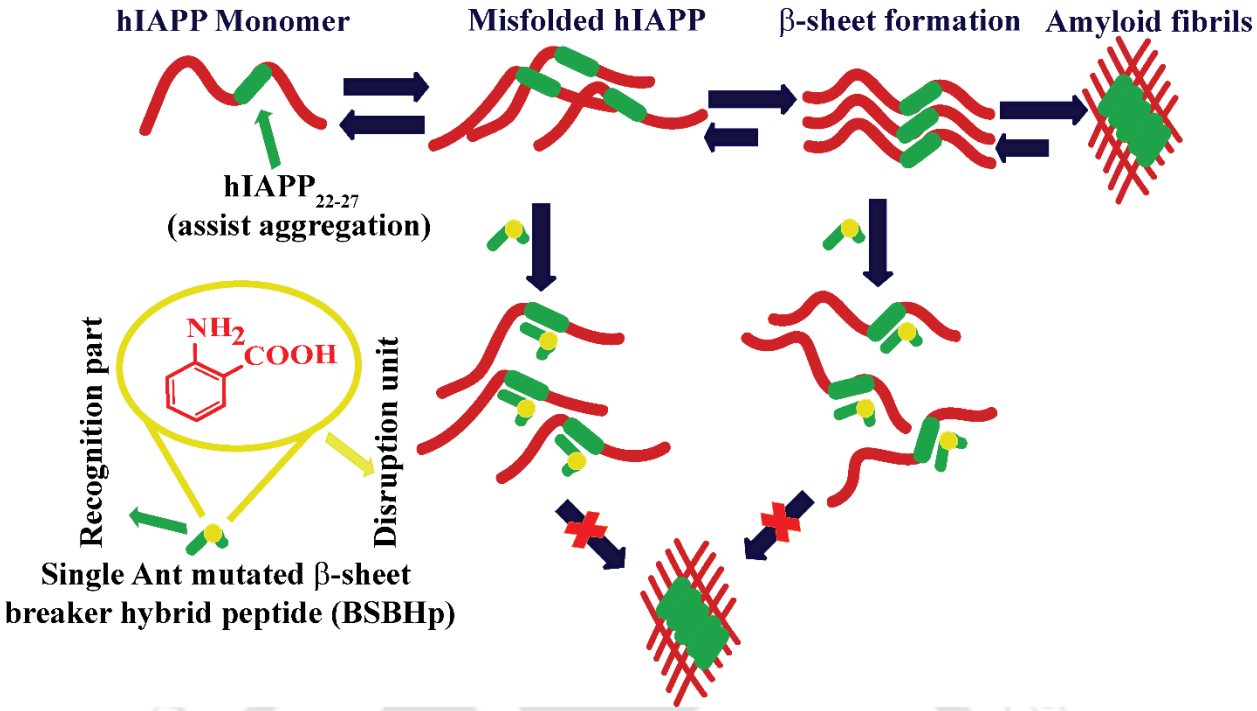

Scheme 2.1: Schematic representation of hIAPP aggregation and proposed hypothesis for the inhibition process of amyloid formation by single mutant BSBHp.

2.3. Design of peptides:

The wild type $hIAPP_{1-37}$ is one of the most highly amyloidogenic polypeptides known to date and is more prone to form amyloid than the wild type $A\beta_{1-42}$ peptide.[99] Therefore, the generation of inhibitors against hIAPP amyloid aggregation is a challenging task. To attain this goal, initially, we synthesized the central hydrophobic segment NFGAIL ($hIAPP_{22-27}$, peptide **2A**), which forms amyloid aggregates similar to hIAPP.[95] Further, we synthesized three BSBHps by inserting various isomers of aminobenzoic acid (2, 3, and 4-aminobenzoic acid) separately as breaker components in the peptide **2A** and finally analysed their efficiencies in inhibiting hIAPP amyloid formation. Along with these, we synthesized one control breaker peptide *via* incorporating α-aminoisobutyric acid (Aib) in the peptide **2A** to compare the results.[127,128] Various breaker components were incorporated in all the BSBHps at the I26 position to maintain the sequence homology for recognition with N-F-G-A

($hIAPP_{22-25}$) tetrapeptide residue. We considered I26 position for the breaker element insertion as several peptide-based inhibitors have been reported using $hIAPP_{20-29}$ fragment as the basic unit.[95,107]

Table 2.1: Sequences of the synthesized peptides for the present study:

peptide no.	peptide sequence	molecular mass $[M+H]^+$ (expected/ observed)	function
2A	NFGAIL	633.3724/ 633.3748	Aggregating
2B	$NFGAX_1L$	605.3411/ 605.3627	control
2C	$NFGAX_2L$	639.3255/ 639.3310	inhibitor
2D	$NFGAX_3L$	639.3255/ 639.3315	inhibitor
2E	$NFGAX_4L$	639.3555/ 639.3335	inhibitor

N.B. Standard amino acids are represented by one letter code, X_1 = α-aminoisobutyric acid (Aib), X_2 = 2-aminobenzoic acid (2-Abz), X_3 = 3-aminobenzoic acid (3-Abz), and X_4 = 4-aminobenzoic acid (4-Abz).

2.4. Synthesis and characterization of the designed peptides:

We have synthesized all the designed peptides by solid-phase peptide synthesis (SPPS) strategy on a Tarson blood tube rotator using standard Fmoc/t-Bu protecting group on Rink Amide MBHA resin following standard protocols (described in chapter 6 section 6.4).[129,130] Solid white powder of pure peptides were obtained after synthesis followed by purification and lyophilization (The details of the yield have been described in the experimental section). Finally, the purity of the peptides was further checked with Waters analytical HPLC instruments and characterized by ESI mass spectrometry. A representative example of the synthetic protocol of **2C** has been depicted in scheme 2.2. All other peptides were synthesized in a similar process. The characterization data for the synthesized peptides are shown below (Figure 2.1-2.10).

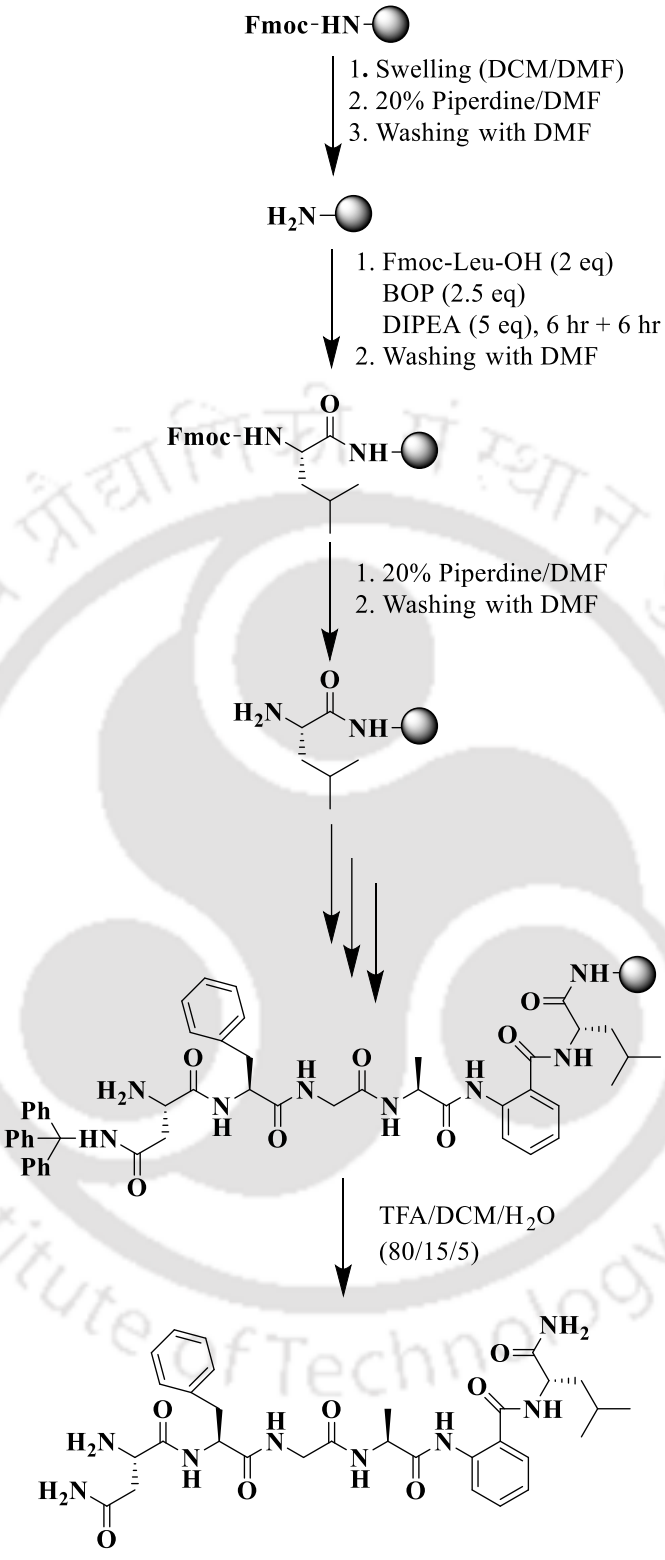

Scheme 2.2 : The synthetic scheme of peptide **2C**.

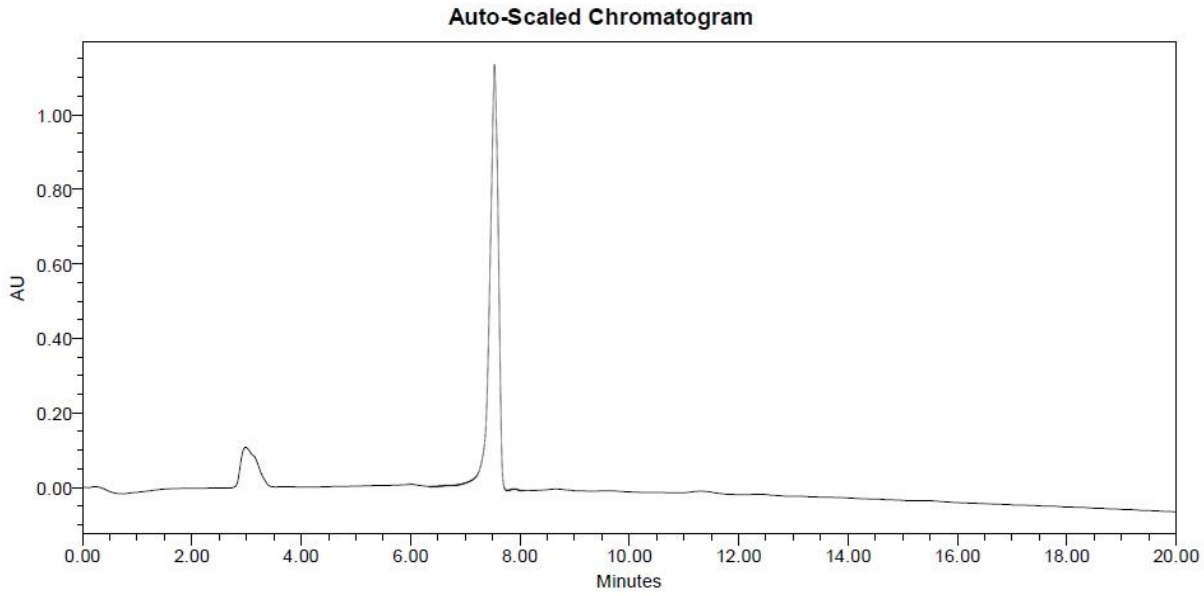

Figure 2.1: HPLC profile of the purified peptide **2A.**

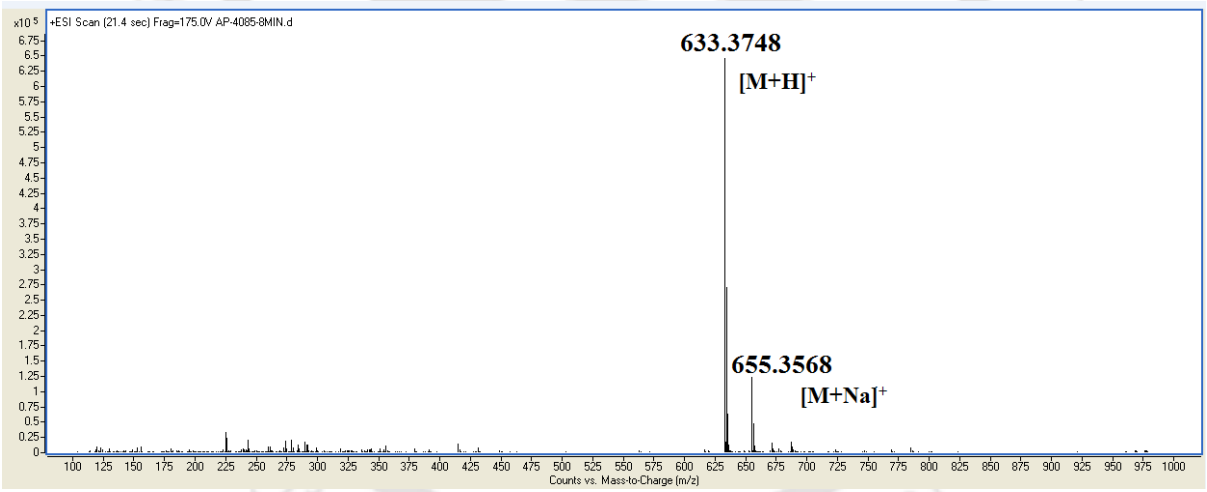

Figure 2.2: ESI mass spectrum of peptide **2A**. Calculated mass for $C_{30}H_{49}N_8O_7$ is 633.3724 $[M+H]^+$, observed 633.3748 $[M+H]^+$and calculated mass for $C_{30}H_{48}N_8O_7Na$ is 655.3544 $[M+Na]^+$, observed 655.3568 $[M+Na]^+$.

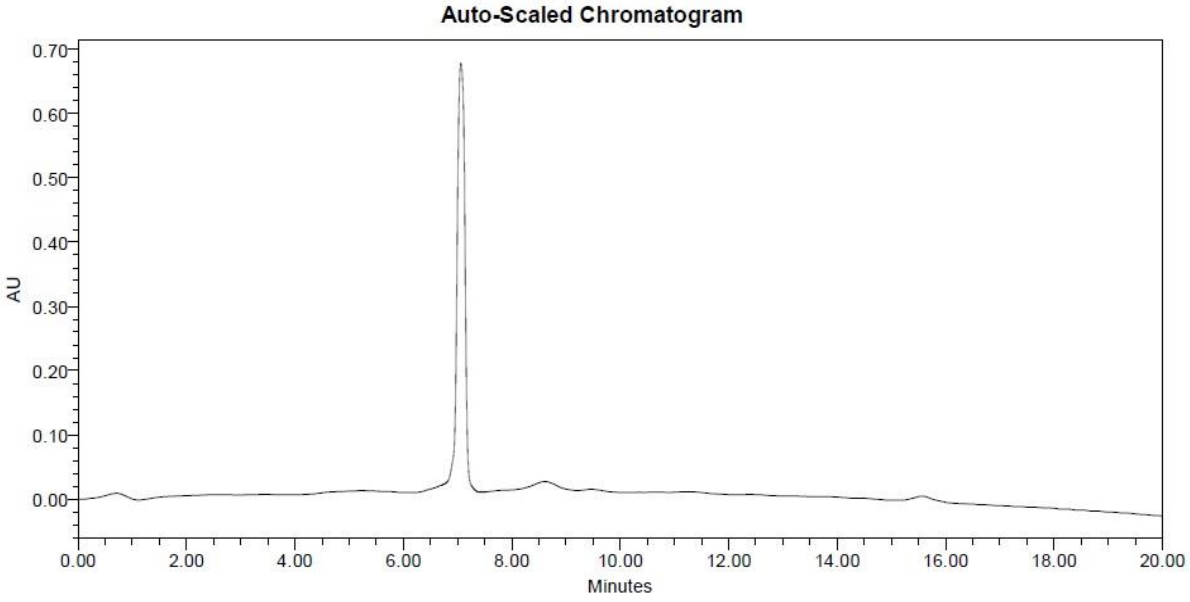

Figure 2.3: HPLC profile of the purified peptide **2B.**

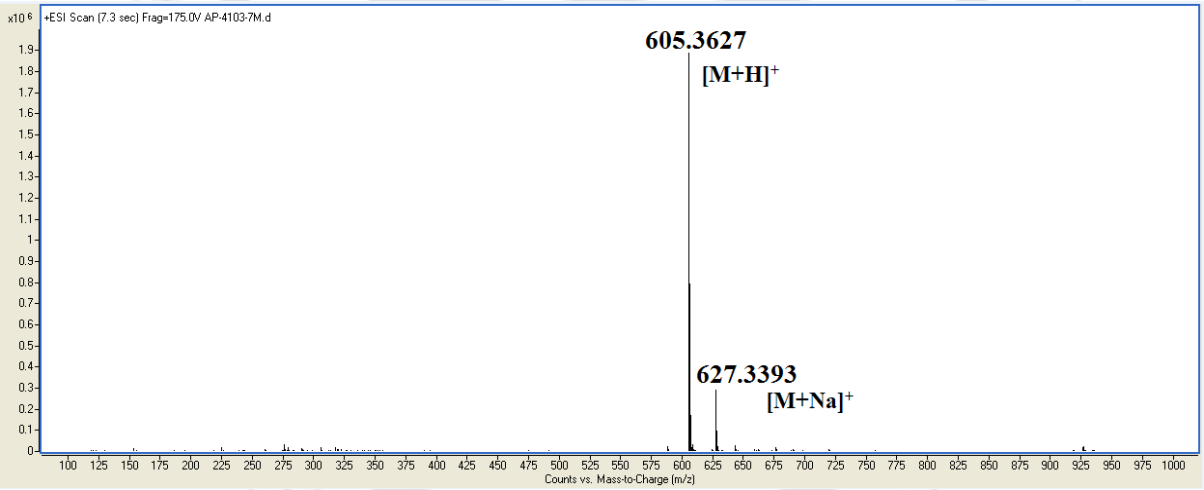

Figure 2.4: ESI mass spectrum of peptide **2B**. Calculated mass for $C_{28}H_{45}N_8O_7$ is 605.3411 $[M+H]^+$, observed 605.3627 $[M+H]^+$ and calculated mass for $C_{28}H_{44}N_8O_7Na$ is 627.3231 $[M+Na]^+$, observed 627.3393 $[M+Na]^+$.

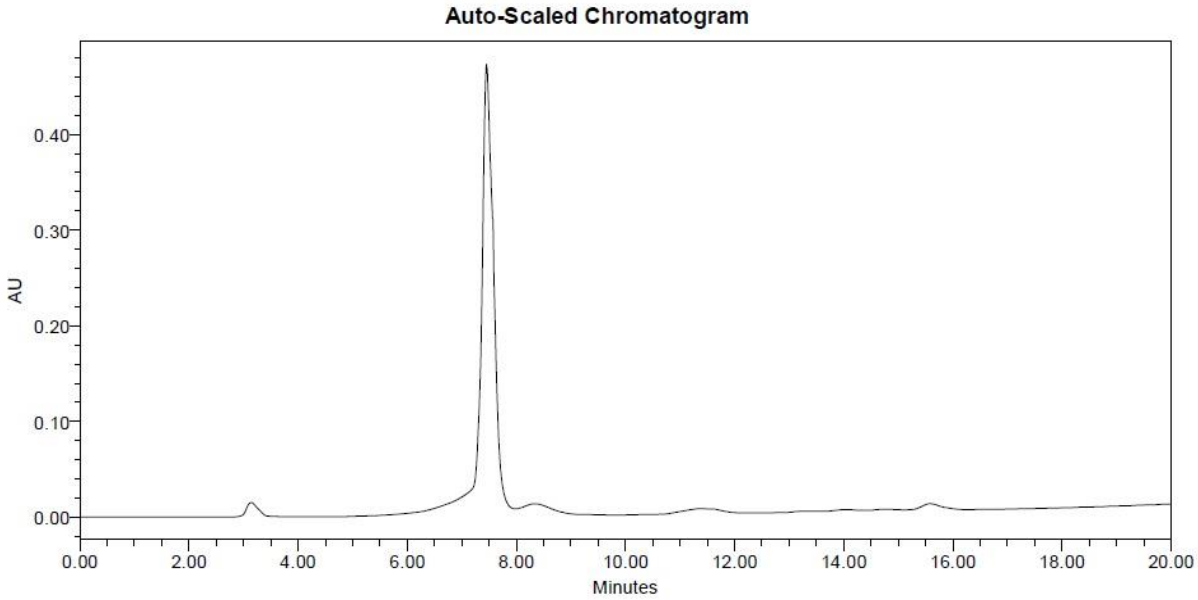

Figure 2.5: HPLC profile of the purified peptide **2C.**

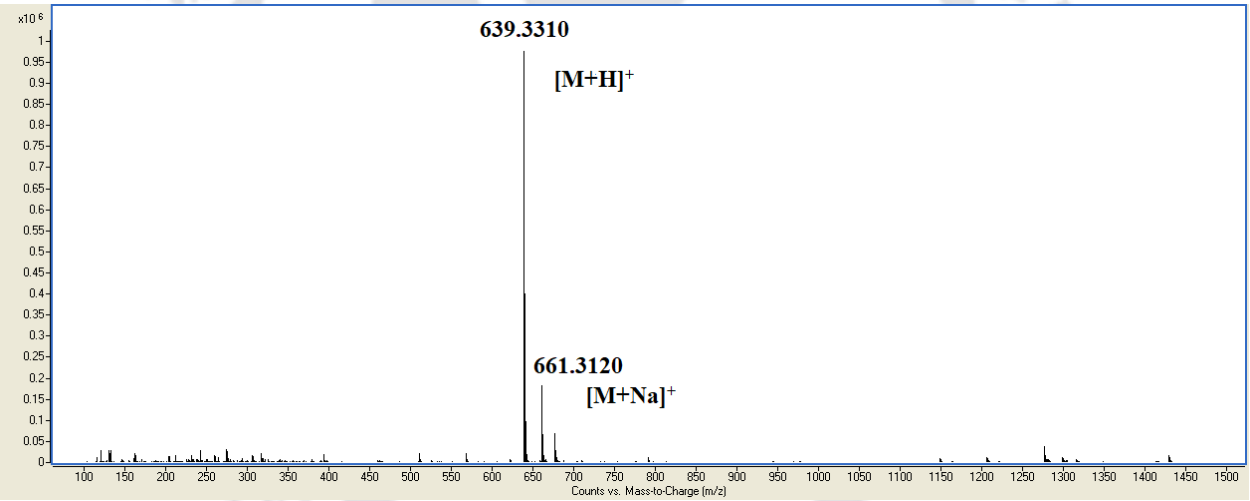

Figure 2.6: ESI mass spectrum of peptide **2C**. Calculated mass for $C_{31}H_{43}N_8O_7$ is 639.3255 $[M+H]^+$, observed 639.3310 $[M+H]^+$ and calculated mass for $C_{31}H_{42}N_8O_7Na$ is 661.3074 $[M+Na]^+$, observed 661.3120 $[M+Na]^+$.

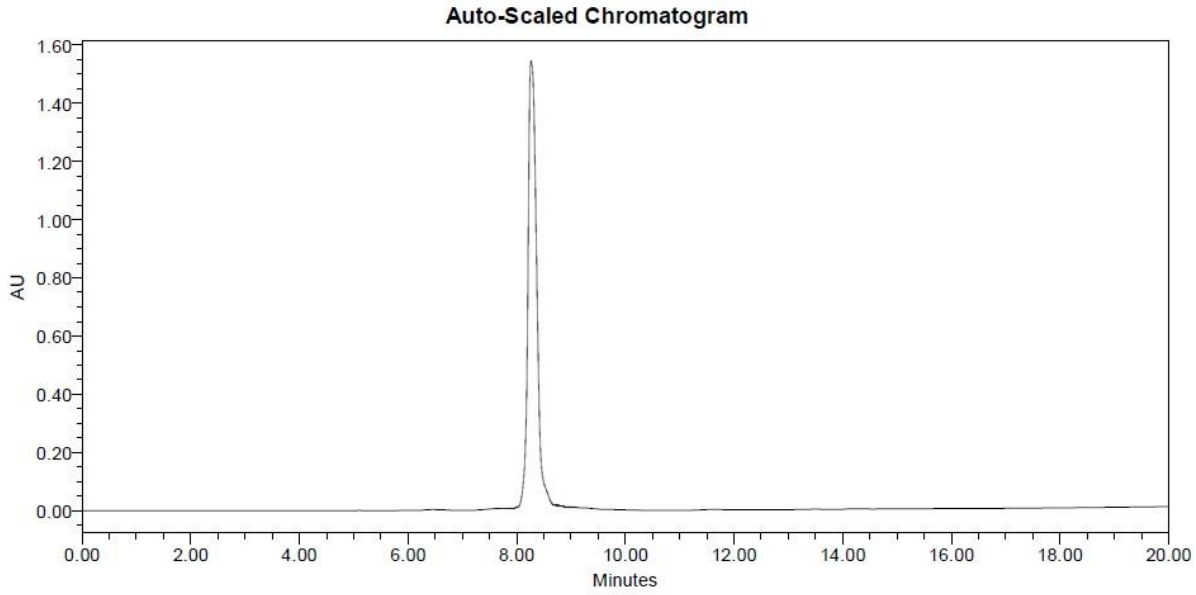

Figure 2.7: HPLC profile of the purified peptide **2D.**

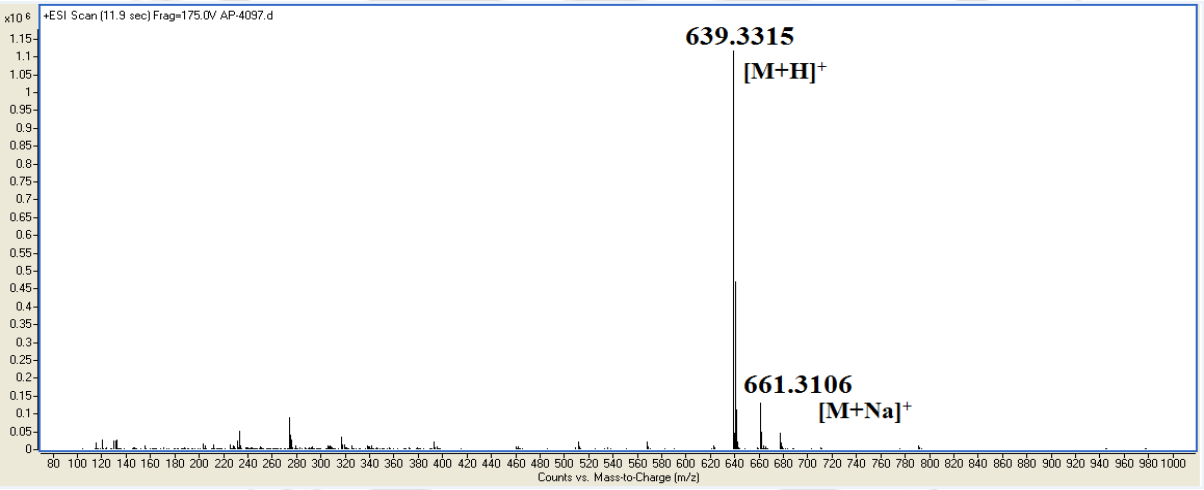

Figure 2.8: ESI mass spectrum of peptide **2D**. Calculated mass for $C_{31}H_{43}N_8O_7$ is 639.3255 $[M+H]^+$, observed 639.3315 $[M+H]^+$ and calculated mass for $C_{31}H_{42}N_8O_7Na$ is 661.3074 $[M+Na]^+$, observed 661.3106 $[M+Na]^+$.

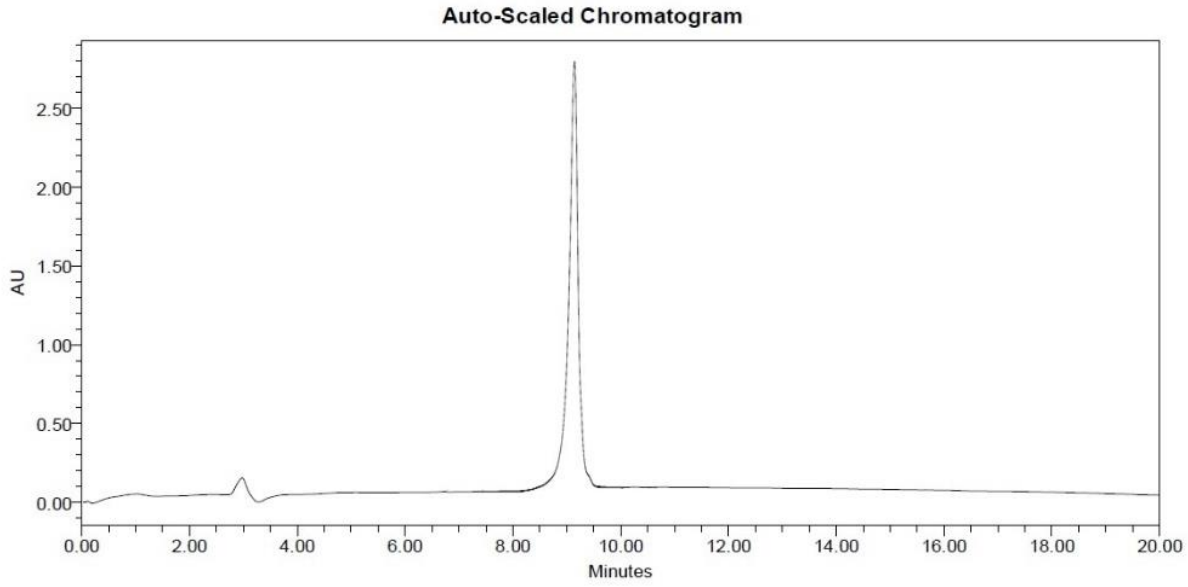

Figure 2.9: HPLC profile of the purified peptide **2E.**

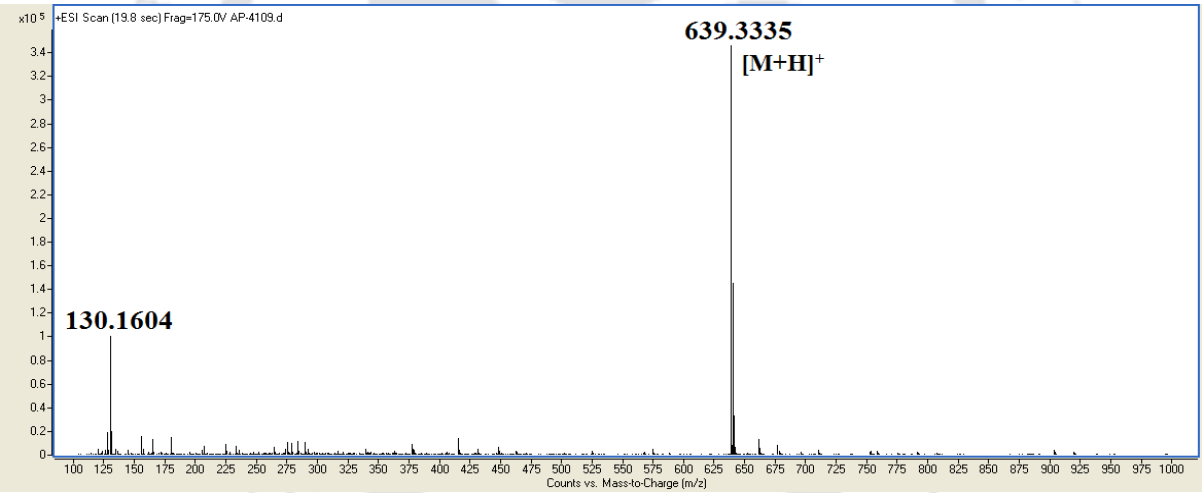

Figure 2.10: ESI mass spectrum of peptide **2E**. Calculated mass for $C_{31}H_{43}N_8O_7$ is 639.3255 $[M+H]^+$, observed 639.3335 $[M+H]^+$.

2.5. Amyloidogenic nature of the designed β-sheet breaker hybrid peptidomimetics (BSBHps):

Before applying the BSBHps in inhibiting the aggregation of the aggregating peptide, it is crucial to find the amyloidogenic nature of the peptides. Hence, we first investigated the amyloidogenicity of the synthesized peptides using various biophysical tools.

2.5.1. Conformational characterization of BSBHps by CD and FTIR studies:

The conformational analyses of the BSBHps were monitored by circular dichroism (CD) and Fourier transform infrared (FTIR) spectroscopic assays. To perform the biophysical studies, the peptides were dissolved in 50 mM PBS (phosphate buffer solution, pH 7.4) containing 3% DMSO to prepare a stock solution of concentration 40 μM. The stock solutions of the peptides were kept in incubation on a water bath at 37 °C for five days. After five days of incubation, the conformations of the BSBHps were investigated using CD and FTIR (Figure 2.11).

From the CD spectrum of **2A**, we observed a negative band at ~ 220-225 nm and a positive band at ~ 195-200 nm, suggesting the peptide attains a β-sheet conformation.[23] On the other hand, such specific bands were missing for the peptides **2B**, **2C**, and **2D**, indicating non-β-sheet and a mixture of conformations. However, for the peptide **2E**, some β-sheet rich conformation was observed from the CD experiment.

Similarly, from the FTIR spectra, we noticed an amide I band at 1631 cm^{-1} for the peptide **2A**, indicating β-sheet rich conformation.[23] On the contrary, the amide I band shifted up to 1653 cm^{-1}, 1654 cm^{-1} and 1654 cm^{-1} for the peptides **2B**, **2C**, and **2D**, respectively, indicating non-β-sheet conformation. However, peptide **2E** showed some β-sheet conformation, as evident from FTIR as the band appeared at 1638 cm^{-1}.

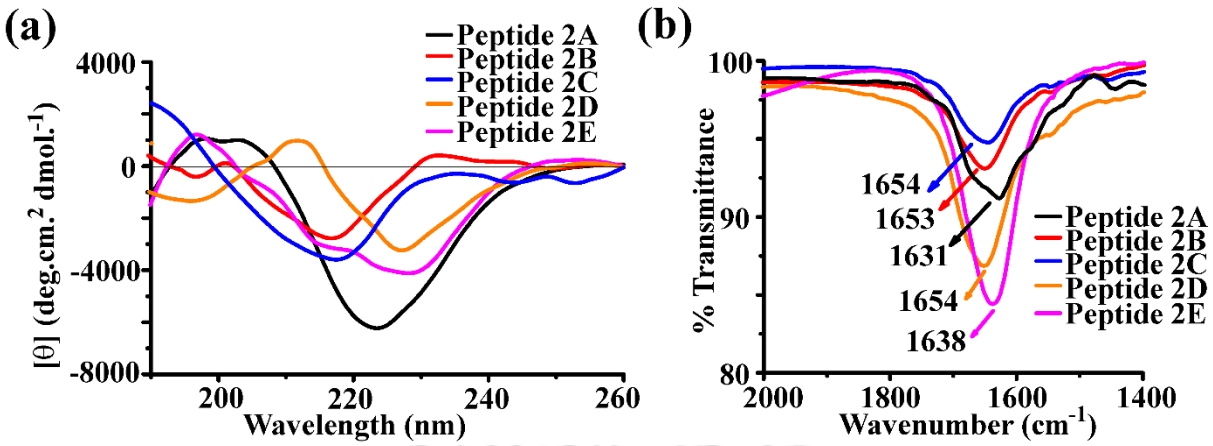

Figure 2.11: (a) CD and (b) FTIR spectra of peptide **2A** (black), **2B** (red) **2C** (blue), **2D** (orange) and **2E** (magenta). Spectra were recorded after 5 days of incubation of the peptides in PBS (50 mM) at pH 7.4 and 37 °C.

2.5.2. Amyloidogenic characterization of the synthesized peptides by TEM and Congo red stained birefringence studies:

From the conformational analysis of BSBHps, it was evident that peptides **2A** and **2E** exist in β-sheet rich conformation at physiological condition. However, the other peptides **2B**, **2C**, and **2D** existed in mixed conformations at the same conditions. To elucidate the amyloidogenicity of the peptides, we further investigated TEM and Congo red stained birefringence experiments (Figure 2.12).

10 μL aliquot of the peptide solution from the stock solutions (as described in section 2.5.1) was spotted on the dark side of the carbon-coated copper grid and air-dried for 2 minutes. After that, the samples were negatively stained by adding 2% uranyl acetate solution (10 μL) and were allowed to float for 2 min, and the additional solution was withdrawn with blotting paper. The sample was dried at room temperature and examined by TEM at 200 kV on a JEOL instrument. Similarly, for the Congo red stained birefringence study, 10 μL aliquot from the five days incubated peptide solution was added over a microscopic glass slide and kept for 6h for complete air dry. After that 10 μL of the filtered Congo red solution was

added over the samples and air-dried at room temperature for 6h. Finally, the prepared samples were examined under a Leica ICC50 HD polarizable microscope.

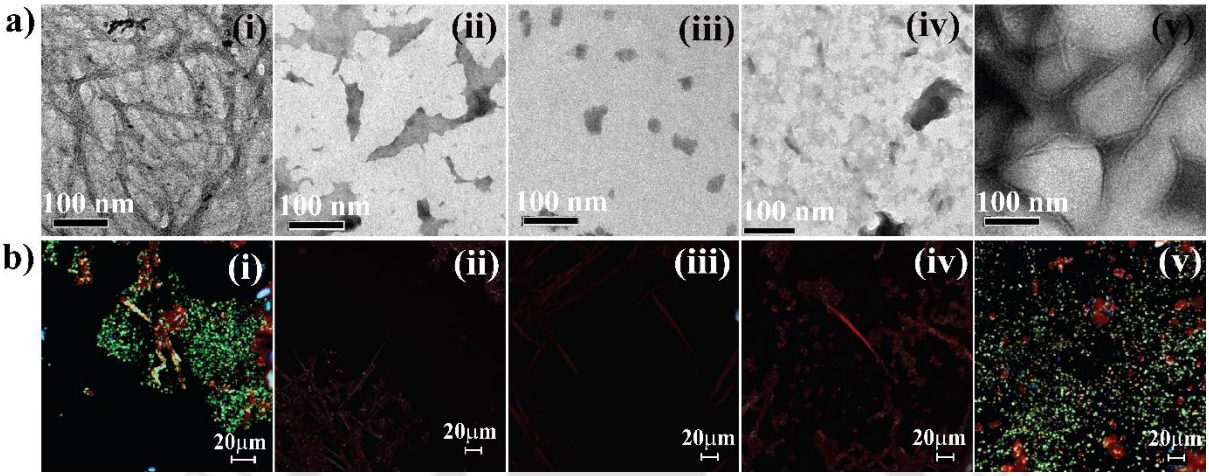

Figure 2.12: (a) TEM and (b) Congo red stained birefringence images of peptide **2A** (i), **2B** (ii), **2C** (iii), **2D** (iv) and **2E** (v). Images were captured after five days of incubation of the peptides in PBS (50 mM) at pH 7.4 and 37 °C.

The presence of fibrillar morphology under an electron microscope is a characteristic feature of amyloid formed by a peptide.[23] Peptide **2A** showed fibrillar morphology (Figure 2.12 (a) (i)) when viewed under TEM, indicating amyloid formation. However, no such fibrillar assemblies were observed for breaker peptidomimetics **2B**, **2C**, and **2D** (Figure 2.12 (a) (ii, iii, iv respectively)). On the other hand, we noticed some fibrillar morphology for peptidomimetic **2E**, indicating its amyloidogenic nature**.** (Figure 2.12 (a) (v)). Again, the appearance of green-gold birefringence under cross-polarized light upon staining with Congo red is a specific property of amyloid, and we noticed the specific birefringence for peptide **2A** (Figure 2.12 (b) (i)) and slight birefringence for the peptide **2E** (Figure 2.12 (b) (v)) supporting their amyloidogenic nature. However, we did not notice any such birefringence for breaker peptidomimetics **2B**, **2C**, and **2D**, indicating their non-amyloidogenic nature (Figure 2.12 (b) (ii, iii, iv)).[23]

The experimental investigations showed that the peptide **2A** (NFGAIL) developed amyloid fibrils similar to hIAPP. We observed the non-amyloidogenic nature of 2-Abz (X_2) and 3-Abz (X_3) containing peptidomimetics, **2C** and **2D**. Further, we also observed the non-amyloidogenic nature of the control peptide **2B** containing Aib (X_1) unit. However, peptidomimetics **2E** containing 4-Abz (X_4) unit exhibited some amyloidogenic properties.

2.6. Inhibition of amyloid formation of hIAPP by BSBHps:

To examine the inhibitory efficacy of the single breaker element (I26X) containing BSBHps (**2C**, **2D**, and **2E**) and compare the results with control peptide **2B**, we carried out several biophysical studies with aggregating hIAPP. hIAPP was co-incubated in the absence and presence of BSBHps and the control peptide at physiological conditions up to 7 days. The kinetics of amyloid formation was monitored using different biophysical experiments. To examine the dose-dependence effect, 2-, 5-, and 10-fold molar ratios of the BSBHps were incubated with 40 μM of hIAPP in PBS (50 mM).

2.6.1. Monitoring conformational transition by CD and FTIR studies:

At first, we checked the changes in conformation of the aggregating peptide, hIAPP in the absence and presence of the BSBHps. We assembled four distinct sets of solutions for performing the conformational study, where the concentration of hIAPP remained 40 μM in each sets. In the first set, only hIAPP was present in PBS of pH 7.4, while in the other three sets; hIAPP was mixed with the BSBHps in a molar ratio of 1:2, 1:5, and 1:10, maintaining the same concentration of hIAPP. Each set contains two replicate solutions. All the different sets were prepared in PBS of pH 7.4 and incubated at 37 °C on a water bath for seven days and checked the conformation of hIAPP (40 μM) in the absence and presence of the 80 μM, 200 μM and 400 μM of BSBHps respectively using CD and FTIR studies (Figure 2.13).

For CD analysis, a total volume of 200 µL of the peptide solution without further dilution was taken in a 1 mm path length quartz cuvette. An average of three scans was accumulated for each sample on a JASCO J-1500 spectrometer. For FTIR analysis, 20 µL of the stock peptide solution was drawn off, combined with KBr, prepared the pellets, and analysed with background subtraction to obtain the final spectra.

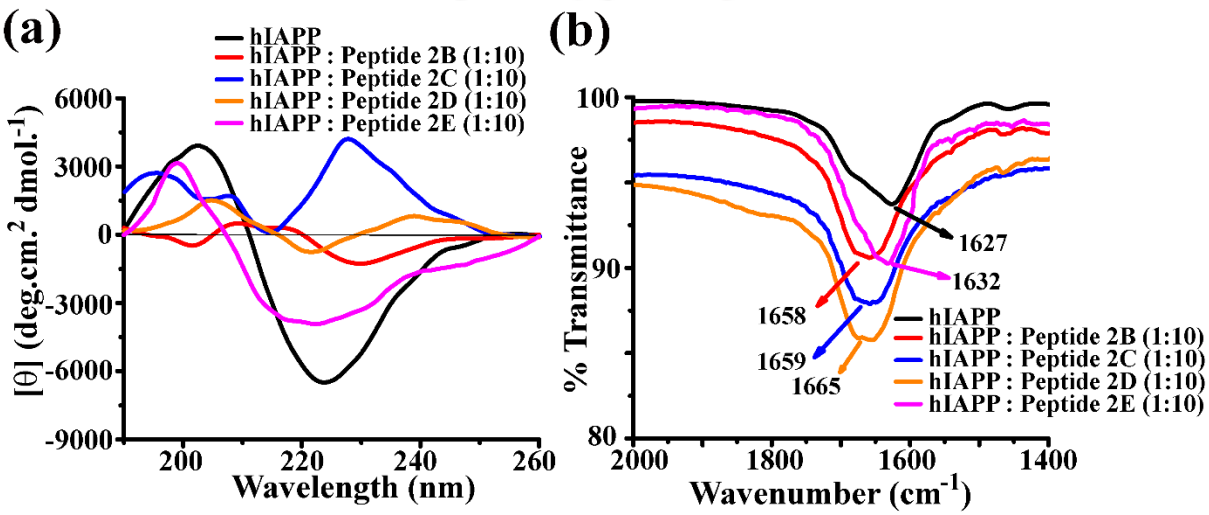

Figure 2.13: (a) CD and (b) FTIR spectra of hIAPP alone (black) and in co-incubation with 10 fold molar ratios of peptidomimetics **2B** (red), **2C** (blue), **2D** (orange) and **2E** (magenta). Spectra were recorded after 7 days of incubation of the peptides in PBS (50 mM) at pH 7.4 and 37 °C.

The aggregating peptide hIAPP, when incubated alone, exhibited a negative band at ~220-225 nm and a positive band at ~200 nm in CD profile (black, Figure 2.13 (a)) and a strong band at 1627 cm^{-1} in FTIR spectra (black, Figure 2.13 (b)), which indicated the precise β-sheet conformation of hIAPP. On the other hand, hIAPP, when co-existed with peptidomimetics **2C** and **2D** (10-fold molar excess)**,** no such specific β-sheet conformations were noticeable from CD spectra (Figure 2.13 (a)). There was no characteristic band for β-sheet in CD profile, whereas, in FTIR, the amide I band shifted up to 1659 cm^{-1} and 1665 cm^{-1}, respectively, indicating significant inhibition of hIAPP aggregation in the presence of **2C** and **2D** (10-fold molar excess, Figure 2.13 (b)). The control peptidomimetics **2B** also showed

significant inhibitory efficacy in 10 fold molar excess, as evident from CD and FTIR. However, in the presence of peptide **2E** in that same ratio, minor β-sheet characteristic conformation persisted in the CD and FTIR analyses, signifying non-inhibition of aggregation (Figure 2.13).

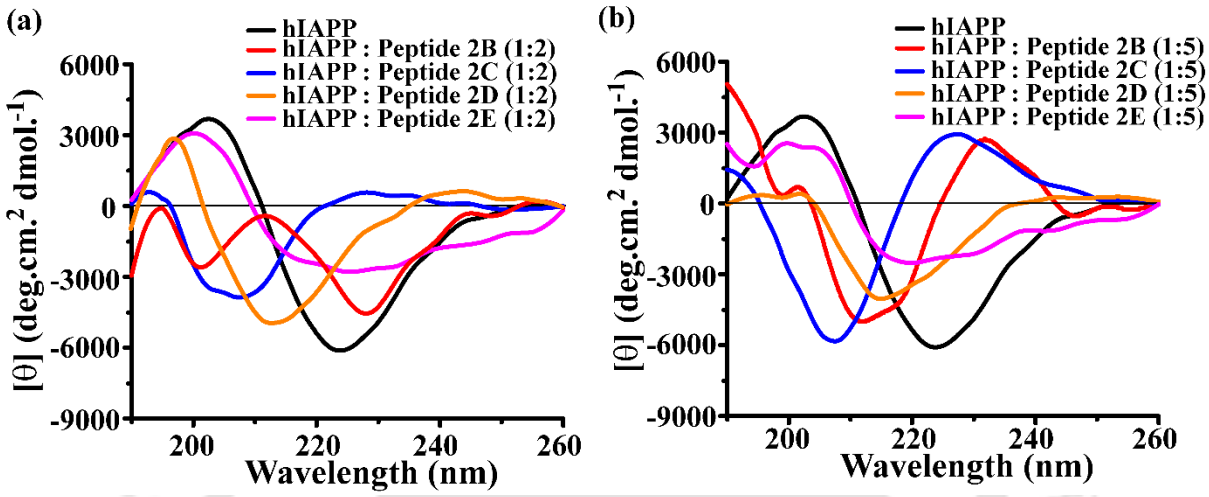

Figure 2.14: CD spectra of hIAPP alone (black) and in co-incubation with (a) 2-fold and (b) 5-fold molar ratios of peptidomimetics **2B** (red), **2C** (blue), **2D** (orange) and **2E** (magenta). Spectra were captured after seven days of incubation of the peptides in PBS (50 mM) at pH 7.4 and 37 °C.

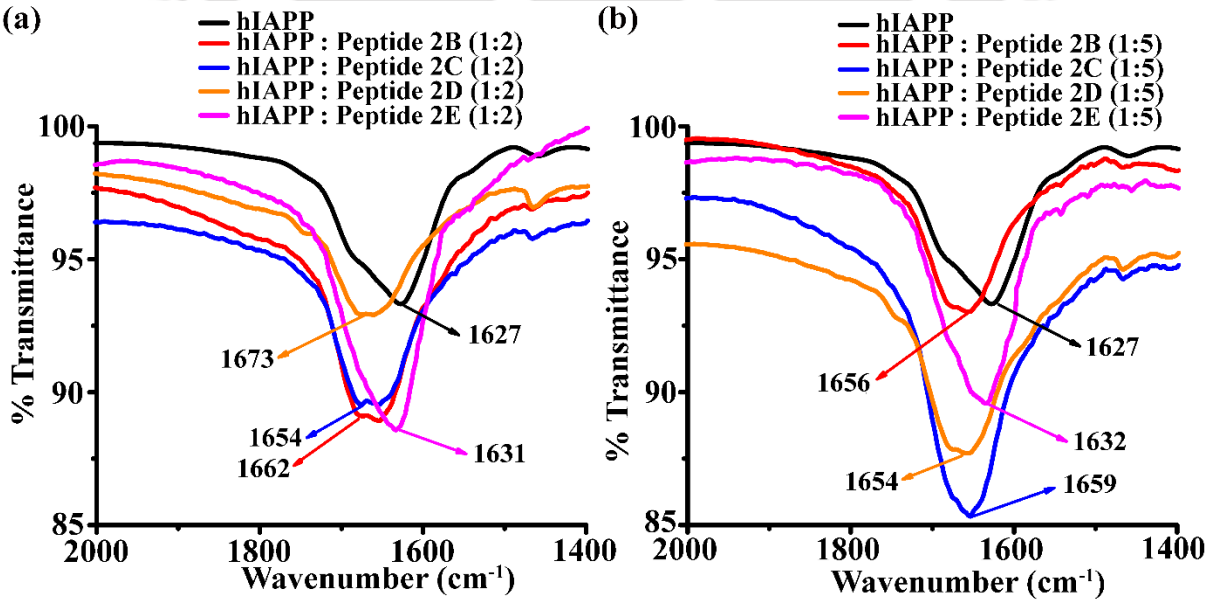

Figure 2.15: FTIR spectra of hIAPP alone (black) and in co-incubation with (a) 2-fold and (b) 5-fold molar ratios of peptidomimetics **2B** (red), **2C** (blue), **2D** (orange) and **2E** (magenta). Spectra were captured after seven days of incubation of the peptides in PBS (50 mM) at pH 7.4 and 37 °C.

Again, in the presence of 2-fold and 5-fold molar excesses of the breaker peptides, hIAPP exhibited similar results with lesser efficiency than the 10-fold molar ratio in both CD and FTIR analyses. (Figure 2.14 and Figure 2.15)

2.6.2. Monitoring the kinetics of amyloid formation and its subsequent inhibition by BSBHps *via* ThT fluorescence assay:

The elevation in fluorescence intensity of a protein or peptide upon binding with Thioflavin T (ThT) dye is a specific feature of the presence of amyloid in the solution, which provides quantitative direction on the growth of amyloid in the peptide sample.[23] The kinetics of amyloid fibril formation of hIAPP and its inhibition efficacy by the BSBHps were observed by a time-dependent ThT fluorescence assay. For the ThT fluorescence assay, stock solutions were prepared in a similar process as in CD and FTIR experiments (described in 2.6.1 section) and incubated at 37 °C in PBS of pH 7.4 up to 7 days. At an interval of 12h, 40 μL of the stock solution was mixed with 160 μL of PBS (pH 7.4, 50 mM) and added 200 μL of ThT solution (50 μM) to make up the final volume of 400 μL. However, 200 μL of PBS solution was mixed with 200 μL of Thioflavin T solution for the reference sample. Fluorescence emission was measured at 485 nm, fixing the excitation at 440 nm, with each scan repeating three times using a slit of 5 nm on a Fluoromax-4 Horiba Fluorospectrometer. We have prepared two sets of samples for each measurement, and three readings were scanned separately for each set. Thus, an average of six readings was taken and plotted as F/F_0 along the y-axis (where, F= average fluorescence value of the samples at time t, F_0= fluorescence value of the reference in the absence of sample at time t) against time (h) along the x-axis with observed standard deviation set as y-error. It is important to mention that the mutant

peptides (BSBHps) are itself non-fluorescent and non-aggregating. Hence, they do not interfere with the ThT fluorescence through quenching mechanism.

From the same study, the relative % of amyloid present in the sample was also calculated at the highest incubation time, i.e., at 168h, using the following formula.

$$\%\ \text{of amyloid} = \frac{(\text{Observed fluorescence in the presence of the peptide} - 1)}{(\text{Observed fluorescence in the absence of the peptide} - 1)} \times 100\ \%$$

where, 1 was considered as a normalisation factor.

The fluorescence intensity was observed to increase significantly when hIAPP existed alone in the solution (black, Figure 2.16 (a)). However, hIAPP in co-incubation with 10-fold molar ratio of peptidomimetic **2C** (blue, Figure 2.16 (a)) and **2D** (orange, Figure 2.16 (a)) the fluorescence intensity restrained to ~55% (blue, Figure 2.16 (b)) and ~50% (orange, Figure 2.16 (b)) respectively, suggesting significant inhibition of amyloid formation. Likewise, control peptidomimetic **2B** (red, Figure 2.16 (a)) also inhibited the amyloid formation appreciably up to ~40% (red, Figure 2.16 (b)). On the contrary, the presence of peptidomimetic **2E** (magenta, Figure 2.16 (a)) enhanced the fluorescence intensity up to ~5% (magenta, Figure 2.16 (b)) instead of showing inhibition of amyloid formation.

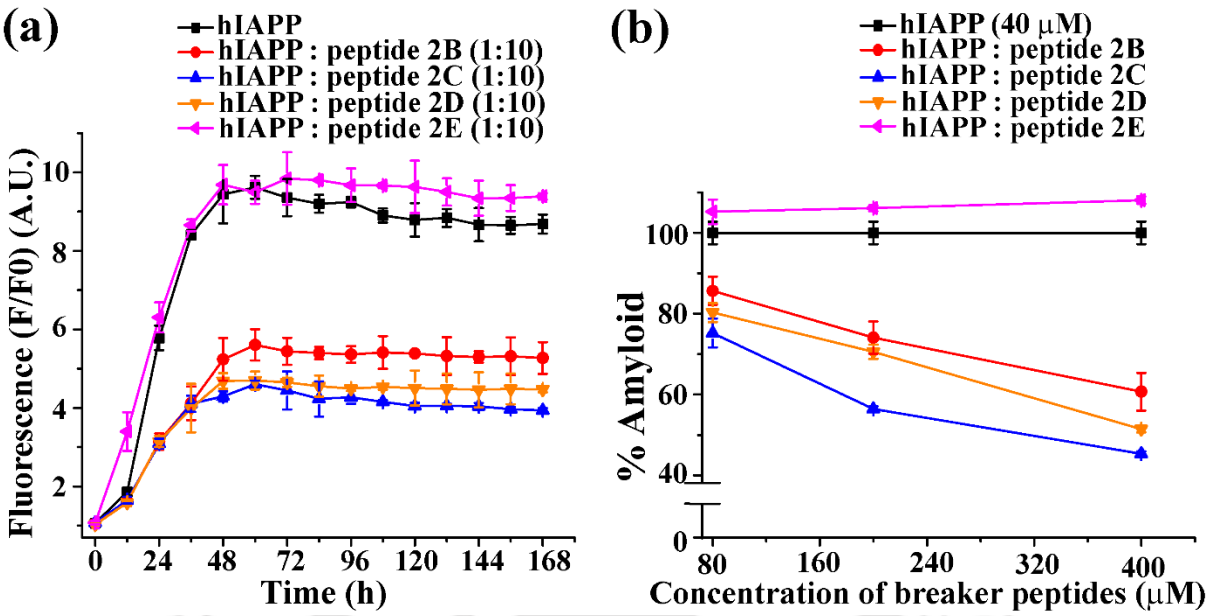

Figure 2.16: (a) Time dependent ThT fluorescence spectra of hIAPP (40 μM) alone (black) and in co-incubation with 10-fold molar ratios of **2B** (red), **2C** (blue), **2D** (orange) and **2E** (magenta). (b) Dose dependent ThT fluorescence spectra at 168h of hIAPP (40 μM) alone (black) and in co-incubation with different molar ratios of **2B** (red), **2C** (blue), **2D** (orange) and **2E** (magenta).

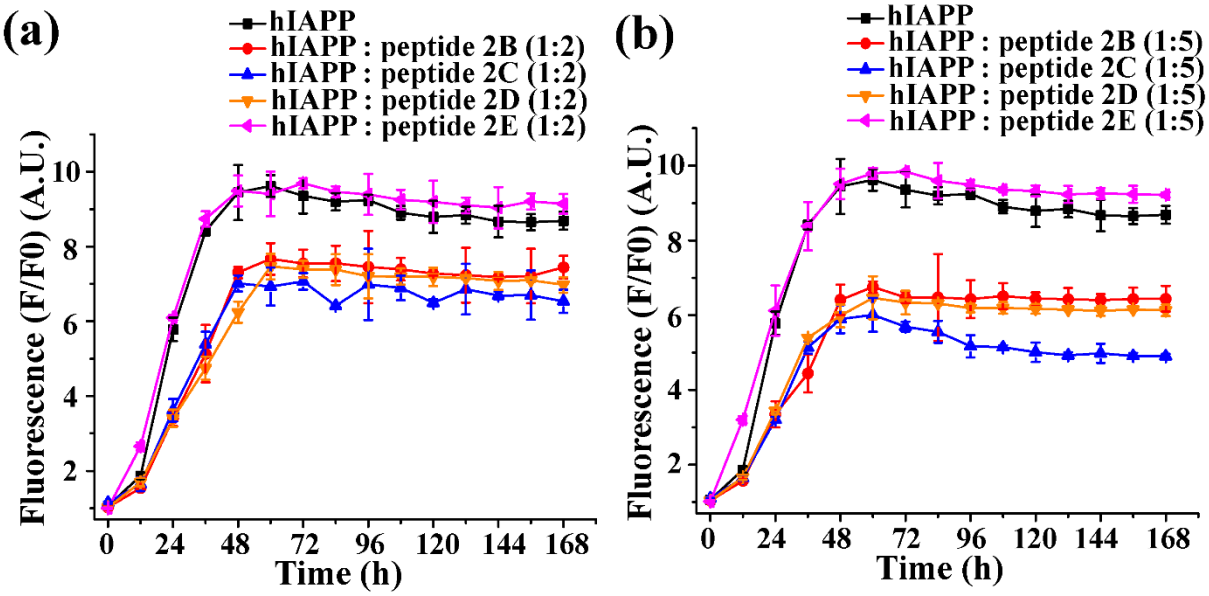

Figure 2.17: Time dependent ThT fluorescence spectra of hIAPP (40 μM) alone (black) and in co-incubation with (a) 2-fold (b) 5-fold molar ratios of peptidomimetics, **2B** (red), **2C** (blue), **2D** (orange) and **2E** (magenta).

From the dose-dependent study, we observed that 2-fold molar ratio (Figure 2.17 (a)) of the peptidomimetics, **2B**, **2C** and **2D**, when co-incubated with hIAPP, were inefficient for

inhibiting the amyloid formation of hIAPP. However, increasing the molar ratio to 5-fold (Figure 2.17 (b)), the efficiency of inhibition was found to increase and observed to be more pronounced with 10-fold molar ratio (Figure 2.16) of the peptidomimetics.

2.6.3. Monitoring the amyloid formation by TEM and Congo red birefringence studies:

Fibrillar assembly under TEM and appearance of characteristic green-gold birefringence under cross polarised light when a peptide is stained with Congo red dye are direct evidences for amyloid formation.[23] After seven days of incubation at physiological conditions, from the stock solution (as discussed in section 2.6.1) 10 μL aliquot of each solution was taken out and analysed the sample under TEM (prepared the samples as described in section 2.5.2). The hIAPP sample when present alone, exhibited clear fibrillar morphology when viewed under TEM (Figure 2.18 (a) (i)), specifying the presence of amyloid. However, hIAPP in co-incubation with 10-fold molar ratio of peptidomimetics **2B** (Figure 2.18 (a) (ii), **2C** (Figure 2.18 (a) (iii)) and **2D** (Figure 2.18 (a) (iv)), such fibrillar assembly was not observed, which demonstrated significant inhibition of hIAPP amyloid. On the other hand, when the peptidomimetic **2E** (Figure 2.18 (a) (v)) was co-incubated with hIAPP, fibrillar assembly was noted, indicating the inefficiency of **2E** in inhibiting fibrillization.

As another complimentary evidence of amyloid formation, Congo red stained birefringence study was also performed (prepared the samples as described in section 2.5.2.) The hIAPP, when present alone, exhibited green-gold birefringence (Figure 2.18 (b) (i)), denoting amyloid formation. In contrast, hIAPP in co-incubation with a 10-fold molar ratio of peptidomimetics **2B** (Figure 2.18 (b) (ii), **2C** (Figure 2.18 (b) (iii) and **2D** (Figure 2.18 (b) (iv), no such specific birefringence was noticed, suggesting remarkable inhibition of hIAPP amyloid formation. Whereas, in the presence of peptidomimetic **2E** (Figure 2.18 (b) (v), we

noticed some characteristic green-gold birefringence, which again indicated the negative efficiency of **2E** in inhibiting the growth of hIAPP amyloid fibrils.

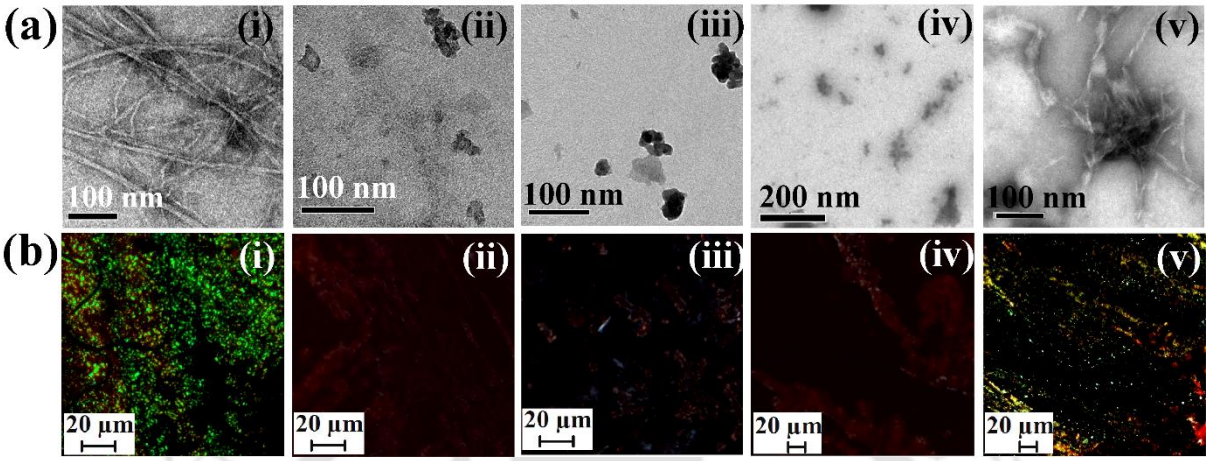

Figure 2.18: (a) TEM and (b) Congo red birefringence images of hIAPP alone (i) and in co-incubation with 10-fold molar ratios of peptidomimetics, **2B** (ii), **2C** (iii), **2D** (iv) and **2E** (v). Images were captured after 7 days of incubation of the peptides in PBS (50 mM) at pH 7.4 and 37 °C.

2.7. Disruption of preformed amyloid fibril of hIAPP by BSBHps:

From the earlier inhibition study, we observed effective inhibition of hIAPP amyloid formation while co-incubating hIAPP with BSBHps (**2C** and **2D**). The hIAPP-induced cytotoxicity may arise due to the presence of the oligomers and amyloid of the aggregating peptide. Hence, to be an effective therapeutic agent, the peptidomimetics must disrupt the preformed amyloid into a non-oligomeric state. Therefore, we analysed the potential of the BSBHps in disrupting the preformed hIAPP amyloid *in vitro*. From the initial ThT fluorescence assay (black, Figure 2.16 (a)), we witnessed that hIAPP fibrillization attained its maximum at ~45-50h. Hence, to study the effects of the BSBHps on preformed hIAPP amyloid, we sketched a study where the BSBHps were added to the preformed mature fibrils of hIAPP. The hIAPP was incubated exclusively at the physiological condition in PBS for 48h to allow to form matured amyloid fibrils. Different molar ratios (2-, 5- and 10-fold) of

BSBHps were added to it. Fibrillogenesis was monitored by various biophysical techniques. The samples for the different studies were prepared similarly as described above in section 2.6. Since BSBHp **2E** was inefficient in inhibiting the fibrillization of hIAPP, we excluded it from the disruption study.

2.7.1. Monitoring conformational transition by CD and FTIR studies:

Incubating for 7 (2+5) days, it was observed from the CD analysis that hIAPP alone showed a negative band centered at ~ 220 nm and a simultaneous positive band centered at ~ 200 nm, confirming β-sheet conformation of hIAPP (Figure 2.19 (a)). However, when hIAPP was co-incubated with 10-fold molar ratios of **2C** and **2D** (Figure 2.19 (a)), such β-sheet conformation was not observed, suggesting appreciable disruption of hIAPP amyloid. The dose-dependent study revealed that in the presence of the BSBHps, β-sheet content reduced gradually (Figure 2.18) as the doses were increased, giving mixtures of conformation. Similar results were obtained in the presence of the control peptide **2B** (Figure 2.19 (a) and 2.20), which also indicated the conversion of β-sheet conformation into a mixture of conformations.

From the FTIR spectra, we noticed a sharp band of amide I at 1630 cm^{-1} when only hIAPP was incubated at physiological condition, confirming characteristic β-sheet conformation (Figure 2.19 (b)). However, the band shifted to 1650 cm^{-1} and 1652 cm^{-1} in co-incubation with 10-fold molar ratios of **2C** and **2D** respectively indicating conversion of β-sheet conformation. In contrast, in the presence of 2-fold and 5-fold molar ratios of BSBHps with hIAPP, similar results with less efficiency were observed (Figure 2.21). Meanwhile, in the presence of the control peptidomimetics, **2B** with various doses (Figure 2.19 (b) and 2.21), reduction of β-sheet conformation of hIAPP was also achieved.

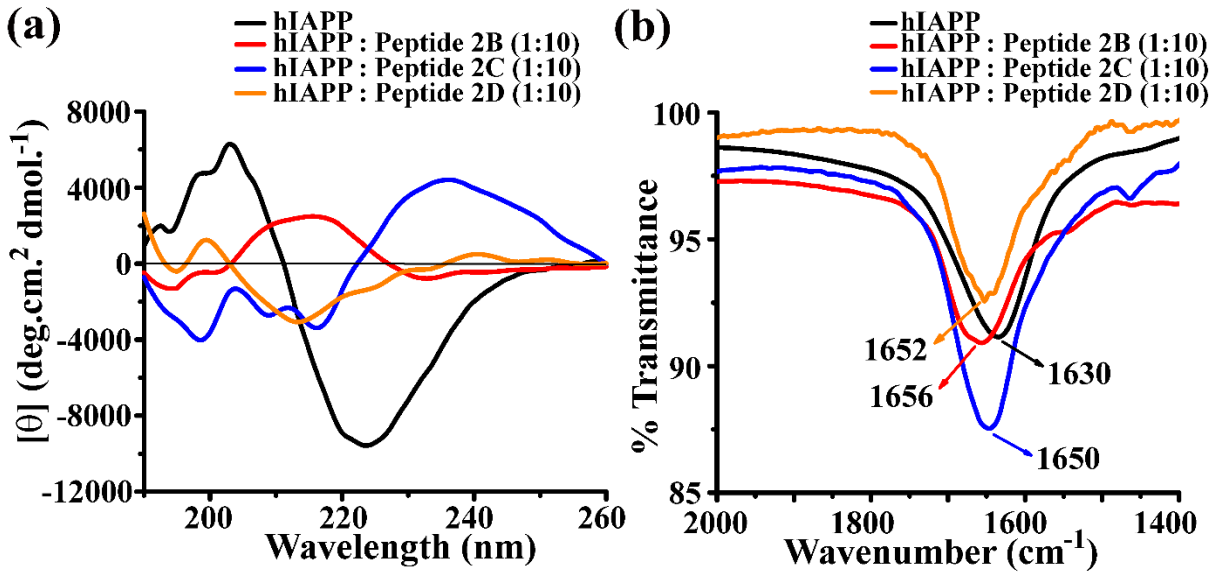

Figure 2.19: (a) CD and (b) FTIR spectra of hIAPP alone (black) and in co-incubation with 10 fold molar ratios of peptidomimetics **2B** (red), **2C** (blue) and **2D** (orange). Spectra were recorded after seven days of incubation of the peptides in PBS (50 mM) at pH 7.4 and 37 °C.

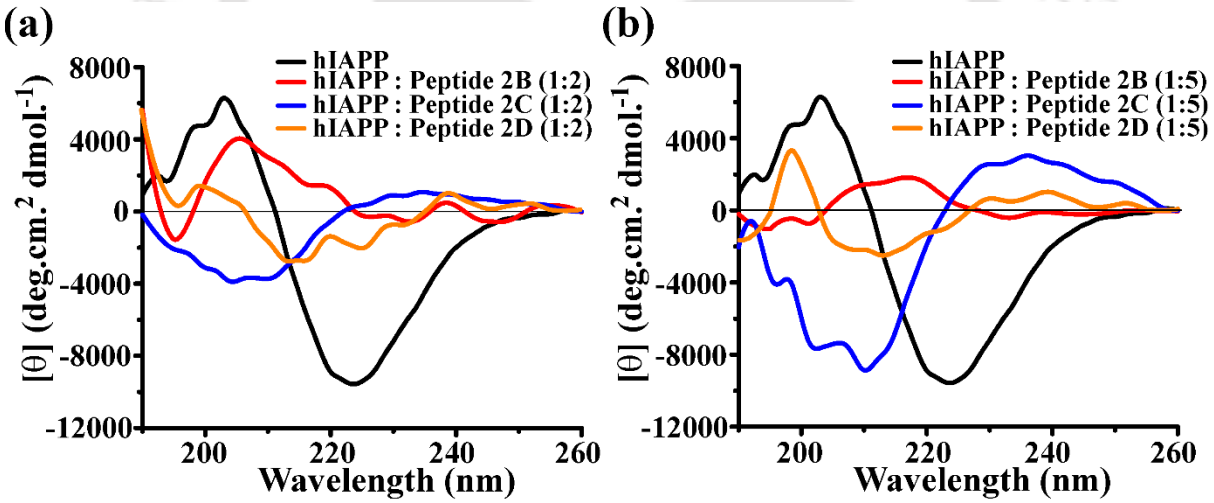

Figure 2.20: CD spectra of hIAPP alone (black) and in co-incubation with (a) 2-fold and (b) 5-fold molar ratios of peptidomimetics **2B** (red), **2C** (blue) and **2D** (orange). Spectra were recorded after seven days of incubation of the peptides in PBS (50 mM) at pH 7.4 and 37 °C.

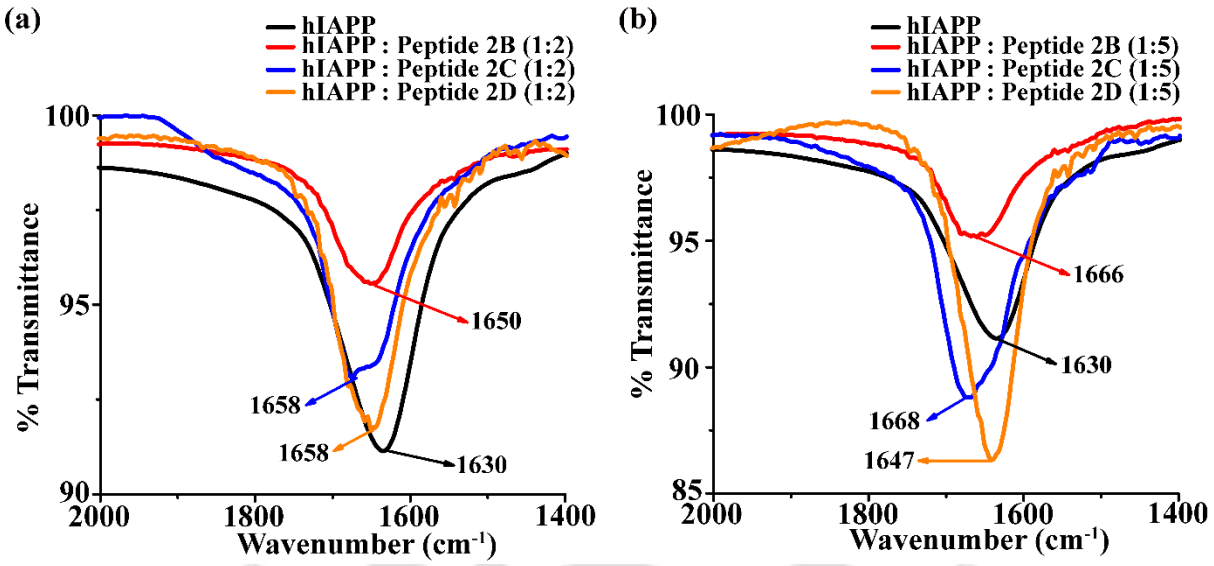

Figure 2.21: FTIR spectra of hIAPP alone (black) and in co-incubation with of (a) 2-fold and (b) 5-fold molar ratios of peptidomimetics **2B** (red), **2C** (blue) and **2D** (orange). Spectra were recorded after seven days of incubation of the peptides in PBS (50 mM) at pH 7.4 and 37 °C.

2.7.2. Monitoring the kinetics of amyloid disruption by ThT fluorescence assay:

The kinetics of the disruption of preformed amyloid was monitored by Thioflavin T (ThT) fluorescence experiments, where the BSBHps were added to the aggregating hIAPP after incubating 48h in PBS (50 mM) at pH 7.4 and 37 °C. The ThT fluorescence analysis distinctly showed that fluorescence intensity exhibited increment with time when hIAPP was incubated exclusively and reached a maximum after which it becomes saturated (black, Figure 2.22 (a); however, in co-incubation with 10-fold molar ratio of control peptidomimetic **2B** we noticed ~ 23% disruption (red, Figure 2.22) of preformed amyloid. On the contrary, when peptidomimetic **2C** (blue, Figure 2.22) was added to the solution of hIAPP, we witnessed a sharp decrease in fluorescence intensity up to ~ 40%, indicating disruption of preformed hIAPP amyloid. While in the presence of peptidomimetic **2D** (orange, Figure 2.22), we noted disruption of ~ 33% of the preformed amyloid fibril.

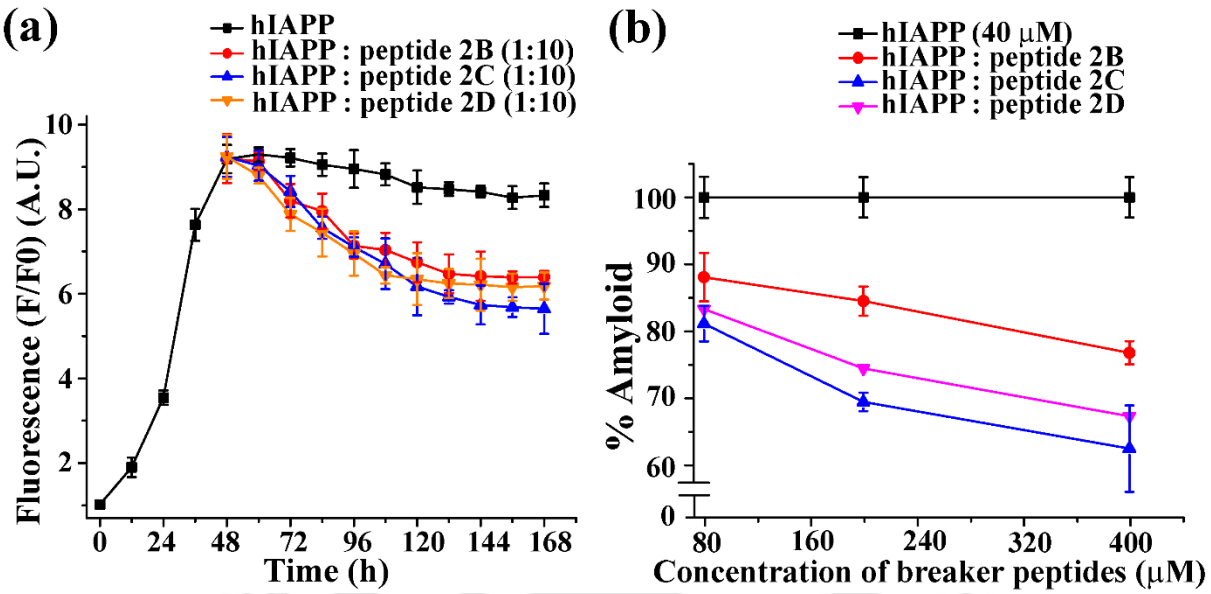

Figure 2.22: (a) Time dependent ThT fluorescence spectra of hIAPP (40 μM) alone (black) and in co-incubation with 10-fold molar ratios of **2B** (red), **2C** (blue) and **2D** (orange). (b) Dose dependent ThT fluorescence spectra at 168h of hIAPP (40 μM) alone (black) and in co-incubation with different molar ratios of **2B** (red), **2C** (blue) and **2D** (orange).

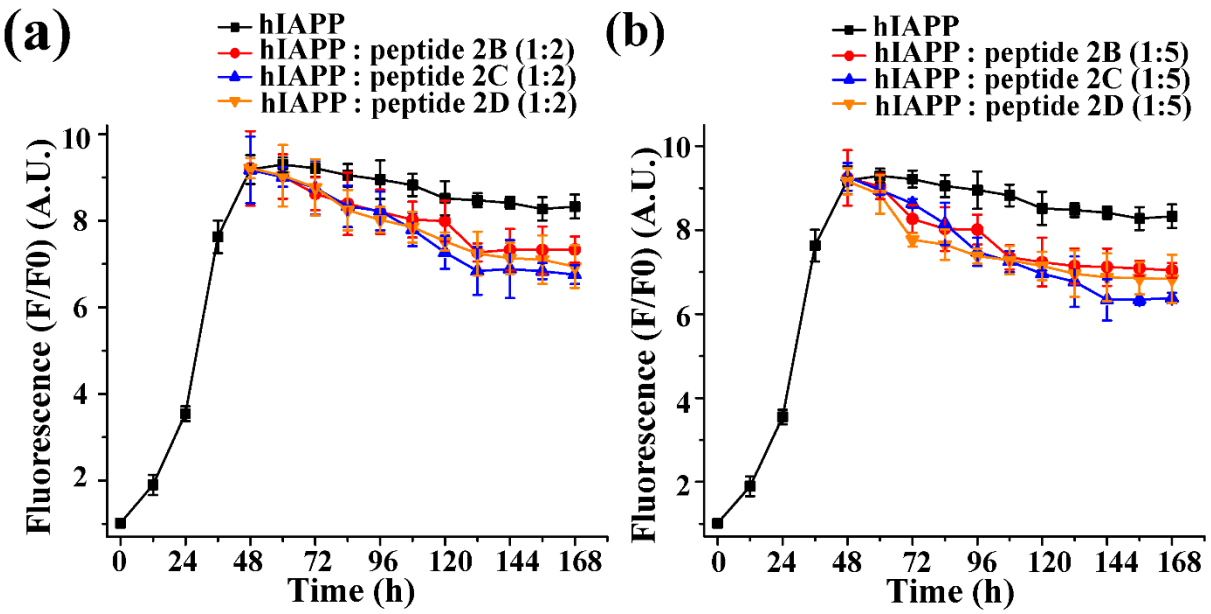

Figure 2.23: Time dependent ThT fluorescence spectra of hIAPP (40 μM) alone (black) and in co-incubation with (a) 2-fold and (b) 5-fold molar ratios of peptidomimetics **2B** (red), **2C** (blue) and **2D** (orange).

The dose-dependent disruption of preformed amyloid with 2- and 5-fold molar ratios (Figure 2.23) of BSBHps was also performed. Better results were achieved by increasing the doses from 2- to 10-fold molar excess.

2.7.3. Monitoring disruption of preformed amyloid by TEM and Congo red stained birefringence assay:

Incubating for 7 (2+5) days in PBS at physiological conditions, hIAPP alone showed distinct fibrillar morphology under TEM (Figure 2.24 (a) (i)), supporting the formation of amyloid. However, hIAPP in co-incubation with 10-fold molar ratio of peptidomimetic **2B** (Figure 2.24 (a) (ii)), significant fibrillar morphology was observed, indicating less efficiency of **2B** in disrupting the amyloid. On the other hand, in the presence of BSBHps **2C** (Figure 2.24 (a) (iii)) and **2D** (Figure 2.24 (a) (iv)) with the same molar ratio, no such fibrillar assembly was detected, suggesting sufficient disruption of preformed hIAPP amyloid.

Again, the disruption of amyloid was further monitored by Congo red stained birefringence assay. hIAPP alone displayed green-gold birefringence under cross-polarized light upon staining with Congo red (Figure 2.24 (b) (i)), indicating the development of hIAPP amyloid. On the contrary, hIAPP in co-incubation with 10-fold molar ratio of **2B** with hIAPP, sufficient green-gold birefringence persisted (Figure 2.24 (b) (ii)), signifying inefficient disruption. However, when BSBHps **2C** (Figure 2.24 (b) (iii)) and **2D** (Figure 2.24 (b) (iv)) were present with hIAPP in the same molar ratio, no characteristic birefringence was displayed, supporting sufficient disruption of hIAPP amyloid by BSBHps.

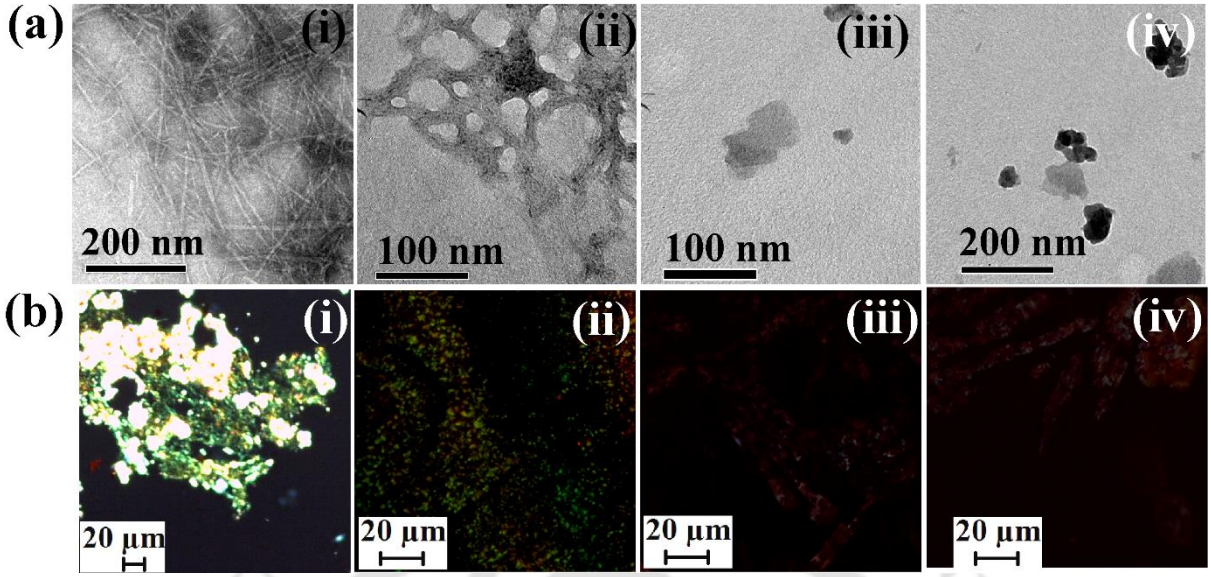

Figure 2.24: (a) TEM and (b) Congo red birefringence images of hIAPP alone (i) and in co-incubation with 10-fold molar ratios of peptidomimetics, **2B** (ii), **2C** (iii) and **2D** (iv). Images were captured after seven days of incubation of the peptides in PBS (50 mM) at pH 7.4 and 37 °C.

2.8. *In vitro* toxicity study using dye loaded LUV leakage study:

Although the amyloids can disrupt cell membranes, the soluble oligomers of the amyloidogenic peptide are the main culprits for the damage of cell membranes.[131-133] They may disrupt the cellular membrane by forming ion channels, thereby disturbing cellular homeostasis.[134] Membrane fragmentation and amyloid fibrillogenesis are two independent processes in hIAPP. Brender *et al*. outlined that amyloid fibril formation is not essential for disrupting the cell membrane by the hIAPP peptide. The small fragment, $hIAPP_{1-19,}$ which does not form mature amyloid fibres, is highly active to disrupt the cellular membrane, similar to that of the $hIAPP_{1-37}$.[135]

Hence, it was crucial to know the exact state of disaggregated hIAPP after disruption by the BSBHps. Therefore, we have carried out a membrane leakage assay on carboxyfluorescein-loaded large unilamellar vesicles (LUVs) to elucidate the presence or absence of toxic oligomeric species in the solution.[136-138] Amount of toxic oligomer species is directly

proportional to the dye leakage as the toxicity arises from the pore formation in the artificial cell membrane or vesicle. The carboxyfluorescein dye entrapped LUVs of 2 mM concentration were prepared using three different lipids, DPPC, Cholesterol and GM1 with 68:30:2 molar ratios in 50 mM HEPES buffer of pH 7.4 using the reported protocol (described in chapter 6 section 6.1.3.)..[153-154] The formation of LUVs was confirmed by FESEM images (Figure 2.25) in a scale bar of 200 nm.

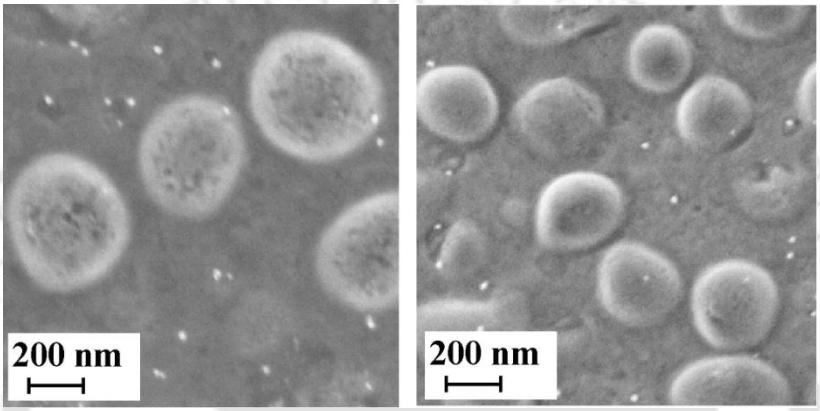

Figure 2.25: FESEM images of the large unilamellar vesicles (LUVs) at a concentration of 2 mM in HEPES buffer (50 mM). Scale bar is indicated as 200 nm.

To carry out the membrane leakage assay, we have taken different sample sets for the experiment, including one untreated LUVs as a control, which does not contain any peptide. Before performing LUV leakage assay, the peptide solutions were prepared in HEPES buffer of pH 7.4 and added to 48h incubated hIAPP solution (as similar to the process of section 2.7) and incubated for a total of 168h (48h + 120h), i.e., up to 7 days at 37 °C. After incubation, individual peptide solutions were added to the LUVs separately, and dye leakage studies were carried out. The various sample solutions prepared for the study are as follows:

Sample 1 Untreated LUVs

Sample 2- LUVs + hIAPP (incubated for 12h)

Sample 3- LUVs + hIAPP (incubated for 7 days)

Sample 4- LUVs + hIAPP: peptidomimetic **2B** (1:10)

Sample 5- LUVs + hIAPP: peptidomimetic **2C** (1:10)

Sample 6- LUVs + hIAPP: peptidomimetic **2D** (1:10)

25 μL of the peptide solution (50 μM of hIAPP) were added with 12.5 μL of dye loaded LUVs (2 mM) and diluted to 500 μL to acquire a final concentration of 2.5 μM for hIAPP solution and 50 μM for the lipid solution, maintaining the peptide and lipid molar ratio of 1:20.[137] Fluorescence assay (λ_{ex} = 485 nm, λ_{em} = 516 nm, bandwidth 3 nm) was used to monitor the carboxyfluorescein dye leakage. The emission was recorded at an interval of 10 minutes up to 100 minutes followed by a 12h interval up to 72h. To measure the 100% dye leakage from the LUVs, 10 μL of Triton X-100 was added at the end of the experiment, which induces total disruption of the lipid vesicles. Three different sets of replicate solutions were scanned separately for each data point, and the average was taken with noted standard deviation.

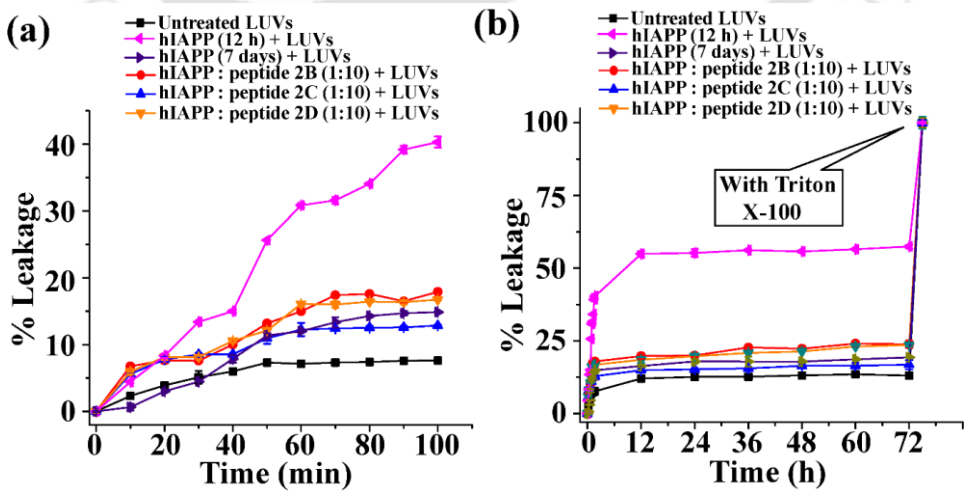

Figure 2.26: Emission of carboxyfluorescein dye with time, in terms of pore formation on LUVs showing the effect of hIAPP. (a) Dye released from LUVs alone and in the presence of different solutions from (a) 0 min to 100 min and (b) 0h to 72h.

The % dye leakage can be calculated using the following formula,[137]

$$\% \text{ Leakage} = \frac{(\text{observed fluorescence} - \text{initial fluorescence})}{(\text{total fluorescence} - \text{initial fluorescence})} \times 100\ \%$$

From the time-dependent dye leakage assay, we noticed a sharp increment of fluorescence intensity for sample 2 (12h old hIAPP) from 0 to 100 min, indicating considerable dye leakage at the early stages. Significant dye leakage was observed (~40% in 100 min and ~55% in 72h) from the 12h old hIAPP (sample 2, magenta Figure 2.26), indicating the presence of pore-forming toxic soluble oligomers in it. On the other hand, 7 days old hIAPP (sample 3, purple Figure 2.26) showed less LUV leakage (~13% in 100 min and ~17% in 72h), confirming the less toxic effect of matured fibrils on LUVs in terms of pore formation and dye leakage as compared to the soluble oligomers. Oligomers are abruptly more destructive which may give rise to significant numbers of pores on the vesicles. These are the main culprits for the release of the carboxyfluorescein dye from the artificial cell, in turn enhancing the fluorescence intensity of the sample. However, fibril disrupted by the control peptide (sample 4, red Figure 2.26) and the designed BSPHPs (sample 5 and 6, blue and orange, respectively, Figure 2.26) did not form sufficient pore on the LUVs, as the enhancement of their corresponding fluorescence intensities was almost similar to the untreated LUVs (sample 1, black Figure 2.26). Therefore, this result concluded the non-toxic behaviour of the disrupted species of the preformed amyloid of hIAPP by the BSBHps.

2.9. Enzymatic stability study:

One of the prominent issues of peptide-based therapeutics is their poor instabilities in the presence of proteolytic enzymes.[139] The focus of this study is to probe peptide stability *in vitro* in the presence of serum, which contains a sufficient amount of proteolytic enzymes.[139,140] From the earlier inhibition and disruption profiles, it was clear that BSBHp **2C** was the best among all the synthesized peptidomimetics, so we selected **2C** for the stability study. We correlated the stability of BSBHp **2C** with its native analog **2A** using time-dependent HPLC and ESI mass spectrometry. To check the stability of the peptides, we carried out a stability study *in vitro* in the presence of Roswell Park Memorial Institute (RPMI) 1640 media containing 10% human serum (v/v) procured from Thermo Fischer Scientific. For the stability study, 1 mL of the media was transferred in two different vials and kept in incubation at 37 °C for 15 minutes. After which, an aliquot of 10 μL from the peptide solutions (**2A** and **2C**) in DMSO (5 mg/mL) were mixed individually to the media containing proteolytic enzymes followed by sonication and vortex and again incubated at the same condition. Subsequently, at different time intervals, 100 μL of the mixtures were transferred into 200 μL of 96% ethanol solution for precipitation of the serum.[139] The precipitate was cooled at 4 °C for 10 mins and then centrifuged at 18,000 rpm for 2 mins. The supernatant was collected and analysed through RP-HPLC and mass spectrometry. In HPLC, a binary solvent system was used, encompassing solvent A (H_2O containing 0.1% TFA) and solvent B (CH_3CN containing 0.1% TFA), with a linear gradient of 5-100% CH_3CN for 18 mins followed by 100% CH_3CN up to 20 mins at a flow rate of 4 mL/min using a waters C18-μ-Bondapak column. The fragments were collected at different time intervals and analysed by ESI mass spectrometer.

From the HPLC and ESI mass analyses, it was observed that peptidomimetics **2A** started degrading immediately in the presence of the proteolytic enzymes and no trace of it was observed after 5h of incubation, suggesting complete degradation (Figure 2.27 and 2.28). On the other hand, peptidomimetics **2C** was established as comparatively more stable in the presence of the proteolytic enzymes. For the Ant or 2-Abz mutated peptidomimetics, up to 15h not a single trace of degradation was observed; however, at 25h only some degradation was observed (Figure 2.29 and 2.30). The above result indicated that peptidomimetic **2C** is proteolytically more stable compared to its native analog **2A**. In other words, the insertion of β-amino acid (Ant) into peptide residue instead of α-amino acid increases the proteolytic stability of the peptide.

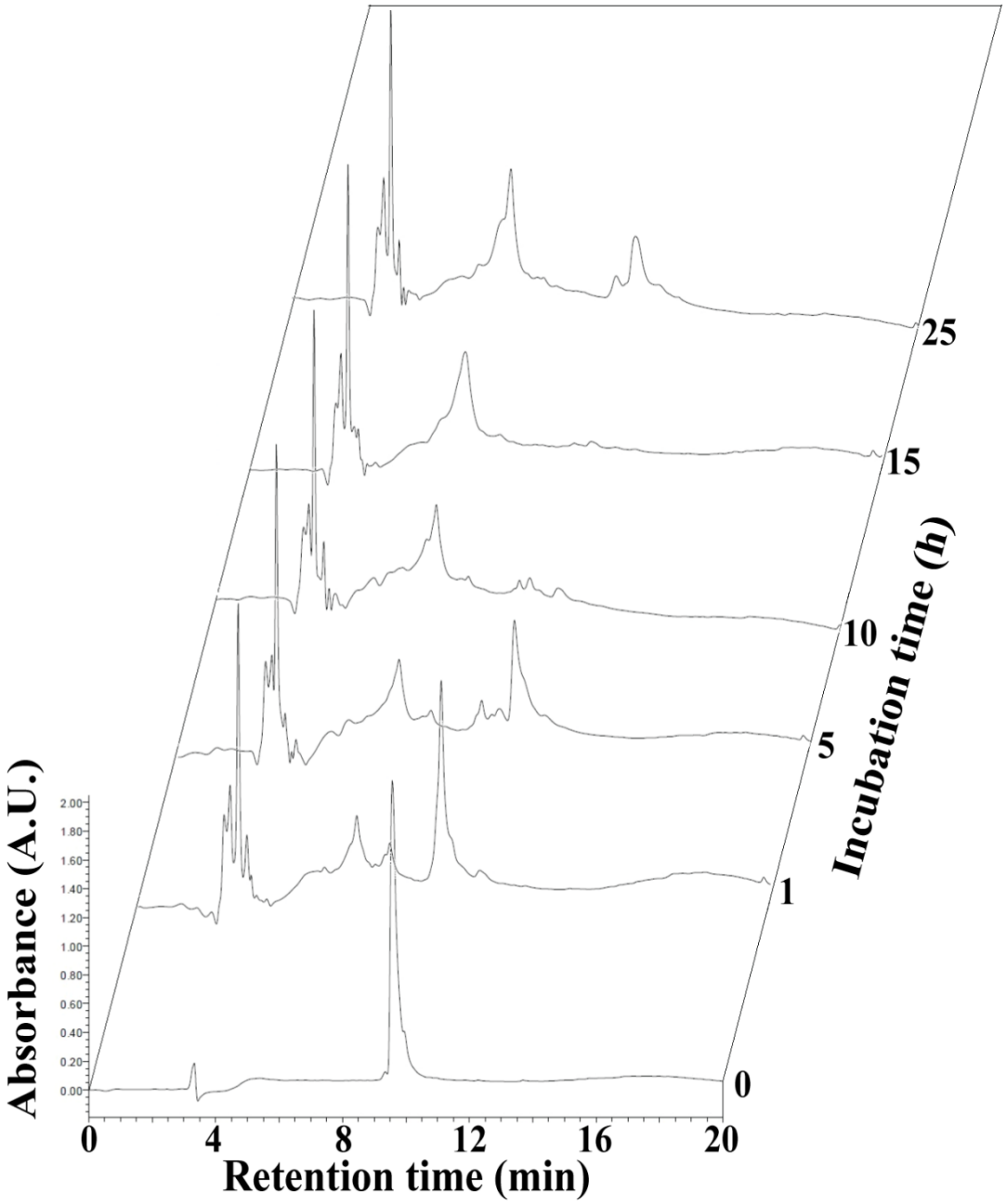

Figure 2.27: Kinetics of stability of peptide **2A** in the presence of proteolytic enzymes (human serum) monitored by RP-HPLC.

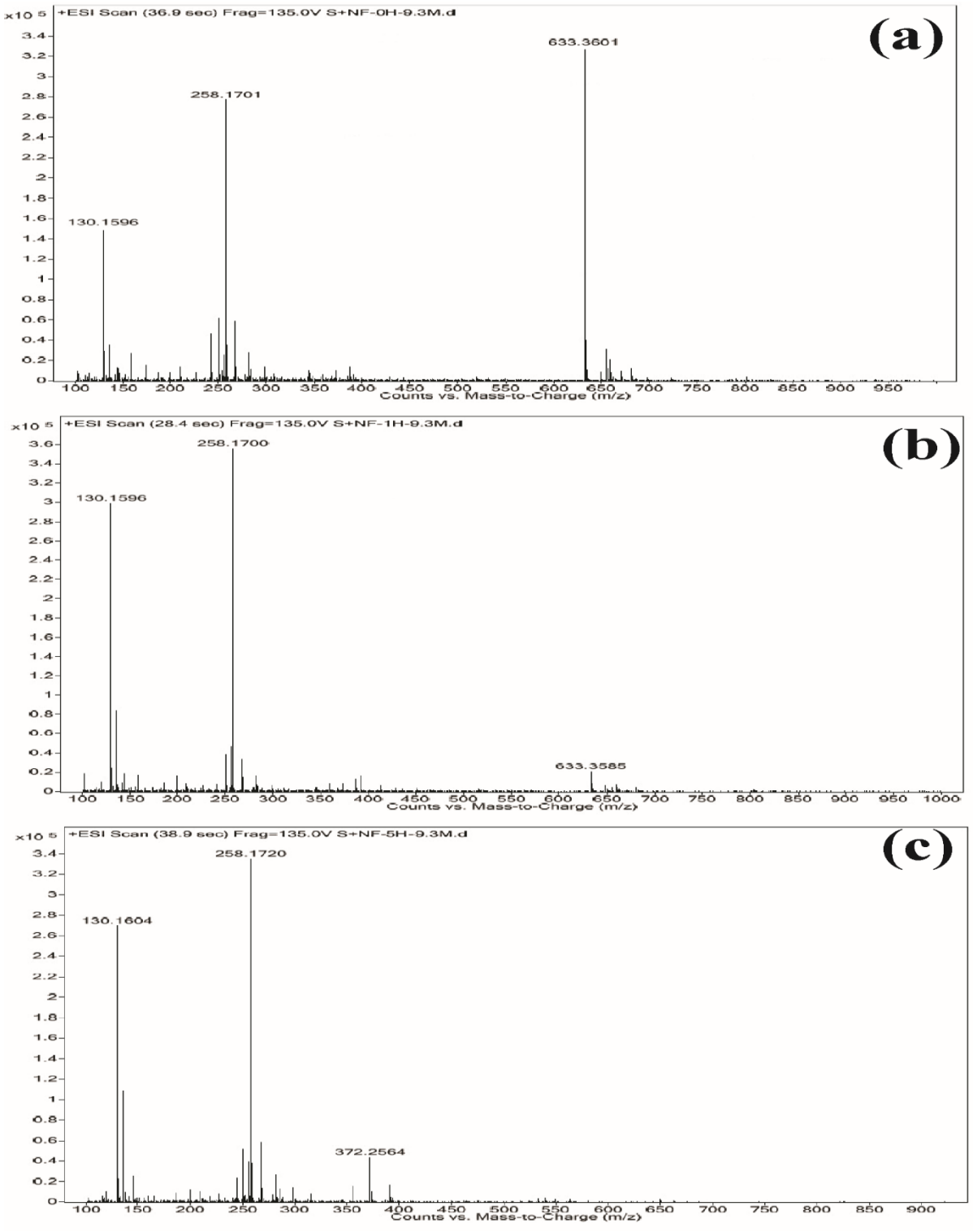

Figure 2.28: ESI mass spectra of peptide **2A** after the addition of human serum at (a) 0h, (b) 1h and (c) 5h. Calculated mass for peptide **2A** for $C_{30}H_{49}N_8O_7$ is 633.3724 $[M+H]^+$.

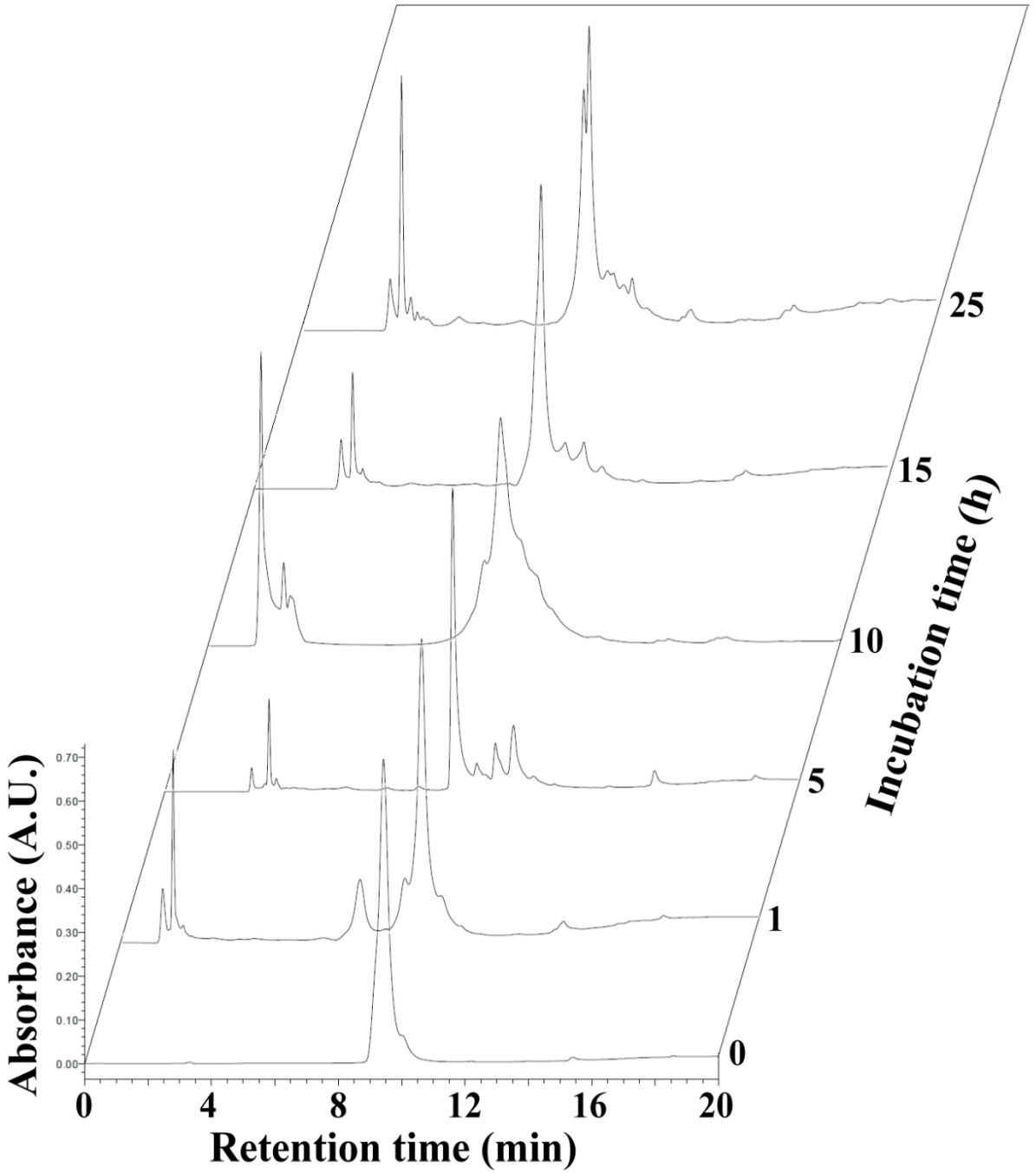

Figure 2.29: Kinetics of stability of peptide **2C** in the presence of proteolytic enzymes (human serum) monitored by RP-HPLC.

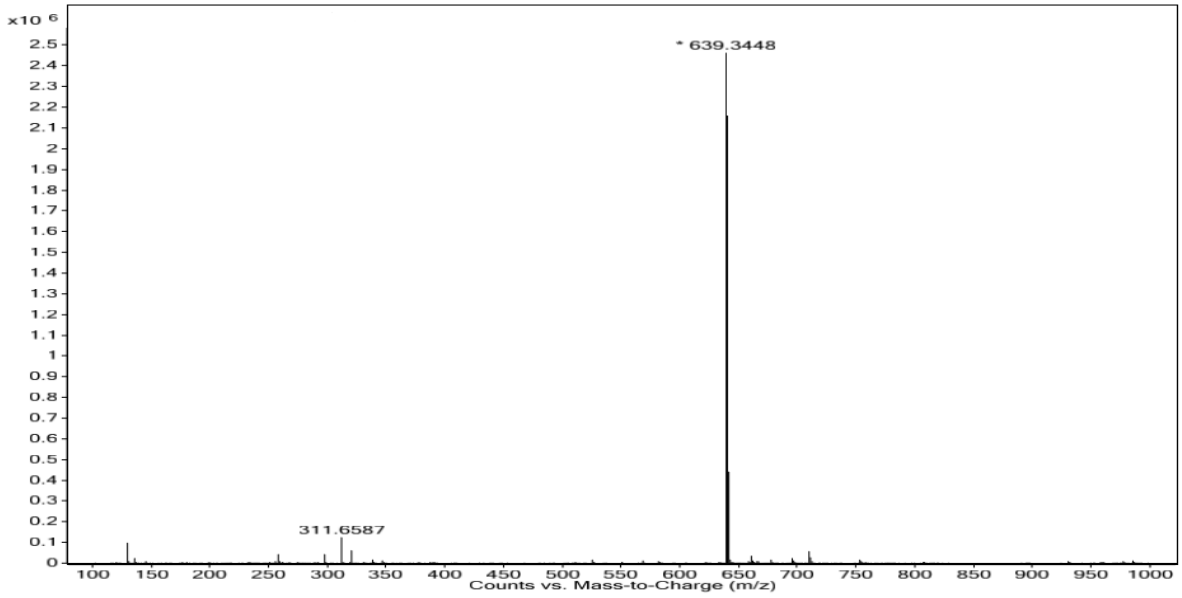

Figure 2.30: ESI mass spectrum of peptide **2C** after the addition of human serum at 15h. The calculated mass for peptide **2C** for $C_{31}H_{43}N_8O_7$ is 639.3255 $[M+H]^+$ and observed mass is 639.3448 $[M+H]^+$.

2.10. Conclusion:

From earlier reports, it was evident that the conformationally restricted β-sheet breaker hybrid peptides containing anthranilic acid (Ant) as a breaker element are potent inhibitors against Aβ amyloid formation.[118] Conformational restriction imposed outstanding potential for amyloid inhibition in protein aggregation diseases. Some of those designed peptides have been exercised for a clinical trial to be used as therapeutics against T2D.[106,118,123,141,142,143] Here, we have outlined an innovative strategy of β-sheet breaker hybrid peptidomimetics (BSBHps) as impressive inhibitors of hIAPP amyloid fibril formation and its disruption. In this context, we have used three different isomers (ortho, meta, and para) of aminobenzoic acid and demonstrated that BSBHps containing ortho (2-Abz) and meta (3-Abz) isomer were highly effective inhibitors against hIAPP amyloid formation *in vitro*. However, the para (4-Abz) isomer did not act as an inhibitor; rather, it enhanced the aggregation process.

Since the amine and carboxylic acid functionalities in para (4-Abz) isomer is 180° apart from each other and because of its planarity, it preferably forms β-sheet structure when present within the peptide sequence. However, in ortho (2-Abz) and meta (3-Abz) isomers, the amine and carboxylic acid functionalities are 60° and 120° apart respectively. Such orientation of the molecules do not allow the peptide chain to form β-sheet structures, rather some helical or turn like distorted structures evolve. These distorted orientations of the peptidomimetics generate kink in the structure, which prevents them to align with the β-sheet assembly of hIAPP, resulting in inhibition of hIAPP aggregation. However, the para isomer can align with the β-sheet assembly of hIAPP and enhance its aggregation instead of inhibition.[118, 119]

Moreover, we also expressed that these BSBHps containing the ortho and para isomers effectively disrupt the preformed amyloid of hIAPP into non-toxic fragments *in vitro* as confirmed by membrane leakage assay. As peptides containing β-amino acids are proteolytically more stable and the BSBHps having ortho- and meta- isomers of aminobenzoic acid exhibited superior inhibitory and disruption efficiency than breaker peptides containing α-aminoisobutyric acid (Aib); hence, these results may emerge as a better candidate for developing efficient therapeutic tool against hIAPP based amyloidogenesis.

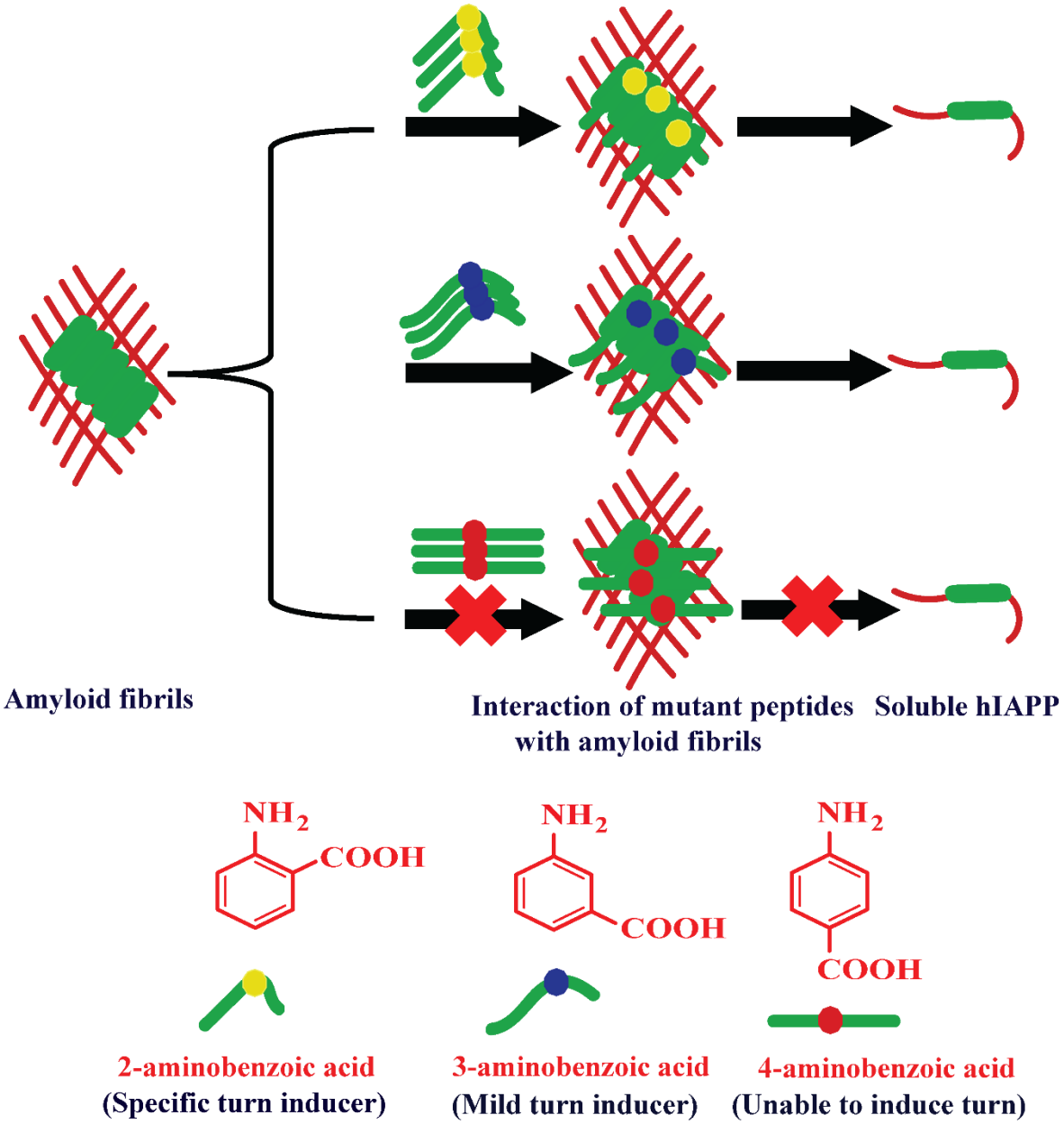

Figure 2.31: Effectiveness in the inhibition and disruption process of hIAPP amyloid by singly mutated BSBHps.

Chapter 3: Application of double breaker unit *via* incorporating isomers of aminobenzoic acid as β-sheet breaker hybrid peptides in the anti-amyloidogenic activity of hIAPP

3.1. Proposed hypothesis:

We have already discussed in chapter 2 that a novel class of BSBHps involving various isomers of aminobenzoic acid as a single breaker unit exhibited profound efficiency in inhibiting hIAPP amyloid aggregation and the disrupting preformed hIAPP amyloid. Although these single breaker peptidomimetics were efficient inhibitors, to gain better efficiencies, we wanted to insert the breaker elements in two different positions of $hIAPP_{22-27}$ (NFGAIL) simultaneously (Scheme 3.1). Then we wished to investigate their inhibitory and disrupting ability over the aggregation of wild-type hIAPP and anticipated that these might be more effective in fighting against the amyloidosis.

3.2. Design of peptides:

To test our hypothesis for the inhibition and disruption of hIAPP amyloid, we have incorporated the three different isomers of aminobenzoic acid as breaker elements in two different positions of $hIAPP_{22-27}$ (**2A**). Further, we also synthesized one control breaker peptide by incorporating α-aminoisobutyric acid (Aib) in the same positions of the peptide **2A** to compare the results. The various breaker elements were incorporated in the BSBHps at G24 and I26 to maintain the sequence homology for recognition with N-F ($hIAPP_{22-23}$) dipeptide residue sequence homology.[95] We considered these two positions, i.e., G24 and I26, as numerous peptide-based inhibitors using $hIAPP_{20-29}$ fragment have been recognised.[95,107]

Commercially available wild-type $hIAPP_{1-37}$ was used as a native aggregating system for the present study.

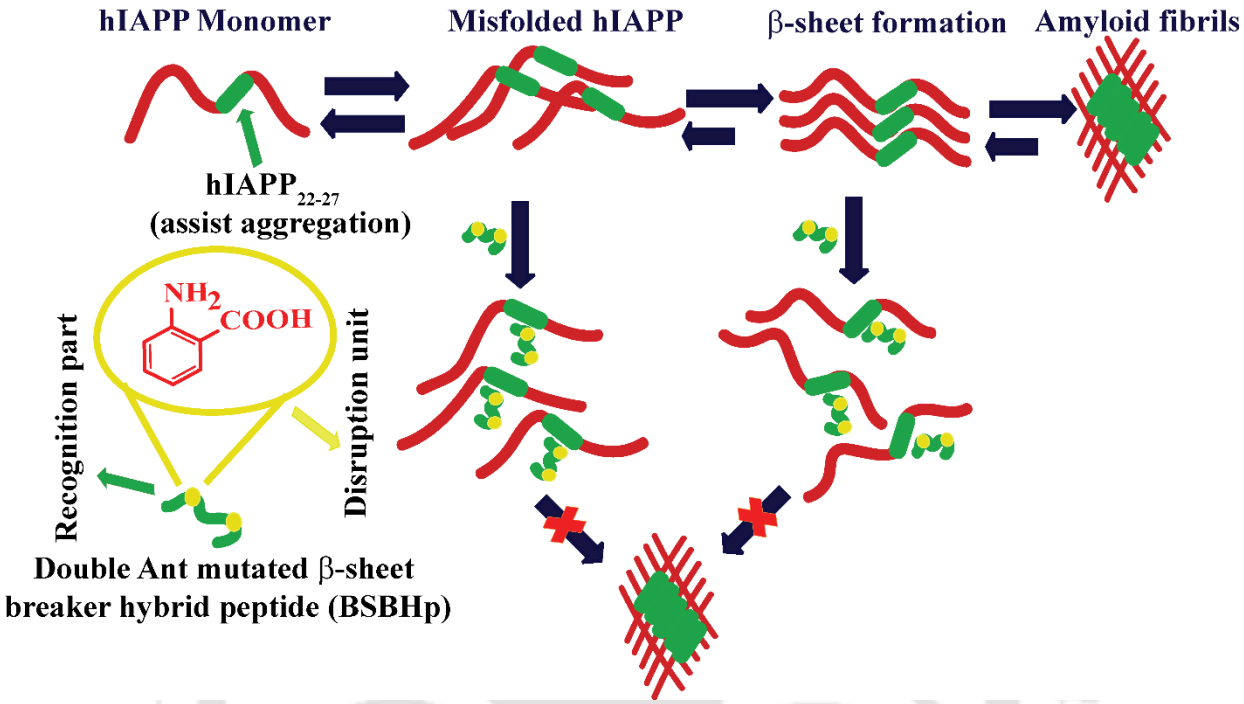

Scheme 3.1: Schematic representation of hIAPP aggregation and proposed hypothesis for the inhibition process of amyloid formation by double mutant BSBHp

Table 3.1: Sequences of all the synthesized peptides for the present study

peptide no.	peptide sequence	molecular mass $[M+H]^+$ (expected/ observed)	function
3A	NFX_1AX_1L	633.3724/ 633.3749	inhibitor/control
3B	NFX_2AX_2L	701.3411/ 701.3414	inhibitor
3C	NFX_3AX_3L	701.3411/ 701.3410	inhibitor
3D	NFX_4AX_4L	701.3411/ 701.3419	inhibitor

N.B. Standard amino acids are represented by one letter code, X_1 = α-aminoisobutyric acid (Aib), X_2 = 2-aminobenzoic acid (2-Abz), X_3 = 3-aminobenzoic acid (3-Abz), and X_4 = 4-aminobenzoic acid (4-Abz).

3.3. Synthesis and characterisation of the designed peptidomimetics:

We have synthesized all the designed peptides by solid-phase peptide synthesis (SPPS) strategy using Fmoc/t-Bu strategy on Rink Amide MBHA resin as the solid support (described in chapter 6 section 6.4).[146,147] The designed peptidomimetics were purified by reverse phase HPLC and purity was confirmed by analytical HPLC and MALDI mass spectrometry. The characterization data for the synthesized peptides are shown below (Figure 3.1-3.8).

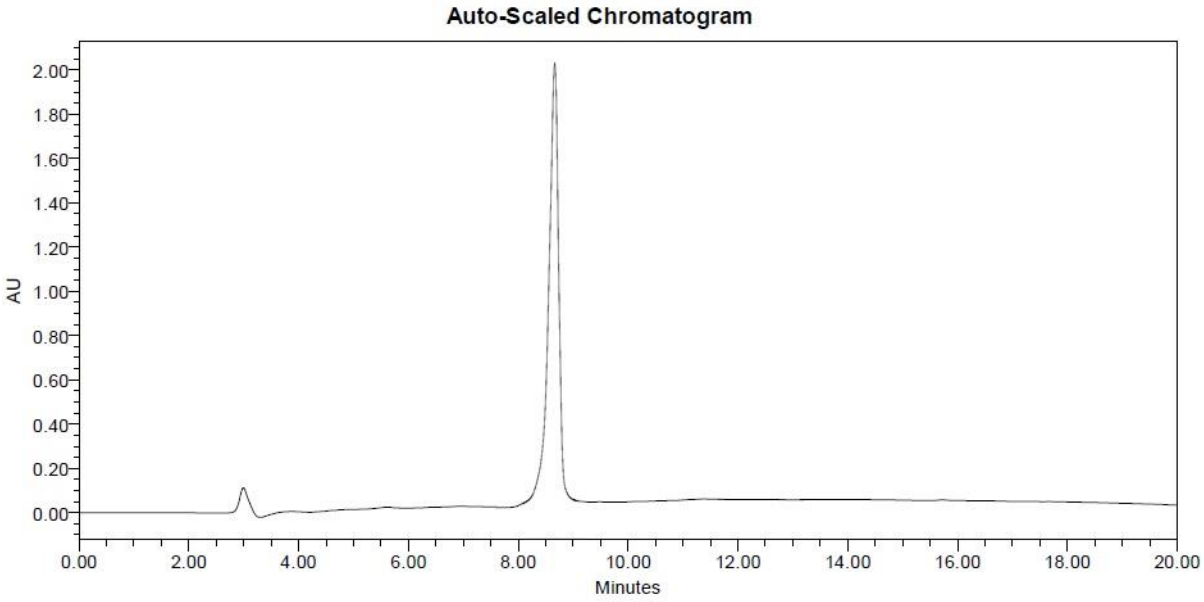

Figure 3.1: HPLC profile of the purified peptide **3A.**

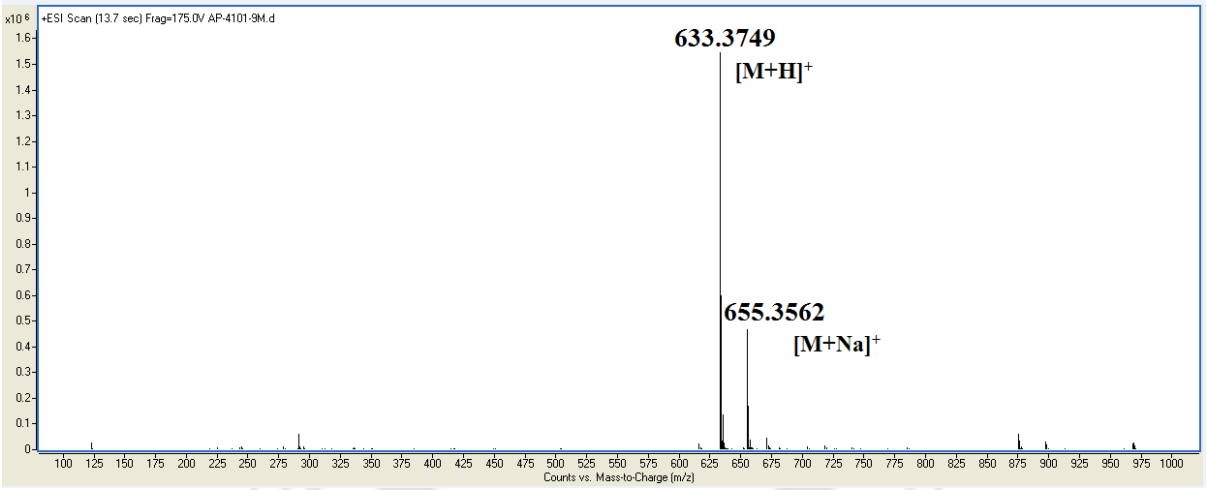

Figure 3.2: ESI mass spectrum of peptide **3A**. Calculated mass for $C_{30}H_{49}N_8O_7$ is 633.3724 $[M+H]^+$, observed 633.3749 $[M+H]^+$and calculated mass for $C_{30}H_{48}N_8O_7Na$ is 655.3544 $[M+Na]^+$, observed 633.3562 $[M+Na]^+$.

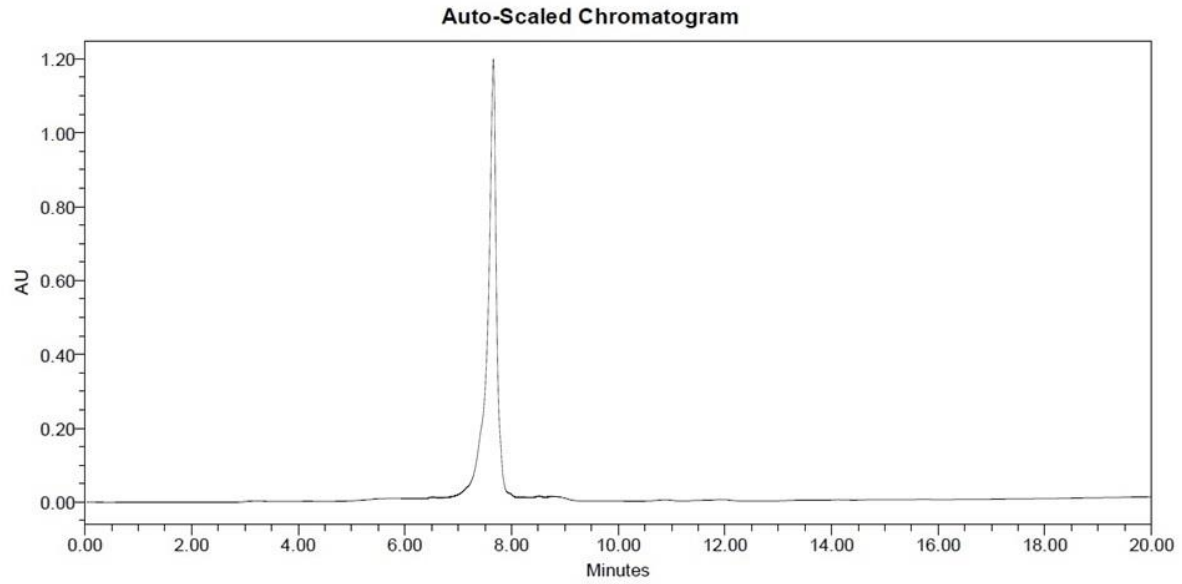

Figure 3.3: HPLC profile of the purified peptide **3B.**

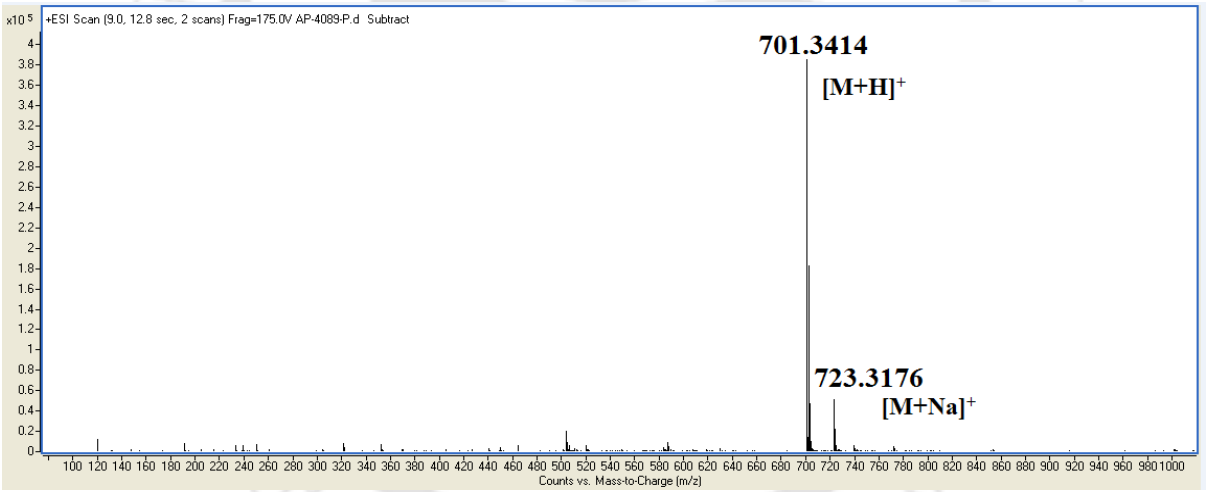

Figure 3.4: ESI mass spectrum of peptide **3B**. Calculated mass for $C_{36}H_{45}N_8O_7$ is 701.3411 $[M+H]^+$, observed 701.3414 $[M+H]^+$and calculated mass for $C_{36}H_{44}N_8O_7Na$ is 723.3231 $[M+Na]^+$, observed 723.3176 $[M+Na]^+$.

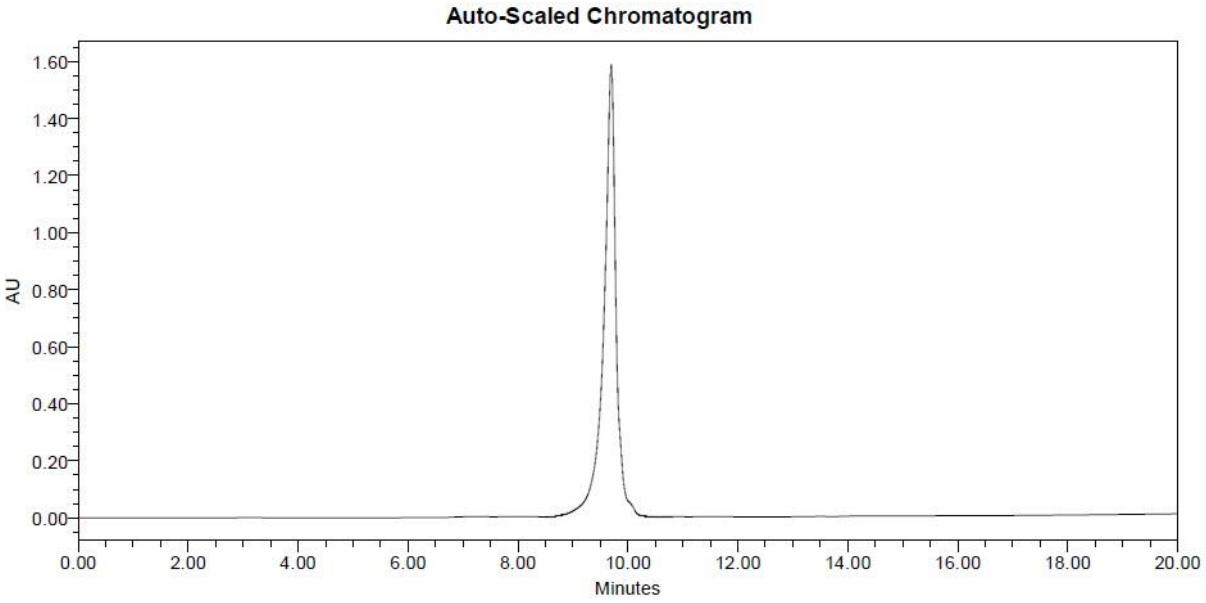

Figure 3.5: HPLC profile of the purified peptide **3C.**

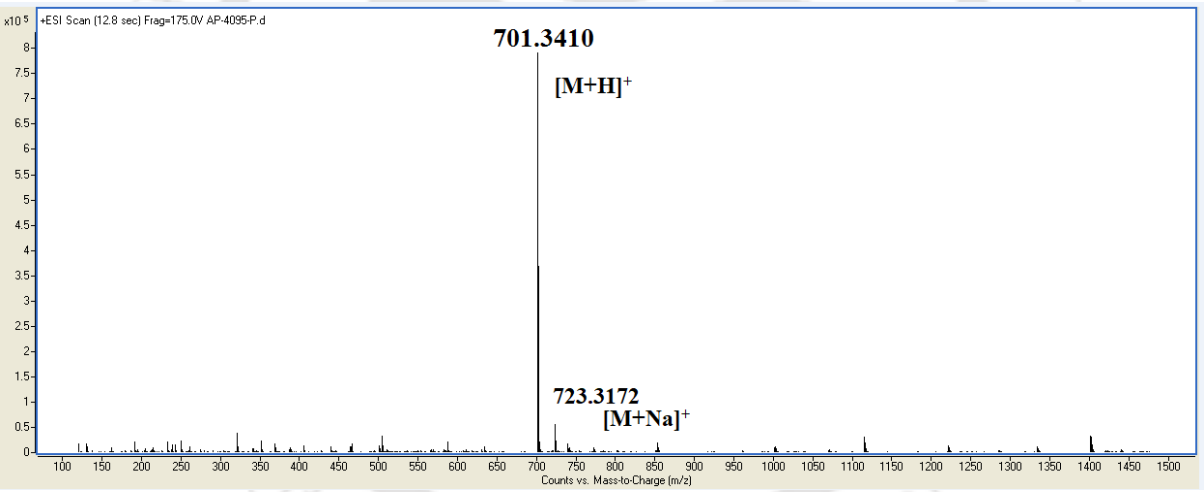

Figure 3.6: ESI mass spectrum of peptide **3C**. Calculated mass for $C_{36}H_{45}N_8O_7$ is 701.3411 $[M+H]^+$, observed 701.3410 $[M+H]^+$and calculated mass for $C_{36}H_{44}N_8O_7Na$ is 723.3231 $[M+Na]^+$, observed 723.3172 $[M+Na]^+$.

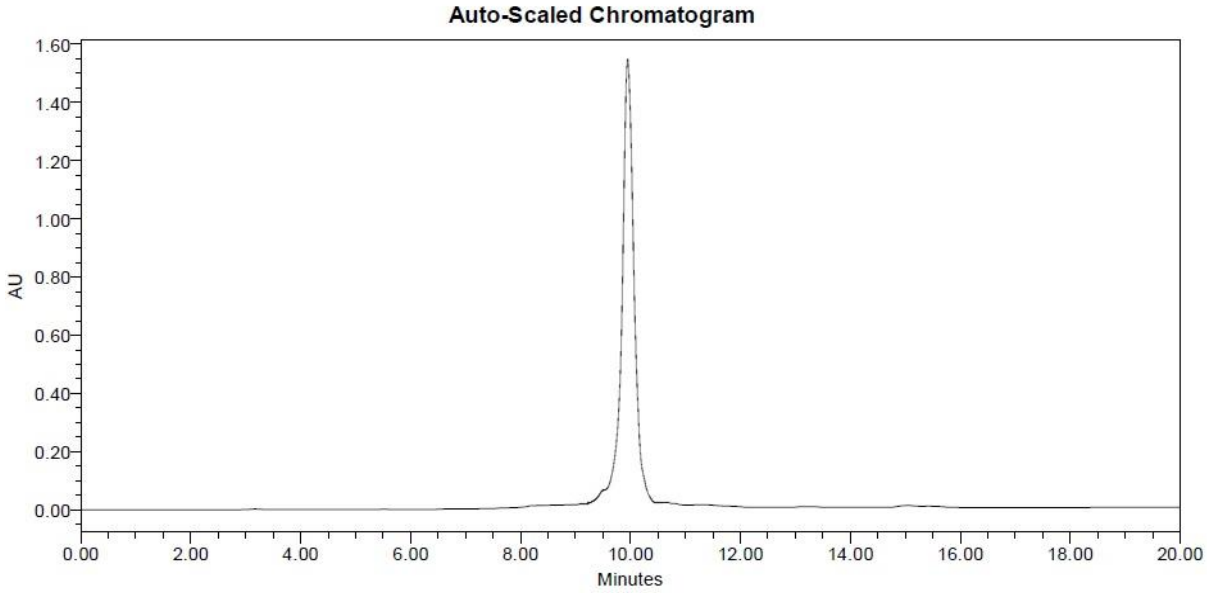

Figure 3.7: HPLC profile of the purified peptide **3D.**

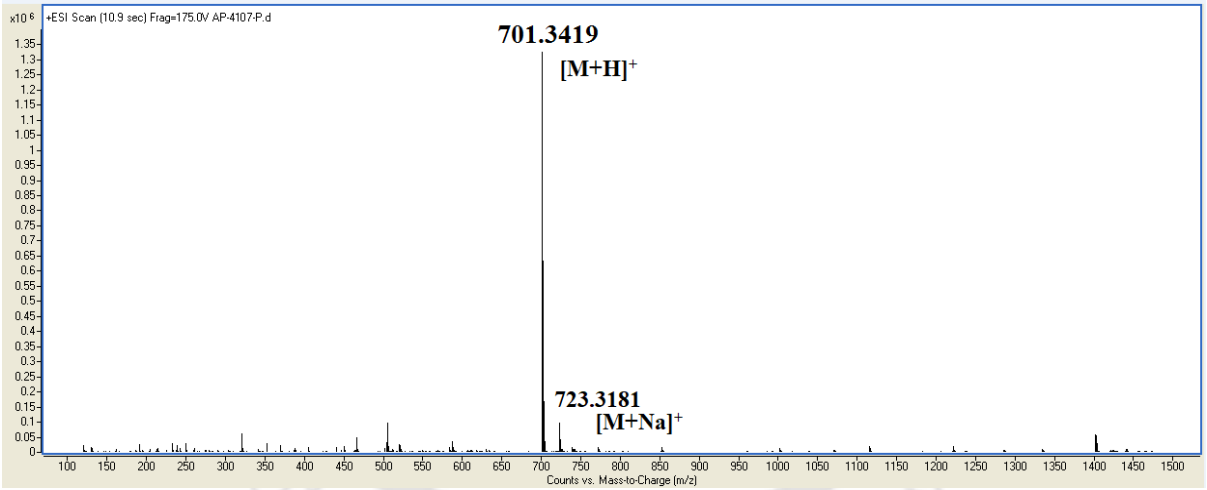

Figure 3.8: ESI mass spectrum of peptide **3D**. Calculated mass for $C_{36}H_{45}N_8O_7$ is 701.3411 $[M+H]^+$, observed 701.3419 $[M+H]^+$and calculated mass for $C_{36}H_{44}N_8O_7Na$ is 723.3231 $[M+Na]^+$, observed 723.3181 $[M+Na]^+$.

3.4. Non-amyloidogenicity of the synthesized BSBHps:

In chapter 2, section 2.5, we have already shown that the BSBHps containing a single breaker unit except the 4-aminobenzoic acid were non-amyloidogenic at physiological conditions (at pH 7.4 and 37 °C). Hence, the BSBHps containing double breaker units are also expected to be non-amyloidogenic in the same conditions. However, we wished to investigate the amyloidogenic behaviour of the BSBHps using various biophysical tools for confirmation.

3.4.1. Conformational characterization of BSBHps by CD and FTIR studies:

To verify the conformation of the BSBHps through the CD and FTIR analysis, the peptides were dissolved in 50 mM PBS (Phosphate buffer solution) of pH 7.4 to prepare a stock solution of 40 μM concentration and kept the solutions in incubation at 37 °C on a water bath. After five days of incubation, the conformational change of the BSBHps was checked using CD and FTIR (Figure 3.9). From the CD spectrum of **3A**, **3B**, and **3C**, we did not observe any specified band of β-sheet conformation for the peptides.[23] To the contrary, for the peptide **3D**, we noticed a negative band at ~220 nm and a positive band at ~195-200 nm, indicating a β-sheet rich conformation for the peptide.

Similarly, from the FTIR spectra of peptides **3A**, **3B**, and **3C**, we noticed the amide I band at 1657 cm^{-1}, 1652 cm^{-1} and 1651 cm^{-1}, respectively, showing non-β-sheet conformation for the peptides. However, for the peptide **3D**, the amide I band was observed at 1641 cm^{-1}, indicating β-sheet rich confirmation for the peptide.

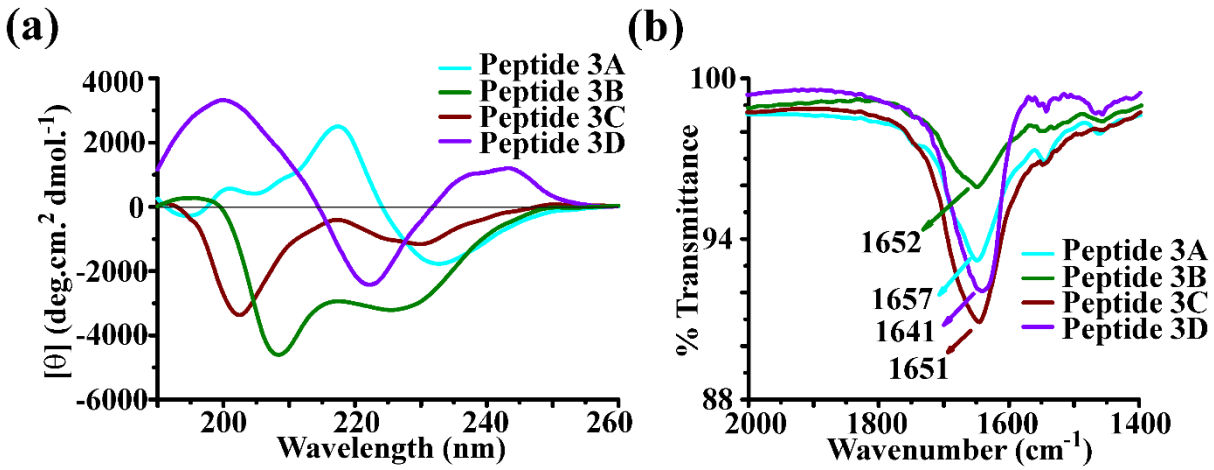

Figure 3.9: (a) CD and (b) FTIR spectra of peptide **3A** (cyan), **3B** (olive), **3C** (wine) and **3D** (violet). Spectra were recorded after five days of incubation of the peptides in PBS (50 mM) at pH 7.4 and 37 °C.

3.4.2. Amyloidogenic characterization of the synthesized BSBHps by TEM and Congo red stained birefringence studies:

From the CD and FTIR analyses of BSBHps, it was evident that peptides **3A**, **3B**, and **3C** exist in mixed conformations at physiological condition. However, the other peptide **3D** exists in β-sheet rich conformation at the same conditions. Further, the amyloidogenicity of the peptides was investigated through TEM and Congo red stained birefringence studies (Figure 3.10).

After five days of incubation of the peptide solution at physiological conditions, 10 μL aliquot of the peptide solution was taken out from the stock solution (as described in section 3.4.1) for TEM analysis (sample preparation was described in chapter 2, section 2.5.2). Under the electron microscope, we did not notice any fibrillar structure for the peptides **3A**, **3B**, and **3C**, indicating the non-amyloidogenic nature of the peptides (Figure 3.10 (a) (i), (ii) and (iii)). However, for the peptide **3D**, we observed clear fibrillar assembly, indicating its amyloidogenic behaviour (Figure 3.10 (a) (iv)).

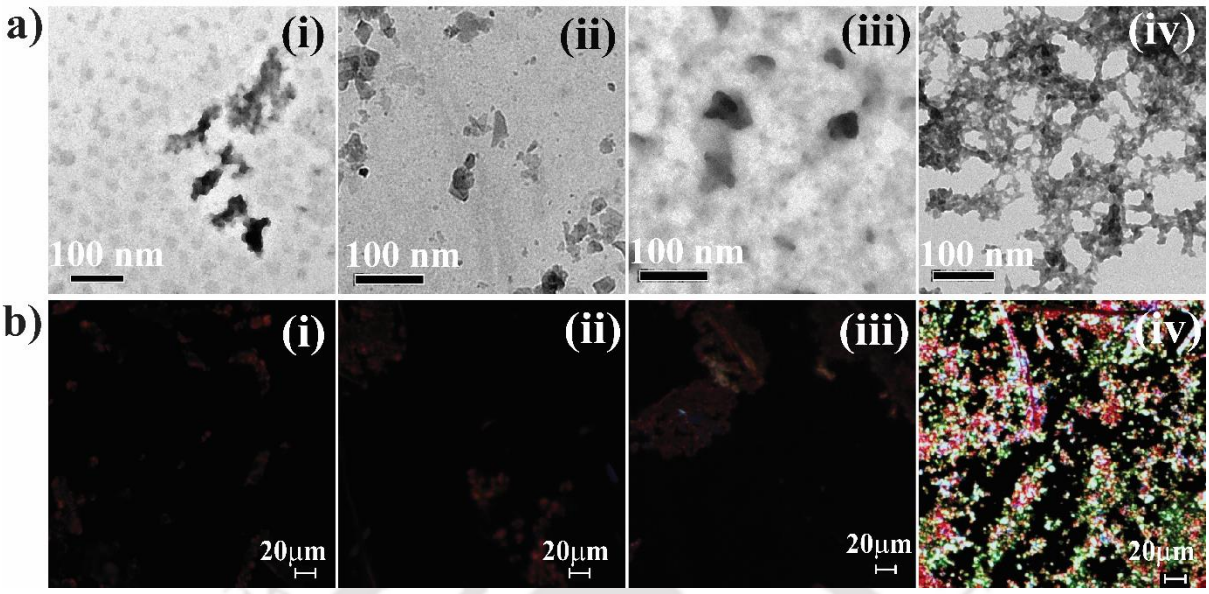

Figure 3.10: (a) TEM and (b) Congo red stained birefringence images of peptide **3A** (i), **3B** (ii), **3C** (iii) and **3D** (iv). Images were taken after five days of incubation of the peptides in PBS (50 mM) at pH 7.4 and 37 °C.

Similarly, 10 μL aliquot was taken from the five days incubated peptide solution (as described in section 3.4.1) for performing the Congo red-stained birefringence study (sample preparation described in chapter 2 section 2.5.2). From the study, we did not observe any green-gold birefringence for the peptides **3A**, **3B**, and **3C**, indicating their non-amyloidogenic nature (Figure 3.10 (a) (i), (ii) and (iii)). However, peptide **3D** showed clear green-gold birefringence under the cross-polarised light, supporting its amyloidogenicity of the peptide (Figure 3.10 (b) (iv))

Hence, from the above experimental results, it was clear that the peptidomimetics, 3B and 3C, containing two 2-Abz (X2) and 3-Abz (X3) units in two different positions of hIAPP22-27 were found to be non-amyloidogenic. We also observed the non-amyloidogenic nature of the control peptide 3A containing two Aib (X1) units in the same positions. However, peptidomimetics 3D containing 4-Abz (X_4) exhibited particular amyloidogenic properties, which might be due to the linear structure of X_4.

3.5. Inhibition of amyloid formation of hIAPP by BSBHps:

In chapter 2, section 2.6., we investigated the inhibitory efficiency of the BSBHps containing a single breaker element (**2B**, **2C**, **2D**, and **2E**). Here, we continued the investigation against the aggregation of hIAPP with the double breaker element (G24X and I26X) containing peptidomimetics (**3A**, **3B**, **3C**, and **3D**) similarly as discussed in Chapter 2. hIAPP in the absence and presence of the breaker and the control peptidomimetics were co-incubated at physiological condition up to seven days, and the kinetics of the amyloid aggregation was studied using different biophysical experiments. To examine dose-dependence activity, 2-, 5-, and 10-fold molar ratios of peptidomimetics were co-incubated with 40 μM of hIAPP in PBS (50 mM of pH 7.4).

3.5.1. Monitoring conformational transition by CD and FTIR studies:

After seven days of incubation, when we checked the CD spectrum of hIAPP alone, we noted a positive band centered at ~ 200 nm and a negative band centered at ~ 220 nm, indicating β-sheet conformation of the peptide (black, Figure 3.11 (a)). Nevertheless, in the presence of a 10-fold molar ratio of peptidomimetics **3B** and **3C**, such specific bands for β-sheet conformation were missing, indicating sufficient inhibition (olive and wine, Figure 3.11 (a)). However, in the presence of 10-fold molar excess of the control peptidomimetic, **3A** shifting of the band from β-sheet conformation was observed (cyan, Figure 3.11 (a)). On the other hand, in the presence of peptidomimetic **3D** in the same concentration**,** significant β-sheet conformation was pointed from CD, suggesting a negative indication for inhibition (violet, Figure 3.11 (a)).

From the FTIR spectrum, we observed an intense amide I band at 1627 cm^{-1} when hIAPP was incubated alone in the solution, indicating β-sheet rich confirmation of hIAPP (black,

Figure 3.11 (b)). However, with a 10-fold molar ratio of peptidomimetics **3B** and **3C**, the band shifted up to 1656 cm^{-1} and 1652 cm^{-1}, indicating non-β-sheet conformation (olive and wine, Figure 3.11 (b)). Nevertheless, in the presence of the control peptidomimetic **3A** in the same concentration, we observed the shifting of the band up to 1656 cm^{-1}, which also supported the inhibition of aggregation (cyan, Figure 3.11 (b)). On the contrary, in the presence of a 10-fold molar ratio of peptidomimetics **3D**, the band was observed at 1632 cm^{-1}, which supported the non-inhibition of aggregation of hIAPP (violet, Figure 3.11 (b)). The same study of inhibition of hIAPP was carried out with 2-fold and 5-fold molar ratios of the designed peptidomimetics. We observed similar results from CD and FTIR as found with 10-fold molar excess; however, lower efficiency was observed with the lesser equivalent of the breaker peptides (Figure 3.12 and 3.13).

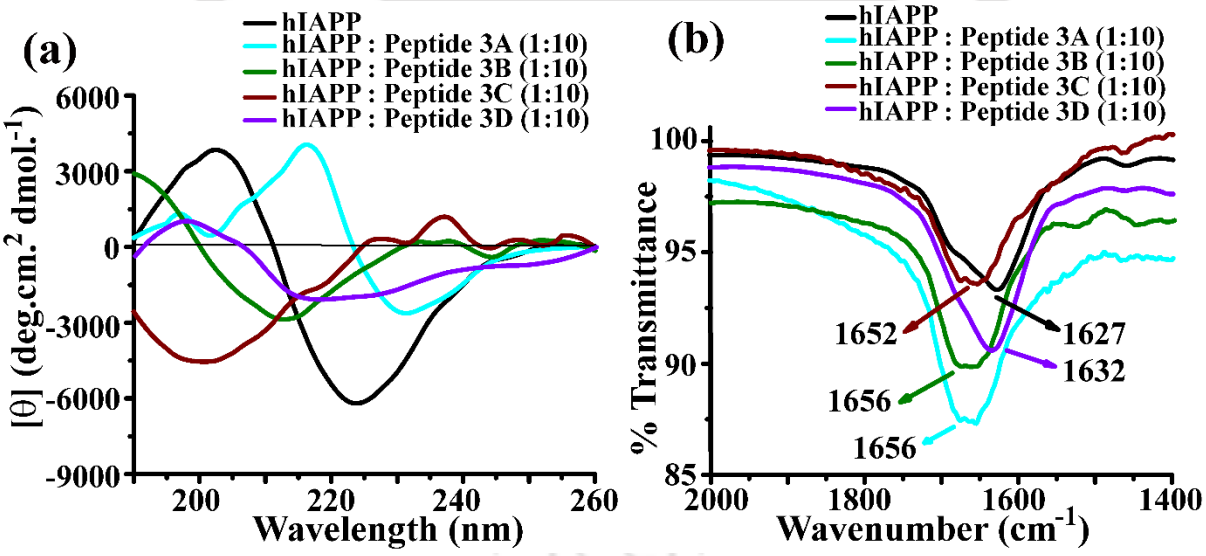

Figure 3.11: (a) CD and (b) FTIR spectra of hIAPP alone (black) and in co-incubation with 10 fold molar ratios of peptidomimetic **3A** (cyan), **3B** (olive), **3C** (wine) and **3D** (violet). Spectra were recorded after seven days of incubation of the peptides in PBS (50 mM) at pH 7.4 and 37 °C.

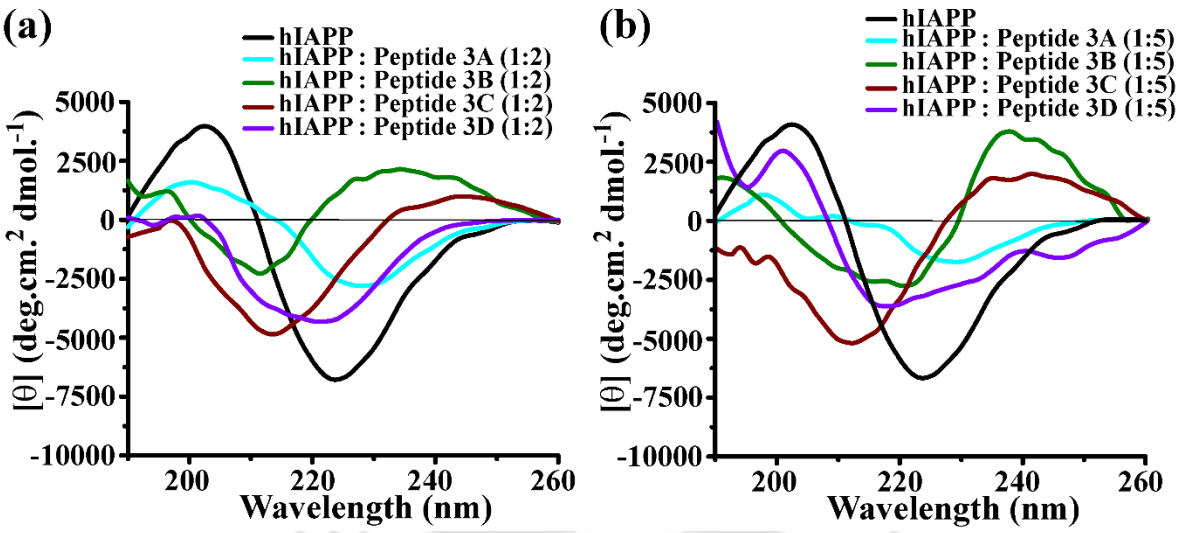

Figure 3.12: CD spectra of hIAPP alone (black) and in co-incubation with (a) 2-fold and (b) 5-fold molar ratios of peptidomimetics **3A** (cyan), **3B** (olive), **3C** (wine) and **3D** (violet). Spectra were recorded after seven days of incubation of the peptides in PBS (50 mM) at pH 7.4 and 37 °C.

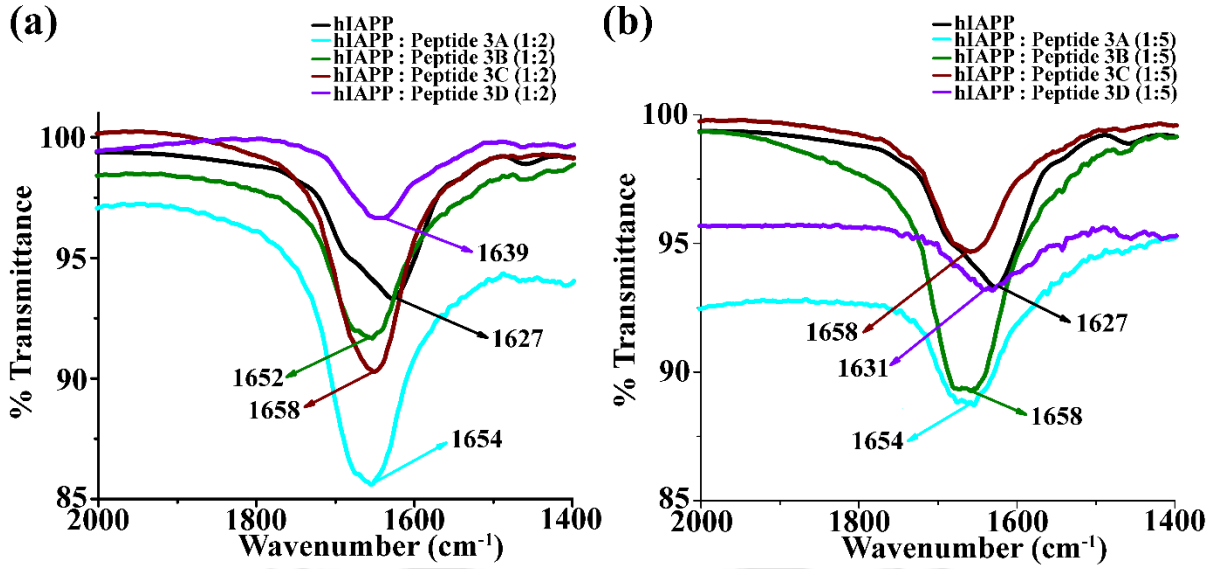

Figure 3.13: FTIR spectra of hIAPP alone (black) and in co-incubation with (a) 2-fold and (b) 5-fold molar ratios of peptidomimetics **3A** (cyan), **3B** (olive), **3C** (wine) and **3D** (violet). Spectra were recorded after seven days of incubation of the peptides in PBS (50 mM) at pH 7.4 and 37 °C.

3.5.2. Monitoring the kinetics of amyloid formation and its subsequent inhibition by BSBHps *via* ThT fluorescence assay:

For the ThT fluorescence assay, stock solutions were prepared in a similar process as in chapter 2 (section 2.6.1) and incubated at 37 °C in PBS of pH 7.4 up to 7 days. At an interval

of 12h, 40 μL of the stock solution was mixed with 160 μL of PBS (pH 7.4, 50 mM) and added 200 μL of ThT solution (50 μM) to make up the final volume of 400 μL and the fluorescence was measured (λ_{ex} =440 nm, λ_{em} =485 nm and slit 5) on a Fluoromax-4 Horiba Fluorospectrometer. At every interval, the reference was measured by mixing 200 μL of PBS (pH 7.4, 50 mM) and 200 μL of ThT solution (50 μM). We have prepared two sets of samples for each measurement, and three readings were scanned separately for each set. Thus, an average of six readings was taken and plotted as F/F_0 along the y-axis (where, F= average fluorescence value of the samples at time t, F_0= fluorescence value of the reference in the absence of sample at time t) against time (h) along the x-axis with observed standard deviation set as y-error.

The noticeable enhancement of fluorescence intensity was noted when hIAPP was incubated alone (black, Figure 3.14 (a)). In contrast, in co-incubation with 10-fold molar ratio of BSBHp **3B** (olive, Figure 3.14 (a)) and **3C** (wine, Figure 3.14 (a)), the intensity was decreased significantly up to ~70% (olive, Figure 3.14 (b)) and ~65% (wine, Figure 3.14 (b)), suggesting significant inhibition of amyloid formation. Further, control peptidomimetic **3A** (cyan, Figure 3.14 (a)) also inhibited hIAPP aggregation reasonably (~52%, cyan, Figure 3.14 (b)). However, in the presence of peptidomimetic **3D** (violet, Figure 3.14 (a)), instead of inhibition, ~12% (violet, Figure 3.14 (b)) enhancement of fluorescence intensity was noted.

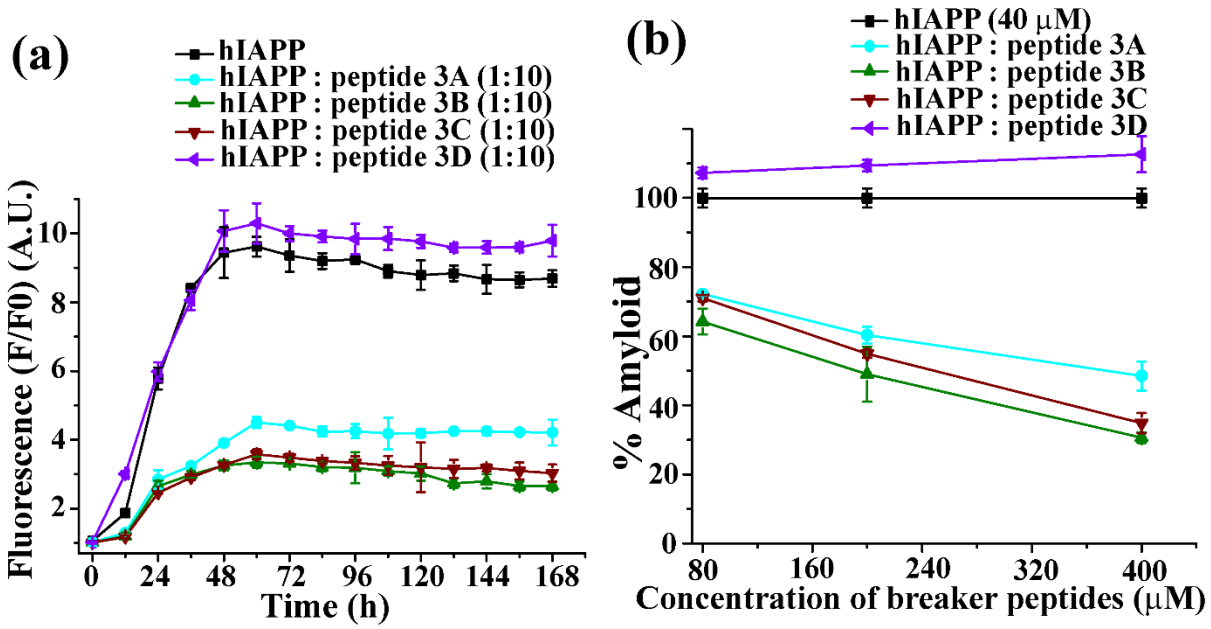

Figure 3.14: (a) Time dependent ThT fluorescence assay of hIAPP (40 μM) alone (black) and in co-incubation with 10-fold molar ratios of **3A** (cyan), **3B** (olive), **3C** (wine) and **3D** (violet). (b) Dose dependent ThT fluorescence assay at 168h of hIAPP (40 μM) alone (black) and in co-incubation with different molar ratios of **3A** (cyan), **3B** (olive), **3C** (wine) and **3D** (violet).

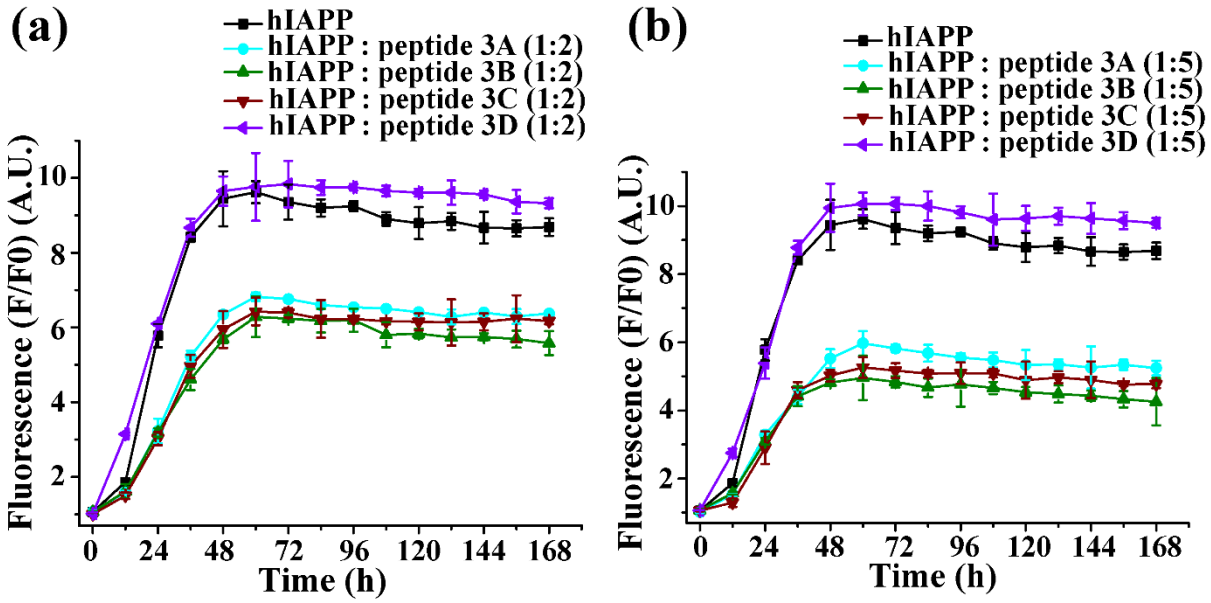

Figure 3.15: Time dependent ThT fluorescence assay of hIAPP (40 μM) alone (black) and in co-incubation with (a) 2-fold and (b) 5-fold molar ratios of peptidomimetics, **3A** (cyan), **3B** (olive), **3C** (wine) and **3D** (violet).

Further, from the dose-dependent study, we observed that 2-fold molar ratio (Figure 3.15 (a)) of the peptidomimetics, **3A**, **3B**, and **3C**, were not efficient in inhibiting hIAPP amyloid formation. Nevertheless, in co-incubation with a 5-fold molar ratio (Figure 3.15 (b)), the amyloid inhibition was observed to be more prominent. From the above results, it was concluded that the BSBHps could inhibit the amyloid formation of hIAPP significantly in a dose-dependent manner, as anticipated.

3.5.3. Monitoring the amyloid formation by TEM and Congo red stained birefringence studies:

The appearance of fibrillar assembly under an electron microscope and green-gold birefringence under cross-polarised light when a peptide stained with Congo red dye is direct evidence of amyloid formation. After seven days of incubation of the peptide solution at 37 °C in 50 mM PBS of pH 7.4, 10 μL aliquot of the peptide solution was taken out from the stock solution (as described in section 3.5) for TEM analysis (sample preparation was described in chapter 2, section 2.5.2). The hIAPP sample, incubated alone exhibited fibrillar assembly under TEM (Figure 3.16 (a) (i)), suggesting amyloid formation. On the other hand, when the 10-fold molar ratio of peptidomimetics **3B** (Figure 3.16 (a) (iii) and **3C** (Figure 3.16a (iv)) were co-incubated with hIAPP, fibrillar assembly was not observed, suggesting appreciable inhibition of hIAPP amyloid. Similarly, in the presence of a 10-fold molar ratio of the control peptidomimetic, **3A** (Figure 3.16 (a) (ii)), we did not observe any fibrillar structure, indicating sufficient inhibition of hIAPP aggregation. However, when the peptidomimetic **3D** (Figure 3.16 (a) (v)) was co-incubated with hIAPP with the same concentration as the earlier, the fibrillar structure was observed, indicating inefficiency of peptidomimetic **3D** to inhibit the hIAPP fibrillization.

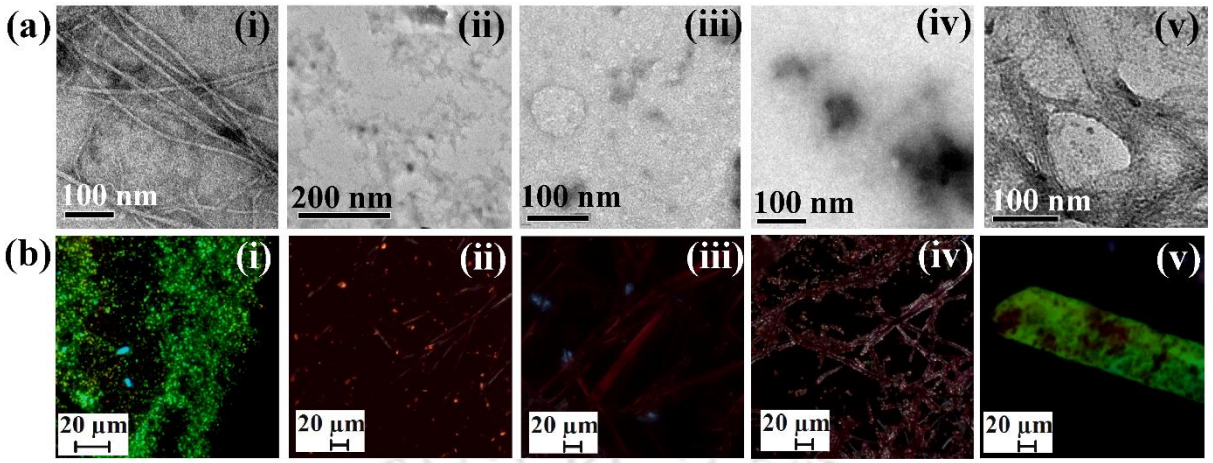

Figure 3.16: (a) TEM and (b) Congo red birefringence images of hIAPP alone (i) and in presence of 10-fold molar ratios of peptidomimetics, **3A** (ii), **3B** (iii), **3C** (iv) and **3D** (v). Images were taken after seven days of incubation of the peptides in PBS (50 mM) at pH 7.4 and 37 °C.

For the birefringence study, 10 µL aliquot from the stock solution (as discussed in section 3.5) was placed upon a glass slide followed by Congo red solution and dried the sample (as described in section 2.5.2). When hIAPP sample was present alone, it displayed green-gold birefringence (Figure 3.16 (b) (i)), suggesting hIAPP amyloid formation. On the contrary, when hIAPP was co-incubated with a 10-fold molar ratio of peptidomimetics **3B** (Figure 3.16 (b) (iii)) and **3C** (Figure 3.16 (b) (iv)), no characteristic green-gold birefringence was visible, suggesting significant inhibition of amyloid formation. Similarly, with the control peptidomimetic **3A** (Figure 3.16 (b) (ii)) in the same concentration, no characteristic birefringence was noticed, suggesting the peptide's efficiency in inhibiting the aggregation. Whereas, in the presence of peptidomimetic **3D** (Figure 3.16 (b) (v)), we noticed characteristic green-gold birefringence, which again indicated the inefficiency of **3D** in inhibiting the hIAPP fibril formation.

Summing up all the results, it could be concluded that the BSBHps, **3B**, and **3C** were found to be highly significant inhibitors for the hIAPP amyloid formation. Moreover, it can also be pointed out that the incorporation of double breaker units over the single breaker unit in

BSBHps significantly increased the inhibitory efficiency from 55% to 70% (**2C** vs. **3B)**. Furthermore, instead of inhibitory activity, some enhancement in amyloidogenic properties was observed in the presence of peptidomimetic **3D** with hIAPP.

3.6. Disruption of preformed amyloid fibril of hIAPP by BSBHps:

From the inhibition study carried out earlier, when BSBHps (**3B** and **3C**) were co-incubated with hIAPP, we observed effective inhibition of hIAPP amyloid formation. Hence, our next step was to investigate the ability of the BSBHps to disrupt preformed amyloid fibrils of hIAPP *in vitro*. From the ThT fluorescence analysis (black, Figure 3.14 (a)), we observed that hIAPP fibrillization attained its maximum at ~45-50h. Hence, the BSBHps at different doses were added into the hIAPP after 48h of incubation (2 days) to form mature fibrils for this study. The samples for the different studies were prepared similarly, as described above in section 2.6. Since **3D** was inefficient in inhibiting the fibril formation of hIAPP, we excluded it from the disruption study.

3.6.1. Monitoring conformational transition by CD and FTIR studies:

After 7 (2+5) days of incubation, when we analyzed CD, hIAPP alone showed a negative band centered at ~ 220 nm and a simultaneous positive band centered at ~ 200 nm, indicating the formation of β-sheet (Figure 3.17 (a)). However, in co-incubation with a 10-fold molar ratio of **3B** and **3C** (Figure 3.17 (a)), such β-sheet conformation was disappeared, suggesting sufficient disruption of hIAPP amyloid. From the dose-dependent study, it was observed that in the presence of the BSBHps, such β-sheet content reduced gradually (Figure 3.18). Similar results were obtained in the presence of the control peptide **3A** (Figure 3.17 (a) and 3.18), which also indicated the conversion of β-sheet conformation into a mixture of conformations.

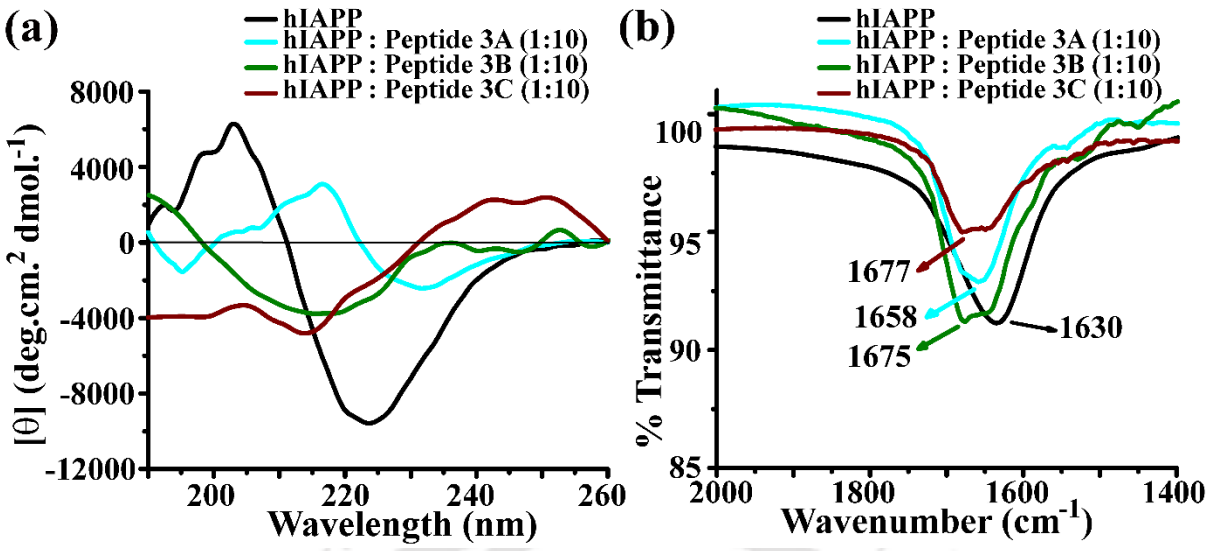

Figure 3.17: (a) CD and (b) FTIR spectra of hIAPP alone (black) and in co-incubation with 10 fold molar ratios of peptidomimetics **3A** (cyan), **3B** (olive) and **3C** (wine). Spectra were recorded after seven days of incubation of the peptides in PBS (50 mM) at pH 7.4 and 37 °C.

From the FTIR spectra, we noticed a sharp band of amide I at 1630 cm^{-1} when only hIAPP was incubated in the solution, confirming characteristic β-sheet conformation (Figure 3.17 (b)). However, with a 10-fold molar ratio of **3B** and **3C**, the band shifted to 1675 cm^{-1} and 1677 cm^{-1}, respectively, indicating the reduction of β-sheet conformation hIAPP by BSBHps. Similar results with less efficiency were noted when 2-fold and 5-fold molar ratios of BSBHps were co-incubated with hIAPP (Figure 3.19). Meanwhile, in the presence of the control peptidomimetics, **3A**, with various doses (Figure 3.17 (b) and 3.19), reduction of β-sheet conformation of hIAPP was also observed.

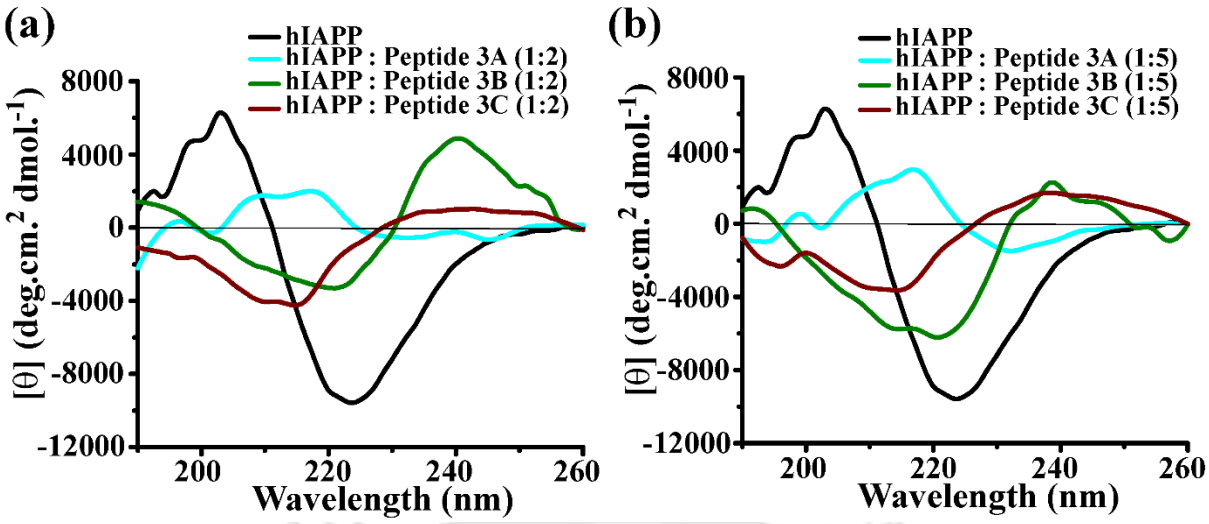

Figure 3.18: CD spectra of hIAPP alone (black) and in co-incubation with (a) 2-fold and (b) 5-fold molar ratios of peptidomimetics **3A** (cyan), **3B** (olive) and **3C** (wine). Spectra were recorded after seven days of incubation of the peptides in PBS (50 mM) at pH 7.4 and 37 °C.

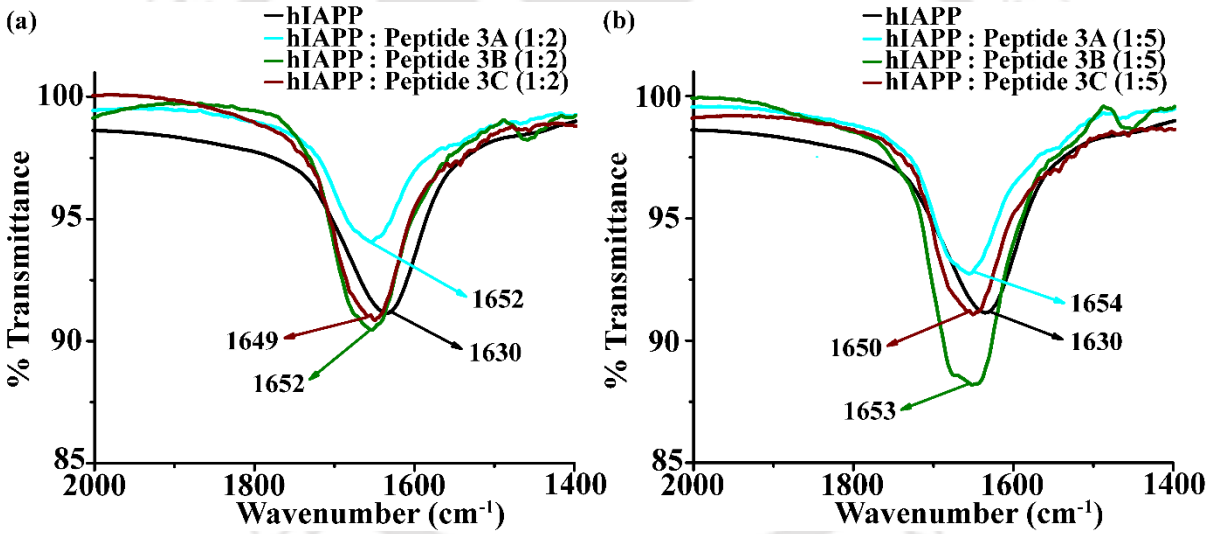

Figure 3.19: FT-IR spectra of hIAPP alone (black) and in co-incubation with (a) 2-fold and (b) 5-fold molar ratios of peptidomimetics **3A** (cyan), **3B** (olive) and **3C** (wine). Spectra were recorded after seven days of incubation of the peptides in PBS (50 mM) at pH 7.4 and 37 °C.

3.6.2. Monitoring the kinetics of amyloid disruption by ThT fluorescence assay:

The kinetics of the amyloid disruption was monitored by time-dependent Thioflavin T (ThT) fluorescence analysis, where the BSBHps were added to the aggregating hIAPP after incubating 48h in PBS (50 mM) at pH 7.4 and 37 °C. From the fluorescence assay, it was

cleared that fluorescence intensity was increased with time and reached a maximum, after which it becomes saturated when hIAPP was incubated alone (black, Figure 3.20 (a)).

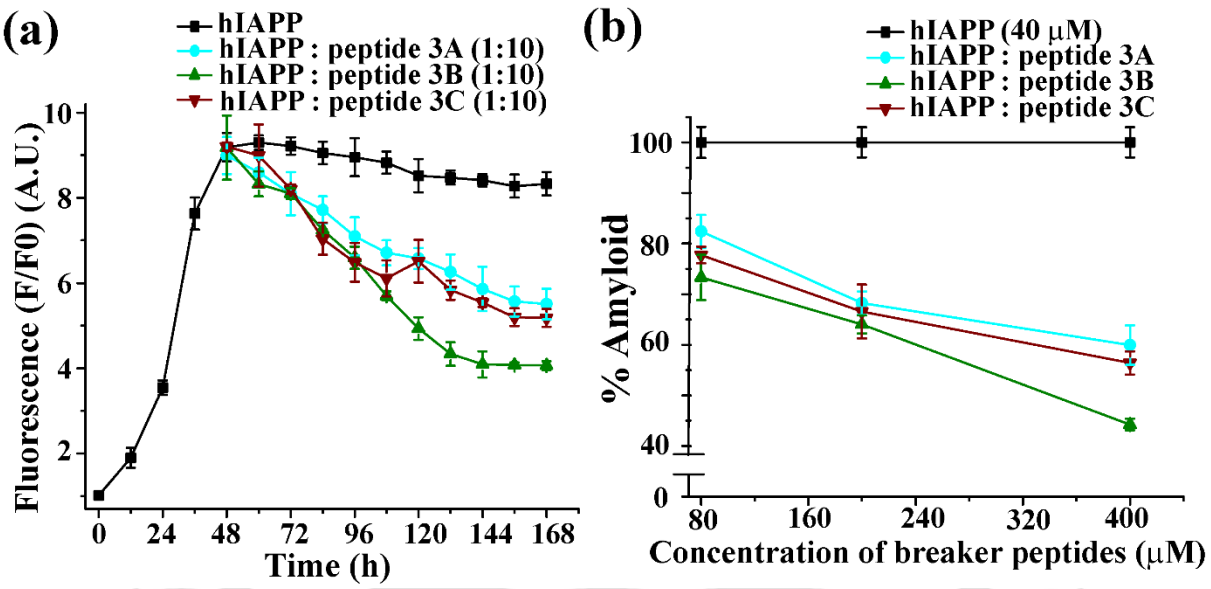

Figure 3.20: a) Time dependent ThT fluorescence assay of hIAPP (40 μM) alone (black) and in co-incubation with 10-fold molar ratios of **3A** (cyan), **3B** (olive) and **3C** (wine). (b) Dose dependent ThT fluorescence assay at 168h of hIAPP (40 μM) alone (black) and in co-incubation with different molar ratios of **3A** (cyan), **3B** (olive) and **3C** (wine).

However, hIAPP in co-incubation with a 10-fold molar ratio of control **3A,** ~40% disruption (cyan, Figure 3.20 (a) and (b)) of preformed amyloid was observed. On the contrary, in co-incubation with a 10-fold molar ratio of BSBHp **3B** (olive, Figure 3.20 (a)) and **3C** (wine, Figure 3.20 (a)), the fluorescence intensity was suppressed up to ~57% (olive, Figure 3.20 (b)) and ~44% (wine, Figure 3.20 (b)) respectively, suggesting significant disruption of preformed fibrillar aggregates. From the dose-dependent analysis with varied molar ratios of BSBHps (Figure 3.21), better results were observed with increasing the molar ratio from 2-fold to 10-fold.

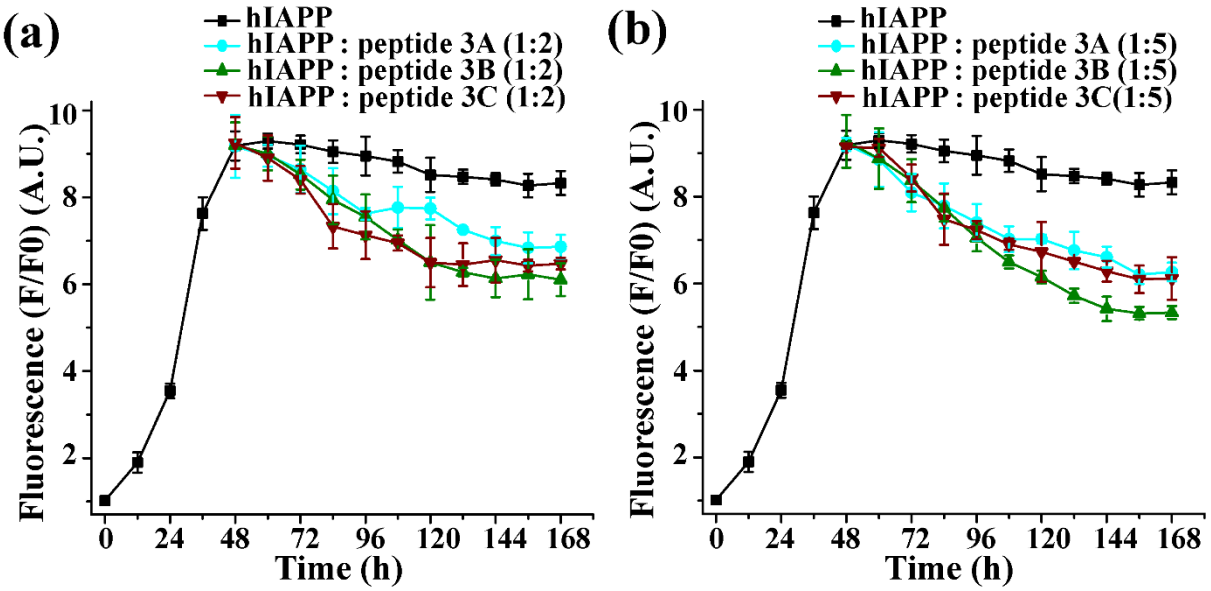

Figure 3.21: Time dependent ThT fluorescence assay of hIAPP (40 µM) alone (black) and in co-incubation with (a) 2-fold and (b) 5-fold molar ratios of peptidomimetics **3A** (cyan), **3B** (olive) and **3C** (wine).

3.6.3. Monitoring amyloid disruption by TEM and Congo red stained birefringence studies:

Incubating for 7 (2+5) days in PBS at physiological condition, hIAPP alone showed fibrillar assembly (Figure 3.22 (a) (i)), suggesting the presence of amyloid under TEM. On the contrary, hIAPP in co-incubation with a 10-fold molar ratio of BSBHps **3A** (Figure 3.22 (a) (ii)), **3B** (Figure 3.22 (a) (iii)) and **3C** (Figure 3.22 (a) (iv)), we did not find any such fibrillar structure, recommending sufficient disruption of hIAPP preformed amyloid.

Again, the Congo red-stained birefringence assay also monitored the disruption of preformed hIAPP amyloid. When incubated alone, hIAPP exhibited green-gold birefringence under cross-polarized light upon staining with Congo red (Figure 3.22 (b) (i)), suggesting the presence of amyloid. On the contrary, in co-incubation with a 10-fold molar ratio of BSBHps **3A** (Figure 3.22b (ii)), **3B** (Figure 3.22 (b) (iii)), and **3C** (Figure 3.22 (b) (iv)) with hIAPP,

we did not notice any such characteristic birefringence, supporting sufficient disruption of hIAPP amyloid.

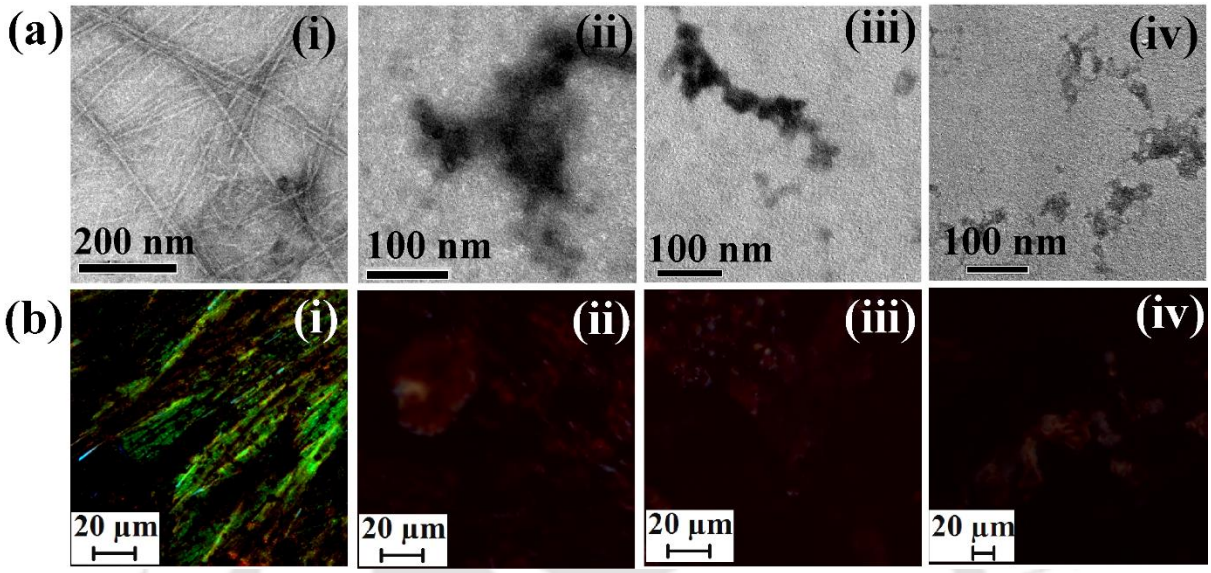

Figure 3.22: (a) TEM and (b) Congo red birefringence images of hIAPP alone (i) and in co-incubation with 10-fold molar ratios of peptidomimetics, **3A** (ii), **3B** (iii) and **3C** (iv). Images were captured after seven days of incubation of the peptides in PBS (50 mM) at pH 7.4 and 37 °C.

3.7. *In vitro* toxicity study using dye loaded LUV leakage study:

As mentioned in chapter 2, section 2.8, the soluble oligomers of hIAPP are more toxic than the matured fibrils formed, as the former are more prone to form pores and cause cellular dysfunction in the cell membrane.[131-133] The LUV dye leakage mechanism by the oligomers has been described in chapter 2. Next, we wished to check the disrupted hIAPP amyloid state by the BSBHps using carboxyfluorescein dye-loaded vesicles (LUVs) to investigate the presence or absence of toxic oligomeric species in the solution.[136-138] From the amount of dye leakage, one could estimate the number of toxic oligomers as both are directly proportional to each other. The LUVs were prepared similarly, as described in chapter 2, section 2.8. The formation of LUVs was confirmed by FE-SEM images (Figure 3.23) in a scale bar of 200 nm.

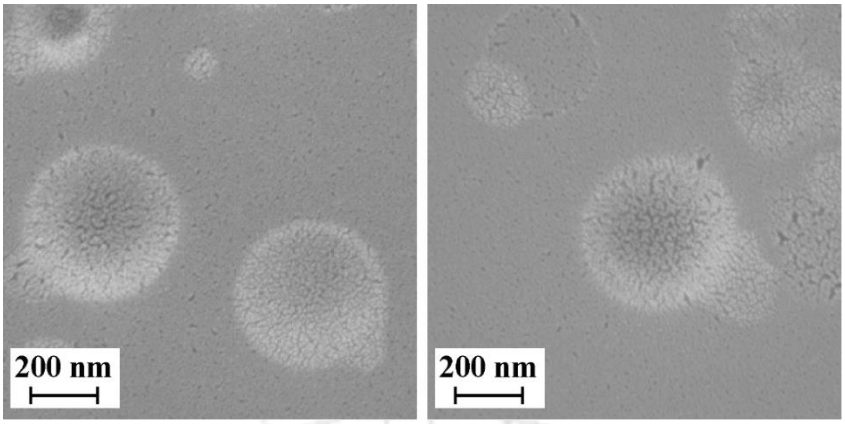

Figure 3.23: FE-SEM images of the large unilamellar vesicles (LUVs) at a concentration of 2 mM in HEPES buffer (50 mM). Scale bar is indicated as 200 nm.

To carry out the membrane leakage assay, we have taken different sample sets for the experiment, including one untreated LUVs as a control, which does not contain any peptide. Before performing LUV leakage assay, the peptide solutions were prepared in HEPES buffer of pH 7.4 and added to hIAPP solution after 48h of incubation (as similar to the process of section 3.6) and incubated for seven days (168h = 48h + 120h) at 37 °C, followed by addition of different peptide solutions individually to the LUVs and dye leakage studies were carried out. The various solutions prepared for the study are as follows:

Sample 1 Untreated LUVs

Sample 2- LUVs + hIAPP (incubated for 12h),

Sample 3- LUVs + hIAPP (incubated for 7 days)

Sample 4- LUVs + hIAPP: peptidomimetic **3A** (1:10)

Sample 5- LUVs + hIAPP: peptidomimetic **3B** (1:10)

Sample 6- LUVs + hIAPP: peptidomimetic **3C** (1:10)

The peptide and the lipid were kept in a 1:20 molar ratio during the analysis and performed similarly as described in chapter 2.

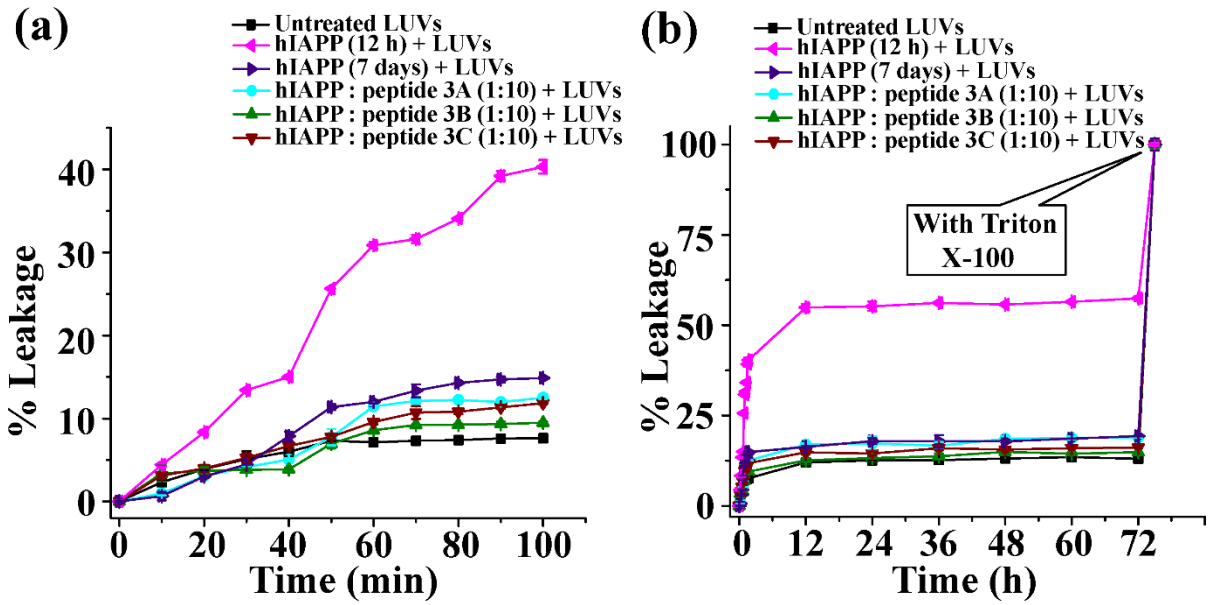

Figure 3.24: Emission of carboxyfluorescein dye with time, in terms of pore formation on LUVs showing the effect of hIAPP. Dye released from LUVs alone and in the presence of different solutions from (a) 0 min to 100 min and (b) 0h to 72h.

Similar to our previous experiment in chapter 2, section 2.8, from the LUV leakage assay, we noted a sharp increment of dye leakage for the 12h old hIAPP (sample 2, magenta Figure 3.24) from 0 to 100 min. The same sample showed significant dye leakage (~40% in 100 min and ~55% in 72h), indicating the presence of pore-forming toxic soluble oligomers in it. However, seven days old hIAPP (sample 3, purple, Figure 3.24) showed less LUV leakage (~13% in 100 min and ~17% in 72h), confirming the more toxic effect of soluble oligomers on LUVs in terms of pore formation and dye leakage as compared to the matured fibrils.

However, fibril disrupted by the control peptide (sample 4, cyan, Figure 3.24) and the designed BSPHPs (sample 5 and 6, olive and wine, Figure 3.24) minimal no of pores on the LUVs were , generated, as the enhancement of their corresponding fluorescence intensities was as similar as the untreated LUVs (sample 1, black, Figure 3.24). Hence, it can be inferred that in the presence of the BSBHps, the disaggregation of the hIAPP amyloid converts into non-toxic species *in vitro* at the physiological conditions.

3.8. Proteolytic stability study:

One of the significant drawbacks of peptide-based drugs is their less stability in the presence of proteolytic enzymes.[139] Hence, we decided to study the stability of our synthesized BSBHps *in vitro* in the presence of a serum, which contains a sufficient amount of proteolytic enzymes.[139,140] From the earlier inhibition and disruption profiles, it was clear that BSBHp **3B** was found to be the best among all the synthesized peptidomimetics, so we selected **3B** for the stability study. We compared the stability of BSBHp **3B** with its native analog **2A** (NFGAIL) using time-dependent HPLC and ESI mass spectrometry. The solutions for the stability study were prepared similarly, as described in chapter 2, section 2.9.

In the presence of the serum, the native peptide **2A** started degradation instantly, and after 5h only, it degraded completely (Figure 3.25 and 3.26), as observed in chapter 2, section 2.9. On the contrary, BSBHp **3B**, which bears two Ant (2-Abz) moieties in the sequence, was observed to be relatively stable in the presence of the proteolytic enzymes. We did not find any sign of degradation; instead, absolute retention in the HPLC peak of the pure compound was observed until 25h (Figure 3.27 and 3.28). In chapter 2, section 2.9, we observed that BSBHp **2C** containing single Ant (2-Abz) moiety also increased the peptide's stability compared to the native peptide. However, the stability of the **3B** peptide is more pronounced than the **2C** peptide. Hence, the above result indicates that the insertion of β-amino acid into peptide sequence instead of α-amino acid increases the stability of the peptide in the presence of proteolytic enzymes.

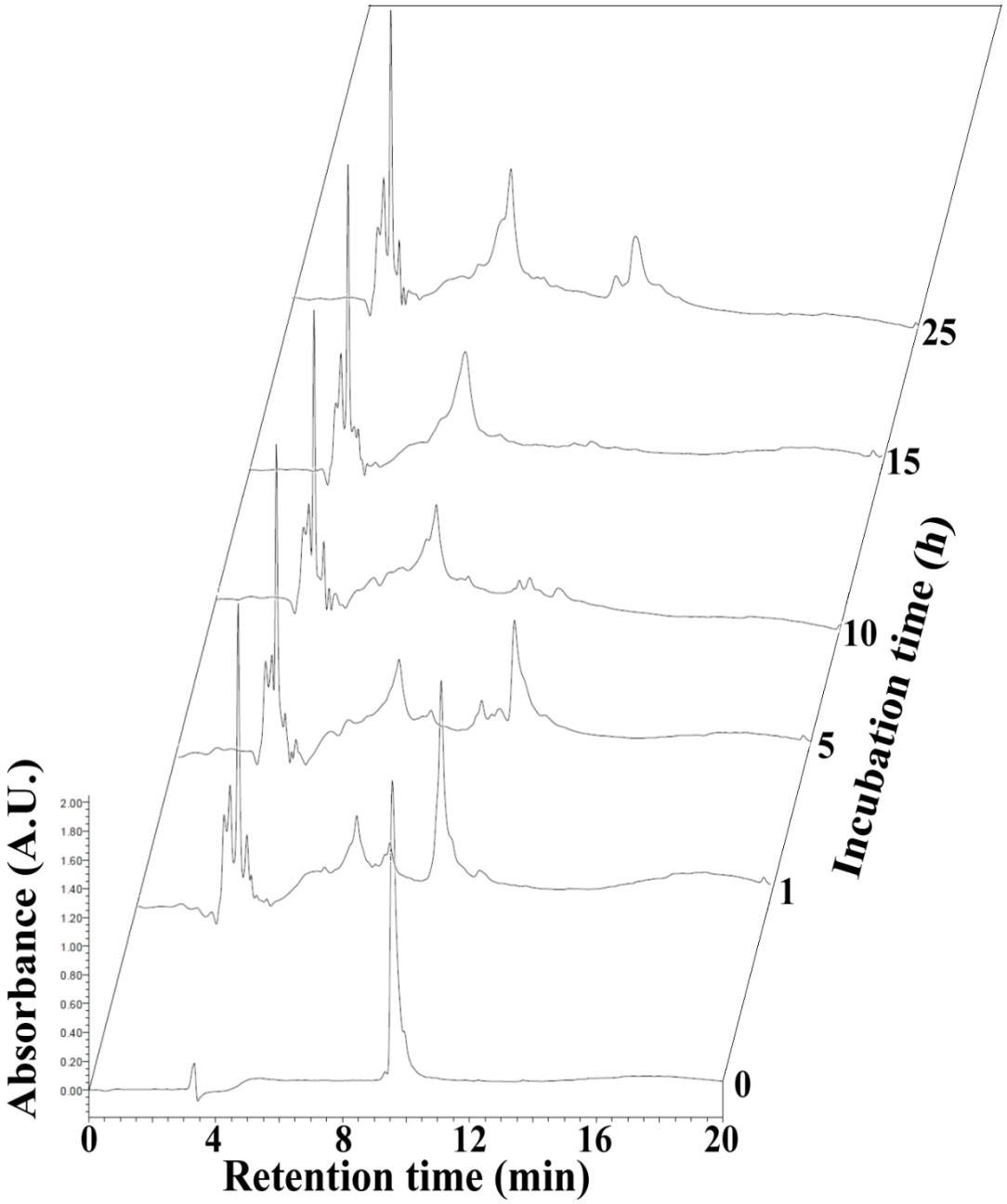

Figure 3.25: Kinetics of stability of peptide **2A** in the presence of proteolytic enzymes (human serum) monitored by RP-HPLC.

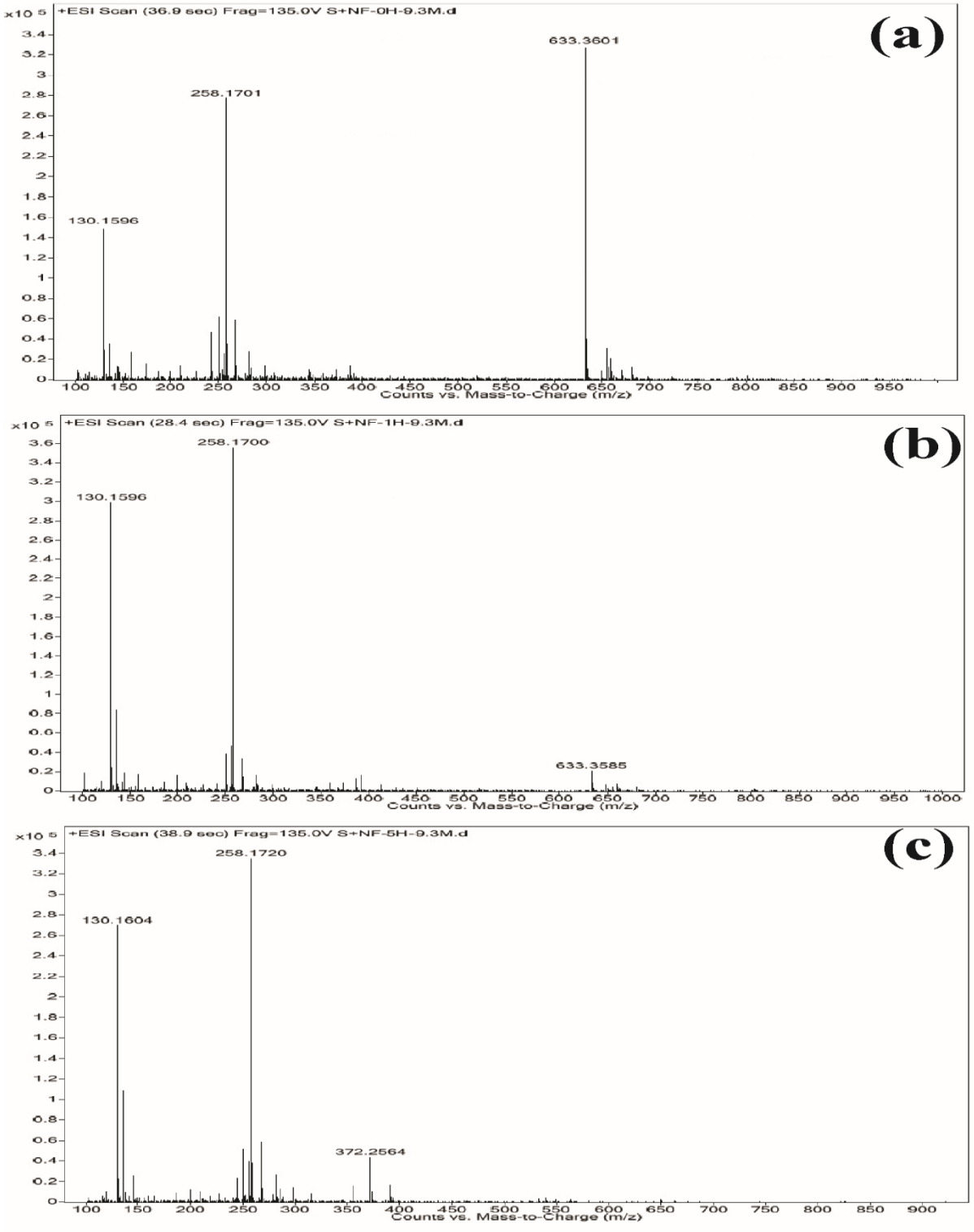

Figure 3.26: ESI mass spectra of peptide **2A** after the addition of human serum at (a) 0h, (b) 1h, and (c) 5h. The calculated mass for peptide **2A** for $C_{30}H_{49}N_8O_7$ is 633.3724 $[M+H]^+$.

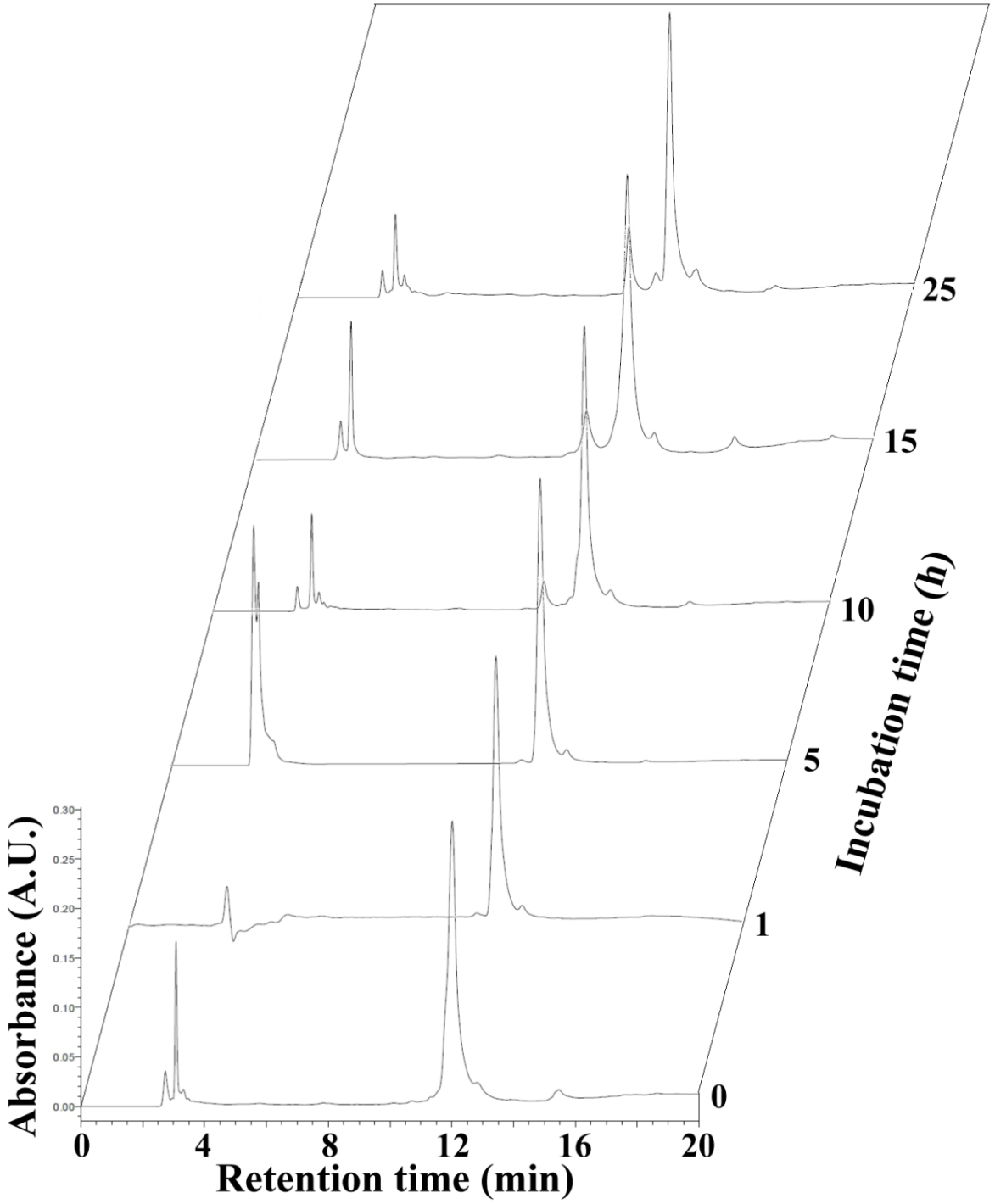

Figure 3.27: Kinetics of stability of peptide **3B** in the presence of proteolytic enzymes (human serum) monitored by RP-HPLC from 0h to 25h.

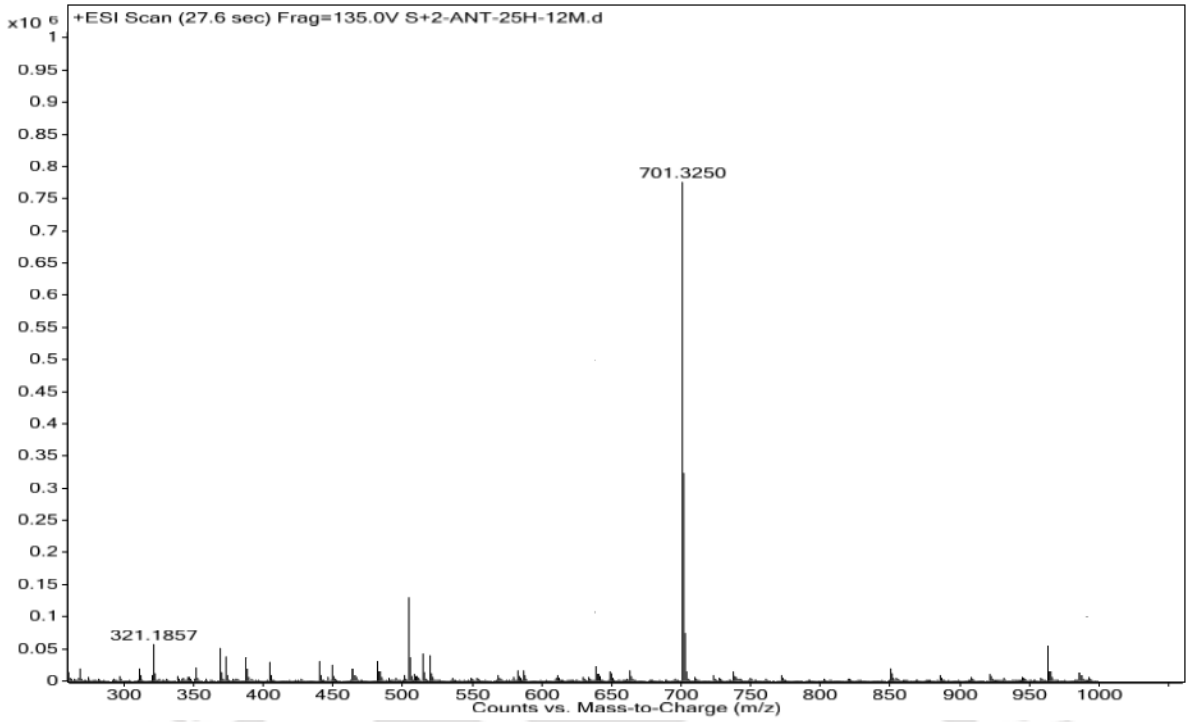

Figure 3.28: ESI mass spectrum of peptide **3B** after the addition of human serum at 25h. Calculated mass for peptide **3B** is 701.3411 $[M+H]^+$, observed 701.3250 $[M+H]^+$.

3.9. Conclusion:

Conformationally restricted anthranilic acid containing β-sheet breaker hybrid peptidomimetics were established as potent inhibitors against Alzheimer's Aβ peptide aggregation.[118] Further in chapter 2, we designed and synthesized novel peptidomimetics by incorporating various isomers of aminobenzoic acid in $hIAPP_{22-27}$ at I26 position, and the resulting peptide construct turned out to be effective inhibitors and disruptors of preformed hIAPP amyloid. However, to increase the effectiveness of modulation in hIAPP aggregation, we decided to develop a new strategy by incorporating the same moiety at two positions, i.e., at G24 and I26 in $hIAPP_{22-27}$. Hence, we have used the three different isomers of aminobenzoic acid at the two positions and observed that ortho (2-Abz) and meta (3-Abz) isomer containing BSBHps were highly effective inhibitors against the amyloid formation of hIAPP than the single mutant peptidomimetics. However, the para (4-Abz) isomer containing

BSBHp did not act as an inhibitor; instead, it enhanced the aggregation process like its single mutant analog. We have also observed that these double breaker containing BSBHps more efficiently disrupted the preformed amyloid of hIAPP into non-toxic fragments *in vitro* as confirmed by membrane leakage assay. Further, the double breaker comprising BSBHps were found to be more stable than the single mutant one in the presence of proteolytic enzymes. Hence, these results can be used as a scaffold for drug design against T2D and other amyloid-related diseases.

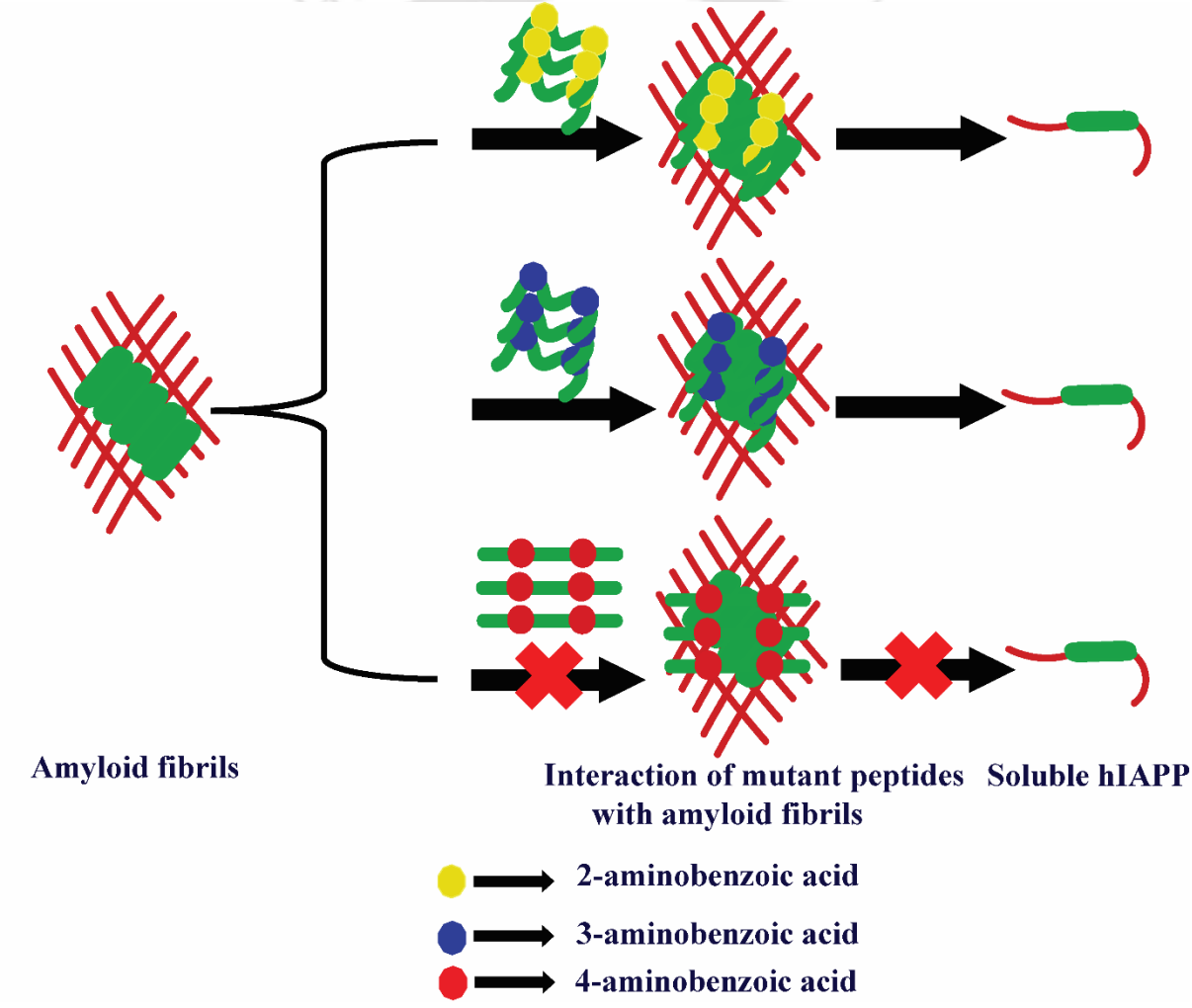

Figure 3.29: Effectiveness in the inhibition and disruption process of hIAPP amyloid by doubly mutated BSBHps.

Chapter 4: Investigation of anti-amyloid activity of peptidomimetics designed by single point mutation by rigid β-amino acid in hIAPP$_{8-37}$ at different positions

4.1. Proposed hypothesis:

In our earlier chapters (Chapter 2 and 3), we have discussed that most of the reported β-sheet breaker hybrid peptides (BSBHPs) contained breaker elements within the recognizing sequences , which included proline,[122] α-aminoisobutyric acid,[110] N-methylated amino acid,[106] and dehydrophenylalanine.[112] Further, we have demonstrated in chapters 2 and 3 that some of the BSBHps incorporating different isomers of aminobenzoic acid in the core hydrophobic region of hIAPP$_{22-27}$ were highly efficient in inhibiting the hIAPP aggregation.[144] However, among the different isomers, 2-aminobenzoic acid or anthranilic acid (Ant) was the best breaker element, and 4-aminobenzoic acid did not act as an inhibitor, rather, the latter enhanced the aggregation process. [144] This effect might be due to the favourable kink formation ability of 2-aminobenzoic acid (Ant) in the sequence. As the conformational rigidity is higher in the anthranilic acid moiety due to the fixed dihedral angle ($\Phi = 0°$), we selected Ant as the β-breaker element inside the peptide backbone.[116-118] Furthermore, the Ant moiety prefers the formation of either a turn or a helical conformation while inserted in the peptide sequence.[119]

Raleigh *et al*. reported that insertion of a single proline in the hydrophobic region of hIAPP emerges the resulting peptide construct as a highly efficient inhibitor.[98] Further, Pramlintide (PM), containing three proline residues in the sequence of hIAPP has been accepted for clinical trials, but due to several drawbacks, including poor solubility, which prevent itself

co-formulation with insulin especially at physiological pH, it failed to emerge as a successful drug candidate.[87] Moreover, one of the significant drawbacks of peptides-based therapeutics is that they are highly susceptible to degradation in the presence of proteolytic enzymes.[139] However, presenting β-amino acids over the α-amino acids into the peptide sequence increases the stability of peptides towards proteolytic degradation.[144]

It is well-known from previous reports that the core hexapeptide (hIAPP$_{22-27}$) is highly amyloidogenic and significant driver for hIAPP aggregation in T2D pathology. Also, G24 and I26 within the core hydrophobic region were the critical residues for hIAPP amyloid formation.[106,107] We, therefore, targeted the hydrophobic core region and designed two peptidomimetics by a single point mutation with Ant at those sites (i.e., G24Ant and I26Ant) within full-length hIAPP$_{8-37}$. In our earlier chapters, we have described that the Ant containing small BSBHPs was effective in inhibiting the aggregation of hIAPP and disrupted its preformed fibrillar structures at comparatively higher doses (10-fold molar ratios). As these BSHBps consists of non-coded β-amino acid, Ant, they were found to be proteolytically stable.[144] But due to the smaller size and deficiency of residual interaction, these BSBHps may not be efficient in binding with the aggregating hIAPP, which might be the reason for the requirement of a higher dose for the inhibition or disruption of hIAPP aggregation.

The inhibition mechanism is not understood entirely yet; however, it is believed that inhibitors binding with the growing fibrillar assembly of the aggregating proteins is essential for showing its inhibition effect. However, the small BSBHPs could not bind with the full-length aggregating hIAPP effectively due to its smaller size; subsequently, a higher dose was required for its inhibition. Therefore, it was believed that a single point mutant of a long sequence of hIAPP might bind more effectively than a small sequence of hIAPP.[61,98] Therefore, we planned to develop a modified set of peptidomimetics, which comprises of a

single point mutant of hIAPP$_{8-37}$ at different positions, expecting to exhibit its inhibitory efficiency at lower fold molar ratios compared to the small fragment of hIAPP$_{22-27}$ (Scheme 4.1)

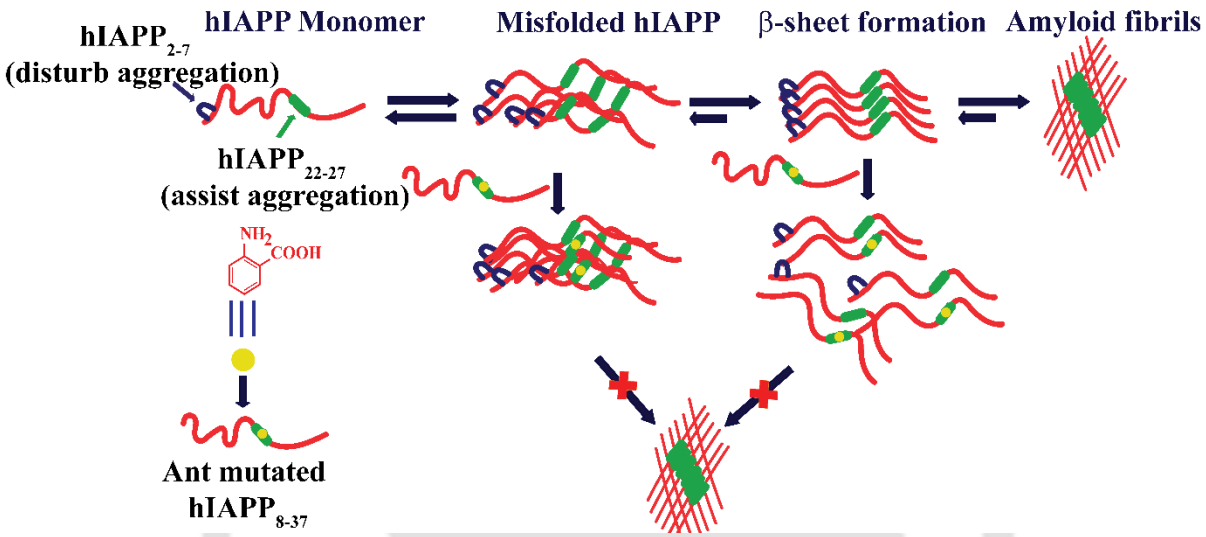

Scheme 4.1: Schematic representation of hIAPP aggregation and proposed hypothesis for the inhibition process of amyloid formation by single point mutated hIAPP$_{8-37}$.

4.2. Design of peptides:

For the present study, we have synthesized hIAPP$_{8-37}$, without any breaker element (**4A**, Table 4.1), to substantiate its property to form fibril similar to hIAPP$_{1-37}$. We initiated our design from eighth residues, as hIAPP$_{2-7}$ contains a disulfide bridge which impose conformational restrictions on the first seven residues, due to which this segment of hIAPP is not involved in β-sheet formation.[61] Further, keeping the above idea in mind, we have designed and synthesized two peptidomimetics by inserting anthranilic acid (Ant) in the hIAPP$_{8-37}$ sequence at two positions (at G24 for **4B** and I26 for **4C**) to prove our hypothesis. These two selected positions belong to the core hydrophobic region, which is primarily responsible for hIAPP aggregation.

A diverse family of peptide-based inhibitors has been reported using the hIAPP$_{20-29}$ fragment.[61,106,145] Moreover, proline as a mutant in the specific sequence may cause the non-amyloidogenic nature of rat amylin.[57] So, for this present study, we selected this particular sequence of hIAPP$_{8-37}$ for incorporation of the breaker elements. Moreover, we also designed a control peptidomimetic inserting the same breaker element in the hIAPP$_{22-27}$ smaller sequence (at I26 as **4D**).

Table 4.1: Sequences of all the Synthesized Peptides for the Present Study

Code	Sequence	Functions
4A	^{8}ATQRLANFLVHSSNNFGAILSSTNVGSNT^{37}Y	Aggregating
4B	^{8}ATQRLANFLVHSSNNF**X**AILSSTNVGSNT^{37}Y	Breaker
4C	^{8}ATQRLANFLVHSSNNFGA**X**LSSTNVGSNT^{37}Y	Breaker
4D	^{22}NFGA**X**^{27}L	Control/Breaker

Note: Standard amino acids are represented by one letter code, X= Anthranilic acid (Ant).

4.3. Synthesis and characterization of the designed peptides:

All the designed peptides were synthesized by standard solid-phase peptide synthesis (SPPS) method using Fmoc/t-Bu strategy on Rink Amide MBHA resin as the solid support (described in Chapter 6, section 6.4)[129,130]. However, in this case, instead of BOP, 2.5 equivalent of o-NosylOXY as a coupling reagent was used for the amino acid coupling. The designed peptidomimetics were purified by reverse phase HPLC and purity was confirmed by analytical HPLC and MALDI-TOF mass spectrometry. A representative example of the synthetic protocol of **4B** has been depicted in scheme 4.2. All other peptides were synthesized in a similar process. The characterization data for the synthesized peptides have been shown below (Figure 4.1-4.8).

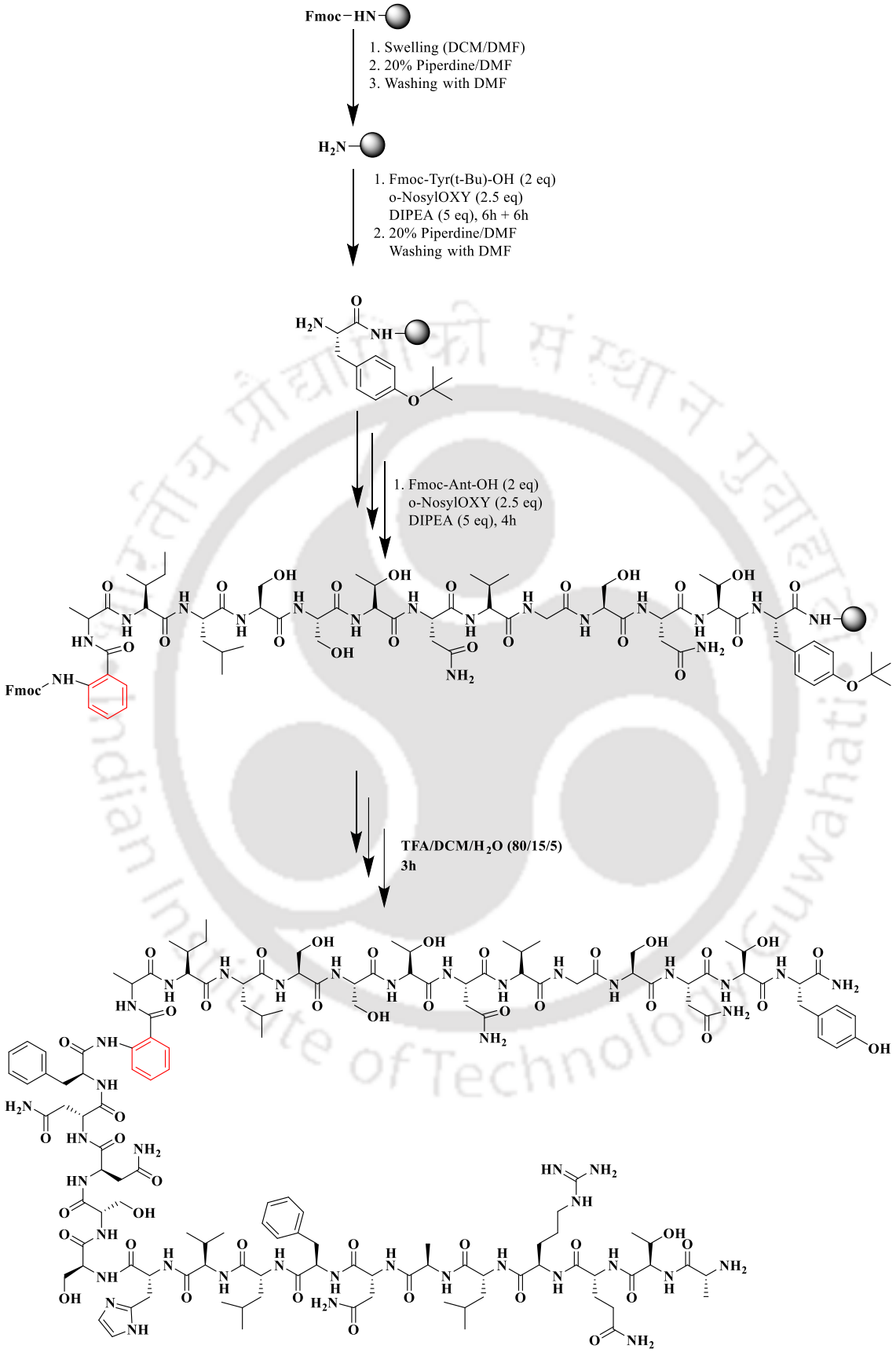

Scheme 4.2: The synthetic scheme of peptide **4B.**

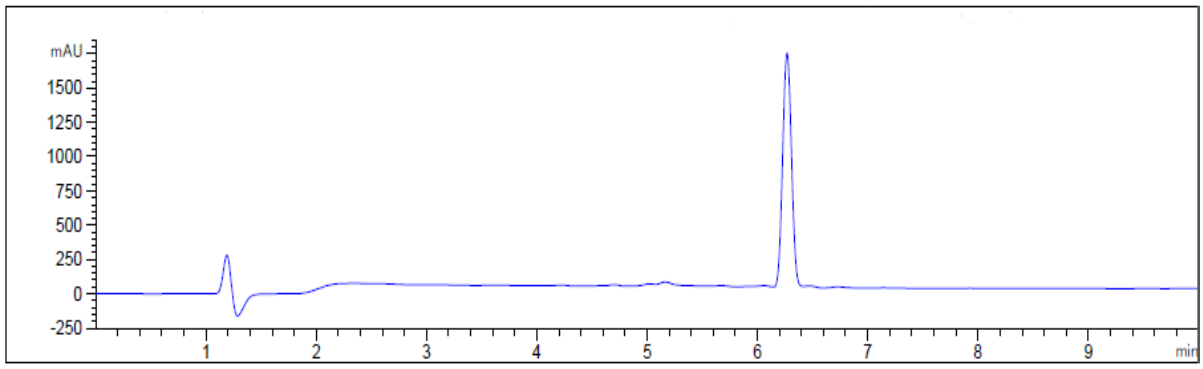

Figure 4.1: RP-HPLC profile of purified peptide **4A.**

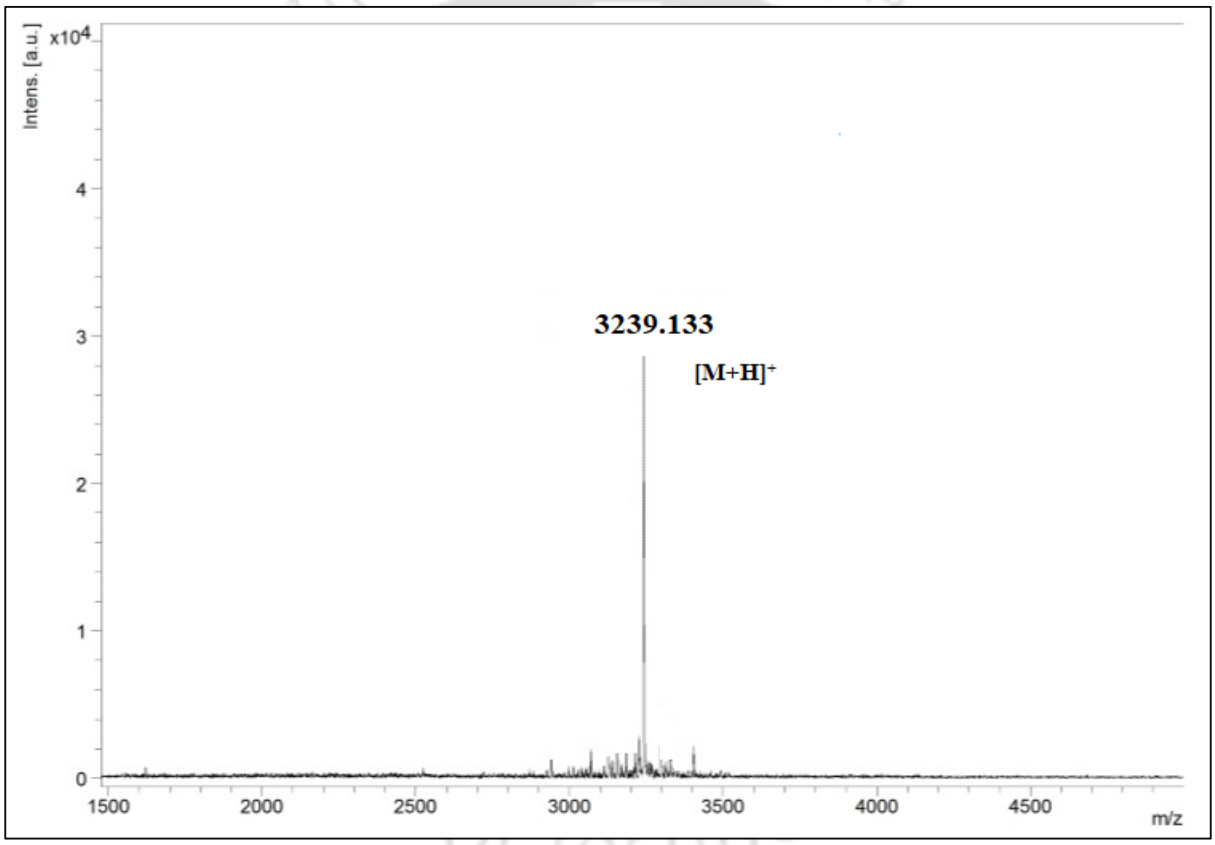

Figure 4.2: MALDI-TOF mass spectrum of peptide **4A**. The calculated mass for $C_{140}H_{219}N_{43}O_{46}$ is 3239.119 $[M+H]^+$; the observed mass is 3239.133 $[M+H]^+$.

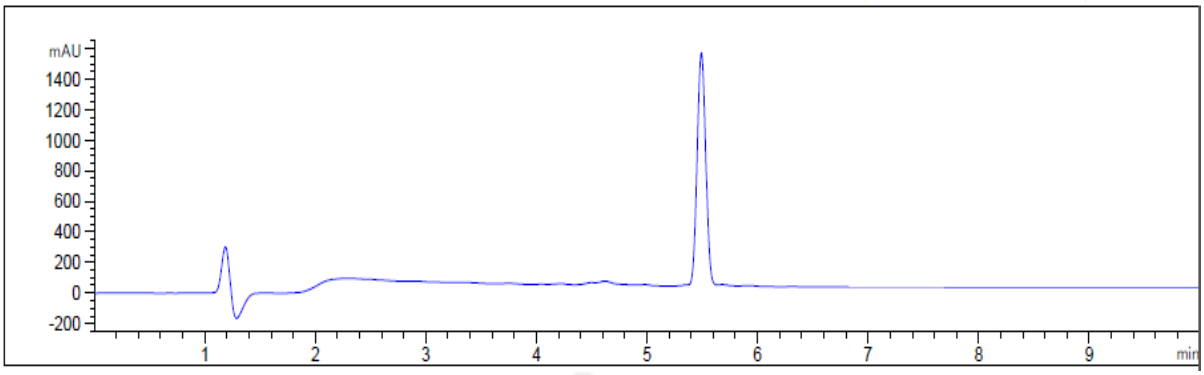

Figure 4.3: RP-HPLC profile of purified peptide **4B**.

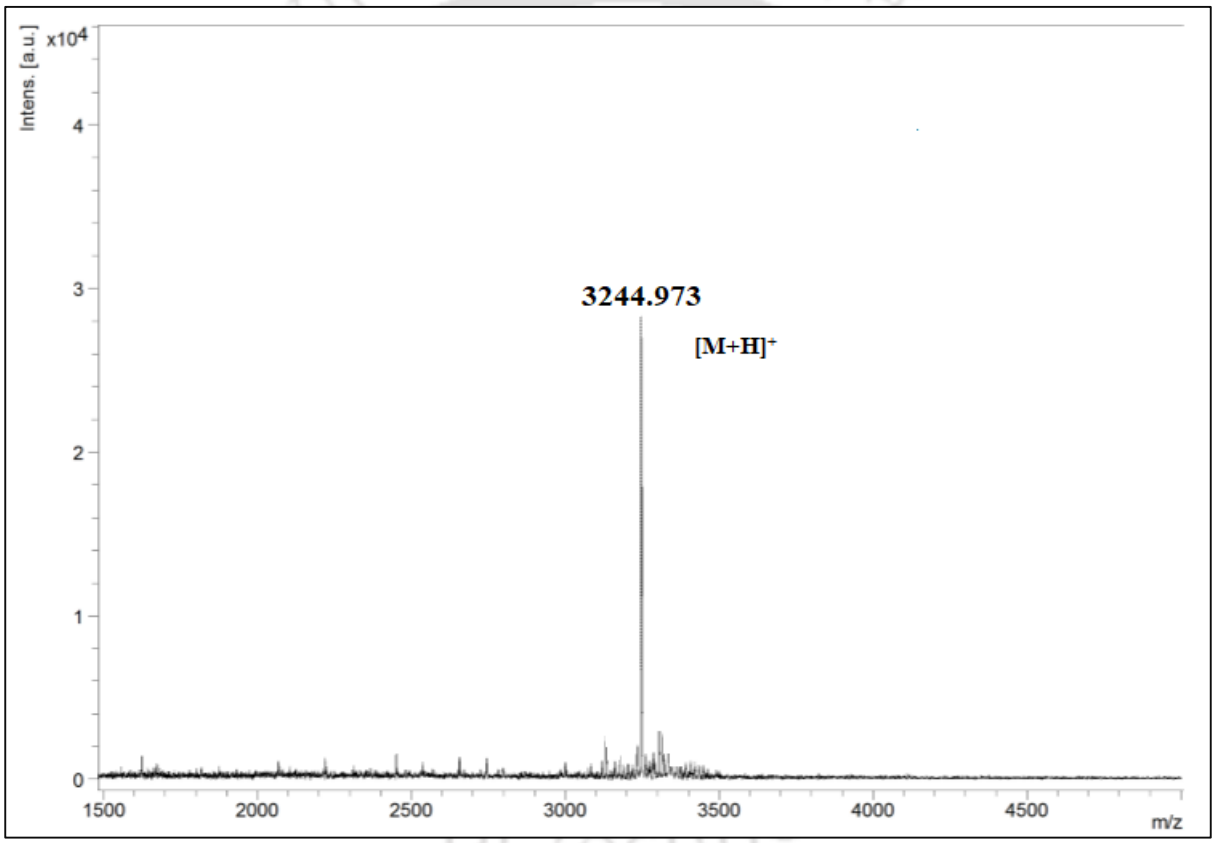

Figure 4.4: MALDI-TOF mass spectrum of peptide **4B**. Calculated mass for $C_{143}H_{218}N_{42}O_{45}$ is 3244.613 $[M+H]^+$, the observed mass is 3244.973 $[M+H]^+$.

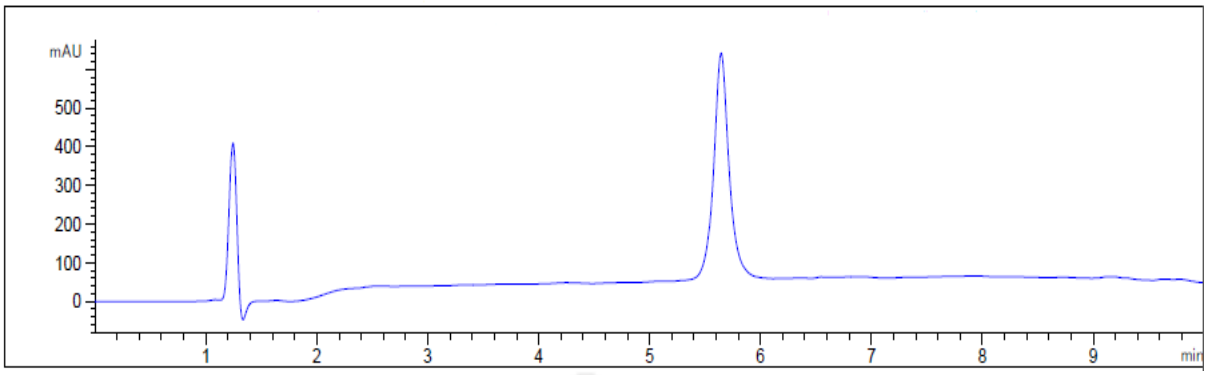

Figure 4.5: RP-HPLC profile of purified peptide **4C**.

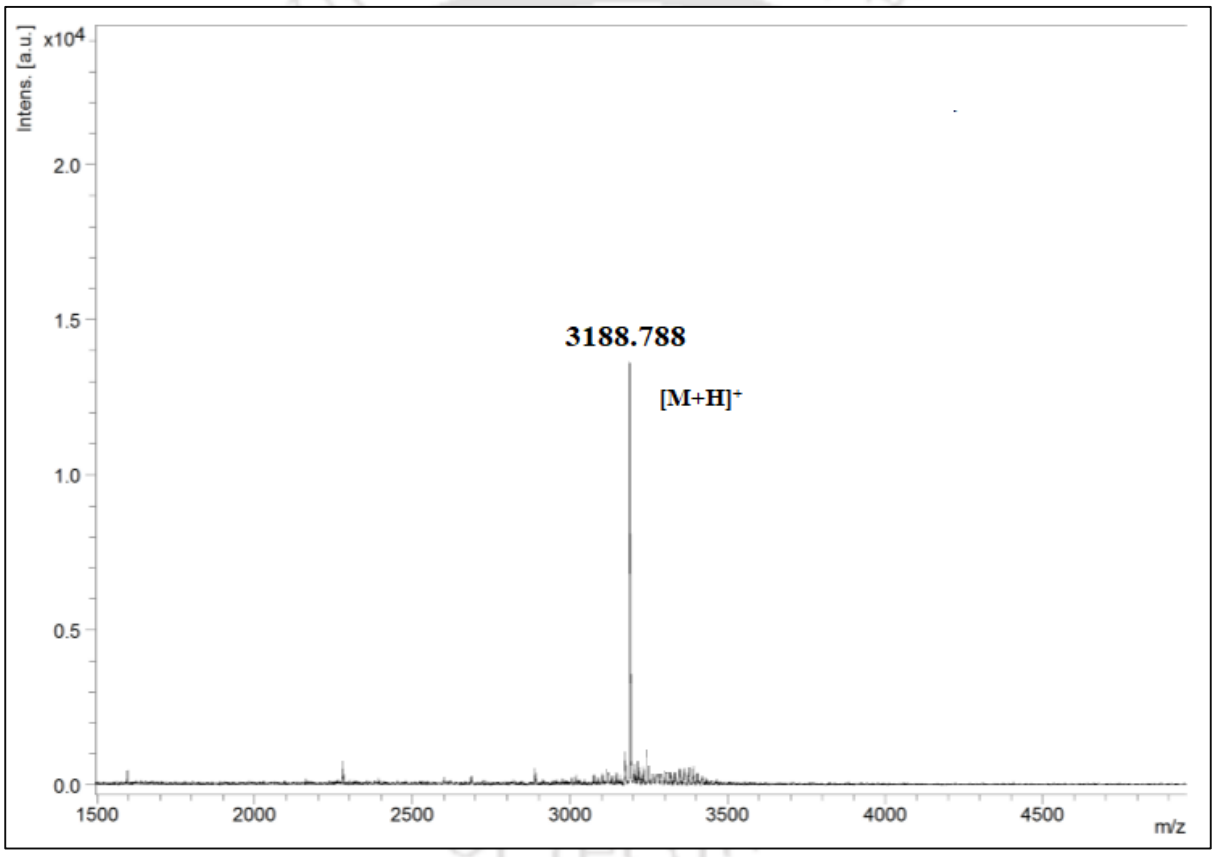

Figure 4.6: MALDI-TOF mass spectrum of peptide **4C**. Calculated mass for $C_{139}H_{210}N_{42}O_{45}$ is 3188.551 $[M+H]^+$, the observed mass is 3188.788 $[M+H]^+$.

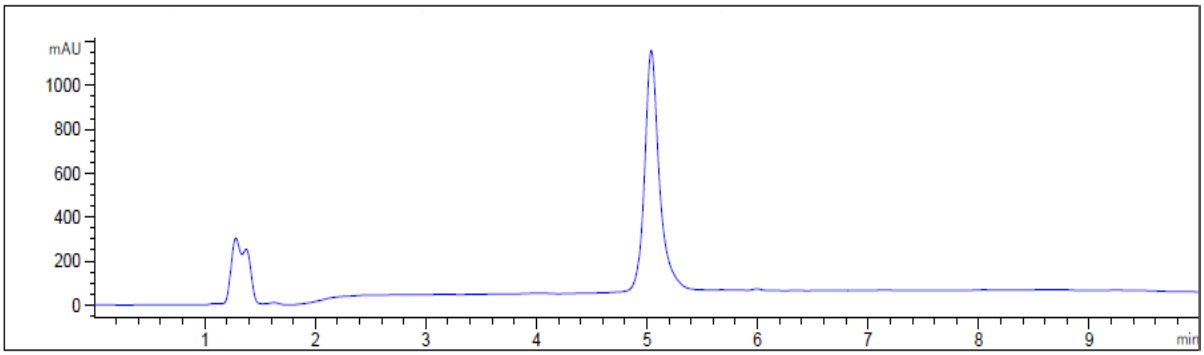

Figure 4.7: RP-HPLC profile of purified peptide **4D**.

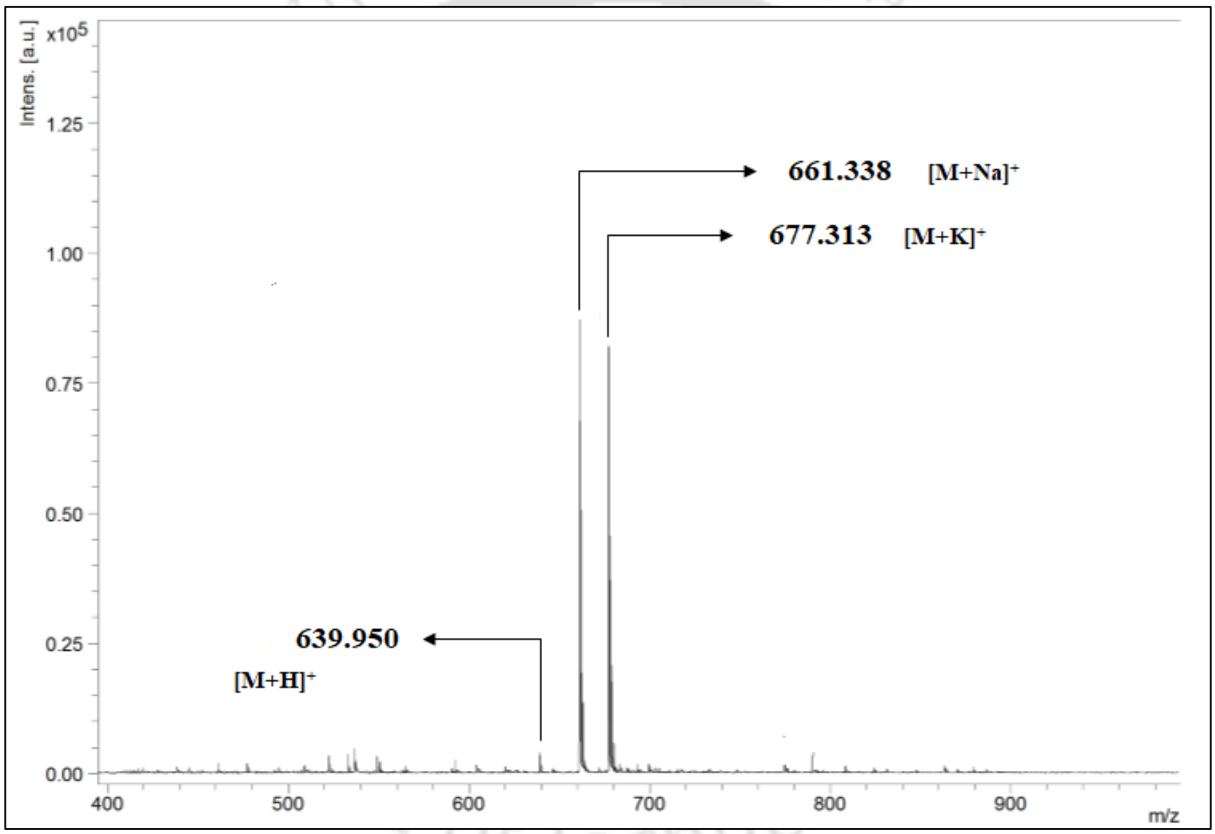

Figure 4.8: MALDI-TOF mass spectrum of peptide **4D**. Calculated mass for $C_{31}H_{42}N_8O_7$ is 639.325 $[M+H]^+$, the observed mass is 639.950 $[M+H]^+$, 661.338 $[M+Na]^+$, 677.313 $[M+K]^+$.

4.4. Non-amyloidogenic nature of the synthesized polypeptides:

Before monitoring the inhibition efficiency of the peptides, it is necessary to examine the amyloidogenic nature of the synthesized polypeptides. Therefore, initially, we wished to check the amyloidogenic behavior of the BSBHPs using various biophysical tools.

4.4.1. Conformational characterization of BSBHPs by CD and FTIR studies:

At first, we analyzed the conformational state of the synthesized polypeptides using circular dichroism (CD) and Fourier transform infrared (FTIR) spectroscopy. For this study, all the purified peptides were dissolved in PBS (50 mM, pH 7.4) to acquire 40 μM concentration and kept in incubation at 37 °C. After five days of incubation, the change in conformation of the peptides was monitored using CD and FT-IR. In CD, peptide **4A** showed a positive band at ~195 nm and a simultaneous negative band centered at ~225 nm (Figure 4.9 (a)), indicating β-sheet rich conformation for the peptide **4A**. On the other hand, in the CD spectrum of the other three peptides, i.e., **4B**, **4C**, and **4D**, the specified β-sheet conformation was not observed ; instead, a negative band at ~195 nm was observed indicating random coil rich conformation. Similarly, in FTIR analysis of **4A** peptide, we detected an amide I band at 1639 cm^{-1} (Figure. 4.9 (b)), suggesting the existence of β-sheet conformation.[23] However, the amide I band shifted up to 1650 cm^{-1}, 1651 cm^{-1} and 1653 cm^{-1}, respectively, for peptides**4B**, **4C**, and **4D** as observed from the FTIR analysis, suggesting the non-amyloidogenic nature of the peptides.[23] Hence, from the above studies, it is evident that peptide **4A**, which lacks the turn inducing moiety, anthranilic acid (Ant), is highly amyloidogenic; however, peptides **4B**, **4C**, and **4D**, which contain one Ant moiety in the sequence, restricts the formation of amyloids at physiological conditions.

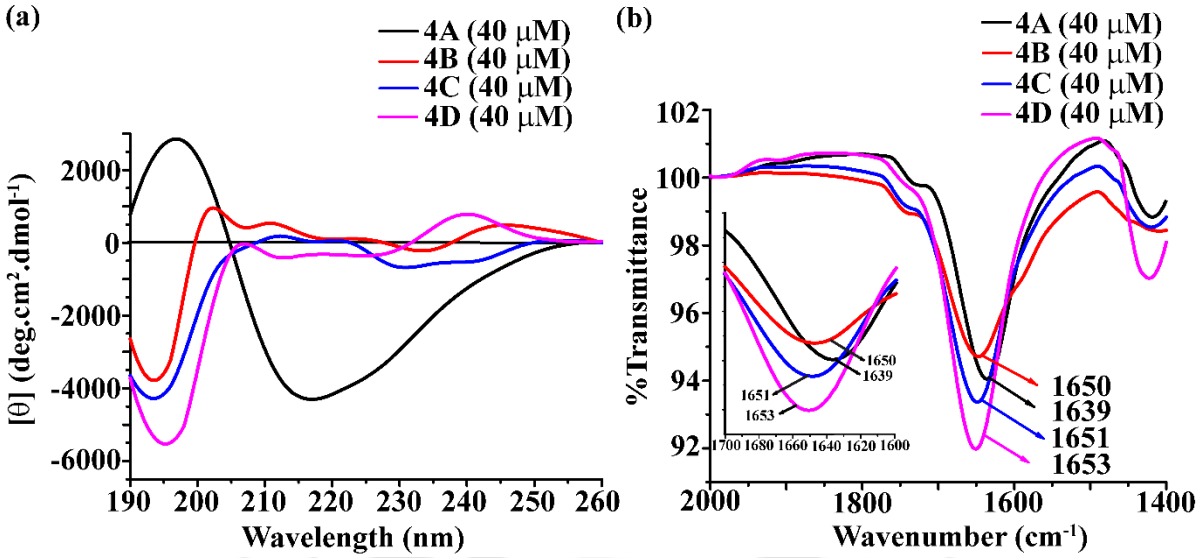

Figure 4.9: (a) CD and (b) FTIR spectra of peptide **4A** (black), **4B** (red) **4C** (blue) and **4D** (magenta). Spectra were recorded after five days of incubation of the peptides in PBS (50 mM) at pH 7.4 and 37 °C.

4.4.2. Amyloidogenic characterization of the synthesized peptides by TEM and Congo red stained birefringence studies:

From the conformational analyses, we observed that only peptide **4A** exhibited β-sheet rich conformation. On the other hand, peptides **4B**, **4C**, and **4D** exist in random coil-rich conformation at physiological conditions. Further, to investigate the amyloidogenic nature of the peptides, we carried out TEM and Congo red stained birefringence studies.

After five days of incubation, 10 μL aliquot of the peptide solution was taken out from the stock solution (as described in section 4.4.1). For TEM and Congo red stained birefringence studies, samples were prepared as discussed in chapter 2, section 2.5.2. Peptide **4A** (Figure. 4.10 (a) (i)) exhibited a transparent network of fibrillar assembly under TEM, indicating the formation of amyloid at physiological conditions. However, peptides **4B**, **4C**, and **4D** (Figure. 4.10 (a) (ii), (iii) and (iv) respectively) did not exhibit any such fibrillar assembly under TEM, indicating their non-amyloidogenic nature at the same condition.

From Congo red stained birefringence study, too, peptide **4A** (Figure. 4.10 (b) (i)) under cross-polarised light exhibited green-gold birefringence, indicating the formation of amyloid by the peptide. On the other hand, peptides **4B**, **4C**, and **4D** (Figure. 4.10 (b) (ii), (iii) and (iv) respectively) did not exhibit such characteristic birefringence under cross-polarised light suggesting the non-amyloidogenic nature of the peptides. Hence, from the above studies, it is evident that **4B**, **4C**, and **4D** cannot form amyloid at physiological conditions; however, peptide **4A** which lacks turn inducer like anthranilic acid is highly amyloidogenic similar to hIAPP.

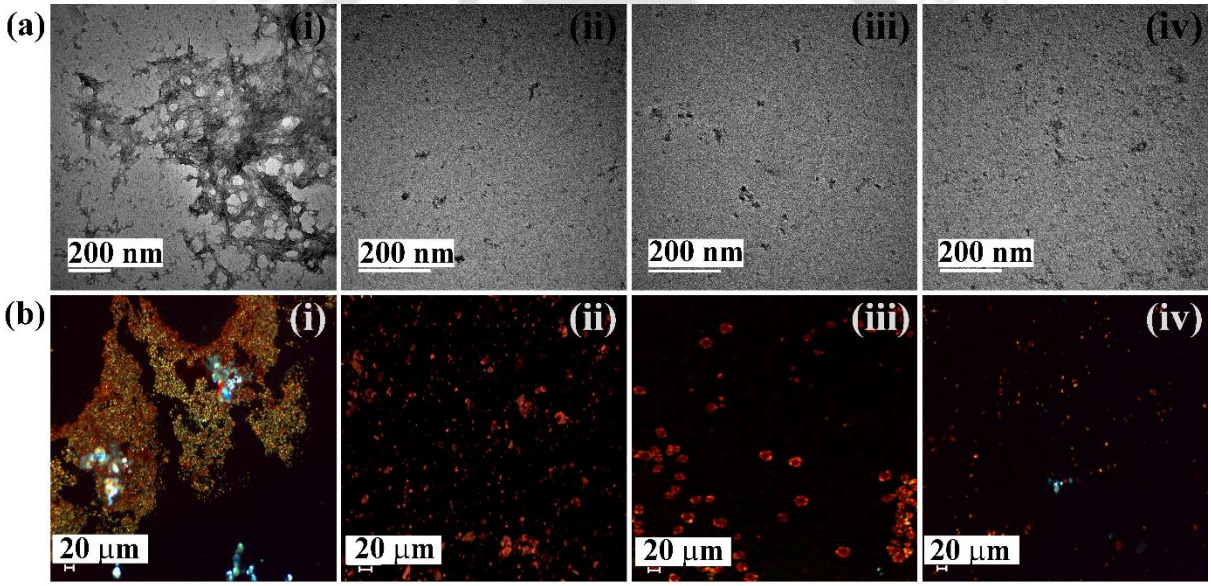

Figure 4.10: (a) TEM and (b) Congo red-stained birefringence images of peptide **4A** (i), **4B** (ii), **4C** (iii) and **4D** (iv). Images were taken after five days of incubation of the peptides in PBS (50 mM) at pH 7.4 and 37 °C.

4.5. Inhibition of amyloid formation of hIAPP by synthesized polypeptides:

To explore the potential of inhibiting the single anthranilic acid (Ant) mutant hIAPP$_{8-37}$ and comparing the consequences with the single Ant mutant hIAPP$_{22-27}$ as a control, we performed several biophysical experiments in the presence or absence of the peptidomimetics. In the earlier study mentioned above, peptide **4A** was amyloidogenic at

physiological conditions; hence we excluded it from further studies. Wild type hIAPP$_{1-37}$ at a concentration of 40 μM was incubated alone and in the presence of the peptidomimetics at 2-fold molar ratios in PBS at physiological conditions in a water bath up to 7 days and thereafter, the kinetics of amyloid formation of hIAPP and its subsequent inhibition by the designed peptidomimetics were monitored by various biophysical tools.

4.5.1. Monitoring conformational transitions by CD and FTIR studies:

Initially, we wished to check the change in conformation of the aggregating peptide, hIAPP, in the absence and presence of the single mutant polypeptides. To carry out the conformational study, we prepared four different sets of solutions, where the concentration of hIAPP was maintained at 40 μM in each set. In the first set, only hIAPP was present in PBS (50 mM) at pH 7.4, while in the other sets, hIAPP was mixed with the single mutant polypeptides in a molar ratio of 1:2, maintaining the same concentration of hIAPP. Each set contained two replicate solutions. All the different sets were prepared in PBS (50 mM) at pH 7.4 and incubated on a water bath at 37 °C for seven days and checked the conformational change of hIAPP (40 μM) in the absence and presence of 80 μM of the polypeptides using CD and FTIR studies (Figure 4.11).

After seven days of incubation, hIAPP displayed a negative band at ~220 nm and a simultaneous positive band at ~195 nm, in the CD spectrum, indicating β-sheet rich conformation of the aggregating peptide (black, Figure 4.11). On the other hand, in the presence of 2-fold molar ratios of **4B** and **4C**, we did not observe such characteristic band for β-sheet conformation; rather, we observed a mixture of conformations. In the presence of the control peptidomimetic, **4D** also, we observed some inhibitory efficaciency, however, the extent of inhibition was far less compared to that of 4B and 4C.

Further, in the FT-IR spectrum, when hIAPP was present alone, we observed a strong amide I band at 1633 cm^{-1}, which indicated β-sheet rich conformation of the peptide after incubation of 7 days. On the contrary, in the presence of **4B** and **4C** in 2-fold molar ratios, the amide I band shifted up to 1655 cm^{-1} and 1659 $cm^{-1,}$ respectively, which indicated significant inhibition of hIAPP in the presence of the breaker peptides. However, in the presence of same fold molar ratio of **4D** also, the amide I band shifted up to 1658 cm^{-1}, indicating inhibition of aggregation of hIAPP by the control peptide.

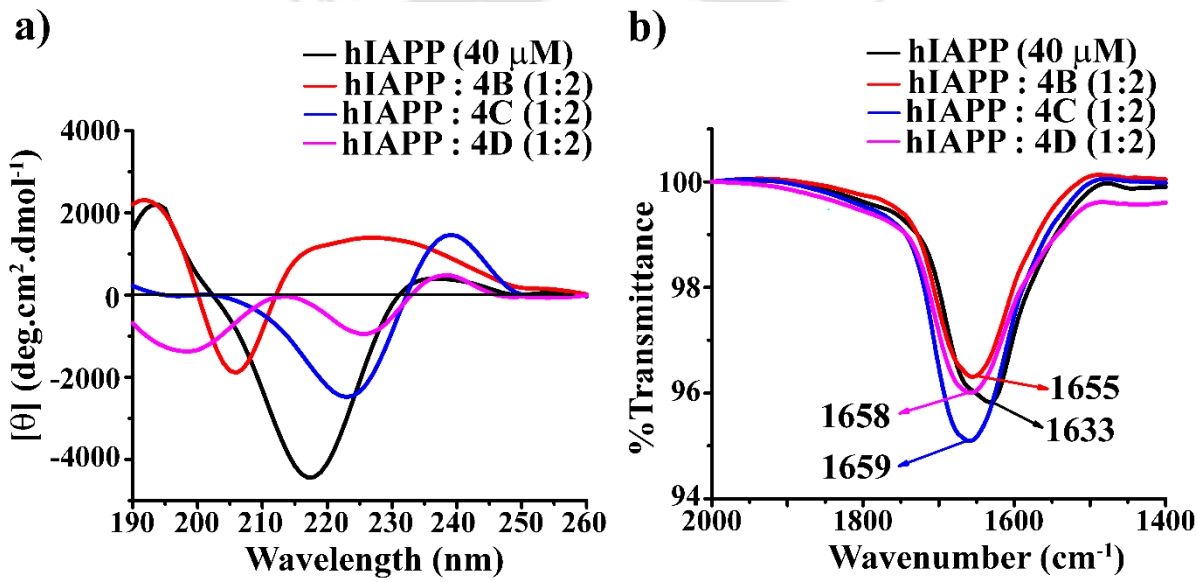

Figure 4.11: (a) CD and (b) FTIR spectra of hIAPP alone (black) and in co-incubation with 2 fold molar ratios of peptidomimetics **4B** (red), **4C** (blue) and **4D** (magenta). Spectra were recorded after seven days of incubation of the peptides in PBS (50 mM) at pH 7.4 and 37 °C.

4.5.2. Monitoring the kinetics of amyloid formation and its subsequent inhibition by ThT fluorescence assay:

The fluorescence intensity of a sample upon binding with Thioflavin T (ThT) provides quantitative information about the amount of fibril formed by the aggregating peptide.[23] Hence, from the ThT based fluorescence study, it can be inferred that as the fluorescence intensity increases, the amount of amyloid in the peptide solution also increases. A ThT

fluorescence assay was performed to monitor the kinetics of amyloid formation of hIAPP and its inhibition process by the synthesized polypeptides. As mentioned earlier, we wished to investigate the inhibitory efficiency of the peptides in lower doses (i.e. hIAPP:peptidomimetics = 1:0.5, 1:1 and 1:2) than used in case of the former BSBHPs. To carry out this study, we prepared four different sets of solutions, where the concentration of hIAPP was maintained at 40 μM in each set. In the first set, only hIAPP was present in PBS (50 mM) at pH 7.4, while in the other three sets hIAPP was mixed with the single mutant polypeptides in a molar ratio of 1:0.5, 1:1 and 1:2, maintaining the same concentration of hIAPP and incubated the samples at 37 °C in PBS at pH 7.4 up to 7 days. The same procedure was followed to carry out the fluorescence assay, as discussed in chapter 2, section 2.6.2. The data received from the software was transferred to an excel file and using these data, graphs were plotted using OriginPro 8 software. We have prepared two sets of samples for each measurement, and three readings were scanned separately for each set. Thus, an average of six readings was taken and plotted as F/F_0 along the y-axis (where, F= average fluorescence value of the samples at time t, F_0= fluorescence value of the reference in the absence of sample at time t) against time (h) along the x-axis with observed standard deviation set as y-error.

From the same study, the relative % of amyloid present in the sample was also calculated at the highest incubation time, i.e., at 132h for the inhibition study and 144h for the disruption study using the following formula.

$$\%\ \text{of amyloid} = \frac{(\text{Observed fluorescence in the presence of the peptide} - 1)}{(\text{Observed fluorescence in the absence of the peptide} - 1)} \times 100\ \%$$

where 1 was considered as a normalization factor, as the minimum value of F/F_0 is 1.

From the time-dependent ThT assay, we observed that the fluorescence intensity increased with time when hIAPP (black; Figure 4.12 (a)) was present alone in thesolution. However, in the presence of 2-fold molar ratios of **4B** (red; Figure 4.12 (a)) and **4C** (blue; Figure 4.12 (a)), the fluorescence intensity suppressed significantly, up to 75-78%, indicating inhibition of amyloid fibrillization. On the contrary, in the presence of the same molar ratios of the control peptide **4D** (magenta; Figure 4.12 (a)), very little inhibition of hIAPP aggregation was observed.

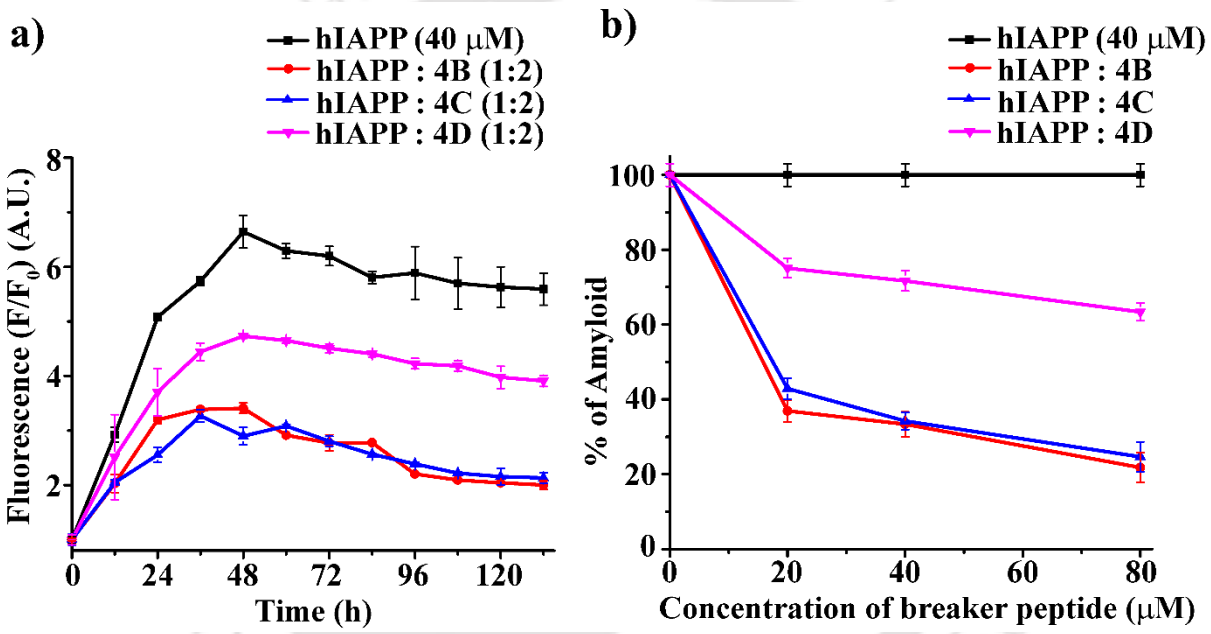

Figure 4.12: (a) Time dependent ThT fluorescence assay of hIAPP (40 μM) alone (black) and in co-incubation with 2-fold molar ratios of **4B** (red), **4C** (blue) and **4D** (magenta). (b) Dose dependent ThT fluorescence assay at 132h of hIAPP (40 μM) alone (black) and in co-incubation with different molar ratios of **4B** (red), **4C** (blue) and **4D** (magenta).

From the dose-dependent study of inhibition, it was observed that 0.5-, 1, and 2-fold molar excesses of **4B** (Figure 4.12 (b) and 4.13) exhibited 63%, 66%, and 78% of inhibition, while the same doses of **4C** (Figure 4.12 (b) and 4.13) exhibited 57%, 65% and 75% of inhibition of hIAPP aggregation respectively. In the presence of the control peptide **4D** (Figure 4.12 (b) and 4.13), we observed 24%, 28%, and 36% of amyloid inhibition, respectively, with the

same molar doses. Hence, an increase in doses of the peptidomimetics with respect to hIAPP suppresses the fluorescence intensity and increases the percentage of amyloid inhibition. However, peptidomimetics **4B** and **4C** were highly efficient in inhibition over the control peptide **4D** as observed from the ThT fluorescence assay.

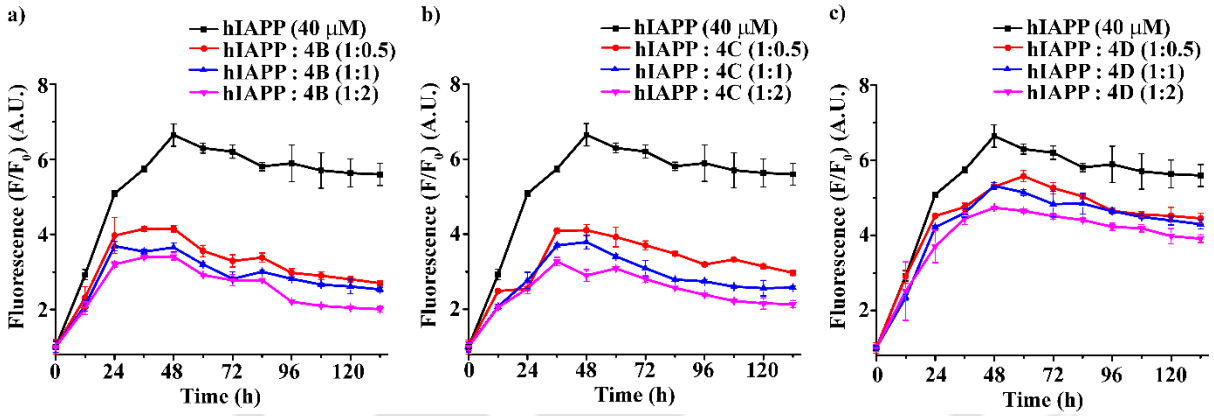

Figure 4.13: Time dependent ThT fluorescence assay of hIAPP (40 μM) alone (black) and in co-incubation with 0.5-(red), 1-(blue) and 2-fold (magenta) molar ratios of a) **4B**, b) **4C** and c) **4D**. Spectra were recorded at an interval of 12 hrs after incubation in PBS (50 mM) at pH 7.4 and 37 °C.

Further, we checked the ThT fluorescence assay of the Ant containing peptides alone and compared with that of the hIAPP peptide at physiological condition. From the study, it was observed that the fluorescence intensity increased with time for the only hIAPP sample, however, no increment in fluorescence intensity was observed for the Ant mutant peptides (4B and 4D), indicating non-aggregating as well as non-interference in the ThT assay.

4.5.3. Monitoring amyloid formation by TEM and Congo red stained birefringence studies:

The existence of fibrillar structures under transmission electron microscope (TEM) and the occurrence of green-gold birefringence of Congo red stained peptide sample under cross-polarised light gives direct evidence of amyloid formation. After seven days of incubation of the peptide solution at 37 °C in 50 mM PBS of pH 7.4, 10 μL aliquot of the peptide solution

was taken out from the stock solution (as described in section 4.5) for TEM analysis (sample preparation was described in chapter 2, section 2.5.2). When hIAPP was incubated alone, it exhibited clear fibrillar rich morphology (Figure 4.14 (a) (i)) when viewed under TEM, indicating amyloid formation by hIAPP. On the contrary, hIAPP, when co-incubated with 2-fold molar ratios of **4B** (Figure 4.14 (a) (ii)) and **4C** (Figure 4.14 (a) (iii)), no such fibrillar assembly was detected, suggesting significant inhibition of hIAPP amyloid formation. However, in co-incubation with 2-fold molar excess of **4D** (Figure 4.14 (a) (iv)), some fibrillar structures were detected, indicating lower efficacy of 2 equivalent of the control peptidomimetic in the process of inhibition.

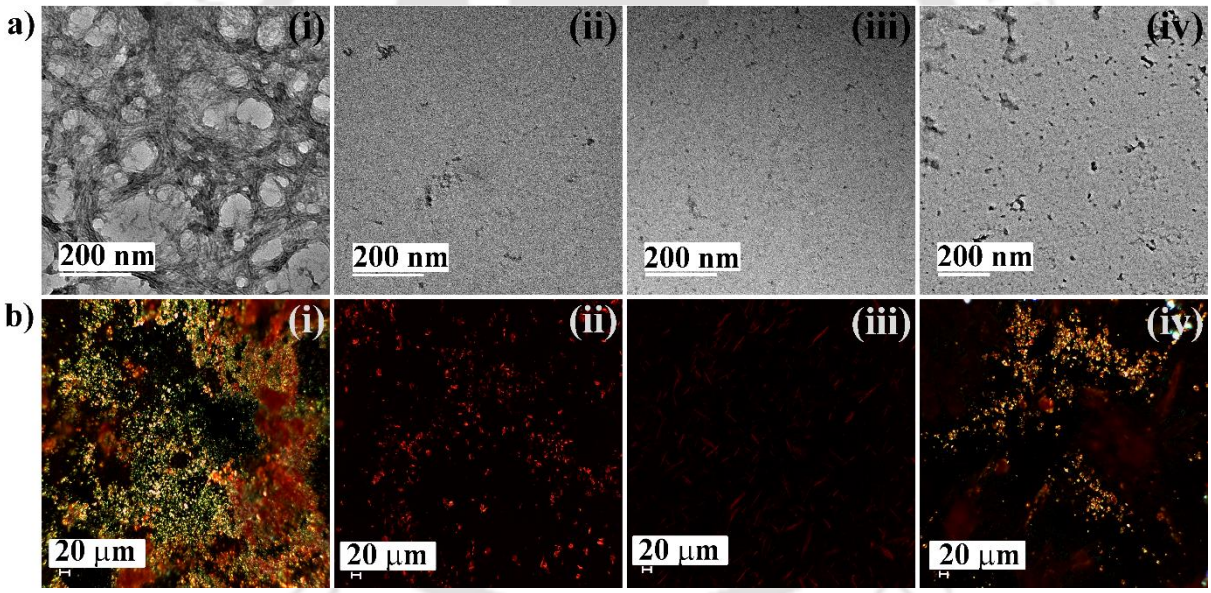

Figure 4.14: (a) TEM and (b) Congo red birefringence images of hIAPP (i) alone and in co-incubation with 2-fold molar ratios of peptidomimetics, **4B** (ii), **4C** (iii) and **4D** (iv). Images were captured after seven days of incubation of the peptides in PBS (50 mM) at pH 7.4 and 37 °C.

When hIAPP was incubated alone, we observed green-gold birefringence under cross-polarised light (Figure 4.14 (b) (i)), indicating the formation of amyloid by hIAPP under Congo red stained birefringence analysis. However, in co-incubation with 2-fold molar ratios of **4B** (Figure 4.14 (b) (ii)) and **4C** (Figure 4.14 (b) (iii)), no characteristic birefringence was noticed, which indicated the inhibitory efficiencies of the peptidomimetics. However, in the

presence of same fold molar ratio of **4D** (Figure 4.14 (b) (iv)) some characteristic birefringence was detected, indicating lower efficacy of the control peptidomimetic in inhibiting hIAPP aggregation to the expected mark.

Therefore, from the experiments described above, it can be inferred that **4B**, **4C**, and **4D** were capable of inhibiting the aggregation of wild-type hIAPP. However, among the peptidomimetics, **4B** and **4C** appeared to be far better inhibitors against the amyloid aggregation of hIAPP compared to the control peptide **4D**. Besides this, the biophysical studies revealed no remarkable difference in the behaviour of **4B** and **4C** in the inhibition process or upon the insertion of breaker element at the two specific positions of the recognizing sequence, as **4B** and **4C** differ only in the position of the breaker element (Ant), i.e., in G24X and I26X. Hence, we proceeded with further studies considering only **4B**, as **4B** and **4C** showed almost similar behaviour in the inhibition process of hIAPP.

4.6. Disruption of preformed amyloid fibrils of hIAPP by synthesized polypeptides:

The above experimental studies confirmed that single point anthranilic acid mutated hIAPP$_{8-37}$ impressively inhibited the aggregation of hIAPP. Hence, in our next step, we wished to examine the potential of the single mutant polypeptide in disrupting the preformed hIAPP amyloid *in vitro*. From the ThT fluorescence analysis (black, Figure 4.14 (a)), it was observed that for hIAPP, fibrillization attained the growth phase at around 45-50h at the mentioned condition. Therefore, to perform the disruption assay, we designed an experiment where hIAPP was incubated alone in PBS (50 mM) at physiological conditions (pH 7.4 and 37 °C) and added the peptidomimetics (**4B** and **4D**) into the hIAPP solution separately in different molar ratios (1:0.5, 1:1, and 1:2) similar to the previous studies. Thereafter, various biophysical tools was performed to monitor the disruption of the preformed hIAPP amyloid

by the single mutant peptidomimetics. The samples for the different studies were prepared in a similar way as in section 4.5.

4.6.1. Monitoring conformational transitions by CD and FTIR studies:

We performed the CD experiment after 7 (2+5) days of incubation, and from the analysis, we observed a negative band at ~218 nm and a simultaneous positive band at ~200 nm when hIAPP was incubated alone (Figure 4.15 (a)), indicating characteristic bands for β-sheet conformation. On the contrary, hIAPP in the presence of a 2-fold molar ratio of **4B** exhibited random coil conformation instead of the β-sheet conformation (Figure 4.15 (a)). But, hIAPP in the presence of the same molar ratio of the control peptide **4D** (Figure 4.15 (a)), β-sheet rich conformation existed predominantly. These results indicated the conversion of β-sheet into non-β-sheet conformation in the presence of **4B**, which supported the disruption efficiency of the preformed amyloid of hIAPP by **4B**. Nevertheless, in the conformational analysis with the control peptidomimetic **4D**, we did not observe such conversion of conformation, confirming its less efficiency in disruption of the same.

Further, after 7 (2+5) days of incubation, from the FT-IR analysis, hIAPP alone exhibited a sharp band at 1634 cm^{-1}, attributed to amide I band for aggregated β-sheet conformation (Figure 4.15 (b)). Again, in the presence of a 2-fold molar ratio of the designed peptidomimetic **4B**, the amide I band shifted up to 1654 cm^{-1}, which indicated effective disruption of preformed hIAPP amyloid. On the contrary, the control peptidomimetic **4D** shifted the band up to 1648 cm^{-1}, which implied certain amount of disruption of preformed amyloid (Figure 4.15 (b)).

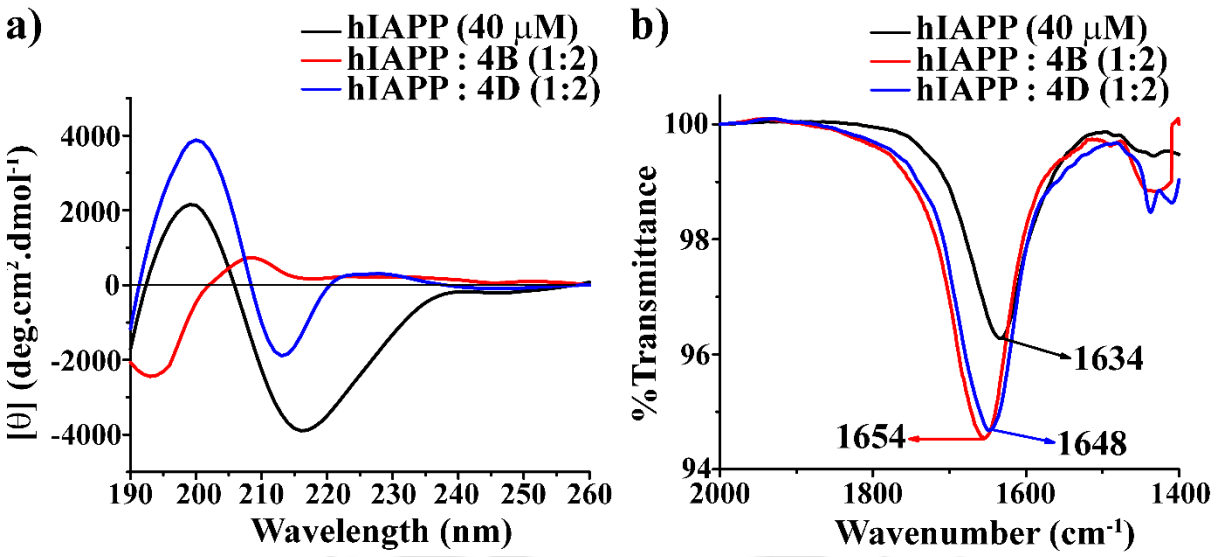

Figure 4.15: (a) CD and (b) FTIR spectra of hIAPP alone (black) and in co-incubation with 2-fold molar ratios of peptidomimetics **4B** (red) and **4D** (blue). Spectra were recorded after seven days of incubation of the peptides in PBS (50 mM) at pH 7.4 and 37 °C.

4.6.2. Monitoring the kinetics of amyloid disruption by ThT fluorescence assay:

After the CD and FT-IR analyses, we proceeded to perform the Thioflavin T (ThT) fluorescence assay, with which we wished to monitor the kinetics of amyloid formation by hIAPP and disruption of its preformed fibrils by the designed peptidomimetics. In this study, hIAPP was incubated alone at physiological conditions up to 48h, and after that, the breaker peptides at different molar ratios were added to the aggregated hIAPP solution. From the time-dependent ThT fluorescence assay, we observed an increment of fluorescence intensity with time for the sample where hIAPP was incubated alone. On the contrary, when hIAPP was co-incubated in the presence of 2-fold molar ratio of **4B**, the fluorescence intensity was suppressed noticeably up to 72% (red; Figure 4.16), indicating disruption of preformed hIAPP amyloids. However, in case where hIAPP was co-incubated in the presence of 2-fold molar ratio of the control peptide, **4D**, the fluorescence intensity decreased up to 38% only (blue; Figure 4.16) at the same time interval, indicating less efficiency in disruption of preformed amyloid in that molar ratio.

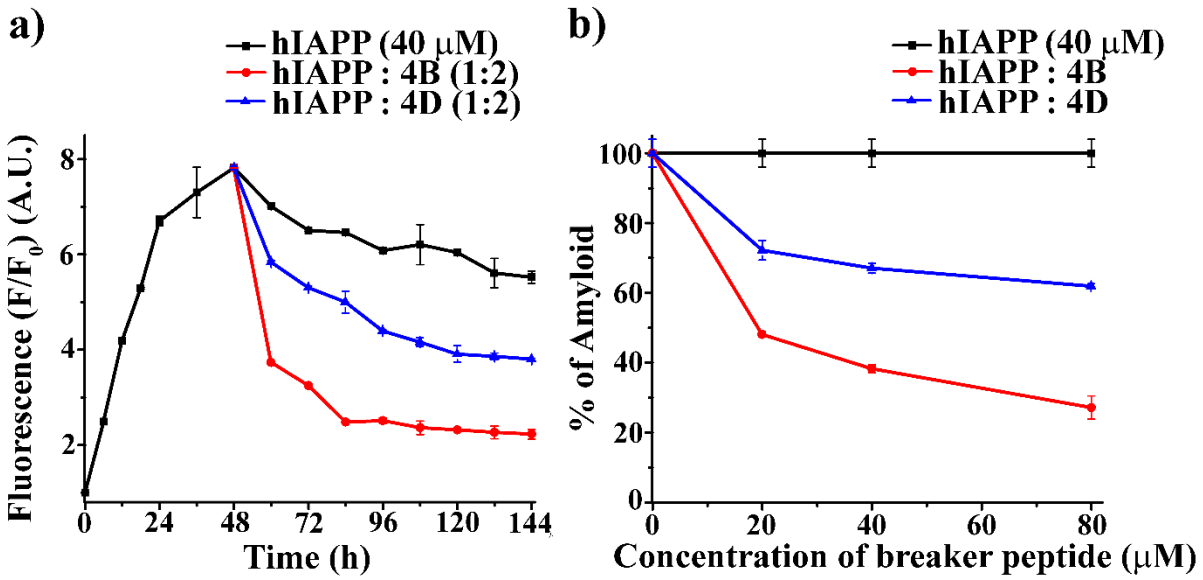

Figure 4.16: a) Time dependent ThT fluorescence assay of hIAPP (40 μM) alone (black) and in co-incubation with 2-fold molar ratios of peptidomimetics, **4B** (red) and **4D** (blue). (b) Dose dependent ThT fluorescence assay at 144h of hIAPP (40 μM) alone (black) and in co-incubation with different molar ratios of peptidomimetics, **4B** (red) and **4D** (blue). Spectra were recorded at an interval of 12 hrs after incubation in PBS (50 mM) at pH 7.4 and 37 °C.

Moreover, when varied (0.5, 1, and 2-fold) molar ratios of the peptides **4B** and **4D** were added to the existing hIAPP fibrillar assembly, the fluorescence intensity decreased gradually with time as the doses increased. To be more precise, we observed that 0.5-, 1- and 2-fold molar ratios of **4B** (Figure 4.16 (b) and 4.17) exhibited 51%, 61%, and 72% of disruption respectively, while the same doses of **4D** (Figure 4.16 (b) and 4.17) exhibited 27%, 32% and 38% of disruption of preformed hIAPP amyloids respectively. Therefore, the preformed fibril of hIAPP was disrupted by peptidomimetic **4B** more significantly than **4D** at different time intervals.

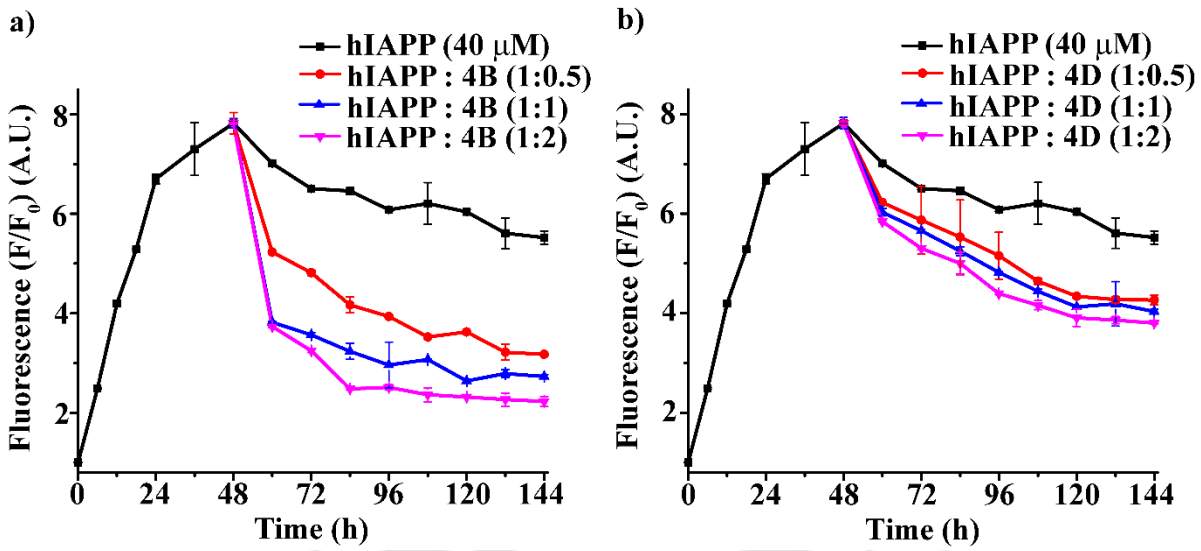

Figure 4.17: Time dependent ThT fluorescence assay of hIAPP (40 μM) alone (black) and in co-incubation with 0.5-(red), 1-(blue) and 2-fold (magenta) molar ratios of a) **4B** and b) **4D**. Spectra were recorded at an interval of 12 hrs after incubation in PBS (50 mM) at pH 7.4 and 37 °C.

4.6.3. Monitoring amyloid disruption by TEM and Congo red stained birefringence studies:

Incubating for 7 (2+5) days in PBS at physiological conditions, we observed that hIAPP alone (Figure 4.18 (a) (i)) exhibited clear fibrillar aggregates under electron microscope (TEM), which confirmed the formation of amyloid, whereas in co-incubation with 2-fold molar ratio of **4B** (Figure 4.18 (a) (ii)), we did not notice any such fibrillar aggregates suggesting significant disruption of preformed hIAPP amyloid. However, some fibrillar assembly was noticed when hIAPP was investigated in co-incubation with 2-fold molar ratio of **4D** (Figure 4.18 (a) (iii)), which indicated insignificant disruption of hIAPP amyloid.

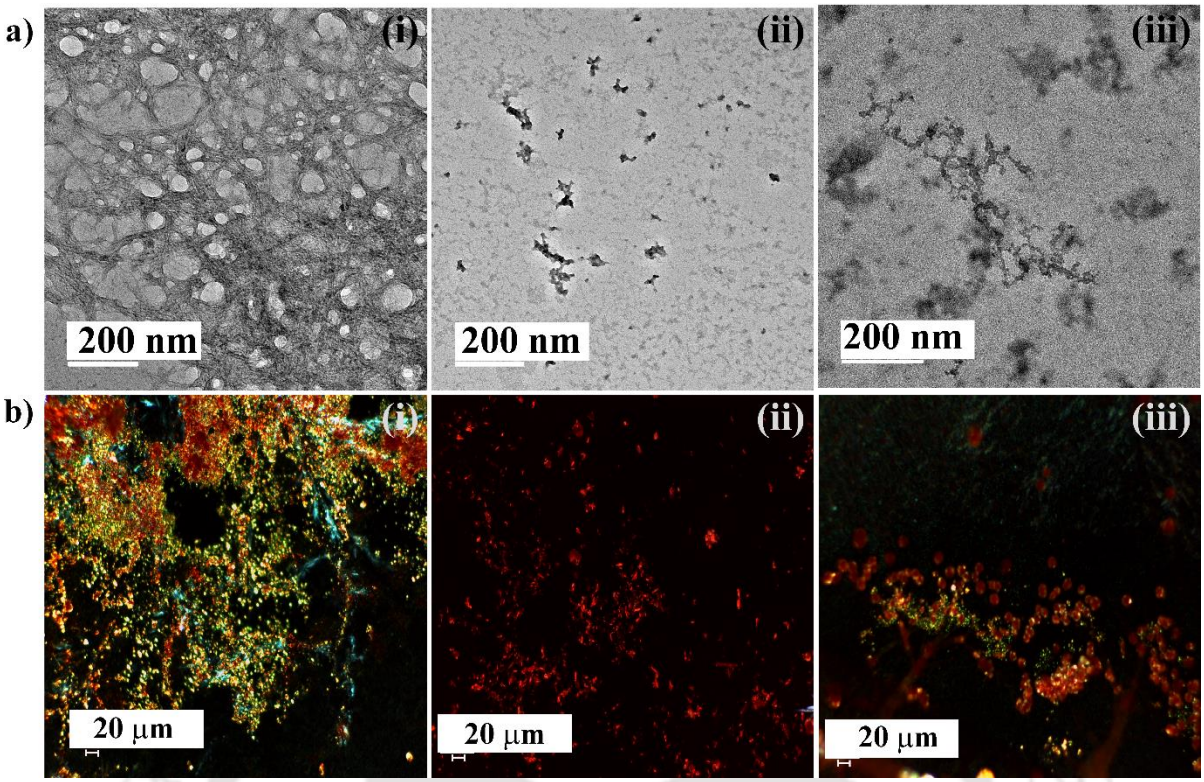

Figure 4.18: (a) TEM and (b) Congo red birefringence images of hIAPP (i) alone and in co-incubation with 2-fold molar ratios of peptidomimetics, **4B** (ii) and **4D** (iii). Images were captured after seven days of incubation of the peptides in PBS (50 mM) at pH 7.4 and 37 °C.

Furthermore, the disruption of preformed amyloid was investigated through a Congo red-stained birefringence study after seven days of incubation of the peptide samples. When we analyzed the sample containing only hIAPP (Figure 4.18 (b) (i)) under a polarisable microscope, we observed a clear appearance of green-gold birefringence under cross-polarised light indicating the formation of amyloid. However, in co-incubation with 2-fold molar ratios of **4B** (Figure 4.18 (b) (ii)), we did not observe any such characteristic birefringence, which indicated significant disruption of preformed amyloid. Further, when hIAPP was incubated with the same molar ratio of **4D** (Figure 4.18 (b) (iii)), some green-gold birefringence was noticed, suggesting incomplete disruption of hIAPP amyloid.

Hence, from the methodical *in vitro* study with the preformed amyloid of hIAPP in the presence of the designed peptidomimetics, our results suggested that peptidomimetics **4B**

could disrupt the amyloid with 2-fold molar excess more significantly than the control peptide **4D** with the same molar ratios at physiological condition.

4.7. *In vitro* toxicity study using dye loaded large unilamellar vesicle (LUV) leakage assay:

The soluble oligomers of any amyloidogenic peptide can damage the cell membrane by forming pores into it, for which such species have been considered much more toxic than the full-grown fibrils. [43,132] They disrupt cell membrane through the formation of ion channels, thereby disturbing cellular homeostasis.[134] Membrane fragmentation and amyloid fibrillogenesis are two independent processes in hIAPP. Brender *et al*. reported that, unlike the full-length hIAPP, the hIAPP$_{1-19}$ fragment is unable to form fibrillar assembly; instead, it boosts the potential of disrupting the lipid vesicles, thereby proposing a model to study the disruption of the artificial membrane by hIAPP.[135]

If we go through the mechanism, disruption of the cellular membrane by hIAPP or other aggregating peptides occurs *via* two-step processes *in vitro*. At first, the soluble oligomers formed from the monomers adhere to the cellular membrane, which forms some smaller size, ion-selective channel-like pores. The pores formed by hIAPP are inconsistent, so during the membrane disruption process, the pores amalgamate into large aggregates, converting them into fibrillar assembly. On the contrary, the next step commences with the disruption of some non-selective biological membranes *via* a detergent-like process by the fibrous material of hIAPP. [134,135]

From the disruption study, it has been confirmed that the peptidomimetics (**4B** and **4D**) were able to disrupt the preformed amyloids of hIAPP. To investigate the toxicity of the species generated after disruption, we performed a dye leakage experiment using carboxyfluorescein

dye, entrapped inside the large unilamellar vesicles (LUVs, Figure 4.19). To carry out the membrane leakage assay, we have taken five sets of samples for the experiment, including one untreated LUVs as a control, which does not contain any peptide as described in chapter 2, section 2.8. The peptide solutions (**4B** and **4D**) were prepared in PBS (50 mM) at pH 7.4 and added to the preformed fibrillar assemblies of 48h aged hIAPP solution (as similar to the process described in section 4.6) and further co-incubated them for another 5 days (168h = 48h + 120h). The various solutions prepared for the study are as follows:

Sample 1- Untreated LUVs,

Sample 2- LUVs + hIAPP (incubated for 5h)

Sample 3- LUVs + hIAPP (incubated for 7 days)

Sample 4- LUVs + hIAPP: **4B** (1:2)

Sample 5- LUVs + hIAPP: **4D** (1:2)

The peptide and the lipid were prepared maintaining 1:20 molar ratios during the analysis and the dye leakage assay was performed similarly as described in chapter 2.

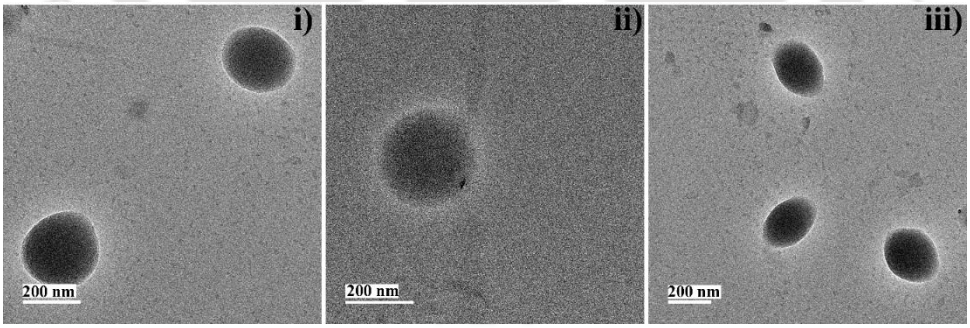

Figure 4.19: TEM images of the large unilamellar vesicles (LUVs) at a concentration of 1 mM in PBS (50 mM). Scale bar is indicated as 200 nm.

From the dye leakage assay (Figure 4.20), we noticed that there was a sharp rise in fluorescence intensity for the 5h aged hIAPP sample (sample 2, red, Figure 4.20 (a) and (b)) until 100 min and attained a plateau after 12h, which indicated the extent of dye leakage from

the LUVs. This sample exhibited significant dye leakage (~45% in 100 min and ~55% in 72h), indicating the presence of pore-forming toxic soluble oligomers. On the contrary, seven days old hIAPP sample (sample 3, blue, Figure 4.20 (a) and (b)) exhibited less dye leakage from the LUVs (~17% in 100 min and ~25% in 72h), confirming the less toxic effect of the matured fibrils on LUVs by pore formation and dye leakage in compared to the soluble oligomers. As the soluble oligomers are responsible for toxicity being generated during the fibrillization of hIAPP, they may form sufficient numbers of pores on the LUVs, due to which there is maximum leakage of carboxyfluorescein dye from the LUVs, as evident from an increment in the fluorescence intensity.

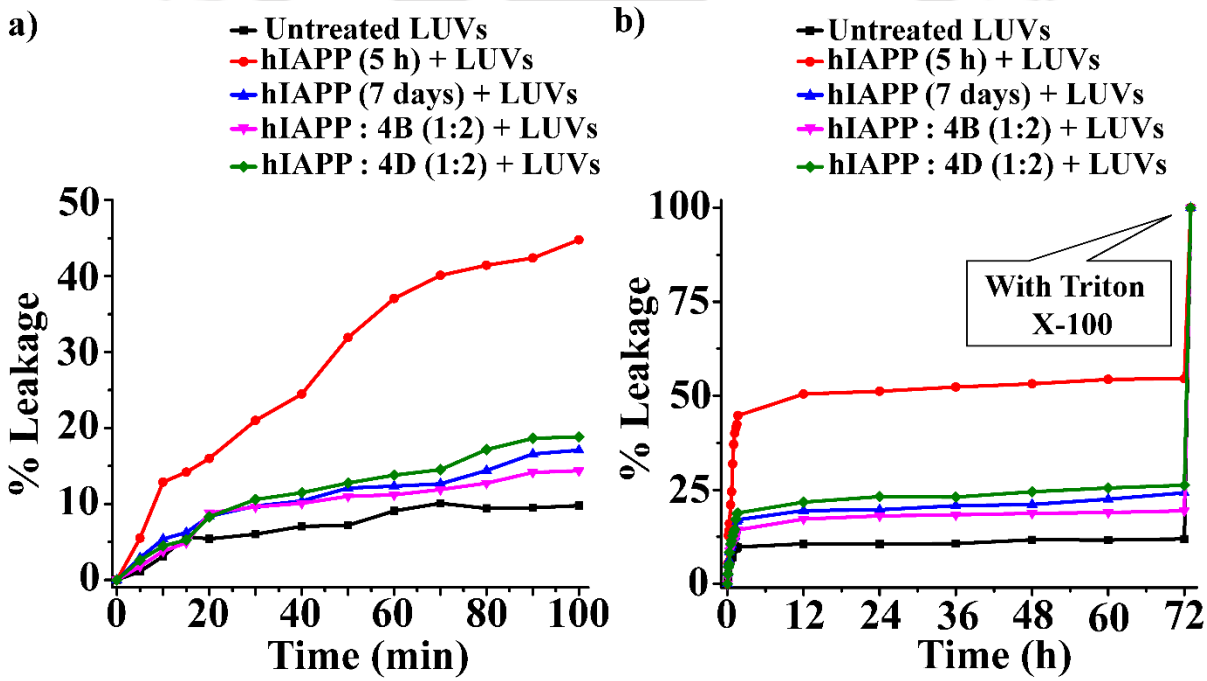

Figure 4.20: Emission of carboxyfluorescein dye with time, in terms of pore formation on LUVs showing the effect of hIAPP. (a) Dye released from LUVs alone and in the presence of different solutions from (a) 0 min to 100 min and (b) 0h to 72h.

However, disruption of preformed fibrils by the designed peptidomimetic, **4B** and the control peptidomimetic, **4D** did not form pores on the artificial cell or the LUVs significantly, as the increment of their corresponding fluorescence intensity (sample 4, magenta, and sample 5

olive, Figure 4.20 (a) and (b)) was found to be as low as that of the untreated LUVs (sample 1, black, Figure 4.20 (a) and (b)). Hence, this result was evident of the non-toxic behaviour of the disrupted preformed fibrillar assembly of hIAPP by the designed peptidomimetics.

4.8. Preliminary investigation of the mode of inhibition of aggregating hIAPP:

To investigate the preliminary mechanism of inhibition of aggregation of hIAPP by the peptidomimetic **4B**, we explored the change in size distributions of the different species generated, and morphology of hIAPP incubated alone and in the presence of **4B** using dynamic light scattering (DLS) and TEM analyses, respectively. [108,146,147] Furthermore, we performed a dye leakage assay using LUVs, prepared by entrapping carboxyfluorescein dye to gain insight into the membrane disrupting ability of the species generated during hIAPP fibrillization and its inhibition by **4B**.[136] For the complete investigation, we incubated hIAPP (40 μM) alone and in co-incubation with a 2-fold molar ratio of **4B** (80 μM) at physiological condition for 48h.

From the DLS study, the change in the size distribution of hIAPP in terms of hydrodynamic diameter (d) was observed to increase in ascending order from 1 nm to higher orders, with simultaneous broadening of the d values. The untreated hIAPP samples, which were incubated for 0h and 6h, exhibited hydrodynamic diameters of ~1 nm and ~100 nm, respectively, suggesting the gradual conversion of monomeric species to oligomeric species at the interval of 0h to 6h (Figure 4.21 (a) (i-ii)). Extending the duration of incubation of untreated hIAPP samples up to 48h resulted in further increase in the size distributions of the particles, ranging from 100–10000 nm (Figure 4.21 (a) (iii-v)). On the contrary, hIAPP in co-incubation with **4B**, a modulated fibrillization process was observed, as in 0h incubated sample two species were generated instantly, one with size distribution centered at 100-1000

nm and another at ~1 nm with reduced intensity (Figure 4.21 (b) (i)). The instant formation of the species with size distribution ranging from 100-1000 nm might indicate the binding of hIAPP to **4B** to generate some aggregated species. However, the size of the species occurring in the size distribution range from 100-1000 nm was found to decrease gradually with increasing incubation time from 12h to 48h (Figure 4.21 (b) (ii-v)). Thus from the above performed DLS study it is conclusive that the presence of **4B** restrict the native hIAPP fibrillization pathway and lead to the generation of some non-fibrillar aggregated species.

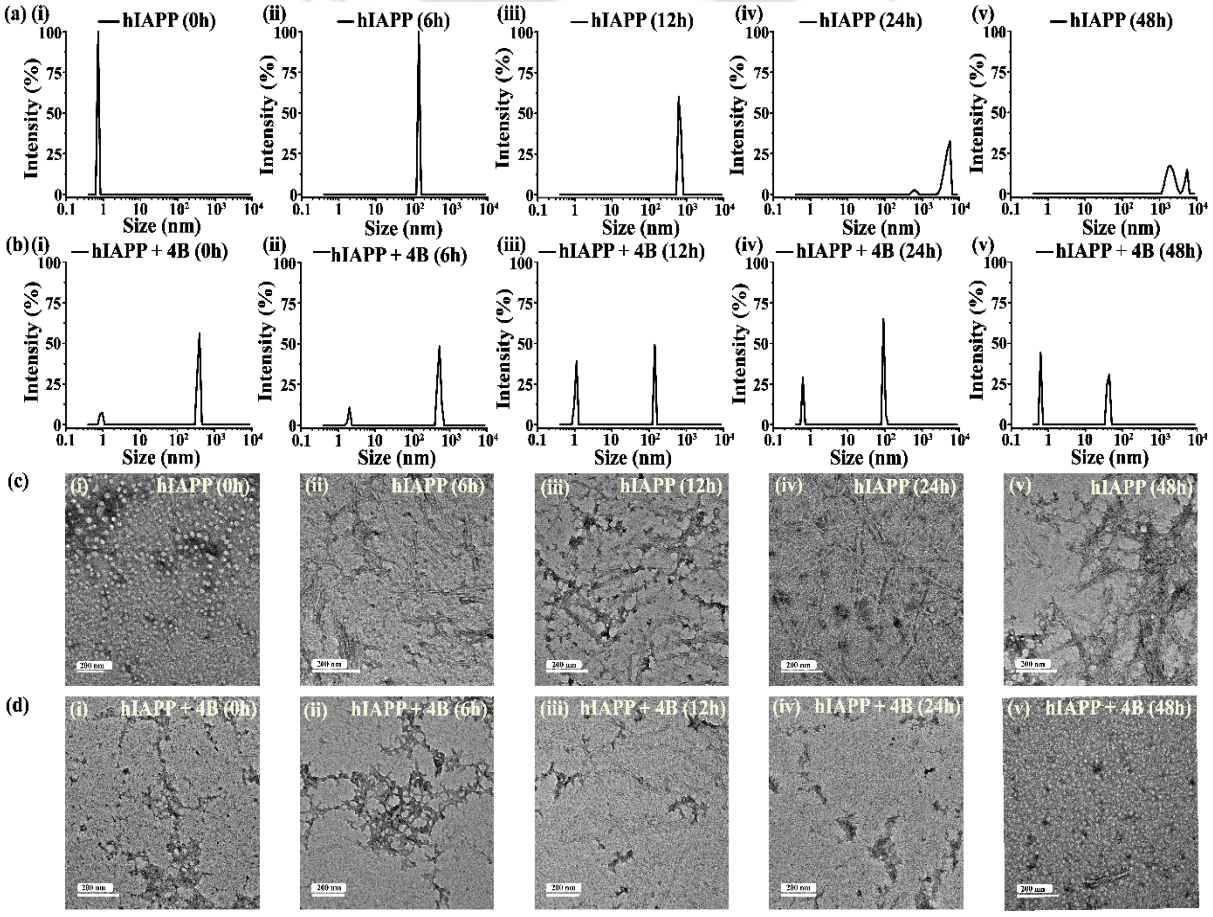

Figure 4.21: DLS study showing the changes in size distributions of hIAPP incubated alone (a) and in co-incubation with 2-fold molar ratio of **4B** (b) at 0h (i), 6h (ii), 12h (iii), 24h (iv) and 48h (v) respectively. TEM images exhibiting the changes in morphology of hIAPP incubated alone (c) and in co-incubation with 2-fold molar ratio of **4B** (d) at 0h (i), 6h (ii), 12h (iii), 24h (iv) and 48h (v) respectively. The scale of TEM images indicates 200 nm.

Moreover, from the TEM analysis, a transitional growth from smaller to longer fibrils of hIAPP was observed, leading to the formation of an extensive fibrillar assembly. At 0h, the only hIAPP-incubated sample exhibited dot-like structures; however, it slowly transformed into intermittent fibrillar species at 6-12h, finally leading to the formation of the mature fibrillar assembly after 24h (Figure 4.21 (c) (i-v)). On the contrary, hIAPP in co-incubation with **4B**, modulated hIAPP fibrillization process was observed. At the initial hours (0h and 6h), hIAPP in co-incubation with **4B** resulted in the formation of some amorphous aggregated species exhibiting morphology which is strikingly different from that of native hIAPP (Figure 4.21 (d) (i-ii)). After 6h, although a rich fibrillar network was not observed, however some small and thin fibrils were visible under TEM, which gradually transformed into smaller dot-like species indicating a significant reduction in aggregation process (Figure 4.21 (d) (iii-v)).

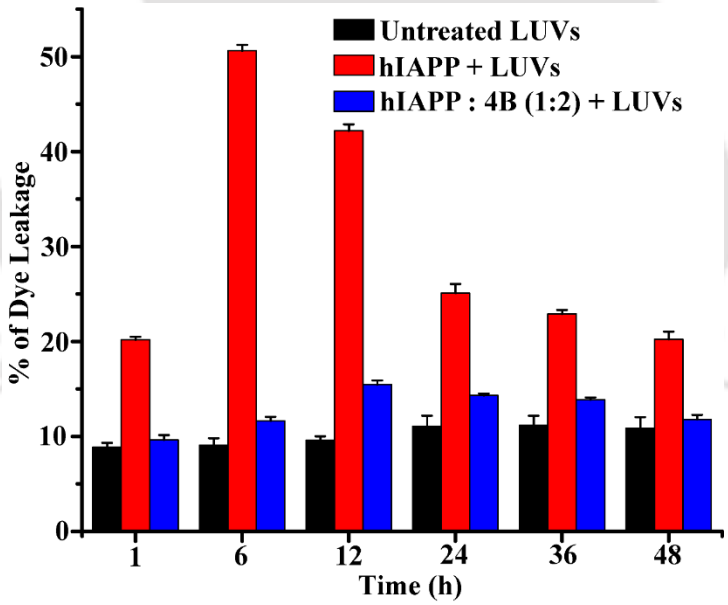

Figure 4.22: The emission of carboxyfluorescein dye showing the effect of hIAPP on the LUVs with time and % of dye leakage during the inhibition process in the absence and presence of **4B** with hIAPP from 1h to 48h.

Next, in the dye leakage analysis, hIAPP was incubated alone and in the presence of **4B** at different time intervals up to 48h in PBS and mixed with LUVs to attain 50 μM final concentration of the lipids. For the only hIAPP-incubated solution, the highest

carboxyfluorescein dye leakage was observed from the 6h aged sample, whereas dye leakage decreased gradually as the incubation time of hIAPP increased from 12h to 48h (red, Figure 4.22). We did not observe any significant dye leakage at the initial hour (1h aged sample), whereas a maximum dye leakage was observed from the 6h aged sample, indicating that the oligomeric species generated at ~ 6h involved higher toxicity. Furthermore we observed a constant decrease in dye leakage upon increasing the incubation time from 12h to 48h, indicating the formation of matured fibrils, which are relatively less toxic than the oligomers. On the other hand, when hIAPP was co-incubated with **4B** (blue, Figure 4.22), we did not observe any significant dye leakage. Rather, the extent of dye leakage was almost similar to that of the untreated LUVs (black, Figure 4.22), indicating the fact that the species generated during the inhibition of hIAPP aggregation by **4B** were relatively non-toxic.

Hence, from the experimental analyses of size distribution and morphological changes, it could be presumed that binding of **4B** (breaker peptide) with hIAPP triggers the generation of non-fibrillar aggregating species, which prevents the generation of toxic oligomeric species associated with amyloid fibrils. Moreover, from the dye leakage assay, it was observed that the aggregates generated in the presence of **4B** did not cause pore formation or rupture the artificial membrane, thus indicating the non-toxic nature of the species. These results strongly correlate with the results acquired from the various biophysical experiments of inhibition and disruption. Hence, convincing binding of **4B** with the aggregating peptide could determine anti-amyloidogenic processing of hIAPP; nevertheless, further studies are essential to understand the proper mechanism.

4.9. Conclusion:

The initial investigations indicated that inserting a conformationally restricted components such as proline, N-methylated amino acids and α-aminoisobutyric acid in an aggregating peptide sequence acquired excellent efficacy in inhibiting or disrupting the amyloid fibrils, and some of them are undergoing clinical trials.[110,112,141,142] We also formerly reported that the insertion of anthranilic acid into hIAPP$_{22-27}$ gained significant success in inhibiting the aggregation of hIAPP at a dose of 10-fold molar ratios.[144] Here, we have demonstrated the superior effect of a single point Ant mutated hIAPP $_{8-37}$ (**4B** or **4C**) at two different positions over its smaller Ant mutant variant in hIAPP $_{22-27}$ (**4D**) at I26 position in aggregation modulating caused by hIAPP.

The systematic experimental results support that peptidomimetics **4B**, **4C** and **4D** containing Ant at different positions were non-amyloidogenic; however, peptide **4A** lacks Ant moiety in its sequence, exhibited amyloidogenic behaviour in a similar way as that of hIAPP. Experimental data supports that peptidomimetics **4B** and **4C** were potent inhibitors of amyloid formation at a significantly lower concentration than the **4D**. Hence, based on the experimental data, **4B** and **4C**, being longer peptides, are more effective as inhibitors than small sequenced peptidomimetics, **4D**. The improved efficacy may be due to the packed binding and better sequence recognition of the long peptidomimetics (**4B** or **4C**) to the fibrillar assembly generated by hIAPP over the smaller one (**4D**).[98,116] On the other hand, differences in the mutant position at G24X and I26X, (X=Ant) did not show any significant variation in their ability to inhibit the amyloid formation of hIAPP. Therefore, we ruled out **4C** for further studies.

Furthermore, we demonstrated the effect of peptidomimetics in terms of disruption of the preformed amyloid of hIAPP. Both the peptidomimetics **4B** and **4D** were able to disrupt the

preformed amyloid into non-toxic species as evident from LUV studies; however, **4B** was much more effective than **4D**. Furthermore, in methodical DLS and TEM experiments, it was observed that the presence of **4B** with hIAPP altered the native aggregation pathway of hIAPP and the soluble oligomers thus originated were able to rupture the lipid membrane slightly. Overall, a single point anthranilic acid mutant of full-length hIAPP$_{8-37}$ at G24X or I26X (X=Ant) enhances significantly anti-amyloidogenic activity associated with hIAPP. Finally, it can be concluded that these peptidomimetics are highly efficient inhibitors and disruptors of the preformed amyloid towards the aggregation of hIAPP at low molar ratios. These peptidomimetics may emerge as lead scaffolds for therapeutic design towards T2D and other amyloid-related diseases.

Chapter 5: Disruption of hIAPP aggregates into non-toxic species by side-chain to tail stapled peptides

5.1. Proposed hypothesis:

From our previous chapters (chapter 2-chapter 4), we observed the effectiveness of the BSBHPs in the inhibition of hIAPP aggregation and disruption of preformed amyloid . In chapter 2 and chapter 3, we used three different isomers of aminobenzoic acid individually in the core hydrophobic region of $hIAPP_{22-27}$ as breaker elements and ortho and meta isomer containg peptidomimetics found to be an effective inhibitor of hIAPP aggregation.[144] From our experimental findings , it was observed that 2-aminobenzoic acid (anthranilic acid) emerged as the best breaker element in inhibiting the hIAPP aggregation among the different isomers. The profound efficiency of the peptidomimetic containing the anthranilic moiety is believed to be due to the kink formation ability of the β-breaker element, as the kink cannot fit into the planar topology of β-sheet which in turn reduces the extent of H-bonding interactions, responsible for aggregation. However, it has been observed that the anthranilic moiety incorporated into the small peptide sequence ($hIAPP_{22-27}$) has shown its β-breaking activity in higher doses, like 10-fold molar excess or more. Although the kink formation provides the anti-amyloid activity, for better breaking efficiency, proper recognition with the aggregating peptide is of utmost importance, as it depends on the number of H-bonds and hydrophobic interactions. Therefore, in chapter 4, we designed and worked out the inhibition of hIAPP aggregation with a new set of peptidomimetics comprising an anthranilic acid mutant of $hIAPP_{8-37}$. With this set of peptidomimetics, we observed better consequences of β-breaking efficiency, as it is a longer breaker peptide, which might be able to bind with the

hIAPP effectively and exhibit its anti-amyloid activity with less molar ratio than the small BSBHPs.[148]

Regardless of tremendous research and scientific development on protein misfolding and amyloid, no complete cure for amyloidogenic diseases has been discovered. In recent years, stapled peptides have emerged as one of the most efficient drug candidates for various biological dysfunctions due to their various structural advantages. The stapling technique has emerged rapidly as one of the most accepted strategies for inhibiting protein-protein interactions (PPI) in living systems.[149] The development of stapled peptides showed potential to facilitate the approach to α-helix mediated PPI drug targets.[150] Further, it has been observed from the studies that stapled peptides could disrupt enzyme and membrane receptors.[151,152] Peptidomimetics made by one component stapled peptides have also been investigated recently to inhibit amyloid fibrillogenesis.[147] Looking into these enormous advantages and clinical activities, the stapled peptides can open up some new possibilities as critical therapeutics for targeting some incurable diseases like T2D.

Herein, we planned to design side-chain to tail stapled peptides for arresting hIAPP aggregation by incorporating a recognition motif into the peptide sequence, maintaining sequence homology with hIAPP (Scheme 5.1).

5.2. Stapled peptides:

Peptide stapling is an approach for peptide macro-cyclization between the two side chains of two amino acids or the side chain to head or tail in a peptide sequence employing covalent binding. If the design of the stapled peptides attains an optimal position and length, the resulting macrocycle emerges out to possess enhanced structural rigidity and the desired α-helical conformation.[153] Stapling is a robust approach for stabilising peptides in α-helical

conformation. Peptide stapling greatly enhances the proteolytic stability and cell permeability of the resulting peptide constructs in addition to the efficiency of binding to a protein target by involving protein-protein interactions (PPI), which may convert previously thought 'undruggable' peptides into different therapeutics.[154]

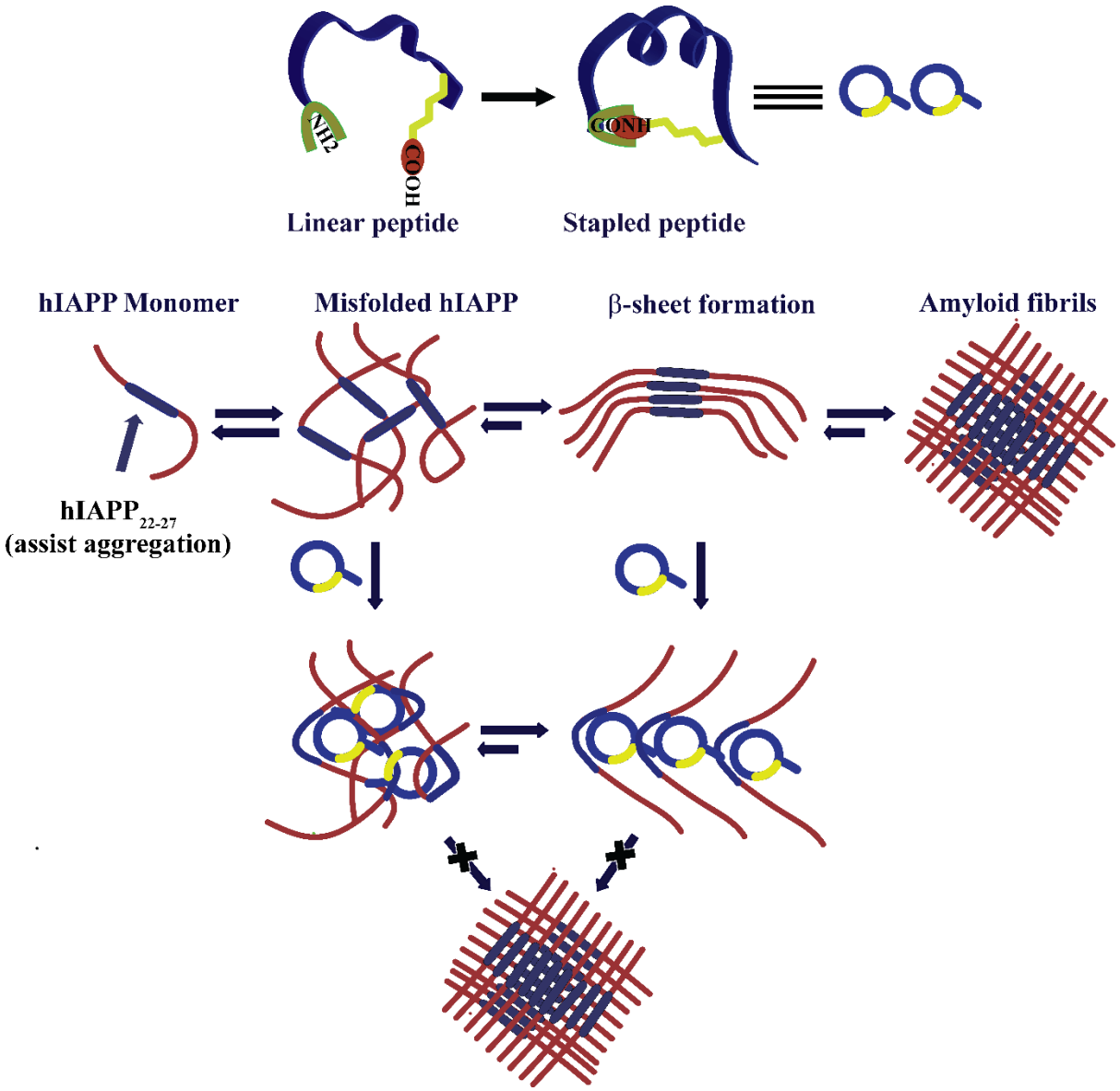

Scheme 5.1: Formation of stapled peptides (SPs) and schematic representation of hIAPP aggregation and proposed hypothesis for the inhibition process of amyloid formation by SPs.

A large number of diverse techniques have been adopted for the stapling process; including lactam formation between Lys and Glu/Asp residues, disulfide bridge, hydrocarbon stapling,

which involve ring-closing metathesis of olefin bearing peptides.[155, 156, 157] In general, the stapling process has been categorized as one-component stapling and two-component stapling. The one-component stapling process involves direct cyclization between the side-chain of two non-native amino acids, while two-component stapling utilizes a separate bi-functional linker to connect the two side chains.[153] However, in our present work, the stapling process has been carried out directly between the side chain of glutamic acid at the C-terminus and the backbone asparagine residue at the N-terminus (Scheme 5.1).

5.3. Design of peptides:

Herein, we have designed two side chain to tail stapled peptides in the absence and presence of a turn-inducing moiety, anthranilic acid (Ant), being incorporated into the highly aggregating fragment of $hIAPP_{22-27}$. Along with these, we also designed two control linear peptides one without the anthranilic moiety and another containing the turn-inducing element maintaining the sequence homology with the hIAPP for proper recognition and binding with the same.

Table 5.1: Sequence of peptides with their functions:

Peptide No	Sequence	Molecular mass $[M+H]^+$ (Expected/Observed)	Functions
5A	NFGAILER-$CONH_2$ └─ **X** ─┘	900.577/ 900.624	Breaker
5B	NFGA(Ant)LER-$CONH_2$ └─ X ─┘	906.530/ 906.629	Breaker
5C	NFGAILER-$CONH_2$	918.588/ 918.623	Control/Breaker
5D	NFGA(Ant)LER-$CONH_2$	924.541/ 924.533	Control/Breaker

Note: Standard amino acids are represented by a one-letter code, Ant = Anthranilic acid and X= amide, -CONH-

The anthranilic moiety was introduced in both the stapled and linear one in the I26 position of $hIAPP_{22-27}$, i.e., the NFGAIL sequence. The I26 position was selected to incorporate anthranilic moiety due to its critical residual effect for hIAPP amyloid formation by keeping the -N-F-G-A- tetrapeptide residue intact for maintaining sequence homology.[57, 95, 106] Besides the said sequence, one glutamic acid (E) and one arginine (R) were introduced at the C-terminus. The arginine group was inserted to increase the aqueous solubility of the peptides. The stapling process was carried out between the side chain of glutamic acid at the C-terminus and the tail of the backbone, i.e., the N-terminus of asparagine.

5.4. Synthesis and characterization of the designed peptides:

All the designed peptides were synthesized by standard solid-phase peptide synthesis (SPPS) method using Fmoc/t-Bu strategy on Rink Amide MBHA resin as the solid support (described in Chapter 6, section 6.4).[119, 120] Proceeding in this way, initially the linear counterpart was synthesized, followed by OtBu deprotection from the side chain of glutamic acid at the C-terminus using 5 eq of $FeCl_3$ for 1.5h[158] and Fmoc-deprotection from the N-terminus using 20% piperidine in DMF. In the next step, on-resin stapling was carried out using BOP as a coupling reagent, and DIPEA as a base for 24h, followed by resin cleavage using TFA mixtures.[147] The designed peptidomimetics were purified by Thermo Fischer RP-HPLC and the purity of the peptides were further confirmed using Agilent analytical HPLC system with Agilent C_{18} analytical column at a flow rate of 1 ml/min. The purified peptides were characterized by HPLC and MALDI-TOF mass spectrometry. A representative example of the synthetic protocol of **5B** has been depicted in scheme 5.2. All other peptides were synthesized in a similar process. The characterization data for the synthesized peptides have been shown below (Figure 5.1-5.8).

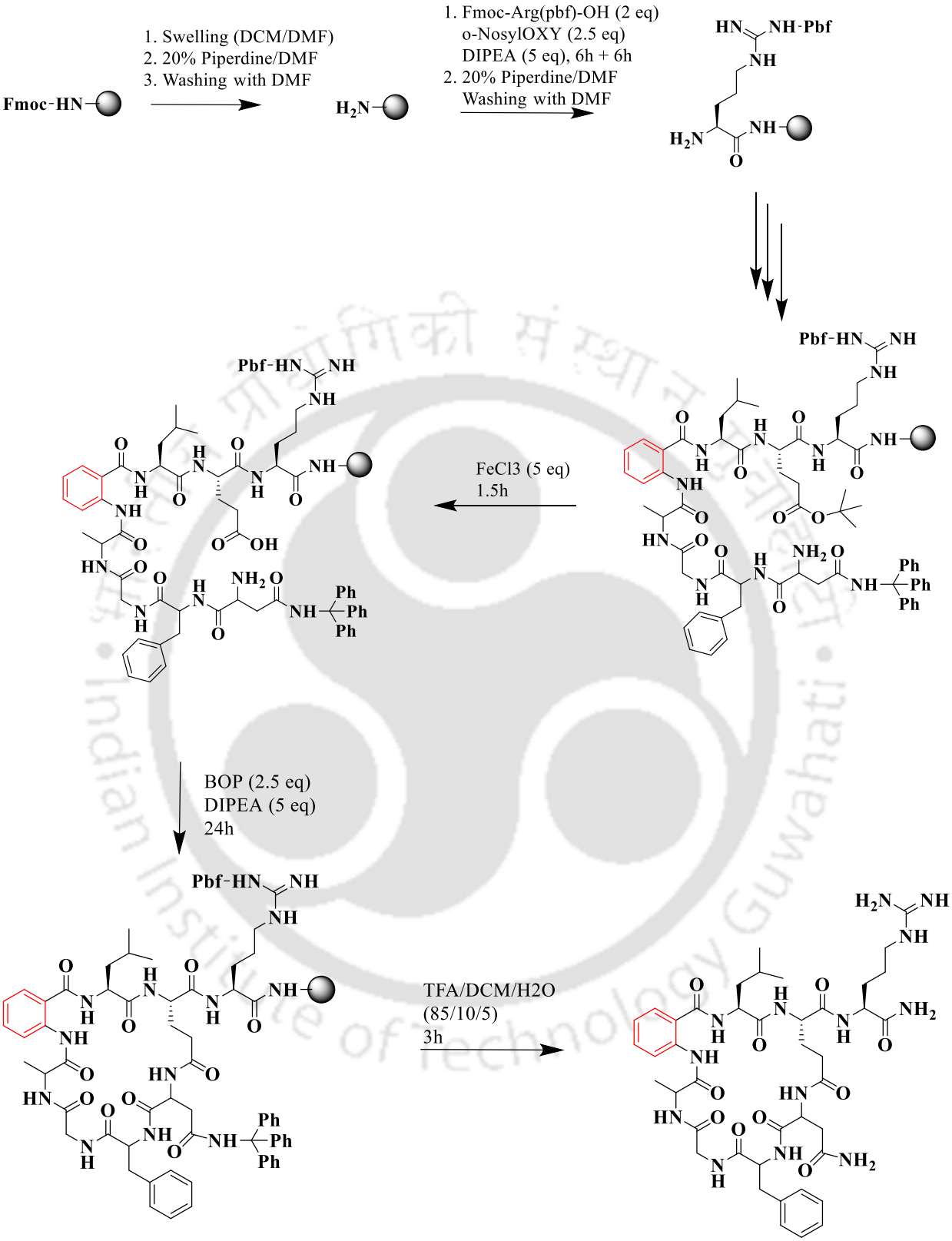

Scheme 5.2: The synthetic scheme of peptide **5B**.

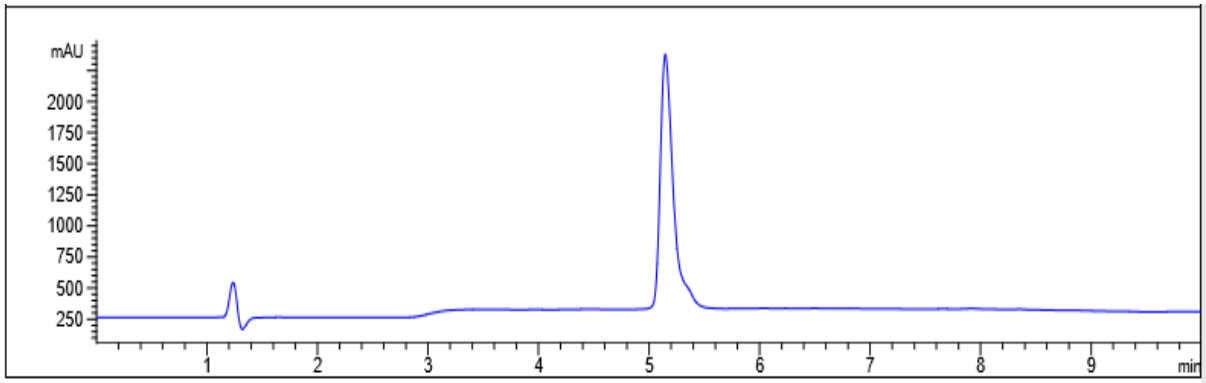

Figure 5.1: RP-HPLC profile of purified peptide **5A**.

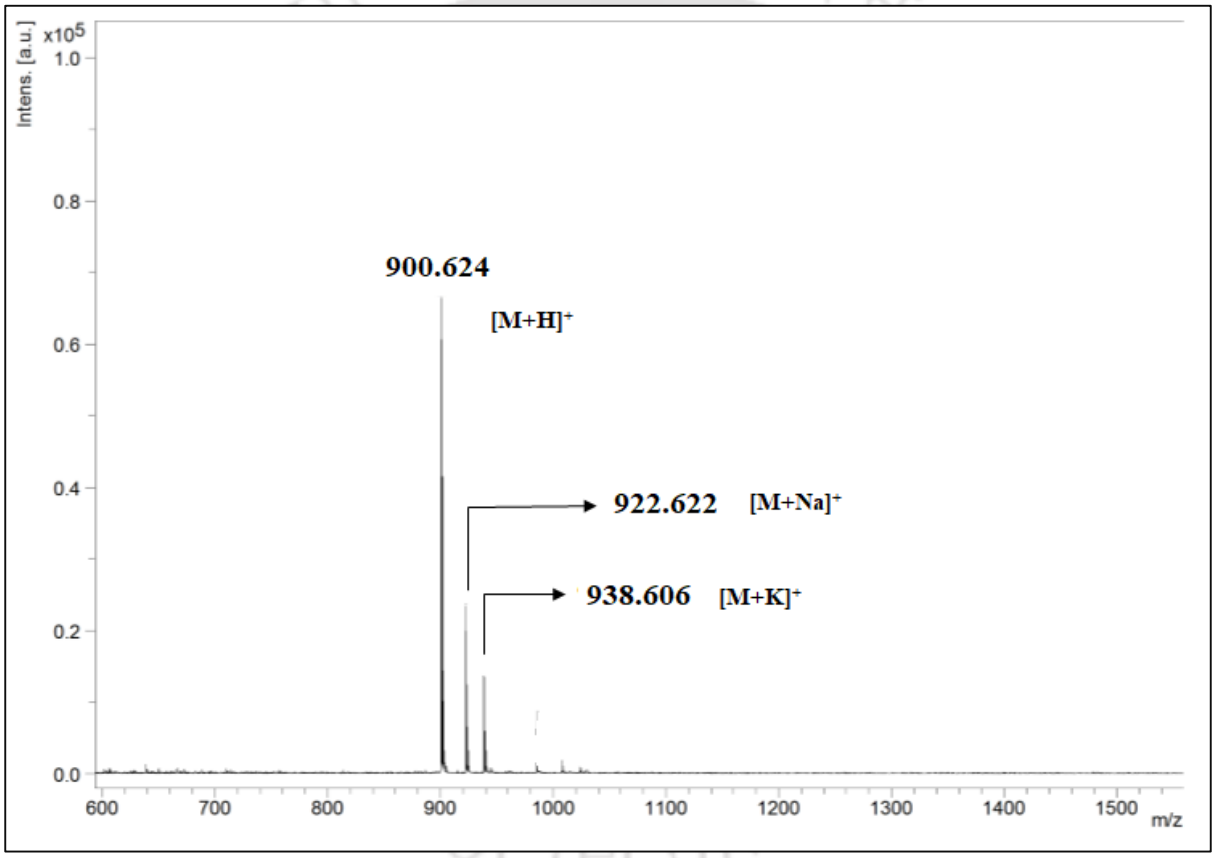

Figure 5.2: MALDI-TOF mass spectrum of peptide **5A**. Calculated mass for $C_{41}H_{66}N_{13}O_{10}$ is 900.577 $[M+H]^+$, observed mass is 900.624 $[M+H]^+$, 922.622 $[M+Na]^+$, 938.606 $[M+K]^+$.

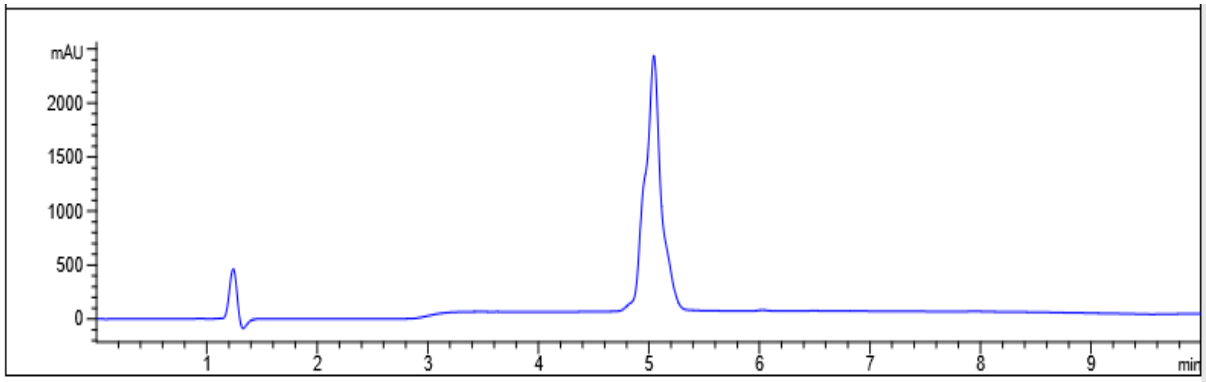

Figure 5.3: RP-HPLC profile of purified peptide **5B**.

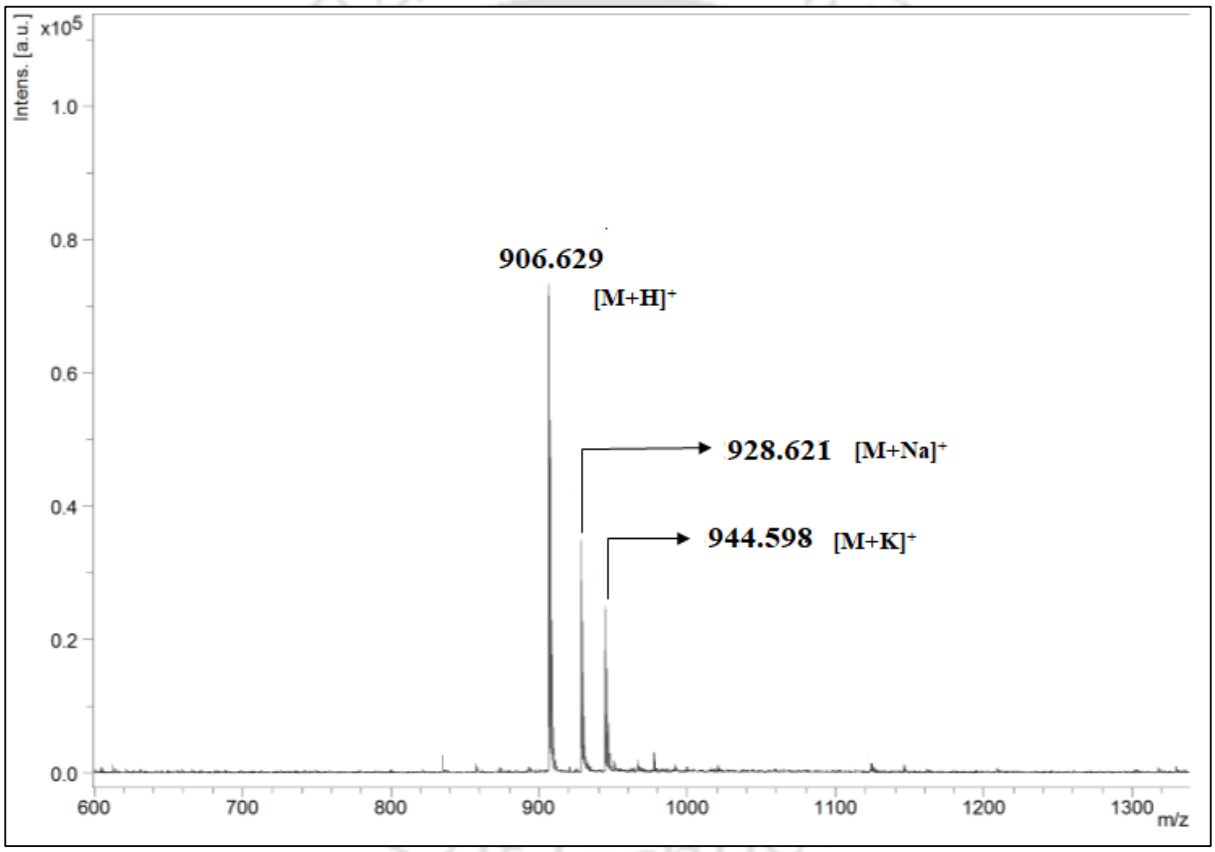

Figure 5.4: MALDI-TOF mass spectrum of peptide **5B**. Calculated mass for $C_{42}H_{60}N_{13}O_{10}$ is 906.530 $[M+H]^+$, observed mass is 906.629 $[M+H]^+$, 928.621 $[M+Na]^+$, 944.598 $[M+K]^+$.

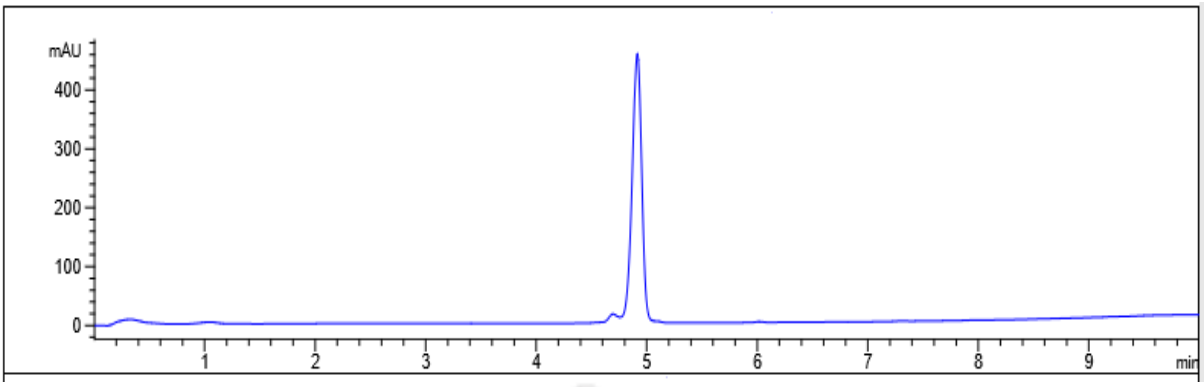

Figure 5.5: RP-HPLC profile of purified peptide **5C**.

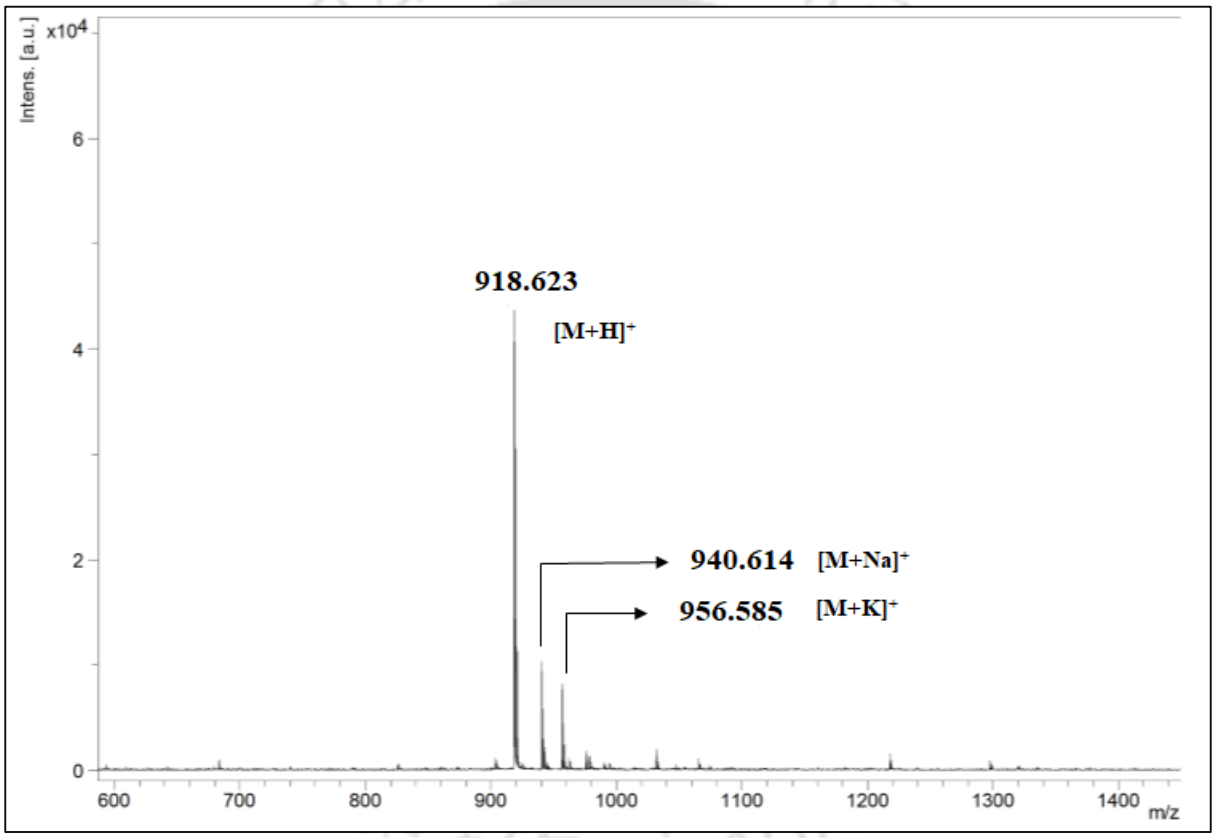

Figure 5.6: MALDI-TOF mass spectrum of peptide **5C**. Calculated mass for $C_{41}H_{68}N_{13}O_{11}$ is 918.588 $[M+H]^+$, observed mass is 918.623 $[M+H]^+$, 940.614 $[M+Na]^+$, 956.585 $[M+K]^+$.

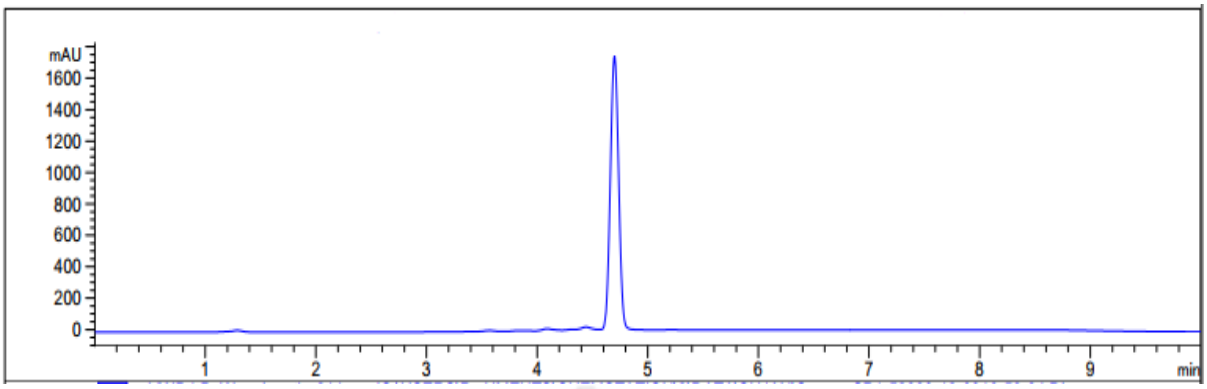

Figure 5.7: RP-HPLC profile of purified peptide **5D**.

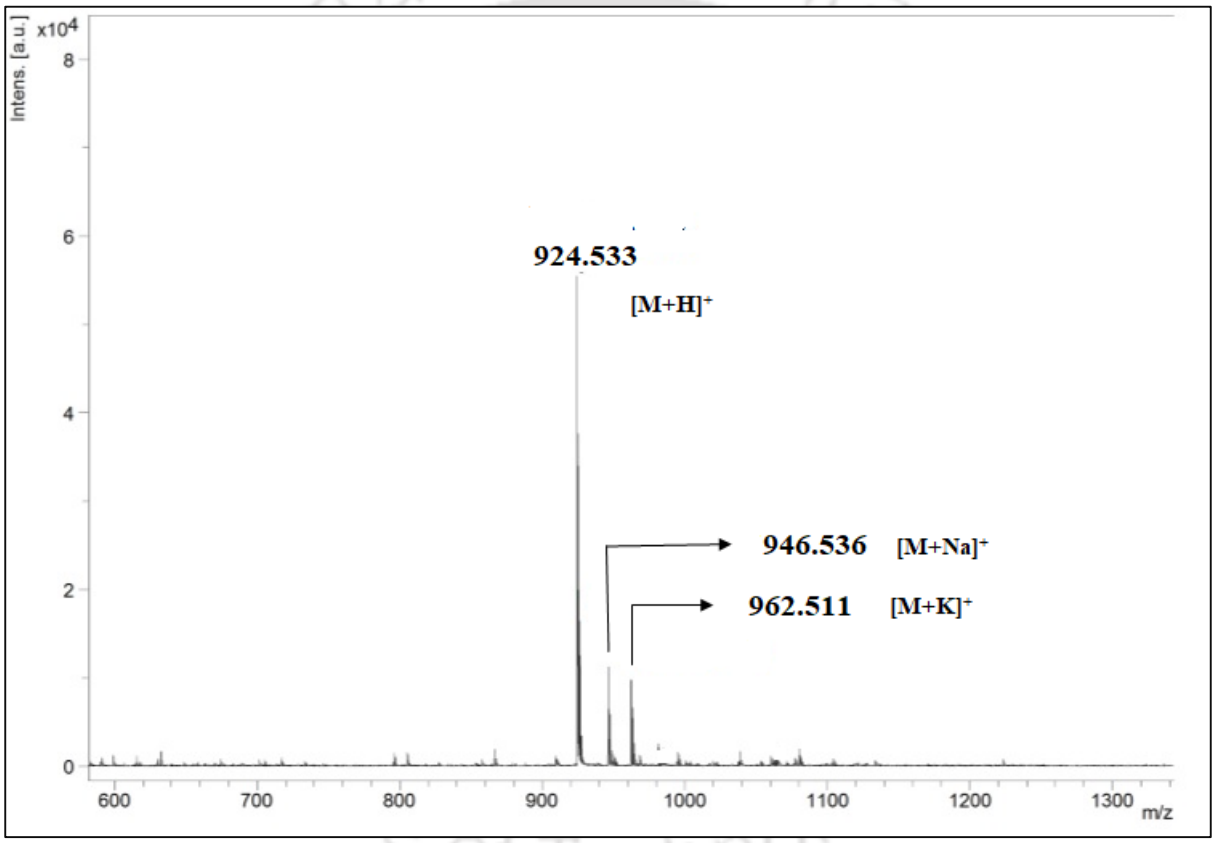

Figure 5.8: MALDI-TOF mass spectrum of peptide **5D**. Calculated mass for $C_{42}H_{62}N_{13}O_{11}$ is 924.541, observed mass is 924.533 $[M+H]^+$, 946.536 $[M+Na]^+$, 962.511 $[M+K]^+$.

5.5. Non-amyloidogenic nature of the synthesized peptides:

Before monitoring the anti-amyloid activity of the stapled peptides and linear peptides, we investigated their native amyloidogenic nature using various biophysical techniques, namely CD, FT-IR, TEM, and Congo red birefringence studies. For these studies, all the HPLC purified peptides were dissolved in 50 mM PBS buffer of pH 7.4 to obtain a final concentration of 40 μM and incubated at 37 °C for five days.

5.5.1. Conformational characterization of the peptides by CD and FTIR studies:

Initially, we checked the conformational state of the synthesized stapled peptides and their linear analogs using circular dichroism (CD) and Fourier Transform Infrared (FTIR) spectroscopy.

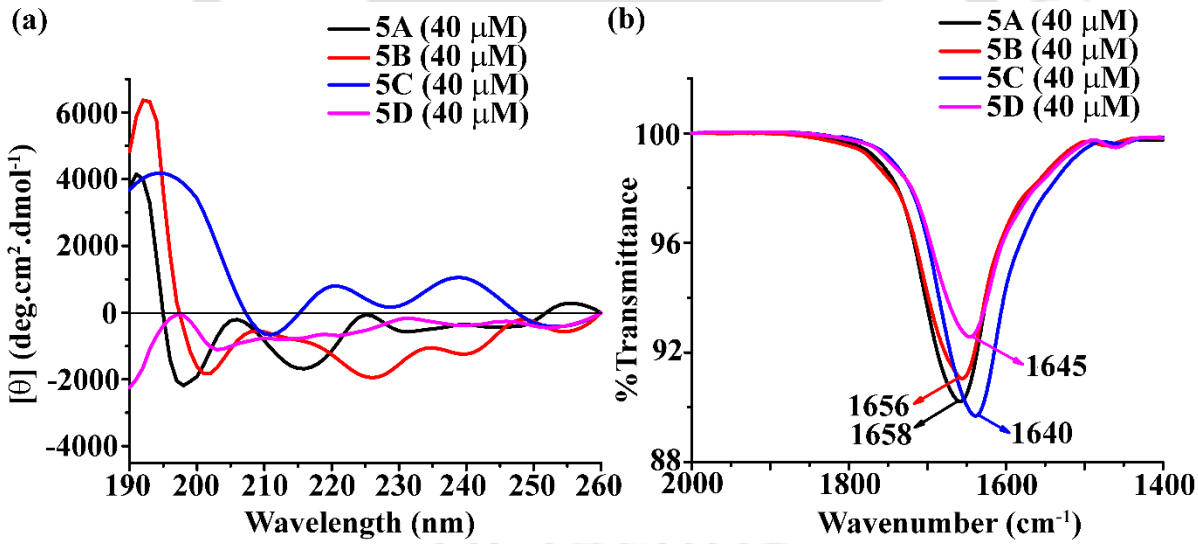

Figure 5.9: (a) CD and (b) FTIR spectra of peptide **5A** (black), **5B** (red), **5C** (blue) and **5D** (magenta). Spectra were recorded after 5 days of incubation of the peptides in PBS (50 mM) at pH 7.4 and 37 °C.

The CD spectra of **5A**, **5B**, and **5D** showed some mixed conformations, indicating non-β-sheet rich conformation of the peptides (Figure 5.9 (a)). On the other hand, in the CD spectrum of **5C**, we observed some characteristic β-sheet rich conformation. Similarly, in FTIR analyses (Figure 5.9 (b)) of **5A**, **5B**, and **5D**, we detected amide I band at 1656 cm^{-1},

1658 cm^{-1}, and 1645 cm^{-1} respectively, suggesting the existence of non-β-sheet conformation.[23] However, the amide I band shifted up to 1640 cm^{-1} for the peptide **5C**, suggesting a β-sheet rich conformation.[23] Hence, from the above studies, it is evident that the linear peptide **5C**, which lacks a turn-inducing moiety like Ant, is converted to β-sheet conformation with time; however, the stapled peptides **5A** and **5B** and the linear peptide with Ant moiety**, 5D** does not form β-sheet conformation at physiological conditions.

5.5.2. Amyloidogenic characterization of the synthesized peptides by TEM and Congo red stained birefringence studies:

From the above conformational study, we observed that peptides **5A**, **5B**, and **5D** exist in non-β-sheet conformation; however, peptide **5C** exhibited a β-sheet rich conformation at physiological conditions. Further, we wished to investigate the amyloidogenicity of the peptides using TEM and Congo red stained birefringence techniques.

After five days of incubation at physiological conditions, 10 μL aliquot of the peptide solution was taken out from the stock solution (as described in section 5.5). The samples for TEM and Congo red stained birefringence study were prepared as discussed in chapter 2, section 2.5.2. The appearance of the fibrillar structure under an electron microscope (EM) is a characteristic property of amyloid formation by any amyloidogenic peptide.[23] Under TEM, peptides **5A**, **5B**, and **5D** did not exhibit any fibrillar assembly, indicating the non-amyloidogenic nature of the peptides at physiological conditions. On the other hand, we observed some amorphous aggregates for the peptide **5C** underTEM , which indicated some aggregating behaviour of the peptide at the same condition (Figure 5.10 (a)).

Moreover, the appearance of green-gold birefringence under cross-polarised light upon staining with Congo red is also a characteristic feature of amyloid formation.[23] When viewed under cross-polarised light, peptides **5A**, **5B**, and **5D** did not exhibit such characteristic

birefringence suggesting the non-amyloidogenic nature of the peptides. However, peptide **5C** showed slight green-gold birefringence under the same condition, indicating the formation of some amyloid in the presence of the peptide. Therefore, from the above studies, it can be interpreted that peptides **5A**, **5B**, and **5D** were found to be non-amyloidogenic; however, peptide **5C** gained little amyloidogenic behaviour at physiological conditions (Figure 5.10 (b)). This may be attributed to the linear structure of the peptide **5C**, which lacks the presence of a turn inducer and restricted conformation in the peptide backbone like the other three peptides.

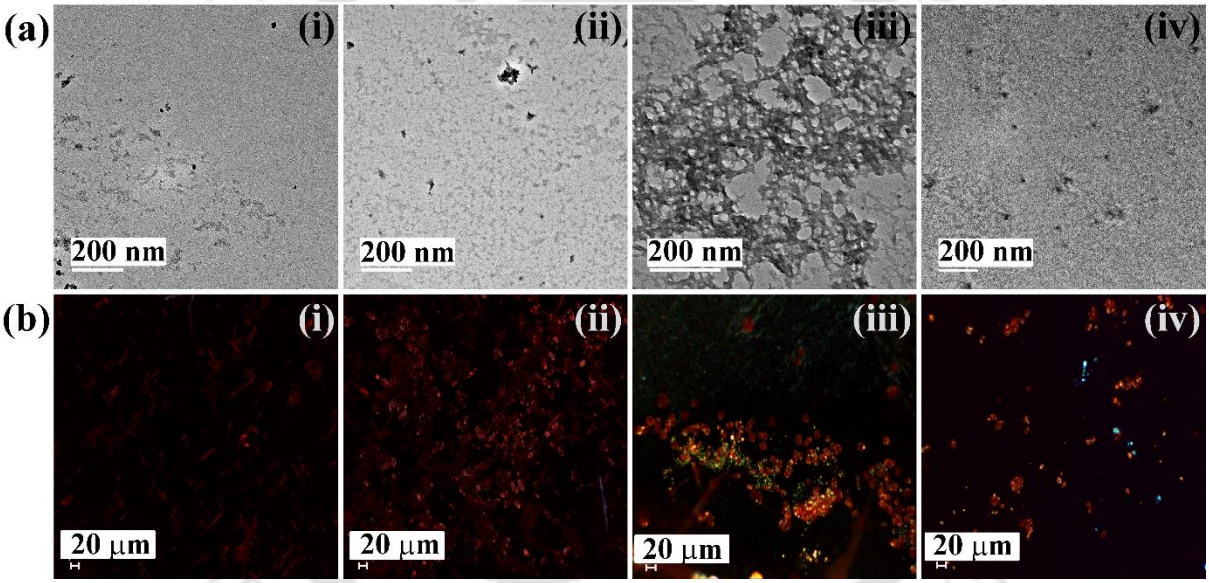

Figure 5.10: (a) TEM and (b) Congo red-stained birefringence images of peptide **5A** (i), **5B** (ii), **5C** (iii) and **5D** (iv). Images were taken after five days of incubation of the peptides in PBS (50 mM) at pH 7.4 and 37 °C.

5.6. Inhibition of amyloid formation of hIAPP by synthesized peptides:

Our primary goal is to investigate the prospective of the synthesized staple peptides (SPs) in blocking the formation of amyloid from the aggregating peptide. To explore the inhibitory efficiencies of the SPs, **5A** and **5B** and to compare the results with their linear analogs **5C** and **5D** as controls, we carried out various biophysical techniques in the absence and

presence of the synthesized peptides in varied doses, namely 0.5-, 1- and 2-fold molar ratios with respect to hIAPP. In addition, the highly aggregating hIAPP at a concentration of 40 μM was incubated in PBS (50 mM) of pH 7.4 at 37 °C in the absence and presence of the peptides up to 7 days and the kinetics of amyloid formation of hIAPP and its subsequent inhibition by the stapled peptides were monitored using various biophysical tools.

5.6.1. Monitoring conformational transition by CD and FTIR studies:

Initially, we wished to check the change in conformation of the aggregating peptide, hIAPP in the absence and presence of the SPs. To carry out the conformational study, we prepared different sets of solutions, where the concentration of hIAPP was maintained as 40 μM in each set. The first set contained only hIAPP, prepared in PBS at pH 7.4, while in the other sets, hIAPP was mixed with the SPs as well as their linear analogs in a molar ratio of 1:2, maintaining the same concentration of hIAPP. Each set containedtwo replicate solutions. All the different sets were prepared in PBS of pH 7.4 and incubated on water bath at 37 °C for seven days and thereafter, checked the conformational change of hIAPP (40 μM) in the absence and presence of 80 μM of the peptides using CD and FTIR studies.

When the CD spectra were recorded after seven days of incubation of the peptide solutions at physiological conditions, we observed that hIAPP alone displayed a positive band at ~196 nm and a simultaneous negative band at ~218 nm specifying a β-sheet rich conformation of the peptide (black, Figure 5.11 (a)). However, in the presence of 2-fold molar ratios of the SPs, i.e., **5A** and **5B** (red and blue respectively, Figure 5.11 (a)), the conformation of hIAPP transformed from β-sheet to α-helical rich conformation. On the other hand, in the presence of the control linear peptides, i.e., **5C** and **5D** (magenta and green respectively, Figure 5.11 (a)), we did not observe any significant conformational changes for the hIAPP peptide; instead, it existed in β-sheet rich conformation in the same molar ratio.

Further, the conformational transitions of the aggregating peptide were also monitored by FT-IR analysis. From the FT-IR spectra, when hIAPP was present alone in the solution, we noticed a sharp band at 1637 cm^{-1}, indicating the β-sheet characteristic conformation of the peptide (black, Figure 5.11 (b)). However, in the presence of 2-fold molar ratios of the SPs, i.e., **5A** and **5B** (red and blue respectively, Figure 5.11 (b)), the band shifted to 1648 cm^{-1} and 1654 cm^{-1} respectively, corresponding to non β-sheet conformation, which indicated inhibition of hIAPP aggregation by the SPs. On the contrary, in the presence of the same molar ratios of the control linear peptides, i.e., **5C** and **5D** (magenta and green respectively, Figure 5.11 (b)), the band shifted to 1643 cm^{-1} and 1647 cm^{-1}, respectively, which also indicated a change in conformation and subsequent inhibition to the aggregating hIAPP peptide to some extent.

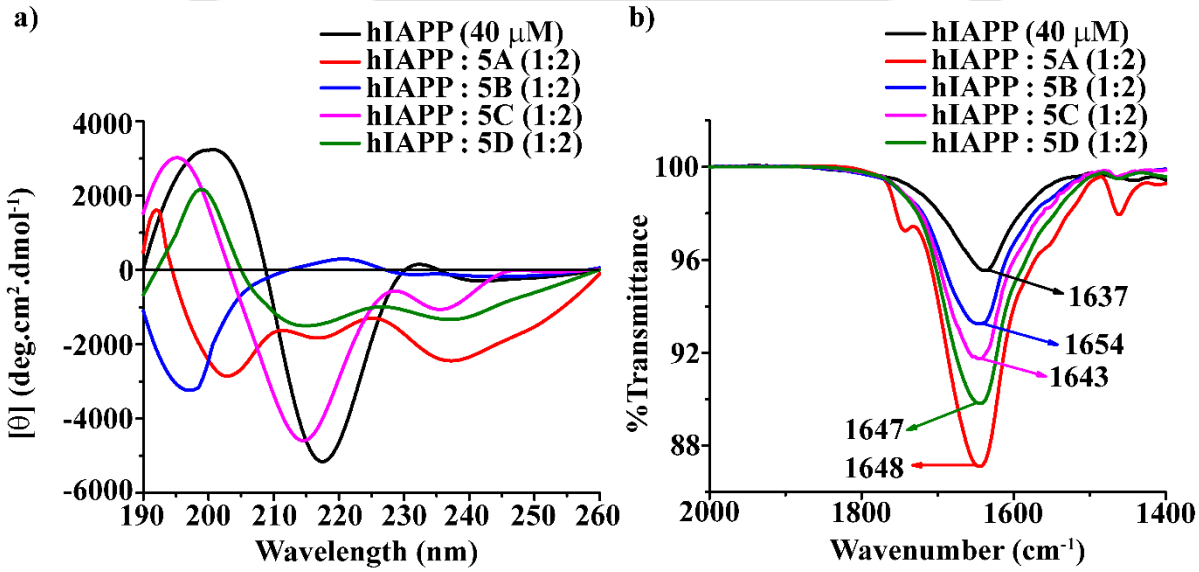

Figure 5.11: (a) CD and (b) FTIR spectra of hIAPP in absence (black) and in presence of 2 fold molar ratios of **5A** (red), **5B** (blue), **5C** (magenta) and **5D** (green). Images were taken after seven days of incubation of the peptides in PBS (50 mM) at pH 7.4 and 37 °C.

5.6.2. Monitoring the kinetics of amyloid formation and subsequent inhibition by the SPs *via* ThT fluorescence assay:

In Thioflavin T (ThT) fluorescence assay, the enhancement of fluorescence intensity with time is considered as a characteristic property of amyloid formation.[23] The time-dependent kinetics study of amyloid formation of hIAPP and its inhibition process by the SPs were monitored by a ThT fluorescence assay. To carry out this assay, we prepared different sets of solutions, where the concentration of hIAPP remained 40 μM in each set. In the first set, the only hIAPP was prepared in PBS at pH 7.4, while in the other sets, hIAPP was mixed with the SPs as well as their linear analogs in molar ratios of 1:0.5, 1:1, and 1:2 respectively, maintaining the same concentration of hIAPP. Thus, each set contained two replicate solutions. All the different sets were prepared in PBS at pH 7.4 and incubated on a water bath at 37 °C for seven days and thereafter, checked the fluorescence assay of hIAPP (40 μM) in the absence and presence of 20 μM, 40 μM and 80 μM of the peptides respectively.

The same procedure was followed to carry out the fluorescence assay, as discussed in chapter 2, section 2.6.2. The relative % of amyloid present in the sample was also calculated at the highest incubation time, using the following formula.

$$\%\ \text{of amyloid} = \frac{(\text{Observed fluorescence in the presence of peptide} - 1)}{(\text{Observed fluorescence in the absence of peptide} - 1)} \times 100\ \%$$

where 1 was considered as a normalization factor, as the minimum value of F/F_0 is 1.

From the time-dependent ThT fluorescence study, when incubated alone in PBS, the fluorescence intensity of hIAPP was found to increase with time (black,Figure . 5.12 (a)), but in the presence of 2-fold molar excess of **5A** (red, Figure 5.12 (a)) and **5B** (blue, Figure 5.12 (a)) the fluorescence intensity was suppressed significantly up to ~ 80-82%, indicating

sufficient inhibition of amyloid formation. However, in the presence of the control peptide, **5D** (olive , Figure 5.12 (a)), inhibition of amyloid aggregation occurred only up to ~40%. However, in the presence of the other control peptide, **5C** (magenta, Figure 5.12 (a)), where no turn-inducing element was present, negligible inhibition of aggregation of hIAPP was observed, roughly exhibiting 20% of amyloid inhibition.

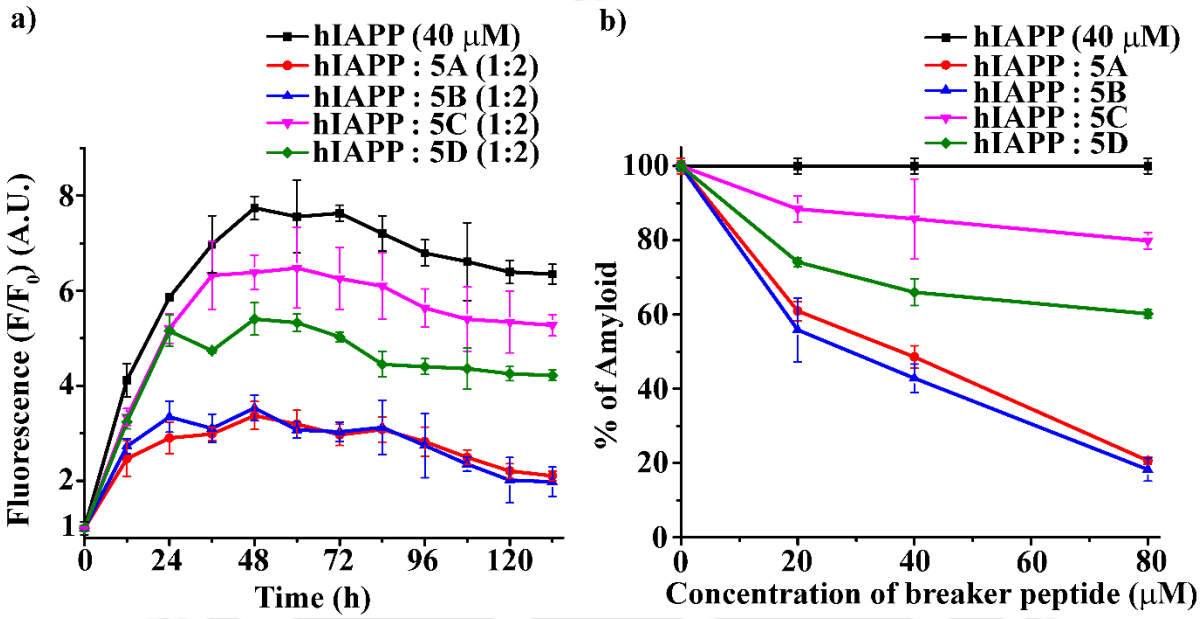

Figure 5.12: (a) Time dependent ThT fluorescence assay of hIAPP (40 μM) in absence (black) and presence of 2-fold molar ratios of peptides, **5A** (red), **5B** (blue), **5C** (magenta) and **5D** (olive). (b) Dose dependent ThT fluorescence assay of hIAPP (40 μM) in absence (black) and presence of varied molar excesses of the peptides **5A** (red), **5B** (blue), **5C** (magenta) and **5D** (olive).

Further, from the dose-dependent study of inhibition, we observed that in the presence of 0.5, 1, and 2-fold molar excesses of **5A** (Figure 5.12 (b) and 5.13 (a)) exhibited 39%, 51%, and 80% of inhibition, while with the same doses of **5B** (Figure 5.12 b and 5.13 b) exhibited 44%, 57% and 82% of inhibition respectively. While, in the presence of the control peptide **5C** (Figure 5.12 (b) and 5.13 (c)), we observed 11%, 14% and 20%, and in the presence of another linear analog **5D** (Figure 5.12 (b) and 5.13 (d)), we observed 26%, 34% and 40% of amyloid inhibition respectively with the same molar doses. Hence, it can be inferred that the

inhibition exhibited by 0.5- and 1-fold molar excess of the SPs is less than that of 2-fold molar excess of the same. In other words, an increase in doses of the peptides with respect to hIAPP, decreases the fluorescence intensity and hence increases the percentage of amyloid inhibition. Further, **5A** and **5B** were found to be better inhibitors of amyloid aggregation compared to **5C** and **5D**.

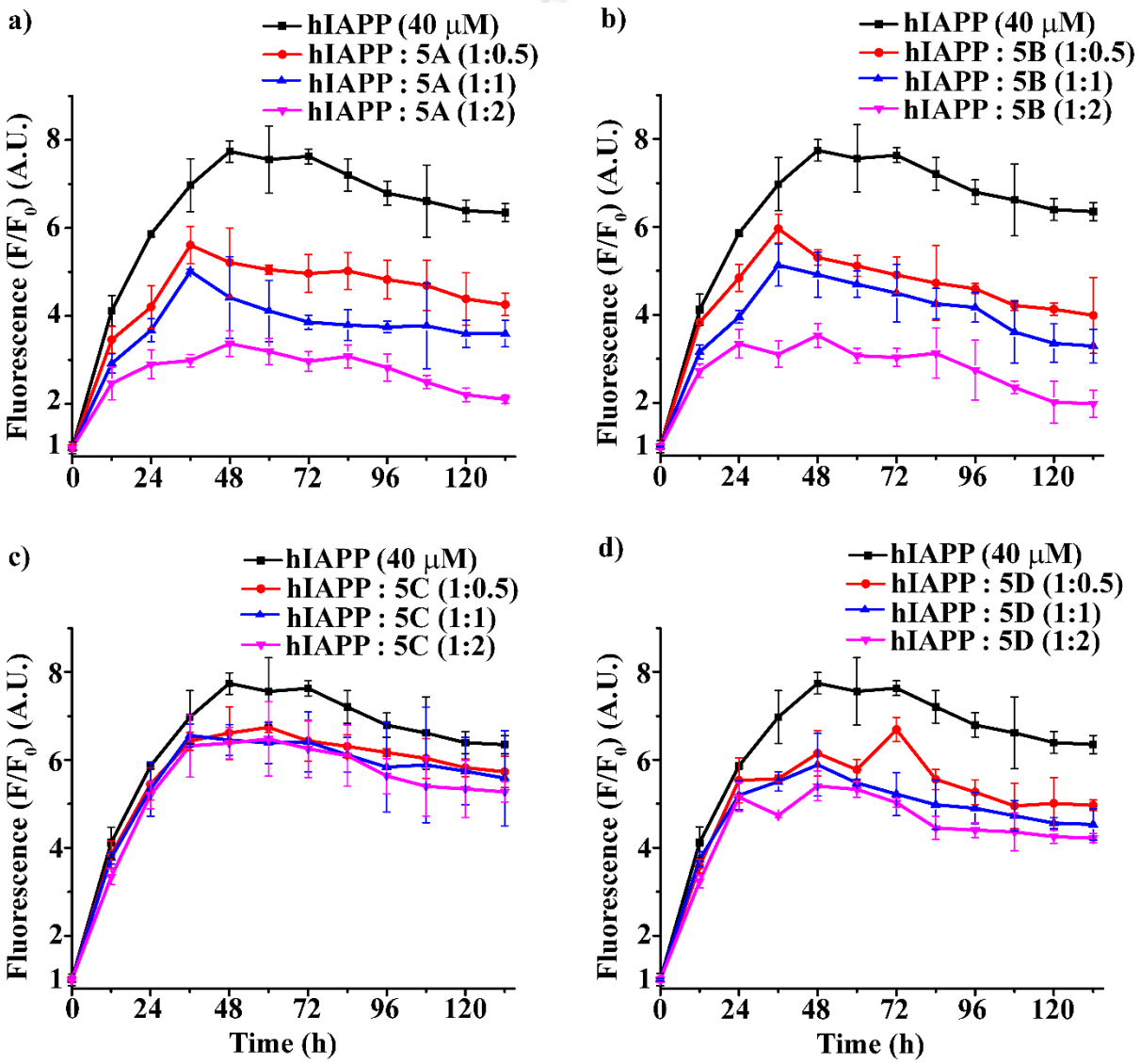

Figure 5.13: Time-dependent ThT fluorescence assay of hIAPP (40 μM) in the absence (black) and presence of 0.5-(red), 1-(blue) and 2-fold (magenta) molar ratios of (a) **5A**, (b) **5B**, (c) **5C** and (d) **5D**. Spectra were recorded at an interval of 12h after incubation of the peptide solutions in PBS (50 mM) at pH 7.4 and 37 °C.

5.6.3. Monitoring the amyloid formation by TEM and Congo red stained birefringence studies:

The existence of fibrillar assembly under transmission electron microscope (TEM) and the occurrence of green-gold birefringence of Congo red stained peptide sample when viewed under cross-polarised light gives direct evidence of amyloid formation.[23] After seven days of incubation of the peptide solutions at 37 °C in 50 mM PBS at pH 7.4, 10 μL aliquot of the peptide solution was taken out from the stock solution (as described in section 5.6) for TEM and birefringence analyses (sample preparation was described in chapter 2, section 2.5.2).

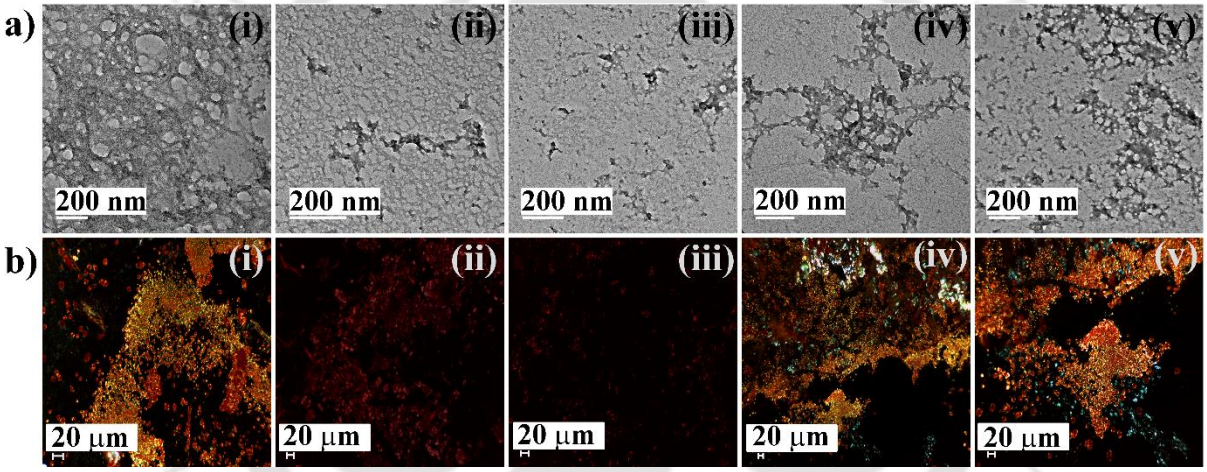

Figure 5.14: (a) TEM and (b) Congo red birefringence images of hIAPP (i) alone and in co-incubation with 2-fold molar ratios of peptidomimetics, **5A** (ii), **5B** (iii), **5C** (iv) and **5D** (v). Images were captured after seven days of incubation of the peptide solutions in PBS (50 mM) at pH 7.4 and 37 °C.

When hIAPP was incubated alone, it exhibited clear fibrillar-rich morphology (Figure 5.14 (a) (i)) when viewed under TEM, indicating amyloid formation of hIAPP. On the other hand, hIAPP, when incubated in the presence of 2-fold molar ratios of **5A** and **5B** (Figure 5.14 (a) (ii) and (iii) respectively), no such fibrillar assembly was observed; instead, some non-fibrillar amorphous aggregates were observed, indicating a substantial inhibition of hIAPP aggregation. While in the presence of similar doses of **5C** and **5D** (Figure 5.14 (a) (iv) and (v)

respectively), some fibrillar structures were observed, reflecting inefficiencies of the control peptides in inhibiting hIAPP aggregation.

Furthermore, from the Congo red stained birefringence analysis, when hIAPP was present alone, we observed clear green-gold birefringence under cross-polarised light (Figure 5.14 (b) (i)), indicating the formation of amyloid. On the contrary, in the presence of 2-fold molar ratios of **5A** and **5B** (Figure 5.14 (b) (ii) and (iii) respectively), green-gold birefringence was not observed , suggesting significant inhibition of hIAPP amyloids. However, in the presence of the linear peptides, **5C** and **5D** (Figure 5.14 (b) (iv) and (v) respectively) with the same molar ratios, some green-gold birefringence was observed, implying less efficiencies of the LPs to inhibit amyloid aggregation to the expected mark.

Therefore, from the investigations performed, it can be hypothesized that the SPs as well as their linear analogs were capable of inhibiting hIAPP aggregation. However, from the studies, both SPs, i.e., **5A** and **5B** appeared to be far better than the LPs, i.e., **5C** and **5D** in inhibiting hIAPP amyloid aggregation. In contrast, **5D** was a far better inhibitor than **5C**, which might be due to the presence of turn inducing moiety in its backbone.[64,129,161] Conversely, in the case of the stapled peptides, stapling itself solely plays a significant role in the inhibition process and the presence or absence of Ant moiety does not play a crucial role in exerting its affect on the inhibitory process. .

5.7. Disruption of preformed amyloid fibrils of hIAPP by synthesized peptides:

From the performed inhibition study with highly aggregating hIAPP, we observed that the SPs and the control peptides effectively inhibited the amyloid aggregation. Next, we explored the potentials of the peptides to disrupt the preformed hIAPP amyloid fibrils *in vitro*. From

the observed. ThT kinetics, the hIAPP fibrillization attained maximum at around after 45-50 hours from its incubation time period. Therefore, we allowed hIAPP to incubate alone in PBS at pH 7.4 and 37 °C up to 2 days (48h) and after that, we added the peptides into the solution of aggregating hIAPP in different molar ratios (i.e., at 0.5-, 1- and 2-fold molar ratios). As the peptide **5C** did not exhibit considerable effect in inhibiting hIAPP aggregation, we eliminated it from the disruption study. The efficiencies of the peptides to alter the structure of preformed amyloid was monitored by various biophysical experiments. The samples for the different studies were prepared in a similar way as in section 5.6.

5.7.1. Monitoring conformational transition by CD and FTIR studies:

Initially, we performed the CD after 7 (2+5) days of incubation, and from the experiment, we noticed a negative band at ~ 218 nm and a simultaneous positive band at ~198 nm when hIAPP was incubated alone (black, Figure 5.15 (a)), indicating characteristic bands for β-sheet rich conformation. However, in the presence of 2-fold molar ratios of the SPs, i.e., **5A** and **5B** (red and blue respectively, Figure 5.15 (a)) with the aggregating hIAPP, the β-sheet content was found to decrease with gradual transformation to random coil conformation, indicating significant disruption of hIAPP aggregation by the SPs. On the other hand, in the presence of a similar molar ratio of the control linear peptide **5D** (magenta, Figure 5.15 (a)), we observed minor β-sheet rich conformation, indicating non-significant disruption of the fibrillar network of the aggregating peptide.

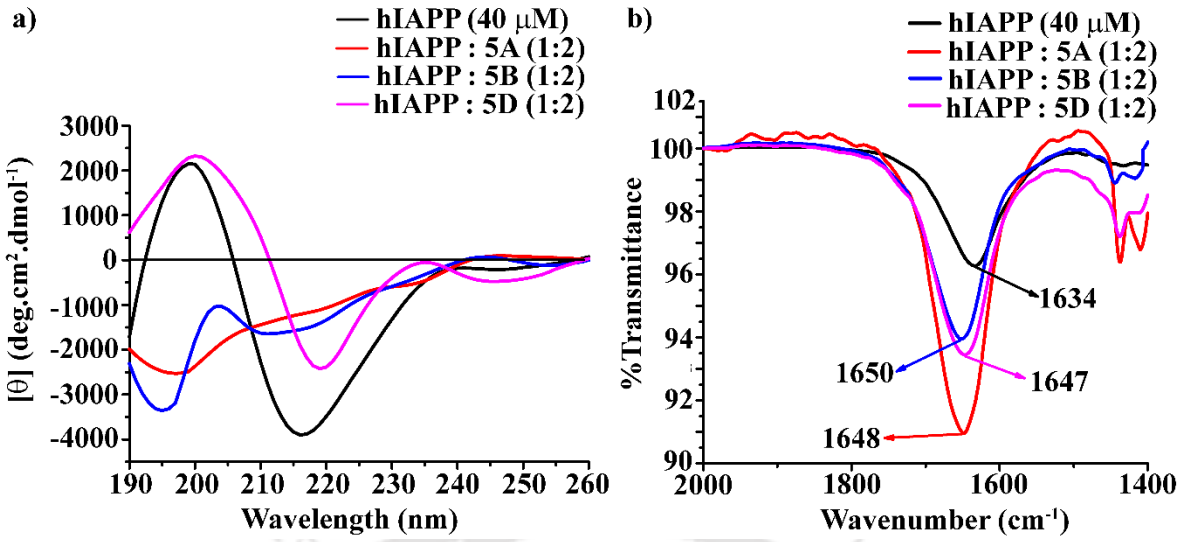

Figure 5.15: (a) CD and (b) FTIR spectra of hIAPP in the absence (black) and presence of 2- fold molar ratios of **5A** (red), **5B** (blue) and **5D** (magenta). Images were taken after seven days of incubation of the peptide solutions in PBS (50 mM) at pH 7.4 and 37 °C.

Further, the change in conformation of the aggregating peptide hIAPP in the presence of the SPs and the control peptides was investigated through FT-IR experiments. From the analysis, when hIAPP was present alone after 7 (2+5) days of incubation, we observed a sharp peak at 1634 cm^{-1}, which was a characteristic amide I band for aggregated β-sheet conformation (black, Figure 5.15 (b)). However, when the stapled peptides, **5A** and **5B** were co-incubated with hIAPP in 2-fold molar ratios, the specific amide band disappeared, while new bands appeared at 1648 cm^{-1} and 1650 cm^{-1} respectively, indicating non-β-sheet conformation (red and blue respectively, Figure 5.15 (b)). Again, in the presence of 2-fold molar ratio of **5D** , a new band was observed at 1647 cm^{-1}, indicating a conformational change of hIAPP (magenta, Figure 5.15 (b)). These results indicated the conversion of β-sheet into non-β-sheet conformation, which supports the disruption efficiency of the preformed amyloid of hIAPP by the SPs.

5.7.2. Monitoring the kinetics of amyloid disruption by ThT fluorescence assay:

After the CD and FT-IR experimental analyses, we proceeded for the Thioflavin T (ThT) fluorescence assay, which would enable us to monitor the kinetics of disruption of preformed amyloid of hIAPP. For this assay, we incubated hIAPP at physiological conditions up to 48h, and the synthesized peptides, i.e. the SPs and the control peptide were added to the aggregated hIAPP after the stipulated time.

From the time-dependent ThT fluorescence assay, we observed that when hIAPP was present alone in solution, the fluorescence intensity was found to increase with time (black, Figure 5.16 (a)). In contrast, after the addition of **5A** and **5B** (red and blue respectively, Figure 5.16 (a)), the intensity was suppressed significantly up to ~75-78%, indicating disruption of preformed fibrils. While in the presence of 2-fold molar excess of the control peptide **5D** (magenta, Figure 5.16 (a)), the fluorescence intensity got suppressed up to ~38% only, indicating minimal disruption of hIAPP fibrillization.

Further, the different molar ratios (0.5, 1, and 2-fold) of the peptides **5A**, **5B** and **5D** were added to the preformed fibrillar assembly of hIAPP; as the doses increased from 0.5 to 2-fold molar ratios, the fluorescence intensity decreased significantly with time. We observed that in the presence of 0.5-, 1, and 2 fold molar ratios of **5A** (Figure 5.16 (b) and 5.17 (a)), hIAPP exhibited 44%, 56%, and 75%, while with the same doses of **5B** (Figure 5.16 (b) and 5.17 (b)) exhibited 47%, 61% and 78% of disruption respectively. However, in the presence of the control peptide, **5D** (Figure 5.16 (b) and 5.17 (c)), disruption of the preformed amyloid of hIAPP was observed only up to 25%, 32%, and 38% with the same doses. Hence, the fibril formed by hIAPP was reduced by peptides **5A** and **5B** more significantly than **5D** at different time intervals.

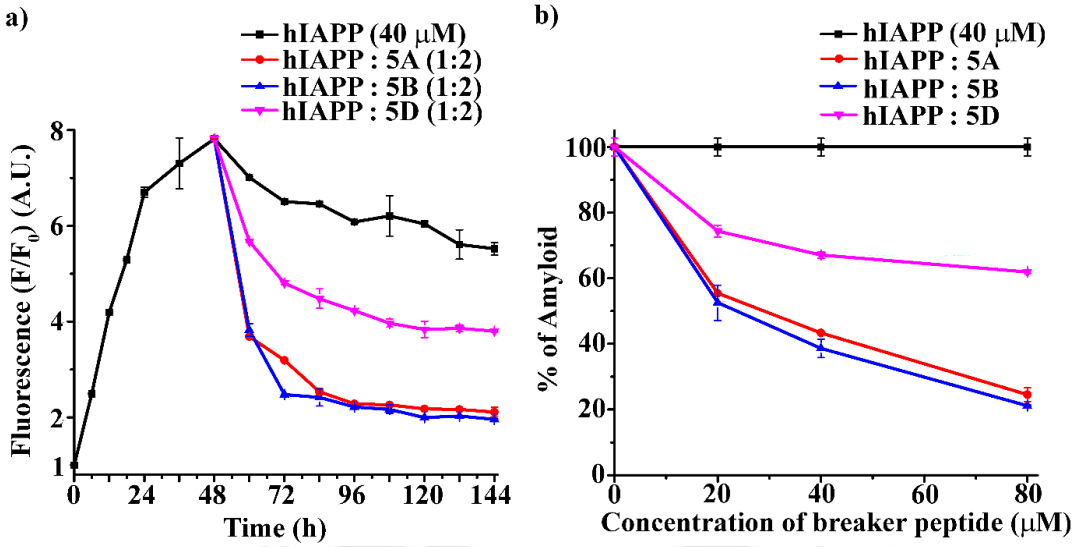

Figure 5.16: Time-dependent ThT fluorescence assay of hIAPP (40 μM) in the absence (black) and presence of 2-fold molar ratios of **5A** (red), **5B** (blue), and **5D** (magenta). (b) Dose-dependent ThT fluorescence assay of hIAPP (40 μM) in the absence (black) and presence of varied molar excesses of **5A** (red), **5B** (blue), and **5D** (magenta). Spectra were recorded at an interval of 12 hrs after incubation in PBS (50 mM) at pH 7.4 and 37 °C.

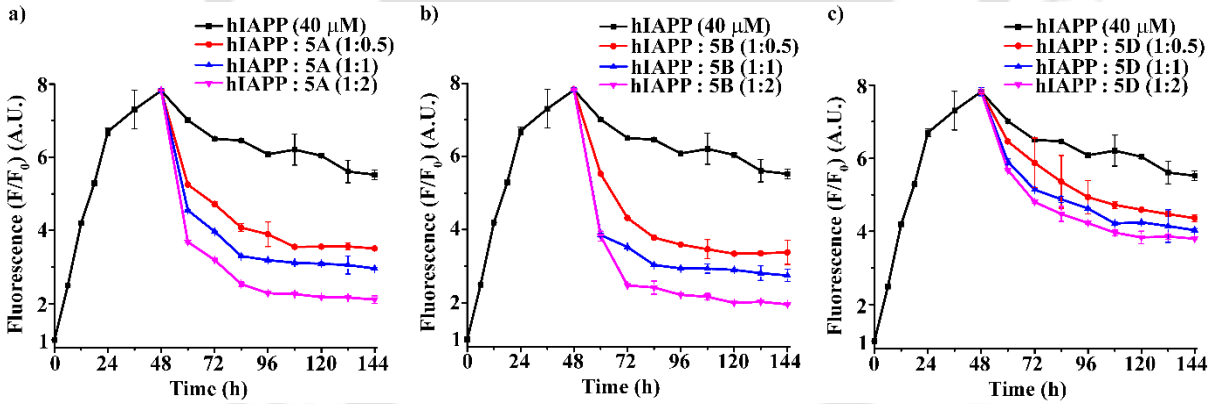

Figure 5.17: Time-dependent ThT fluorescence assay of hIAPP (40 μM) in the absence (black) and presence of 0.5-(red), 1-(blue) and 2-fold (magenta) molar ratios of (a) **5A** (red), (b) **5B** (blue) and (c) **5D** (magenta). Spectra were recorded at an interval of 12h after incubation in PBS (50 mM) at pH 7.4 and 37 °C.

5.7.3. Monitoring disruption of preformed amyloid by TEM and Congo red stained birefringence assay:

Following the conformational study and the ThT fluorescence assay, our next target was to demonstrate the effect of the SPs and the linear control peptide on the preformed amyloid of

hIAPP using TEM and Congo red stained birefringence analyses. The appearance of fibrillar assembly under an electron microscope and green-gold birefringence under crossed polarized light after staining with Congo red are characteristic properties of amyloid formation.

Hence to explore the amyloidogenicity, we performed TEM analysis of hIAPP alone after seven days of incubation in PBS (50 mM) at pH 7.4 and 37 °C and observed transparent fibrillar assembly under the electron microscope (TEM), which confirmed the formation of amyloid (Figure 5.18 (a) (i)). On the other hand, hIAPP when incubated in the presence of 2-fold molar excesses of **5A** (Figure 5.18 (a) (ii)) and **5B** (Figure 5.18 (a) (iii)), we did not observe any such fibrillar assembly indicating significant disruption of preformed amyloid by the stapled peptides. On the contrary, when hIAPP was incubated in the presence of **5D** (Figure 5.18 (a) (iv)) at the same molar ratio, we observed some fibrillar assembly, indicating insignificant disruption of the preformed amyloid by the linear peptide.

In addition, after seven days of incubation, the disruption of preformed amyloid of hIAPP by the stapled peptides was also investigated through Congo red-stained birefringence study. When hIAPP was present alone in the sample (Figure 5.18 (b) (i)) it exhibited green-gold birefringence when viewed under cross-polarised light upon staining with Congo red, which indicated the formation of amyloid. However, hIAPP when incubated in the presence of 2-fold molar excesses of **5A** (Figure 5.18 (b) (ii)) and **5B** (Figure 5.18 (b) (iii)), we did not observe any such characteristic birefringence under the same circumstances, suggesting a significant disruption of preformed amyloid by the stapled peptides. In contrast, when hIAPP was present with the control linear peptide **5D** in a 2-fold molar ratio (Figure 5.18 (b) (iv)), we observed little green-gold birefringence, indicating insufficient disruption of amyloid by the linear peptide.

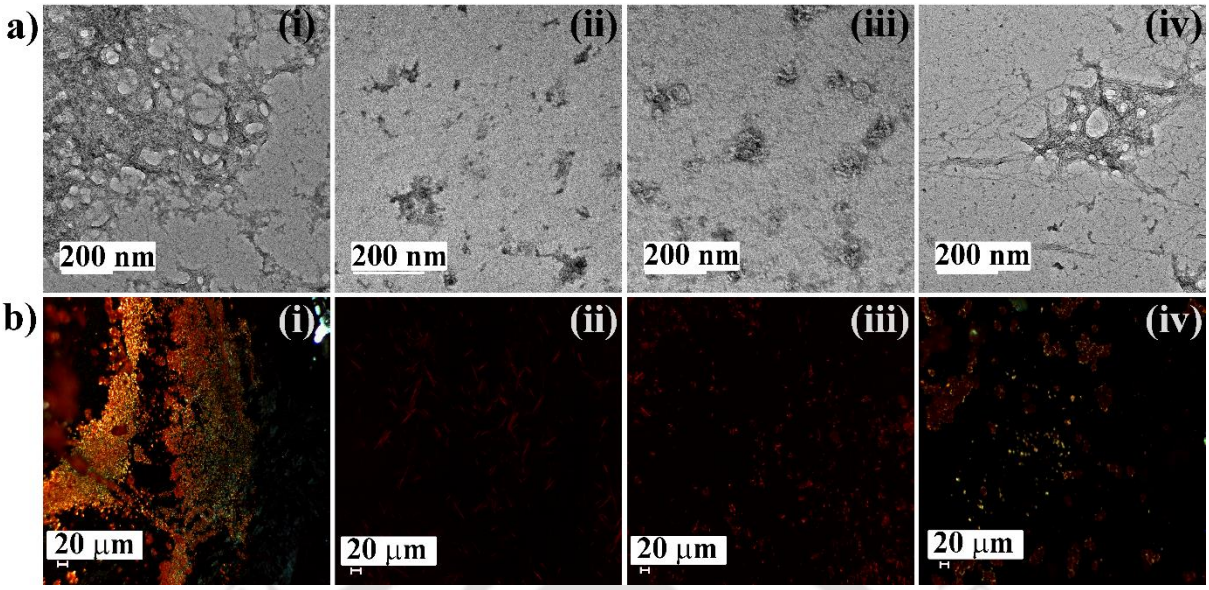

Figure 5.18: (a) TEM and (b) Congo red birefringence images of hIAPP (i) alone and in co-incubation with 2-fold molar ratios of peptidomimetics, **5A** (ii), **5B** (iii) and **5D** (iv). Images were captured after seven days of incubation of the peptides in PBS (50 mM) at pH 7.4 and 37 °C.

Hence, from the systematic *in vitro* biophysical studies on thedisruption of preformed fibril of hIAPP by the stapled peptides along with control linear peptides, we observed that SPs were far more efficient than the control peptide in disrupting the preformed fibrillar amyloid of hIAPP. Further, both the stapled peptides **5A** and **5B** exhibited almost similar disruption efficiencies, indicating that peptide stapling itself plays a crucial role, independent of the presence or absence of breaker moiety to disrupt the fibrillar network. Further, the dose-dependent studies reveal that, as the dose increases from 0.5- to 2-fold molar ratio with respect to the aggregating hIAPP peptide, disruption of the preformed amyloid also increases in ascending order.

5.8. *In vitro* toxicity study using dye loaded LUV leakage study:

As mentioned in the earlier chapters, the amyloid fibril of the amyloidogenic peptides, hIAPP, can disrupt the cell membrane, which is responsible for the destruction of β-cells during T2D disease.[135] However, in fact, the soluble oligomers of hIAPP are the main culprits for the damage of the cell membrane.[43,132]

It was clear from the disruption study of hIAPP that our designed SPs were able to disrupt the preformed amyloid but to confirm the presence of non-toxic species, we performed a carboxyfluorescein dye leakage assay, where the dye was entrapped inside the LUVs.[159] To carry out the vesicle leakage study, we prepared six sets of different samples, including the untreated LUVs (without any peptide) as a control. $hIAPP_{1-37}$ was allowed to incubate up to 48h at physiological conditions, and the peptides (**5A**, **5B**, and **5D**) were added to that solution of hIAPP and again kept for incubation for another five days (168h = 48h + 120h) to form the mature fibrils. After this, the different peptide solutions were added separately to the LUVs, and the dye leakage assay was carried out. The different samples prepared for the study are shown as follows:

Sample 1- Untreated LUVs

Sample 2- hIAPP (incubated for 5h) + LUVs

Sample 3- hIAPP (incubated for 7 days) + LUVs

Sample 4- hIAPP: **5A** (1:2) + LUVs

Sample 5- hIAPP: **5B** (1:2) + LUVs

Sample 6- hIAPP: **5D** (1:2) + LUVs

During the dye leakage study, the peptide and lipid ratio was kept at 1:20 molar ratio, where the samples' concentration was maintained at 2.5 μM and the lipid solution was obtained as 50 μM. To measure the 100% dye leakage from the LUVs, 10 μL of Triton X-100 were added at the end of the experiment, which induces total disruption of the lipid vesicles. The % of dye leakage was calculated as[137]

$$\% \text{ Leakage} = \frac{(\text{observed fluorescence} - \text{initial fluorescence})}{(\text{total fluorescence} - \text{initial fluorescence})} \times 100\ \%$$

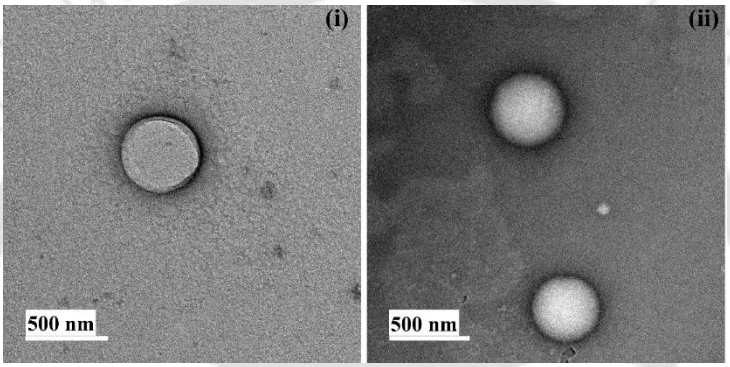

Figure 5.19: TEM images of the large unilamellar vesicles (LUVs) at a concentration of 1 mM in PBS buffer (50 mM). Scale bar is indicated as 500 nm.

From the experiment, a rapid increment in fluorescence intensity was observed for sample 2 (i.e., hIAPP incubated for 5h), which indicated maximum dye leakage from the LUVs from 0 to 100 min, but after 12h, there was no such increment (red, Figure 5.20 (a) and (b)). We observed a significant dye leakage (52% in 100 min and 59% in 72h) from the 5h old hIAPP containing LUV (sample 2), which suggested the presence of sufficient number of pore-forming toxic soluble oligomers. On the other hand, very less % of dye release was observed for sample 3 (15% in 100 min and 20% in 72h) (blue, Figure 5.20 (a) and (b)), which indicated the formation of mature fibrils of hIAPP after incubating for seven days at physiological conditions. Therefore, from the experimental findings of the dye leakage assay, it was noticeable that the soluble oligomers formed after 5h of incubation from hIAPP were

found to be more toxic than the full-grown fibrils obtained from hIAPP after seven days (168h) of incubation. Oligomers generate significant number of pores on the vesicles, thereby leading to the leakage of the carboxyfluorescein dye from the artificial cells, hence, enhancing the sample's fluorescence intensity.

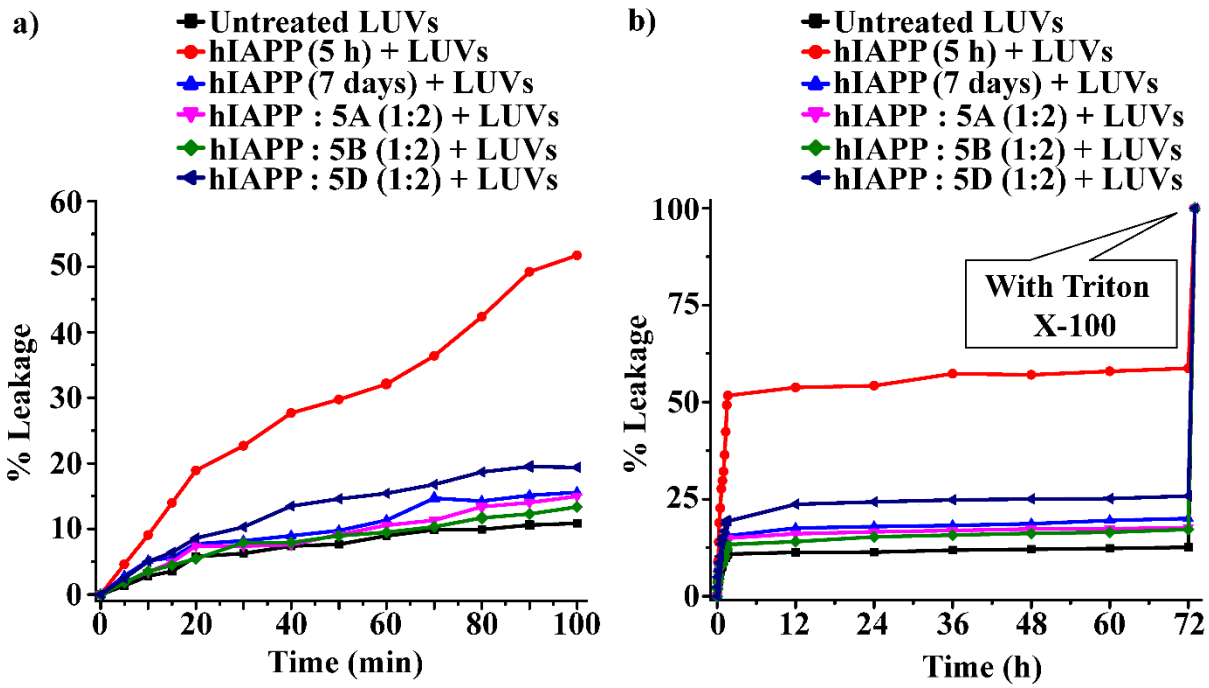

Figure 5.20: Emission of carboxyfluorescein dye from the LUVs with time, in terms of pore formation on LUVs showing the effect of hIAPP. (a) Dye released from LUVs alone and in the presence of different solutions from (a) 0 min to 100 min and (b) 0h to 72h.

On the contrary, disruption of preformed fibrils by the designed SPs (**5A** and **5B**) and the LP (**5D**) did not form pores on the LUVs significantly, as the enhancement of their corresponding fluorescence intensity (sample 4; magenta, sample 5; olive and sample 6; navy respectively, Figure 5.20 (a) and (b)) was observed to be as low as that of the untreated LUVs (sample 1, black, Figure 5.20 (a) and (b)). Hence, from the above investigation, it was clear that the SPs were able to disrupt the hIAPP amyloid, and this result of the dye leakage assay highlighted the non-toxic behaviour of the disrupted components of the preformed fibril of hIAPP.

5.9. Preliminary investigation of the mode of inhibition of aggregating hIAPP by the stapled peptides:

To gain insight into the mode of inhibition of hIAPP aggregation by the SPs, we examined the changes in the size distribution pattern of different particles by DLS and change in morphology *via* TEM analysis of hIAPP alone and in the presence of the SPs at different time intervals.[108,146,147] Further, to check the membrane disrupting nature of the species generated during inhibition of hIAPP agrreagtion in the presence of SP, we carried out another LUV leakage assay by entrapping carboxyfluorescein dye into the LUVs.[136] As the inhibition efficiencies of both the SPs were nearly similar, for the present study, we considered only **5B** with hIAPP. For the mechanistic investigations, hIAPP (40 μM) alone and in the presence of a 2-fold molar ratio of **5B** (80 μM) were incubated at pH 7.4 and 37 °C for 24h.

From the DLS study, the size distribution in terms of hydrodynamic diameter (d) was observed to change in ascending order of the untreated hIAPP samples. The samples incubated for 0h, 6h, 12h and 24h, showed size distribution ~ 1 nm, ~100 nm, 100-1000 nm, and 1000-10000 nm, respectively (Figure 5.21 (a) (i-iv)), indicating the conversion of monomeric species (at 0h) into mature fibrils (at 24h) *via* oligomeric species (6h and 12h) as observed in the previous chapter. On the contrary, when hIAPP was co-incubated with **5B**, modulated fibrillization of hIAPP was observed. At 0h, **5B** treated hIAPP exhibited two types of species, one having size distribution centred at 100-1000 nm with another reduced size distribution of ~1 nm (Figure 5.21 (b) (i)). The formation of higher-sized species implies that hIAPP, after mixing with **5B** assembled instantly to generate some specific aggregated species by altering the native aggregation pathway of hIAPP. Further, the **5B** treated samples exhibited hydrodynamic diameters of 1000-10000 nm species as the time increases from 6h to 24h (Figure 5.21 (b) (ii-iv). These results indicated that upon prolonged incubation of

hIAPP with **5B**, the formation of oligomers or smaller species was prevented. In other words, the presence of **5B** diverted the native aggregation pathway of hIAPP thereby leading to the generation of some larger amorphous aggregates.

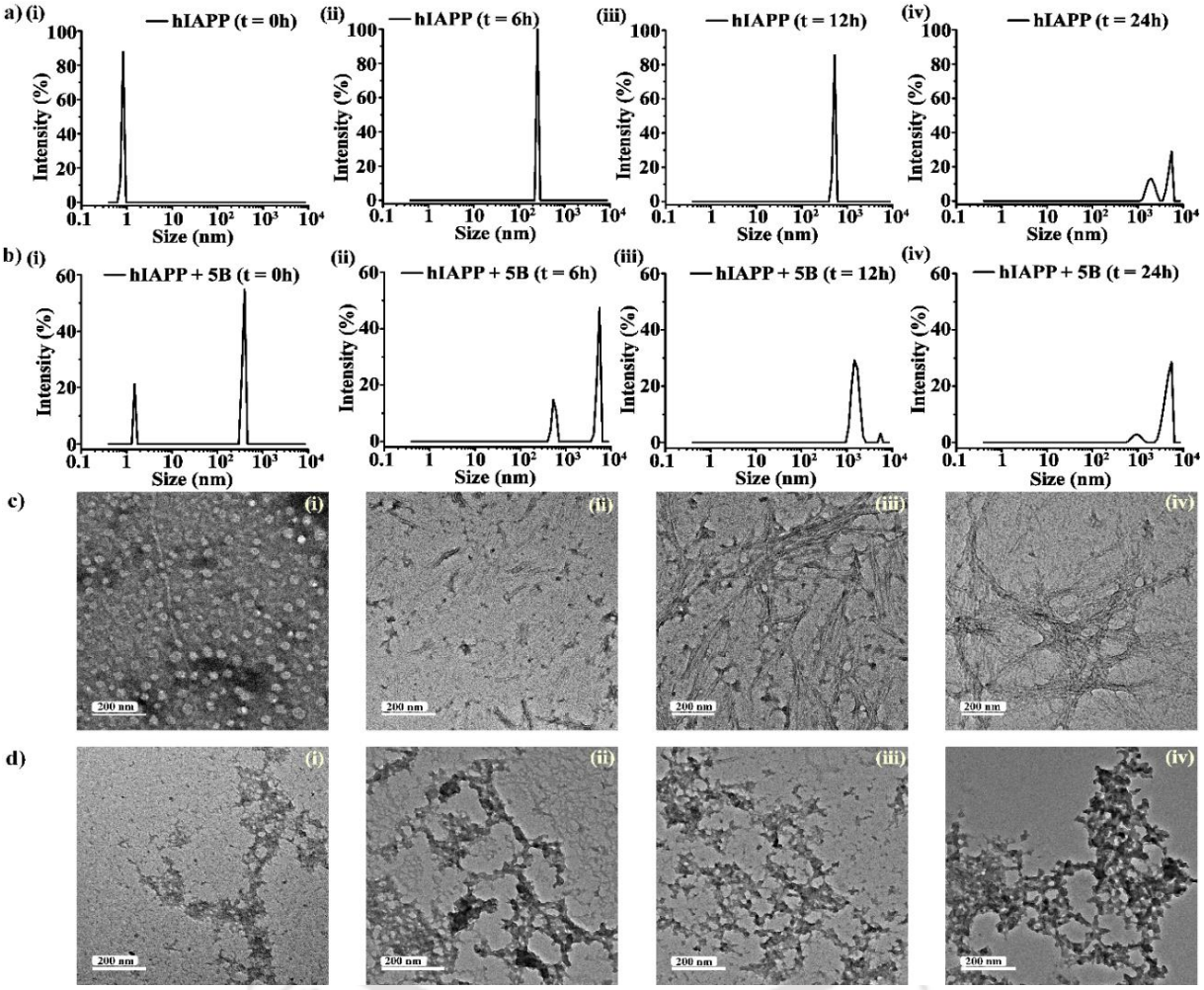

Figure 5.21: DLS study showing the change in size distributions of hIAPP incubated alone (a) and in co-incubation with 2-fold molar ratio of **5B** (b) at 0h (i), 6h (ii), 12h (iii) and 24h (iv) respectively. TEM images exhibiting the change in morphology of hIAPP incubated alone (c) and in co-incubation with 2-fold molar ratio of **5B** (d) at 0h (i), 6h (ii), 12h (iii) and 24h (iv) respectively. The scale of TEM images indicates 200 nm.

Further, to validate this phenomenon, we investigated the morphological changes *via* TEM analysis. In TEM, we observed a transitional growth of untreated hIAPP, converting from small spherical species (at 0h) to mature fibrils (at 24h) *via* oligomeric intermediates (at 6h and 12h) (Figure 5.21 (c) (i-iv)). In contrast, with **5B** treated hIAPP samples, we did not

observe any fibrillar species at all; instead, some amorphous aggregates were observed (Figure 5.21 (d) (i-iv)), indicating altering of the fibrillization process of hIAPP upon binding with **5B**.

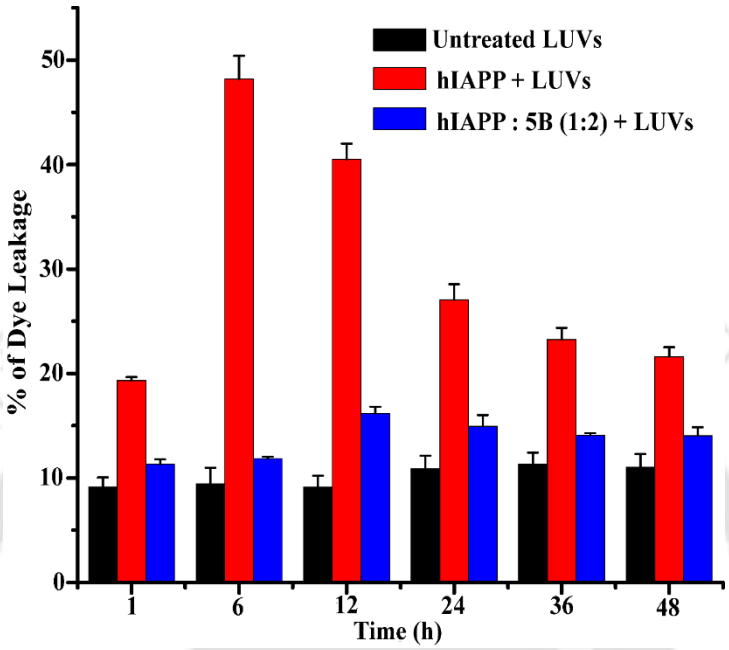

Figure 5.22: The emission of carboxyfluorescein dye showing the effect of hIAPP on the LUVs with time and % of dye leakage during the inhibition process in the absence and presence of **5B** with hIAPP from 1h to 48h.

Further, to examine the toxicity of the species present during the fibrillization of untreated and **5B** treated hIAPP, we carried out a LUV dye leakage assay. In this assay, hIAPP in the absence and presence of **5B** were incubated for 1, 6, 12, 24, 36, and 48h in PBS and then added to LUVs to obtain a final concentration of 50 µM of the lipids, maintaining 1:20 ratio for the peptide and lipid respectively. From the investigation, we observed the highest dye leakage from the 6h incubated untreated hIAPP (red, Figure 5.22), indicating severe toxicity arising from the oligomeric species. On the other hand, the dye leakage was found to decrease as the incubation period increases from 6h to 24h, validating the assumption that mature fibrils are less toxic than the oligomers. On the contrary, with the **5B** treated hIAPP samples (blue, Figure 5.22), we did not observe any significant dye leakage from the LUVs

as the fluorescence intensity was observed to be as low as the untreated LUVs (black, Figure 5.22).

Hence, from the observation of size distribution and morphology, it can be hypothesized that the binding of **5B** with hIAPP restricts the formation of oligomeric species and helps in the formation of some amorphous aggregates by altering the native aggregation process of hIAPP. Moreover, during the fibrillization process of hIAPP, the species generated upon binding with **5B** were found to be non-toxic, as they could not disrupt the membrane of the LUVs. Thus, the formation of non-toxic amorphous species proposes the fact that **5B** triggers the hIAPP aggregation towards an "off-pathway" aggregation route instead of its conventional pathway, which is in line with the previous reports.[163]

5.10. Proteolytic stability study:

The major complication for peptide-based drugs is their proteolytic instability, as they degrade effortlessly in the presence of proteolytic enzymes.[139] In order to check the enzymatic stability of the synthesized peptides, we carried out a stability study *in vitro* in the presence of RPMI (Roswell Park Memorial Institute) 1640 media supplemented with 10% FBS serum (v/v) and 1% Penicillin/Streptomycin Antibiotic, obtained from GIBCO, which contains a sufficient amount of proteolytic enzymes. We compared the stabilities of **5A** and **5B** with their respective linear analogs **5C** and **5D** using analytical HPLC and MALDI-TOF mass spectrometry. For the stability study, 1 mL of the RPMI media was transferred in four different Eppendorf tubes and incubated at 37 °C for 15 minutes. After which, 10 μL of the peptide solutions (**5A**, **5B**, **5C**, and **5D**) in DMSO (10 mg/mL) were added separately to the RPMI media with the same procedure as explained in Chapter 2, section 2.9. From the serum precipitation process, the supernatant was collected and analyzed by RP-HPLC and MALDI-TOF mass analyses. A linear gradient of 5-95% CH_3CN for 8 mins, 95% CH_3CN until 9 mins

followed by 5% CH_3CN up to 10 mins was used at a flow rate of 1 mL/min using an analytical C18 column anda binary solvent system, comprising of solvent A (0.1% TFA in H_2O) and solvent B (0.1% TFA in CH_3CN).

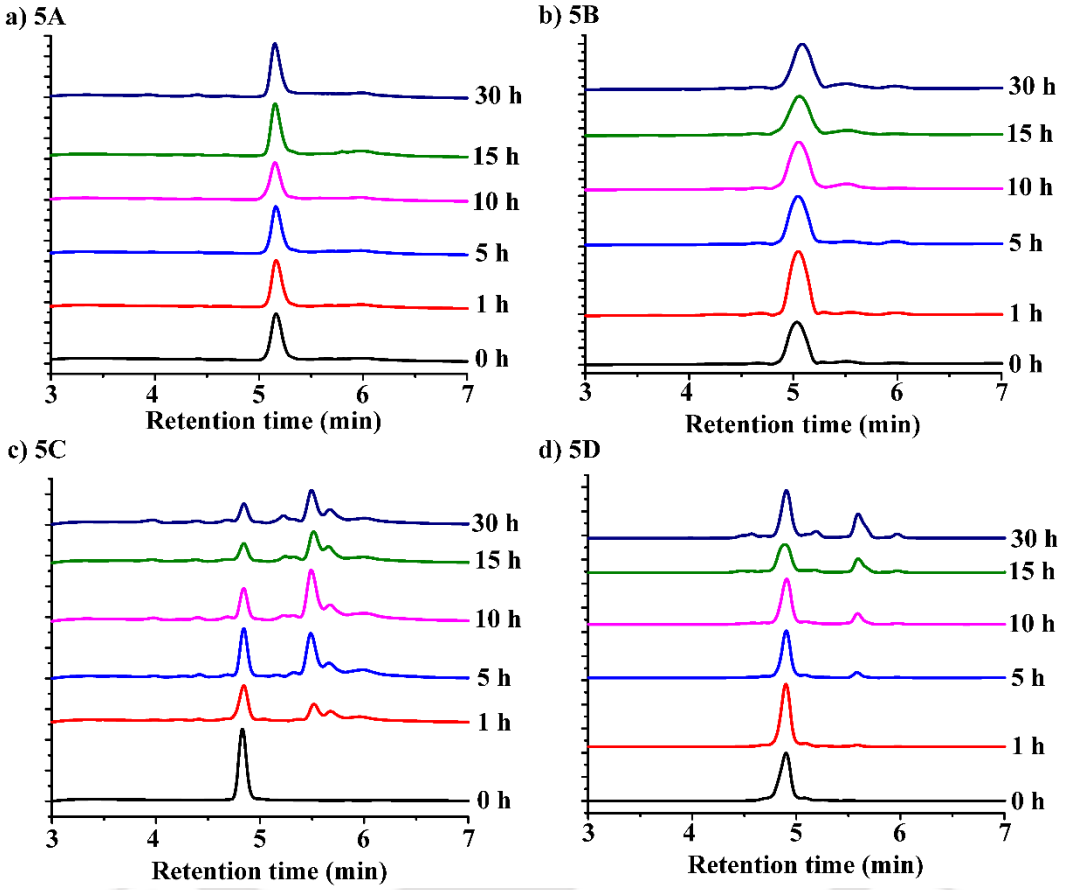

Figure 5.23: Kinetics of stability of peptides **5A** (a), **5B** (b) **5C** (c) and **5D** (d) in the presence of proteolytic enzymes (RPMI media) monitored by RP-HPLC.

From the time-dependent, HPLC study, in the presence of proteolytic enzymes, **5A** and **5B** (Figure 5.23 (a) and 5.23 (b) respectively), not a single trace of degradation was observed up to 30h, rather, absolute retention of the original compound peaks were detected. Contrarily, the linear peptide **5C** (Figure 5.23 (c)), where only α-amino acids were present, started degrading after 1h of incubation in the presence of the enzymes with only a trace of the original compound being observed after 10h. On the other hand, the other linear peptide **5D**

(Figure 5.23 (d)), where one Ant moiety was present, started minimal degradation after 5h. However, after 30h of incubation, around 30% of the peptide was degraded in the presence of the proteolytic enzymes.

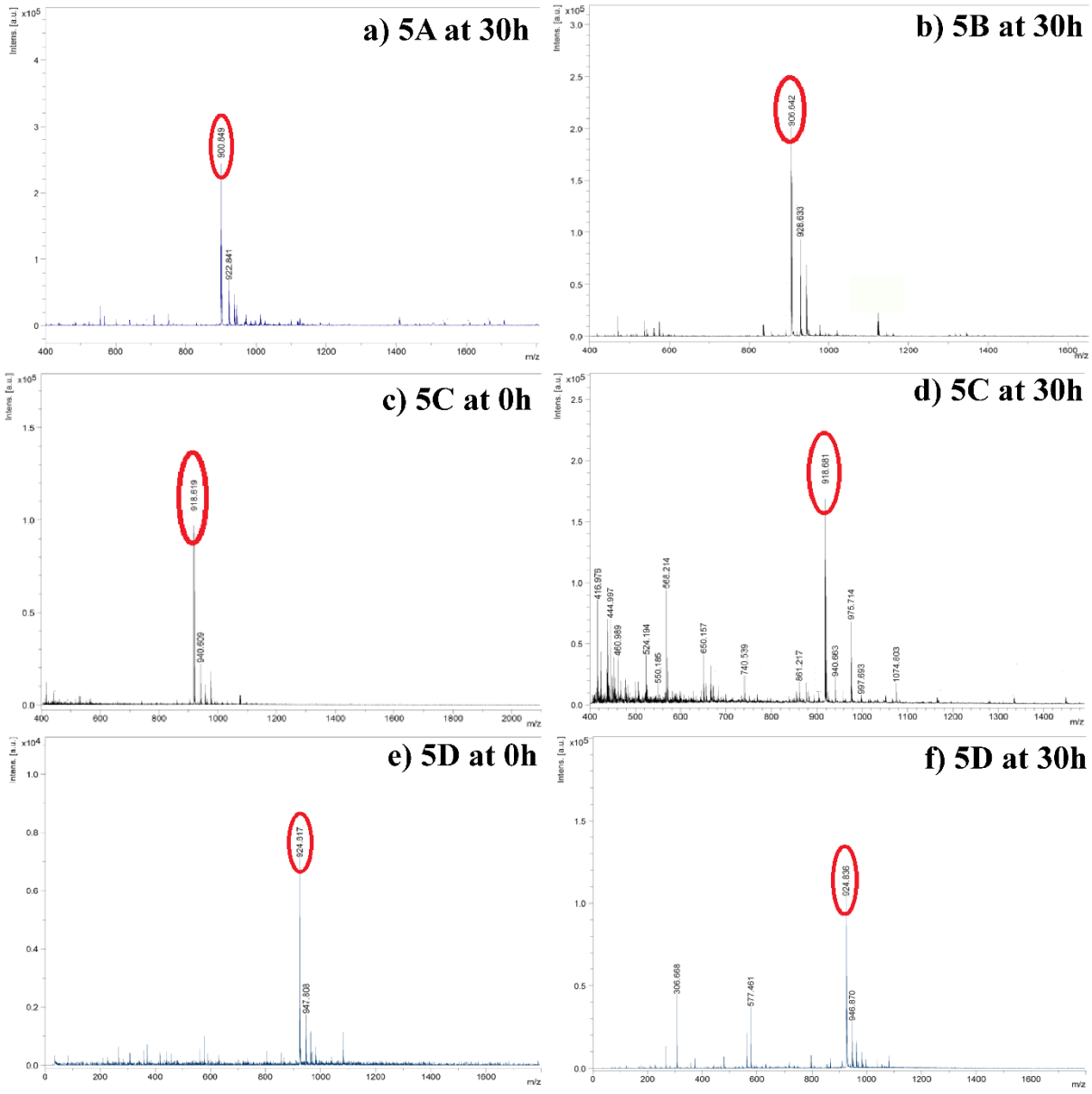

Figure 5.24: MALDI-TOF mass spectra of peptides a) **5A** at 30h b) **5B** at 30h c) **5C** at 0h, d) **5C** at 30h, e) **5D** at 0h and f) **5D** at 30h after the addition of human serum.

Further, from the MALDI-TOF mass analyses, for the peptides **5A** and **5B** we observed complete retention from 0h to 30h (Figure 5.24 (a) and (b)). On the contrary, the pure mass spectra were observed for **5C** at 0h only, but from 1h onwards, some trace of degradation was

observed which continued up to 30h (Figure 5.24 (c) and (d)). Similarly, for the peptide **5D**, original mass spectra were observed up to 5h, but after which some degradation peaks were observed which retained up to 30h (Figure 5.24 (e) and (f)). Hence, it can be presumed that the presence of β-amino acid increases some proteolytic stability compared to α-amino acid-containing peptides.Moreover, stapling itself increases further proteolytic stabilities as the stapled peptides, **5A** and **5B** were relatively resistant to sustain degradation in the presence of proteolytic enzymes compared to their linear precursors **5C** and **5D**.

5.11. Conclusion:

Our earlier reports showed that insertion of a conformationally restricted element in the peptide backbone achieved attractive effectiveness towards modulation of highly aggregating hIAPP or other amyloidogenic peptides. Moreover, from reported articles, we have observed that peptide stapling also brings research output as a therapeutic tool for Alzheimer-related disease. Hence, to give a direction towards the T2D, we wished to investigate the efficiencies of the stapled peptides in anti-amyloid activity with the highly aggregating peptide hIAPP.

Hence, here we demonstrated the design and development of two types of side-chain to tail stapled peptides **5A** and **5B**, one with the presence and another with the absence of a turn inducing moiety (Ant), and compared their efficacies towards hIAPP inhibition with the linear analogs, **5C** and **5D** containing the same moietyin the peptide sequence. Initially, we investigated the amyloidogenic behaviour of the synthesized peptides, and observed that **5A**, **5B** and **5D** were found to be non-amyloidogenic in nature at physiological conditions. However, **5C**, where no turn-inducing moiety was present, showed some characteristics of amyloid aggregates. From the systematic studies, it is clear that both the stapled peptides **5A** and **5B** are potent inhibitors to the highly aggregated amyloid fibrils generated from hIAPP,

with 2-fold molar ratios of them showing the most efficient inhibition abilities. Further, these two SPs can potentially disrupt the preformed amyloid fibril of hIAPP into non-toxic species, as confirmed fromthe dye leakage assay. The higher structural rigidity of the SPs may emerge them as better inhibitors only in two-fold molar excess in contrast to other breaking strategies. In other words, these two SPs, i.e., **5A** and **5B**, showed far better efficiencies toward inhibition and disruption than their linear analogs, **5C** and **5D**.

Further, the efficiency towards suppressing the aggregation of hIAPP was independent of the presence of the turn-inducing moiety (Ant), which indicated that the factor of 'peptide stapling' in terms of conformational restriction solely plays a vital role in arresting the amyloids formed. Moreover, the systematic analysis *via* DLS and TEM analyses established that SPs alter the native aggregation pathway of hIAPP into off-pathway aggregation, and the generated species were found to be non-toxic as revealed from the LUVs dye leakage assay. After that, we demonstrated that the SPs were relatively stable than their linear analogs in the presence of proteolytic enzymes. The enzymatic stability enhancement of the SPs was supposed to be due to the conformational strain imposed by the stapling. Hence, with more fruitful analysis and survey in this direction, the stapled peptides may emerge as new therapeutic implementations towards the society to challenge against T2D or related diseases soon.

Chapter 6: Experimental Section

6.1. Material and methods:

6.1.1. Reagents and Solvents:

Rink Amide MBHA resin (loading 0.7 mmol/g), human Islet Amylin Polypeptide (hIAPP), all Fmoc amino acids with the specific side-chain protecting groups (Boc for lysine, t-Butyl for glutamic acid and Pbf for arginine), Fmoc-chloride (Fmoc-Cl), BOP [(Benzotriazole-1-yloxy) tris (dimethylamino) phosphonium hexafluorophosphate] and PyBOP [(Benzotriazole-1-yloxy-tris-pyrrolidine-phosphonium hexafluorophosphatte] were purchased from GL Biochem (Shanghai, China). The reagent, Ethyl 2-cyano-2-(2-nitrobenzenesulfonyloxyimino) acetate known as o-NosylOXY was used as a coupling reagent and synthesized in the laboratory from Ethyl-hydroxyiminocyanoacetate (Oxyma) and 2-nitrobenzenesulphonyl chloride. 5(6)-Carboxyfluorescein, *N*-Fmoc-*N''*-succinyl-4,7,10-trioxa-1,13-tridecanediamine 1,1,1,3,3,3-hexafluoro-2-propanol (HFIP), Fmoc-Ant-OH (Fmoc-Anthranilic acid), dansyl chloride, Diisopropylethylamine (DIPEA), Thioflavin T (ThT), and Congo red dyes were purchased from Sigma-Aldrich. Zinc bromide ($ZnBr_2$) and Ferric chloride ($FeCl_3$) were purchased from Alfa-Aesar. 1,2-Dipalmitoyl-sn-glycero-3-phosphocholine (DPPC), 1,2-Dimyristoyl-sn-glycero-3-phosphocholine (DMPC), and Ganglioside GM1 were purchased from Avanti Polar Lipid, Inc. Dipotassium hydrogen phosphate (K_2HPO_4), potassium dihydrogen phosphate (KH_2PO_4), and piperidine were purchased from Merck (India). Dimethylformamide (DMF) and dichloromethane (DCM) of extrapure grade and acetonitrile of HPLC grade were purchased from Merck (India). Cholesterol (99%), acetic anhydride (Ac_2O) of synthesis grade, N-methyl-imidazole (NMI) of extrapure grade and trifluoroacetic

acid (TFA) of extrapure grade were purchased from SRL (India). Milli-Q water at 18.2 Ω was used for sample preparation.

6.1.2. hIAPP sample preparation:

The commercially available $hIAPP_{1-37}$ (e.g., 3.1 mg) was dissolved in a small volume (40 µL) of HFIP to obtain disaggregated hIAPP. Then, HFIP was evaporated thoroughly by purging nitrogen gas. This process was repeated thrice. After complete removal of HFIP, hIAPP generates a thin film, and to this, the required volume of 50 mM PBS of pH 7.4, containing 3% DMSO was added, followed by sonication and vortex to obtain soluble hIAPP (40 µM) solution.[160] From the solution, 50 µL of each aliquot was transferred into required portions. For the native hIAPP solution, the final volume was made up to 800 µL with PBS of pH 7.4 to obtain a 40 µM concentration. For the other sets, the required amount of peptide solutions were added to the hIAPP solution to maintain their doses, and the final volume was made up to 800 µL to maintain the same concentration of the aggregating peptide.

We have taken four different concentrations of hIAPP, i.e. 10 µM, 20 µM, 30 µM and 40 µM for the optimisation. We observed a gradual increment in fluoresecnce intensity with increasing concentration of hIAPP, however, a suitable intensity was observed with 40 µM of hIAPP for the biophysical experiments. Hence, we have considered 40 µM of hIAPP for all the biophysical studies. Under physiological condition or in T2DM, 40 µM of hIAPP could be very high. However, it was an *in vitro* study, where we have used only relative concentration of the aggregating and breaker peptides. Hence, in the context of T2DM patients, the relative doses of the inhibitors with respect to the hIAPP concentration may be used.

6.1.3. Large unilamellar vesicles (LUVs) preparation and Carboxyfluorescein entrapment:

The large unilamellar vesicles (LUVs) were prepared using three different lipids; DMPC (or DPPC), Cholesterol, and GM1 with 68:30:2 molar ratios following a reported protocol.[160] Before the vesicle preparation, the required lipids were taken in a clean glass vessel and solubilize in chloroform and methanol (2:1) to make a 2 mM stock solution. Then the solvents were evaporated completely using nitrogen gas to make a thin lipid film. The glass vessel containing the lipid film was placed in a vacuum desiccator for overnight to remove solvents completely. Next, the lipid film was hydrated with 500 µL of carboxyfluorescein solution (200 µM) in 50 mM PBS buffer of pH 7.4. Then, the solution was vortexed vigorously for 30 min to emulsify the lipid mixtures.

Further, the glass vessel was dipped into the liquid nitrogen for instant cooling, and after 5 minutes, the frozen solution was dipped into a water bath at 50-60 °C for thawing.[138] The step was repeated three times for complete entrapment of the dye. The excess dye was removed by ultracentrifugation at 20000 rpm, and the supernatant dye solution was discarded, and the lipid pellet was re-hydrated with 50 mM HEPES buffer. This step was repeated two more times to remove the excess dye, and the final lipid pellet was collected, followed by the addition of 500 µL of PBS buffer and vortexed to obtain a homogenous suspension of 2 mM stock of lipid vesicles.[159] Finally, the lipid solution was filtered through a 0.45 µm polycarbonate membrane to obtain the dye-loaded LUVs. The formation of LUVs was confirmed by TEM or FESEM images. The dye leakage assay was performed on a Fluoromax-4 Horiba Fluorospectrometer instrument. For the dye leakage experiment, all samples, including the carboxyfluorescein entrapped untreated LUV solution, were excited at 485 nm, and fluorescence emission was measured at 516 nm using a slit 5 nm in a 1 mL quartz cuvette of 1 cm path length.

6.2. Instrumentation:

6.2.1. High-performance liquid chromatography (HPLC):

All the crude peptides were purified by RP-HPLC (reverse phase-high performance liquid chromatography) on Waters/ Thermo Fiscer Scientific istrument, using a C18-µ Bondapak semi-preparative column (dimensions 250 × 10 mm, particle size 12 µm, pore size 175 Å) at a flow rate of 4-5 mL/min. A binary solvent system was used, solvent A (0.1% TFA in H_2O) and solvent B (0.1% TFA in CH_3CN). The UV detector was set at dual wavelengths of 214 nm and 254 nm. A total run time of 20 min was used, and the gradient used for purification was 5−100% CH_3CN for 18 min, followed by 100% CH_3CN till 20 min.

For chapter 2 and chapter 3, the purity of the peptides was checked with RP-HPLC on Waters 600E Analytical HPLC system using Waters C_{18} analytical column at a flow rate of 1 mL/min, using linear gradient of 5-100% CH_3CN over 18 minutes in a total run time of 20 min. Dual-wavelength was selected at 214 nm and 254 nm.

Moreover, for chapter 4 and chapter 5, the purity of the peptides was further confirmed with RP-HPLC on Agilent 1260 analytical system, using Agilent C18 analytical column at a flow rate of 1 mL/min for a total run time of 10 min using a linear gradient of 5-100% CH_3CN for 9 min, followed by 100% CH_3CN till 10 min, with the UV detector set at 214 nm and 254 nm.

6.2.2. Mass spectrometry:

The purified peptides were characterized by High-Resolution Mass Spectrometry (HRMS) on Agilent-Q-TOF 6500 instrument (ESI positive mode) with the software Mass Hunter Work Station. $[M+H]^+$ and $[M+Na]^+$peaks were observed for the purified peptides.

6.2.3. MALDI-TOF mass spectrometry:

For characterizing the purified peptides in MALDI-TOF analysis, the peptide solutions were prepared in CH_3CN/H_2O and mixed with CHCA (α-cyano-hydroxy-cinnamic acid) matrix in a 1:1 ratio and analyzed in MALDI-TOF spectrometer using Bruker Daltonics FlexControl software. The mass of the individual peaks of the purified peptides was assigned using the FlexAnalysis software. $[M+H]^+$, $[M+Na]^+$ and $[M+K]^+$ peaks were observed for the purified peptides.

6.2.4. Circular dichroism (CD):

After 5 or 7 days of incubation of the peptide solutions, CD analysis was performed to monitor the conformational changes of the peptides. Solutions of hIAPP (40 μM) alone and mixed with different molar ratios of the breaker peptides (in case of inhibition or disruption study) were dissolved in PBS (50 mM, pH 7.4) to obtain their desired concentration. 400 μL of the sample was taken in a cuvette of 1 mm path length and CD study was performed. Initially, the baseline correction was done by using a blank solution (here, PBS buffer). The spectra were recorded as an average of three measurements, from 190 nm to 260 nm on JASCO J-815/ JASCO J-1500 instrument. Each CD experiment was repeated for at least two times, with each spectra being recorded as an average of three measurements.

Observed ellipticity (mDeg) was obtained from the software, pasted on an excel sheet and converted to mean residue molar ellipticity (θ) using the following equation:

$$\theta\ (\text{deg. cm}^2\text{. dmol}^{-1}) = \text{Ellipticity (mdeg)}.\ 10^6/\ (\text{Pathlength (mm)}.\ [\text{Protein}]\ (\mu\text{M}).\ N)$$

Where [Protein] is the concentration of the peptide samples (in μM) and N is the number of amide bonds in the peptide sequence.

6.2.5. Fourier transform infrared (FTIR) spectroscopy:

Solutions of hIAPP (40 μM) alone and mixed with different molar ratios of the breaker peptides (in case of inhibition or disruption study) were prepared in PBS (50 mM, pH 7.4). After 5 or 7 days of incubation, 10 μL aliquot from the peptide stock solutions was mixed with activated KBr and pellet was prepared. FTIR spectra were recorded on a Perkin Elmer FTIR spectrometer. At first, a background scan was obtained, followed by the sample scan. The final spectra were obtained after baseline correction. The text files were taken and plotted in OriginPro 8 software.

6.2.6. Thioflavin T (ThT) fluorescence assay:

Initially, a stock solution of Thioflavin T (ThT) was prepared at a concentration of 3.2 mM in PBS (50 mM, pH 7.4) and stored at 4 °C with proper protection from light to prevent quenching.[161] Prior to the fluorescence study, the stock solution of ThT was diluted with PBS to obtain a concentration of 50 μM. Stock solution of the aggregating hIAPP peptide of concentration 40 μM was prepared in PBS, and after that, different molar ratios of the breaker peptides were added to the hIAPP solution as required. All the peptide samples were incubated in water bath at 37 °C. The ThT fluorescence assay was carried out manually (without using 96 well plates) on a Fluoromax-4 Horiba Fluorospectrometer.

For the ThT assay, at different time intervals, the required volume of peptide samples (40 μL) was mixed with 200 μL of ThT solution (50 μM), and the total volume was adjusted up to 400 μL with 160 μL of PBS. However, 200 μL of PBS solution was mixed with 200 μL of thioflavin T solution for the reference sample. The excitation wavelength was set at 440 nm, and the fluorescence emission was measured at 485 nm in a 1 mL quartz cuvette of 1 cm pathlength using a slit 5 nm. The software data were copied and pasted on an excel file. The

excel file was taken, and the graphs were plotted on OriginPro 8 software and finalised in Adobe Illustrator software. For each data, three readings were recorded separately, and the average of three was plotted along y-axis and time (h) along the x-axis with observed standard deviation being set as y-error. For each biophysical study, the ThT experiments were repeated twice or thrice.

The relative percentage of amyloid was calculated using the following equation-

$$\text{Relative \% of amyloid} = \frac{(\text{Observed fluorescence in the presence of the peptide} - 1)}{(\text{Observed fluorescence in the absence of the peptide} - 1)} \times 100\%$$

where 1 was considered as a normalization factor.

6.2.7. Transmission electron microscopy (TEM):

For recording TEM images (after 5 or 7 days of incubation as required), 10 μL aliquot from the stock peptide solution (40 μM in case of hIAPP and respective ratios for the mixture of peptides) was added over the dark side of the carbon-coated copper grid and allowed to float for 2 min. Then, the excess solution was discarded using blotting paper. After that, the samples were negatively stained by adding 2% uranyl acetate solution (10 μL) and were allowed to float for 2 min, and the excess solution was removed using blotting paper. The sample was dried at room temperature and was kept in a desiccator before taking TEM analysis. TEM images were captured on JEOL (Model: JEM 2100) and JEOL (Model: JEM-2100F Field Emission Electron Microscope) instrument at 200 kV.

6.2.8. Congo red stained birefringence:

Commercially available Congo red was dissolved in 80% aqueous ethanol to prepare a saturated solution. Then a saturated solution of sodium chloride was added into the saturated Congo red solution and filtered to obtain the required Congo red solution for analysis.[23] For the birefringence analysis, after 5 or 7 days of incubation, 10 μL aliquot of stock peptide

solution (40 μM in case of hIAPP and respective ratios for the mixture of peptides) was drop casted over a cleaned glass slide and kept in an incubator at 37 °C overnight for drying. After that, 10 μL of the saturated solution of Congo red dye was added over the dried samples and then dried further in the incubator at 37 °C. Finally, the prepared samples were examined under a Leica ICC50 HD polarizable microscope.

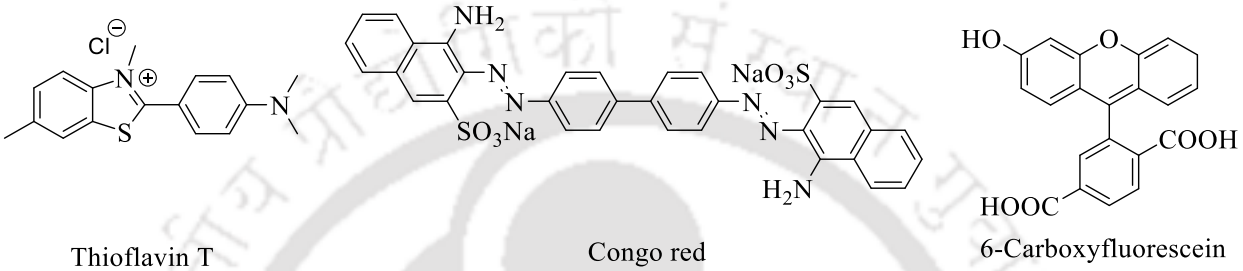

Figure 6.1: Structure of Thioflavin T (ThT), Congo red and Carboxyfluorescein dye used in different techniques to monitor amyloid aggregation

6.2.9. Field emission scanning electron microscopy (FESEM):

In the initial chapters, the formation of LUVs was confirmed by FESEM. 10 μL lipid vesicle solution from the stock solution was drop casted over the clean glass slide covered with aluminium foil. Then the sample was allowed to dry overnight in an incubator at 37 °C. and examined with a Ziess, Sigma VP instrument field-emission scanning electron microscopy system using an accelerating voltage of 3 kV.

6.2.10. Dynamic light scattering (DLS):

DLS measurements of hIAPP alone and in the presence of 2-fold molar ratios of the breaker peptides were performed at different time intervals of incubation at 25 °C using a 633 nm He-Ne laser on a Zetasizer Nano series Nano-ZS90 (Malvern Instruments). For the experiment, a stock solution of hIAPP (40 μM) was prepared in PBS of pH 7.4 (with 3% DMSO) and then added the required amount of the breaker peptide solution to get a final ratio of 1:2 (hIAPP:

breaker peptide). Then the hIAPP alone and the mixture were incubated at 37 °C, and the size distribution measurements were recorded at different time interval using 200 μL of each of the samples in a 1 mL cuvette of 1 cm pathlength. Before scanning, the system was equilibrated for 120 seconds. Each measurement recorded intensity percentage along with size distribution, which was an average of 10 scans. The text values were obtained directly from the Zetasizer software, plotted in OriginPro 8 software, and finalized in Adobe Illustrator.

6.3. Soild phase peptide synthesis (SPPS) protocol:

All the syntheses were performed manually on a Stuart blood tube rotator (20 rpm) using standard SPPS protocols.[129,130] The Rink amide MBHA resin (300 mg of loading of 0.7 mmol/g) was taken into a 5 mL frit-fitted plastic syringe and swollen in DCM for 2h followed by DMF for 1h. Distilled DCM and N_2 purged DMF were used for the syntheses.

6.3.1. Peptide coupling:

For a standard peptide coupling, two equivalent of Fmoc-amino acid was dissolved in DMF and added to the resin and 2.5 equivalents of BOP/ PyBOP/ *o*-NosylOXY as a coupling reagent and five equivalent of DIPEA as a base. Coupling time varied from 2h to 12h (depending on the amino acids coupled). In case of incomplete coupling, the step was repeated twice. After that, the resin was washed with DMF and DCM for 5 min (1 min x 5) after each coupling. All couplings were performed at room temperature.

6.3.2. Fmoc deprotection:

Prior to the subsequent coupling, N_α-Fmoc deprotection was performed by using 20% piperidine in DMF for 21 min (7 min x 3). After Fmoc deprotection, the resin was washed with DMF and DCM for 5 min each (5 x 1 min).

6.3.3. Kaiser test:

Each peptide coupling was monitored by performing the Kaiser test.[162] For carrying out the test, a few resin beads were placed in a small fusion tube, and 50 μL of Kaiser A and 50 μL Kaiser B were added. Further, the tube was heated at 80 °C over a sand bath for 5 min. A positive test is indicated by blue or purple color, which implies free NH_2 groups in the reaction. In such cases, the coupling step was repeated. The composition of the Kaiser solutions are mentioned below:

Kaiser A: 0.5 g ninhydrin in 10 mL ethanol

Kaiser B: 0.4 mL of 0.001 M KCN (aq) in 20 mL pyridine.

6.3.4. Acetylation (capping):

Sometimes, even after repeated coupling, free NH_2 groups remain in the solution. In such cases, acetylation or capping was performed. After coupling, the resin was washed with DCM five times. After that, two equivalent of Ac_2O and three equivalent of *N*-methyl imidazole were mixed in DCM and added to the resin, and the reaction was carried out for 1.5h.

6.3.5. Final cleavage of the peptide from resin:

After completion of peptide synthesis, the Rink amide MBHA resin was treated with a solution of TFA/DCM/H_2O (85/10/5) for 3h.[129,130] Approximately, 2.5-3 mL of the cocktail solution was used for 300 mg resin. After final cleavage of the peptide from the resin, the crude peptide was precipitated in cold diethyl ether, washed thoroughly with ether, then centrifuged to obtain the crude solid product. Thereafter, the crude peptide was purified by semi-preparative HPLC.

6.4. Synthetic procedure of the designed peptides:

6.4.1. Peptide 2A: *(H_2N-Asn-Phe-Gly-Ala-Ile-Leu-$CONH_2$)*

Peptide **2A** was synthesized on 300 mg Rink amide MBHA resin (loading 0.7 mmol/g). The resin was swollen in DCM for 2h, followed by DMF for 1h. Fmoc deprotection was performed using 20% piperidine/DMF for 21 mins (7×3). Coupling at each step was accomplished using 2 eq of Fmoc-amino acids, 2.5 eq of BOP as coupling reagent and 5 eq of DIPEA as a base. Each amino acid coupling was monitored by Kaiser test and if found positive Kaiser test, coupling step was repeated for 2nd time subsequently capping with Ac_2O and NMI (2 and 3 equivalent respectively) in DCM for 1.5h. The exact process was continued for the entire sequence maintaining the same protocol. After completion of peptide synthesis, the final product was cleaved from the resin using a mixture of 85% TFA, 10% DCM and 5% H_2O for 3h. The crude peptide was precipitated in cold diethyl ether, subsequently centrifugated several times and dried with N_2 gas. Later, the dried crude peptide was purified by RP-HPLC with C_{18} μ-Bondapak semi-preparative reverse phase using solvent A (H_2O with 0.1% TFA) and solvent B (CH_3CN with 0.1% TFA) as binary solvent system selecting dual detector wavelength at 214 nm and 254 nm. HPLC was carried out using a linear gradient for purification of the peptides of 5−100% CH_3CN for 18 min leading to 100% CH_3CN until the maximum run time, i.e., 20 min, with a 4 ml/min flow rate. After HPLC, the CH_3CN was evaporated using rotavapor and the aqueous peptide solution was frozen using liquid nitrogen and allowed to lypholise.

Texture: White fluffy powder

Yield: 18.7 mg, 14.06% with respect to the resin loading.

ESI-MS (m/z): 633.3748 $[M+H]^+$, 655.3568 $[M+Na]^+$

HPLC: Retention time (t_R) 7.6 min (C_{18}, a linear gradient from 5 to 100% CH_3CN till 18 mins, followed by 100% CH_3CN till 20 mins).

6.4.2. Peptide 2B: *(H_2N-Asn-Phe-Gly-Ala-Aib-Leu-$CONH_2$)*

Peptide **2B** was also synthesized on 300 mg Rink amide MBHA resin (loading 0.7 mmol/g) in the same way as that of **2A** with α-aminoisobutyric acid instead of I26 position, following the same protocol as mentioned above.

Texture: White fluffy powder

Yield: 15.3 mg, 12.04% with respect to the resin loading.

ESI-MS (m/z): 605.3627 $[M+H]^+$, 627.3393 $[M+Na]^+$

HPLC: Retention time (t_R) 7.1 min (C_{18}, a linear gradient from 5 to 100% CH_3CN till 18 mins, followed by 100% CH_3CN till 20 mins).

6.4.3. Peptide 2C: *(H_2N-Asn-Phe-Gly-Ala-(2-Abz)-Leu-$CONH_2$)*

Peptide **2C** was also synthesized on 300 mg Rink amide MBHA resin (loading 0.7 mmol/g) in the same way as that of **2A** with 2-aminobenzoic acid (2-Abz or Ant) instead of I26 position, following the same protocol as mentioned above. However, more emphasis was given to the coupling next to 3-aminobenzoic acid or anthranilic acid (Ant), as it is complicated due to steric effects. The coupling step was repeated for 2 times and subsequently capped with Ac_2O and NMI.

Texture: Off white solid

Yield: 6.9 mg, 5.14% with respect to the resin loading.

ESI-MS (m/z): 639.3310 $[M+H]^+$, 661.3120 $[M+Na]^+$

HPLC: Retention time (t_R) 7.8 min (C_{18}, a linear gradient from 5 to 100% CH_3CN till 18 mins, followed by 100% CH_3CN till 20 mins).

6.4.4. Peptide 2D: *(H_2N-Asn-Phe-Gly-Ala-(3-Abz)-Leu-$CONH_2$)*

Peptide **2D** was also synthesized on 300 mg Rink amide MBHA resin (loading 0.7 mmol/g) in the same way as that of **2A** with 3-aminobenzoic acid (3-Abz) instead of I26 position, following the same protocol as mentioned above. However, more emphasis was given to the coupling next to 3-aminobenzoic acid, as it is complicated due to steric effects. The coupling step was repeated for 2 times and subsequently capped with Ac_2O and NMI.

Texture: Off white solid

Yield: 7.6 mg, 5.66% with respect to the resin loading.

ESI-MS (m/z): 639.3315 $[M+H]^+$, 661.3106 $[M+Na]^+$

HPLC: Retention time (t_R) 8.3 min (C_{18}, a linear gradient from 5 to 100% CH_3CN till 18 mins, followed by 100% CH_3CN till 20 mins).

6.4.5. Peptide 2E: *(H_2N-Asn-Phe-Gly-Ala-(4-Abz)-Leu-$CONH_2$)*

Peptide **2E** was also synthesized on 300 mg Rink amide MBHA resin (loading 0.7 mmol/g) in the same way as that of **2A** with 4-aminobenzoic acid (4-Abz) instead of I26 position, following the same protocol as mentioned above. However, more emphasis was given to the coupling next to 4-aminobenzoic acid, as it is complicated due to steric effects. The coupling step was repeated for 2 times and subsequently capped with Ac_2O and NMI.

Texture: Off white solid

Yield: 8.9 mg, 6.63% with respect to the resin loading.

ESI-MS (m/z): 639.3335 $[M+H]^+$

HPLC: Retention time (t_R) 9.2 min (C_{18}, a linear gradient from 5 to 100% CH_3CN till 18 mins, followed by 100% CH_3CN till 20 mins).

6.4.6. Peptide 3A: *(H_2N-Asn-Phe-Aib-Ala-Aib-Leu-$CONH_2$)*

Peptide **3A** was also synthesized on 300 mg Rink amide MBHA resin (loading 0.7 mmol/g) in the same way as that of **2A** with α-aminoisobutyric acid in two positions of $hIAPP_{22-27}$ in G24 and I26 position, following the same protocol as mentioned above.

Texture: Off white solid

Yield: 11.9 mg, 8.99% with respect to the resin loading.

ESI-MS (m/z): 633.3749 $[M+H]^+$, 655.3562 $[M+Na]^+$

HPLC: Retention time (t_R) 8.6 min (C_{18}, a linear gradient from 5 to 100% CH_3CN till 18 mins, followed by 100% CH_3CN till 20 mins).

6.4.7. Peptide 3B: *(H_2N-Asn-Phe-(2-Abz)-Ala-(2-Abz)-Leu-$CONH_2$)*

Peptide **3B** was also synthesized on 300 mg Rink amide MBHA resin (loading 0.7 mmol/g) in the same way as that of **2A** with 2-aminobenzoic acid (2-Abz or Ant) in two positions of $hIAPP_{22-27}$ in G24 and I26 position, following the same protocol as mentioned above. However, more emphasis was given to the coupling next to 2-aminobenzoic acid or anthranilic acid (Ant), as it is complicated due to steric effects. The coupling step was repeated for 2 times and subsequently capped with Ac_2O and NMI.

Texture: Off white solid

Yield: 6.3 mg, 4.27% with respect to the resin loading.

ESI-MS (m/z): 701.3414 $[M+H]^+$, 723.3176 $[M+Na]^+$

HPLC: Retention time (t_R) 7.9 min (C_{18}, a linear gradient from 5 to 100% CH_3CN till 18 mins, followed by 100% CH_3CN till 20 mins).

6.4.8. Peptide 3C: *(H_2N-Asn-Phe-(3-Abz)-Ala-(3-Abz)-Leu-$CONH_2$)*

Peptide **3C** was also synthesized on 300 mg Rink amide MBHA resin (loading 0.7 mmol/g) in the same way as that of **2A** with 3-aminobenzoic acid (3-Abz) in two positions of $hIAPP_{22-27}$ in G24 and I26 position, following the same protocol as mentioned above. However, more emphasis was given to the coupling next to 3-aminobenzoic acid, as it is complicated due to steric effects. The coupling step was repeated for 2 times and subsequently capped with Ac_2O and NMI.

Texture: Off white solid

Yield: 7.3 mg, 4.96% with respect to the resin loading.

ESI-MS (m/z): 701.3410 $[M+H]^+$, 723.3172 $[M+Na]^+$

HPLC: Retention time (t_R) 9.6 min (C_{18}, a linear gradient from 5 to 100% CH_3CN till 18 mins, followed by 100% CH_3CN till 20 mins).

6.4.9. Peptide 3D: *(H_2N-Asn-Phe-(4-Abz)-Ala-(4-Abz)-Leu-$CONH_2$)*

Peptide **3D** was also synthesized on 300 mg Rink amide MBHA resin (loading 0.7 mmol/g) in the same way as that of **2A** with 4-aminobenzoic acid (4-Abz) in two positions of $hIAPP_{22-27}$ in G24 and I26 position, following the same protocol as mentioned above. However, more emphasis was given to the coupling next to 3-aminobenzoic acid, as it is complicated due to steric effects. The coupling step was repeated for 2 times and subsequently capped with Ac_2O and NMI.

Texture: Off white solid

Yield: 8.2 mg, 5.56% with respect to the resin loading.

ESI-MS (m/z): 701.3419 $[M+H]^+$, 723.3181 $[M+Na]^+$

HPLC: Retention time (t_R) 9.9 min (C_{18}, a linear gradient from 5 to 100% CH_3CN till 18 mins, followed by 100% CH_3CN till 20 mins).

6.4.10. Peptide 4A: *(H_2N-Ala-Thr-Gln-Arg-Leu-Ala-Asn-Phe-Leu-Val-His-Ser-Ser-Asn-Asn-Phe-Gly-Ala-Ile-Leu-Ser-Ser-Thr-Asn-Val-Gly-Ser-Asn-Thr-Tyr-Gly-$CONH_2$)*

Peptide **4A** was also synthesized on 300 mg Rink amide MBHA resin (loading 0.7 mmol/g) in the same way as that of **2A** following the same protocol as mentioned above. However, in the synthesis 2.5 eq of *o*-NosylOXY was used as a coupling reagent instead of BOP.

Texture: White fluffy powder

Yield: 28.3 mg, 4.16% with respect to the resin loading.

ESI-MS (m/z): 3239.133 $[M+H]^+$

HPLC: Retention time (t_R) 6.3 min (C_{18}, a linear gradient from 5 to 100% CH_3CN till 9 mins, followed by 100% CH_3CN till 10 mins).

6.4.11. Peptide 4B: *(H_2N-Ala-Thr-Gln-Arg-Leu-Ala-Asn-Phe-Leu-Val-His-Ser-Ser-Asn-Asn-Phe-(2-Abz or Ant)-Ala-Ile-Leu-Ser-Ser-Thr-Asn-Val-Gly-Ser-Asn-Thr-Tyr-Gly-$CONH_2$)*

Peptide **4B** was also synthesized on 300 mg Rink amide MBHA resin (loading 0.7 mmol/g) in the same way as that of **4A** with 2-aminobenzoic acid (2-Abz or Ant) instead of G24 position following the same protocol as mentioned above. However, in the synthesis 2.5 eq of *o*-NosylOXY was used as a coupling reagent instead of BOP. More emphasis was given to the coupling next to anthranilic acid, as it is very difficult due to steric effects. The coupling step was repeated for 2 times and subsequently capped with Ac_2O and NMI.

Texture: Off white solid

Yield: 21.3 mg, 3.12% with respect to the resin loading.

ESI-MS (m/z): 3244.973 $[M+H]^+$

HPLC: Retention time (t_R) 5.5 min (C_{18}, a linear gradient from 5 to 100% CH_3CN till 9 mins, followed by 100% CH_3CN till 10 mins).

6.4.12. Peptide 4C: *(H_2N-Ala-Thr-Gln-Arg-Leu-Ala-Asn-Phe-Leu-Val-His-Ser-Ser-Asn-Asn-Phe-Gly-Ala-(2-Abz or Ant)-Leu-Ser-Ser-Thr-Asn-Val-Gly-Ser-Asn-Thr-Tyr-$CONH_2$)*

Peptide **4C** was also synthesized on 300 mg Rink amide MBHA resin (loading 0.7 mmol/g) in the same way as that of **4A** with 2-aminobenzoic acid (2-Abz or Ant) instead of I26 position following the same protocol as mentioned above. However, in the synthesis 2.5 eq of *o*-NosylOXY was used as a coupling reagent instead of BOP. More emphasis was given to the coupling next to anthranilic acid, as it is very difficult due to steric effects. The coupling step was repeated for 2 times and subsequently capped with Ac_2O and NMI.

Texture: Off white solid

Yield: 23.9 mg, 3.57% with respect to the resin loading.

ESI-MS (m/z): 3188.788 $[M+H]^+$

HPLC: Retention time (t_R) 5.7 min (C_{18}, a linear gradient from 5 to 100% CH_3CN till 9 mins, followed by 100% CH_3CN till 10 mins).

6.4.13. Peptide 4D: *(H_2N-Asn-Phe-Gly-Ala-(2-Abz or Ant)-Leu-$CONH_2$)*

Peptide **4D** was also synthesized on 300 mg Rink amide MBHA resin (loading 0.7 mmol/g) in the same way as that of **2A** with 2-aminobenzoic acid (2-Abz or Ant) instead of I26 position following the same protocol as mentioned above. However, in the synthesis 2.5 eq of

o-NosylOXY was used as a coupling reagent instead of BOP. More emphasis was given to the coupling next to anthranilic acid, as it is very difficult due to steric effects. The coupling step was repeated for 2 times and subsequently capped with Ac_2O and NMI.

Texture: Off white solid

Yield: 16.2 mg, 12.08% with respect to the resin loading.

ESI-MS (m/z): 639.950 $[M+H]^+$, 661.338 $[M+Na]^+$, 677.313 $[M+K]^+$

HPLC: Retention time (t_R) 5.1 min (C_{18}, a linear gradient from 5 to 100% CH_3CN till 9 mins, followed by 100% CH_3CN till 10 mins).

6.4.14. Peptide 5A: *(***SP***-Asn-Phe-Gly-Ala-Ile-Leu-Glu)-Arg-*$CONH_2$

Peptide **5A** was also synthesized on 300 mg Rink amide MBHA resin (loading 0.7 mmol/g) in the same way as that of **2A** following the same protocol as mentioned above. However, in the synthesis 2.5 eq of *o*-NosylOXY was used as a coupling reagent instead of BOP. Proceeding by that way, the linear part was synthesized which was followed by O-t-Bu deprotection of the glutamic acid using 5 eq of $FeCl_3$ in DCM for 1.5h.[158] In the next step, on resin stapling were carried out using BOP as a coupling reagent and DIPEA as a base for 24h.

Texture: White fluffy powder

Yield: 18.2 mg, 9.62% with respect to the resin loading.

ESI-MS (m/z): 900.624 $[M+H]^+$, 922.622 $[M+Na]^+$, 938.606 $[M+K]^+$

HPLC: Retention time (t_R) 5.1 min (C_{18}, a linear gradient from 5 to 100% CH_3CN till 9 mins, followed by 100% CH_3CN till 10 mins).

6.4.15. Peptide 5B: *(***SP** *Asn-Phe-Gly-Ala-(2-Abz or Ant)-Leu-Glu)-Arg-CONH*$_2$

Peptide **5B** was also synthesized on 300 mg Rink amide MBHA resin (loading 0.7 mmol/g) in the same way as that of **2A** with 2-aminobenzoic acid (2-Abz or Ant) instead of I26 position following the same protocol as mentioned above. However, in the synthesis 2.5 eq of *o*-NosylOXY was used as a coupling reagent instead of BOP. More emphasis was given to the coupling next to anthranilic acid. The coupling step was repeated for 2 times and subsequently capped with Ac_2O and NMI. Proceeding by that way, the linear part was synthesized which was followed by O-t-Bu deprotection of the glutamic acid using 5 eq of $FeCl_3$ in DCM for 1.5h.[158] In the next step, on resin stapling were carried out using BOP as a coupling reagent and DIPEA as a base for 24h.

Texture: White fluffy powder

Yield: 13.4 mg, 7.05% with respect to the resin loading.

ESI-MS (m/z): 906.629 $[M+H]^+$, 928.621 $[M+Na]^+$, 944.598 $[M+K]^+$

HPLC: Retention time (t_R) 5.0 min (C_{18}, a linear gradient from 5 to 100% CH_3CN till 9 mins, followed by 100% CH_3CN till 10 mins).

6.4.16. Peptide 5C: *(NH_2-Asn-Phe-Gly-Ala-Ile-Leu-Glu-Arg-$CONH_2$)*

Peptide **5C** was also synthesized on 300 mg Rink amide MBHA resin (loading 0.7 mmol/g) in the same way as that of **2A** following the same protocol as mentioned above. However, in the synthesis 2.5 eq of *o*-NosylOXY was used as a coupling reagent instead of BOP.

Texture: Off white solid

Yield: 28.7 mg, 14.94% with respect to the resin loading.

ESI-MS (m/z): 918.623 $[M+H]^+$, 940.614 $[M+Na]^+$, 956.585 $[M+K]^+$

HPLC: Retention time (t_R) 4.9 min (C_{18}, a linear gradient from 5 to 100% CH_3CN till 9 mins, followed by 100% CH_3CN till 10 mins).

6.4.17. Peptide 5D: *(NH_2-Asn-Phe-Gly-Ala-(2-Abz or Ant)-Leu-Glu-Arg-$CONH_2$)*

Peptide **5D** was also synthesized on 300 mg Rink amide MBHA resin (loading 0.7 mmol/g) in the same way as that of **2A** with 2-aminobenzoic acid (2-Abz or Ant) instead of I26 position following the same protocol as mentioned above. However, in the synthesis 2.5 eq of *o*-NosylOXY was used as a coupling reagent instead of BOP. More emphasis was given to the coupling next to anthranilic acid. The coupling step was repeated for 2 times and subsequently capped with Ac_2O and NMI.

Texture: Off white solid

Yield: 18.9 mg, 9.74% with respect to the resin loading.

ESI-MS (m/z): 924.533 $[M+H]^+$, 946.536 $[M+Na]^+$, 962.511 $[M+K]^+$

HPLC: Retention time (t_R) 4.7 min (C_{18}, a linear gradient from 5 to 100% CH_3CN till 9 mins, followed by 100% CH_3CN till 10 mins).

Product Index

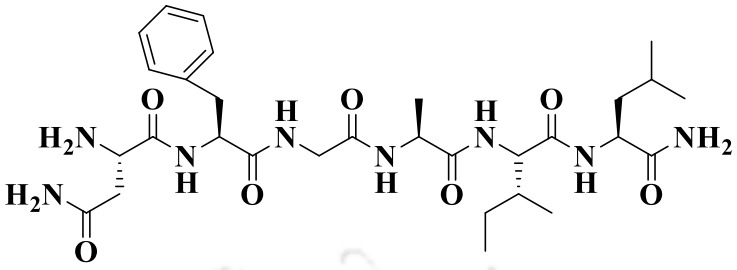

NH_2-NFGAIL-$CONH_2$ (Peptide 2A)

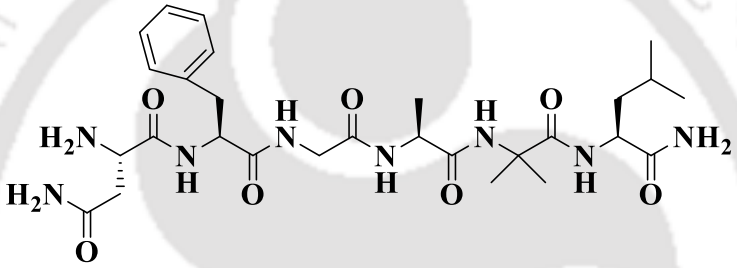

NH_2-NFGA(Aib)L-$CONH_2$ (Peptide 2B)

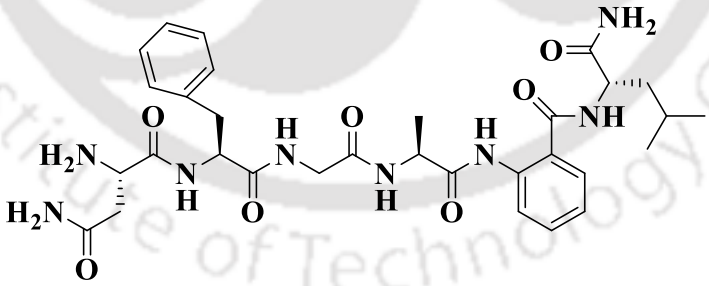

NH_2-NFGA(2-Abz)L-$CONH_2$ (Peptide 2C)

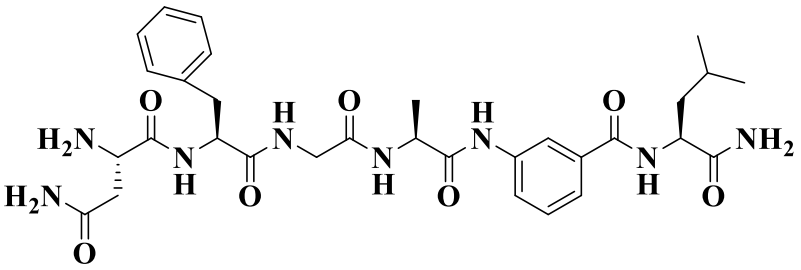

NH_2-NFGA(3-Abz)L-$CONH_2$ (Peptide 2D)

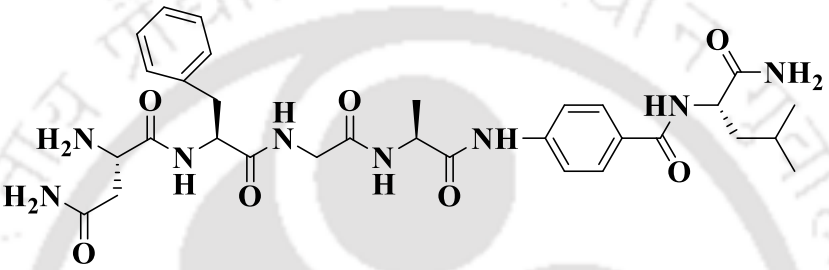

NH_2-NFGA(4-Abz)L-$CONH_2$ (Peptide 2E)

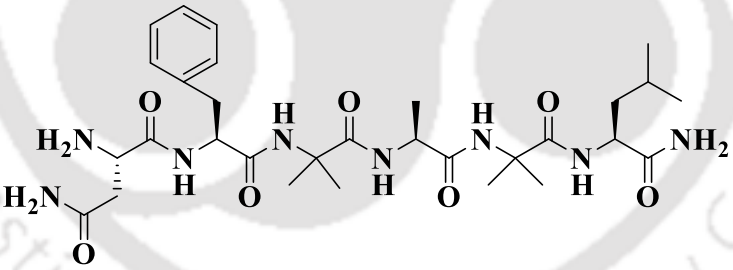

NH_2-NF(Aib)A(Aib)L-$CONH_2$ (Peptide 3A)

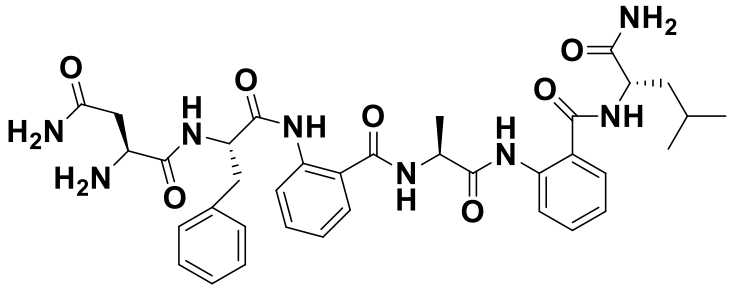

NH_2-NF(2-Abz)A(2-Abz)L-$CONH_2$ (Peptide 3B)

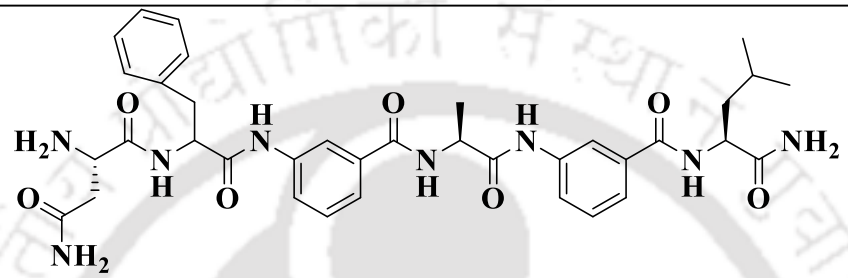

NH_2-NF(3-Abz)A(3-Abz)L-$CONH_2$ (Peptide 3C)

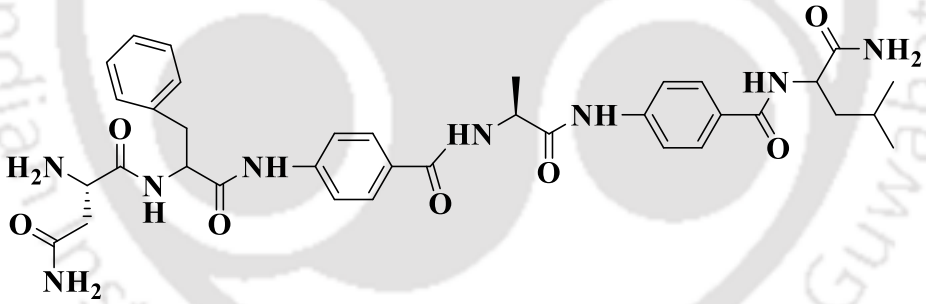

NH_2-NF(4-Abz)A(4-Abz)L-$CONH_2$ (Peptide 3D)

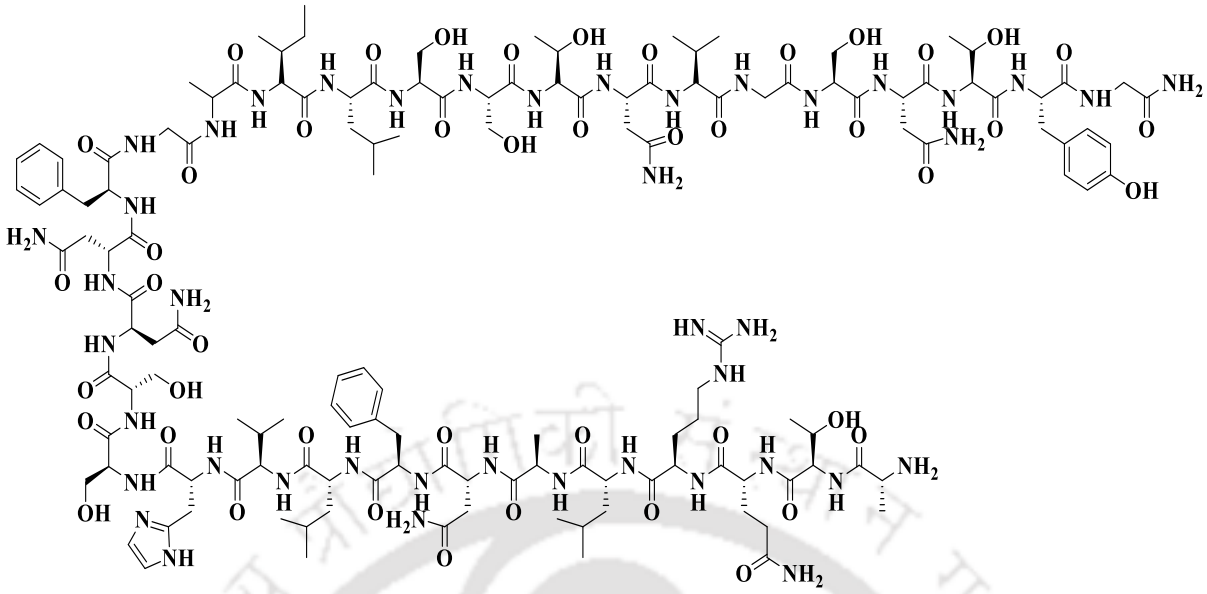

NH_2-ATQRLANFLVHSSNNFGAILSSTNVGSNTYG-$CONH_2$ (Peptide 4A)

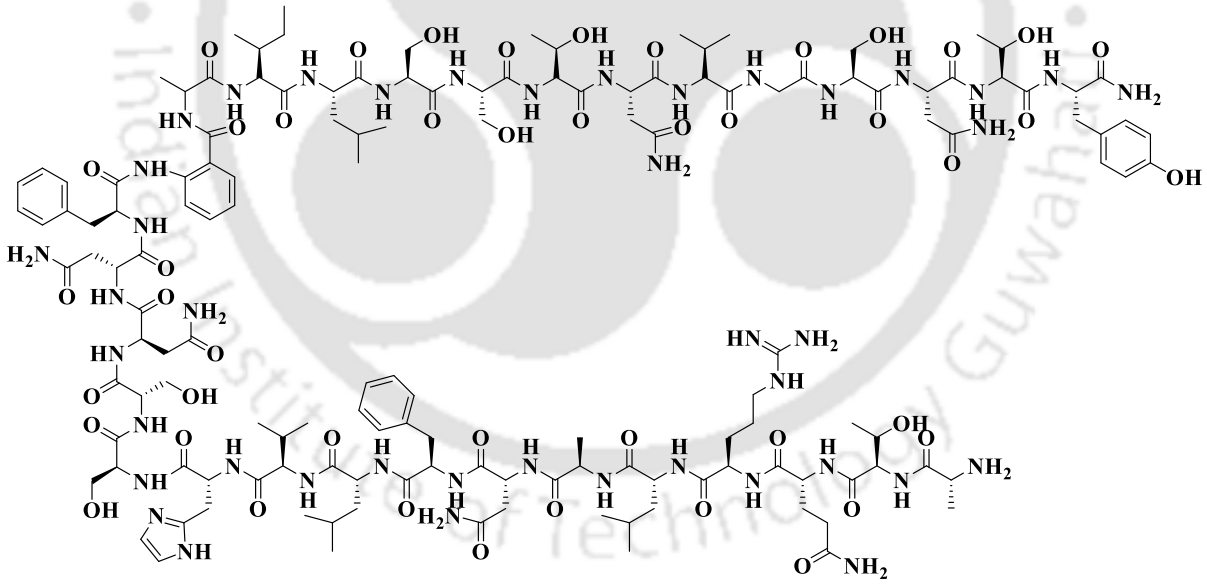

NH_2-ATQRLANFLVHSSNNF(Ant)AILSSTNVGSNTY-$CONH_2$ (Peptide 4B)

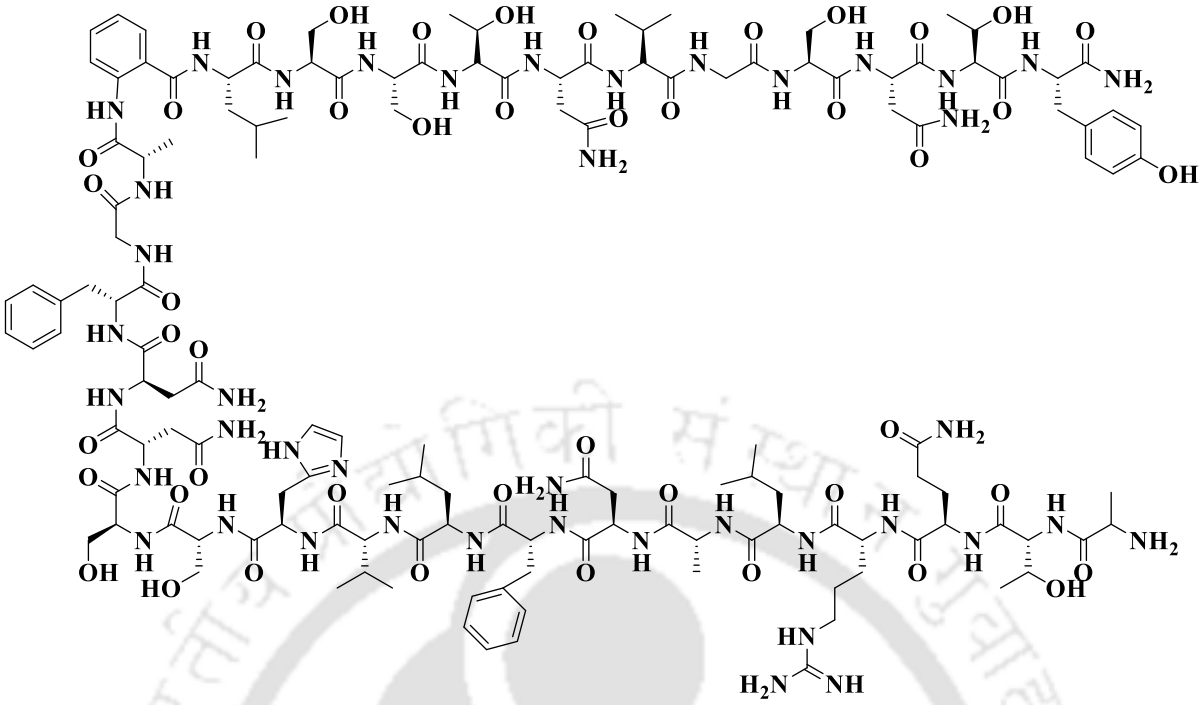

NH_2-ATQRLANFLVHSSNNFGA(Ant)LSSTNVGSNTY-$CONH_2$ (Peptide 4C)

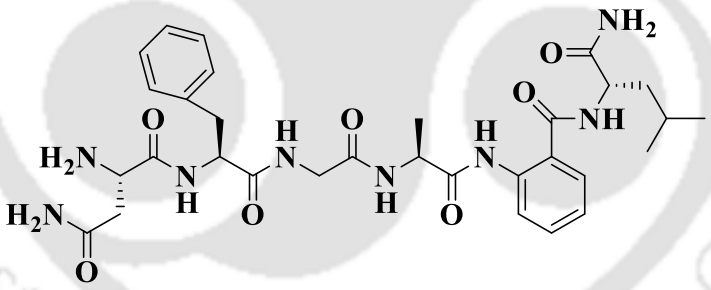

NH_2-NFGA(Ant)L-$CONH_2$ (Peptide 4D)

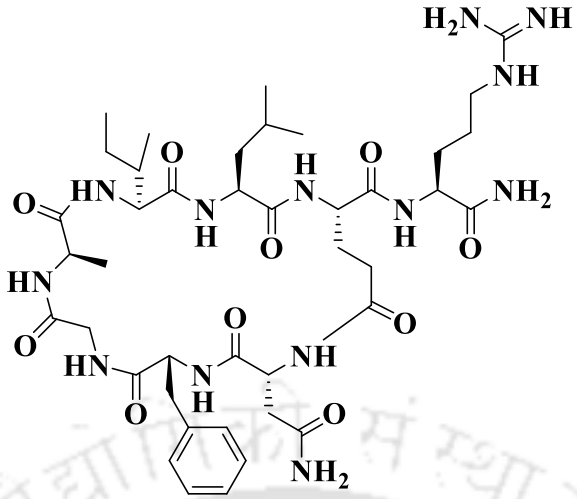

SP-NFGAILER-CONH$_2$ (Peptide 5A)

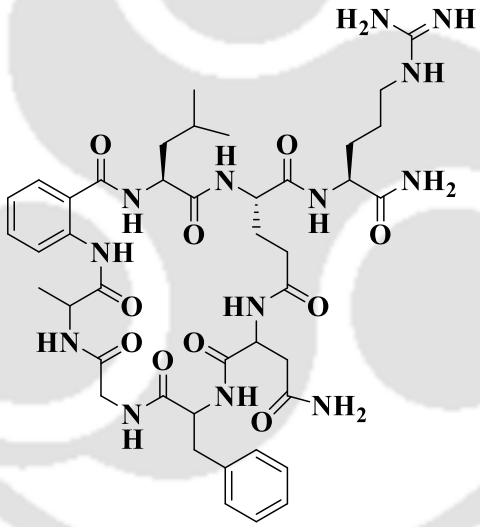

SP-NFGA(Ant)LER-CONH$_2$ (Peptide 5B)

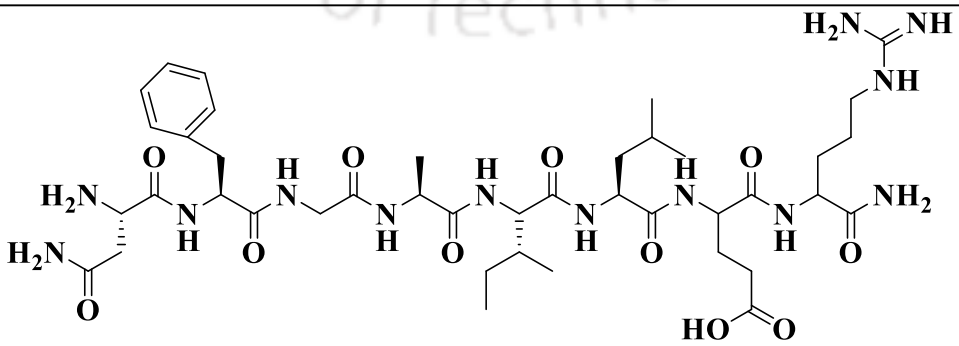

NH$_2$-NFGAILER-CONH$_2$ (Peptide 5C)

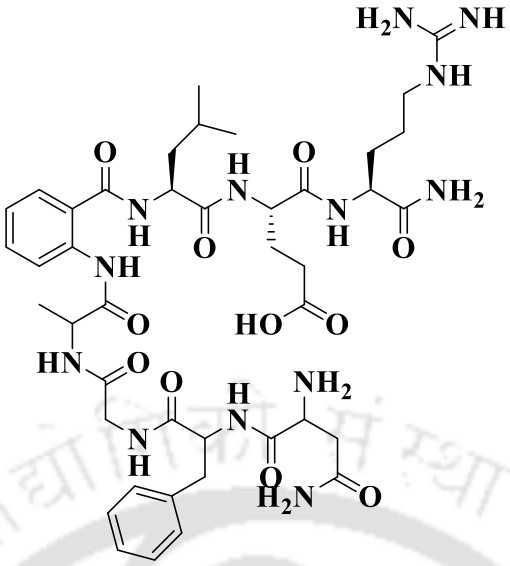

NH_2-NFGA(Ant)LER-$CONH_2$ (Peptide 5D)

Summary and future directions

Summary:

The work presented in this thesis focuses primarily on the design and development of novel peptide-based modulators against T2D via investigating their potentials in inhibiting hIAPP amyloid aggregation and disrupting their preformed fibrillar networks.

In chapter 2, we have demonstrated an innovative strategy for the development of β-sheet breaker peptides (BSBHps) as anti-diabetic agents via inserting three different isomers (ortho, meta, and para) of aminobenzoic acid separately as breaker elements in the peptide sequence $hIAPP_{22-27}$ (NFGAIL) at I26 position. From the investigations, we could outline that BSBHps containing ortho (2-Abz) and meta (3-Abz) isomers were highly efficient as modulators against amyloid aggregation of hIAPP. However, the para (4-Abz) containing BSBHp failed to suppress hIAPP aggregation; instead, it enhanced the aggregation process of hIAPP. The differential behavior of the various isomers towards inhibiting hIAPP aggregation could be interpreted due to their structural variations, as the 4-abz could not generate a kink like the other isomers. Furthermore, BSBHps containing ortho and para isomers could effectively disrupt the preformed amyloids of hIAPP into non-toxic species. Moreover, the peptides containing β and γ-amino acids are more proteolytically stable than α-amino acid.

In chapter 3, we have inserted the same isomers of aminobenzoic acid at two different positions of $hIAPP_{22-27}$ to enhance the efficiencies of the isomers in arresting amyloid aggregation of hIAPP. The three different isomers of aminobenzoic acid were incorporated

individually as breaker elements to the sequence NFGAIL at G24 and I26 positions. From the investigations, we observed that this strategy secured more effectiveness as modulators in preventing hIAPP aggregation. These double unit mutant BSBHps containing 2-Abz and 3-Abz isomers were more effective in arresting the amyloid aggregation and disrupting the preformed amyloid of hIAPP; however, 4-Abz containing BSBHp was ineffective as a modulator. Further, the double mutant BSBHps were observed to be more stable than the single mutant BSBHps in the presence of proteolytic enzymes.

In chapter 4, we have investigated the anti-amyloid activity of single-point mutant with anthranilic acid (Ant) in full-length $hIAPP_{8-37}$. We found that 2-Abz or Ant was found to be the best breaker element among all the isomers from the earlier chapters. However, the small peptide-based BSBHPs were effective only in higher doses (10-fold molar ratios). Therefore, we targeted the long peptide-based breaker peptide to overcome the issue, which might efficiently bind with the aggregating hIAPP. We have inserted Ant individually at G24 and I26 positions and observed that both the peptidomimetics were potent inhibitors of amyloid formation at significantly lower doses.

Moreover, differences in mutant position at G24X or I26X (X= Ant) did not show any significant difference in their ability to inhibit amyloid formation. The long peptidomimetics were highly influential in disrupting the preformed amyloids of hIAPP into non-toxic species at a minimal dose (2-fold molar ratios). Moreover, the peptidomimetic was found to alter the aggregation pathway of hIAPP. Further, MTT assay revealed that Ant-containing peptidomimetics were non-toxic to RIN-5F cells and can rescue from hIAPP-induced toxicity. The superior effect of the long peptidomimetic over the smaller ones in the inhibition and disruption of hIAPP aggregation may be due to the packed binding and sequence recognition to a far better extent.

In chapter 5, we have introduced the concept of side-chain to tail stapled peptides (SPs) with and without incorporating Ant as a turn inducer as therapeutic tools to arrest the aggregation of hIAPP. Here we have demonstrated the effect of SPs in modulating hIAPP assembly and compared their efficacies with their linear analogs. Investigations revealed that both the types of SPs were found to be better inhibitors and disruptors of highly aggregating amyloid of hIAPP compared to their linear precursors. They exhibited significant efficacy in inhibiting and disrupting potentials at minimal doses (2-fold molar ratios) to hIAPP. The structural rigidity of the SPs may impose them as better modulators as the efficiency was independent of the presence or absence of Ant. Moreover, systematic studies established that SPs alter the native aggregation pathway of hIAPP into off-pathway aggregation, and the generated species were found to be non-toxic. Further, SPs were relatively stable than their linear analogs in the presence of proteolytic enzymes, and the enhancement of stability of the SPs might be due to the conformational strain imposed by stapling.

We have introduced four different strategies in arresting the aggregation pathway of hIAPP via several techniques. These strategies may provide lead scaffolds for therapeutic intervention of T2D or other amyloid-related diseases.

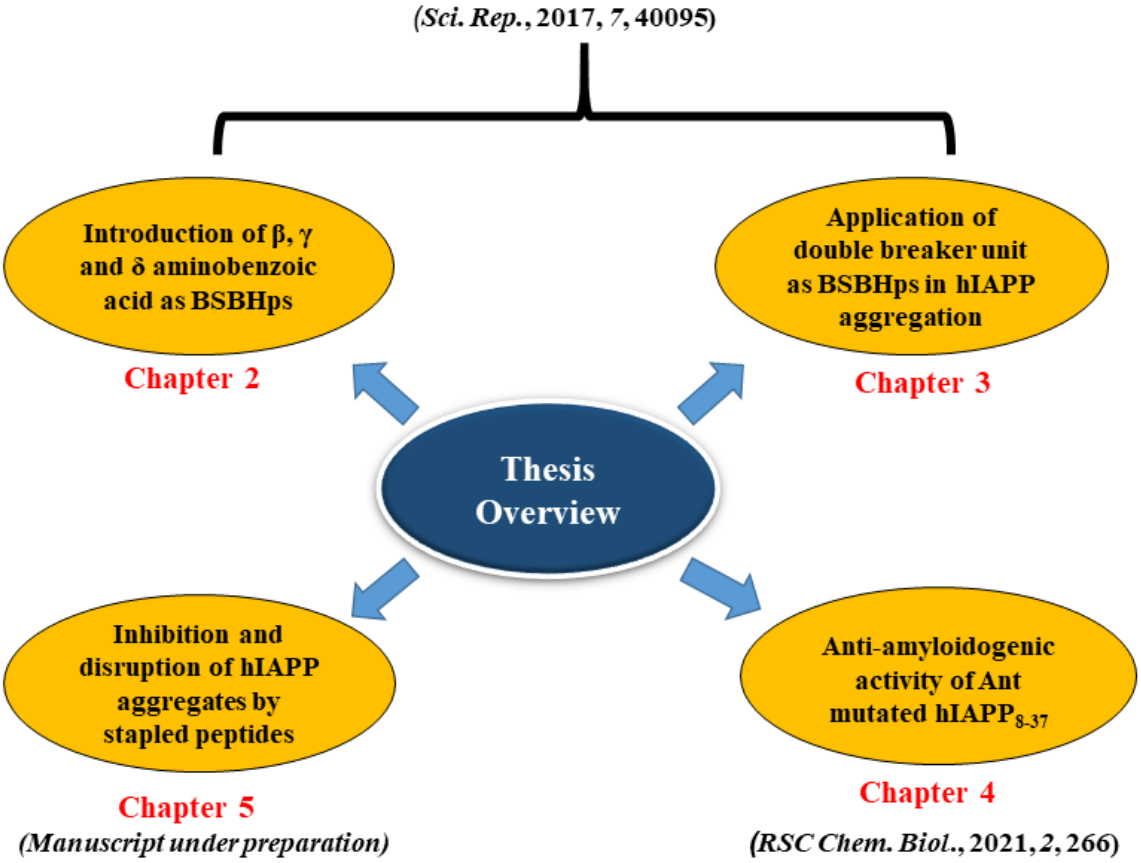

Future directions:

Although we have demonstrated different strategies for inhibiting or disrupting hIAPP aggregation *in vitro* at physiological conditions, more diverse and in-depth investigations are required to establish them as suitable therapeutic agents against T2D. Next, we would like to explore these strategies with pancreatic cell lines *in vitro.* Moreover, we are interested in exploring the exact mechanism of hIAPP aggregation and its interaction with the breaker peptides for successful inhibitory action. Our group has already explored these strategies on Aβ (responsible for Alzheimer's disease) and hIAPP (responsible for T2D). Hence, we would like to apply such techniques on α- Synuclein (responsible for Parkinson's disease) soon.

References:

1. Clamp, M., Fry, B., Kamal, M., Xie, X., Cuff, J., Lin, M. F., Kellis, M., Lindblad-Toh, K. and Lander, E. S. (2007) Distinguishing protein coding and noncoding genes in the human genome. *Proc. Natl. Acad. Sci. U. S. A.*, 104, 19428-19433.
2. Berg, J., Tymoczko, J. and Stryer, L. (2002) *Biochemistry. (5th edition) New York: W H Freeman and Company.*
3. Priller, C., Bauer, T., Mitteregger, G., Krebs, B., Kretzschmar, H. A. and Herms, J. (2006) Synapse formation and function is modulated by the amyloid precursor protein. *J. Neurosci.*, 26, 7212–7221.
4. Petsko, G. and Ringe, D. (2004) *Protein structure and function. (1st edition) London: New Age Press.*
5. Nelson, D. L and Cox, M. M. (2005) *Lehninger's Principles of Biochemistry (4th edition) New York, W. H. Freeman and Company.*
6. Ross, C. A. and Poirier, M. A. (2004) Protein aggregation and neurodegenerative disease. *Nat. Med.*, 10, S10–S17.
7. Takalo, M., Salminen, A., Soininen, H., Hiltunen, M. and Haapasalo, A. (2013) Protein aggregation and degradation mechanisms in neurodegenerative diseases. *Am. J. Neurodegener. Dis.*, 2, 1–14.
8. Raguse, T. L., Lai, J. R., LePlae, P. R. and Gellman, S. H. (2001) Toward β-peptide tertiary structure: self-association of an amphiphilic 14-helix in aqueous solution. *Org. Lett.*, 3, 3963–3966.
9. Das, R. and Baker, D. (2008) Macromolecular modelling with rosetta. *Annu. Rev. Biochem.* 77, 363–382.
10. Rohl, C. A., Strauss, C. E., Misura, K.M. and Baker, D. (2004) Protein structure prediction using rosetta. *Methods Enzymol.*, 383, 66–93.
11. Soto, C. (1999) Alzheimer's and prion disease as disorders of protein conformation: implications for the design of novel therapeutic approaches. *J. Mol. Med.*, 77, 412–418.
12. Gazit, E. (2002) The "correctly folded" state of proteins: is it a metastable state? *Angew. Chem. Int. Ed.*, 41, 257–259.
13. Wang, L., Maji, S.K., Sawaya, M.R., Eisenberg, D. and Riek, R. (2008) Bacterial inclusion bodies contain amyloid-like structure. *PLoS biology*, 6 (8), 1791-1801.
14. Greenwald, J. and Riek, R. (2010) Biology of amyloid: structure, function, and regulation. *Structure*, 18, 1244–1260.

15. Knowles, T. P., Fitzpatrick, A. W., Meehan, S., Mott, H. R., Vendruscolo, M., Dobson, C. M. and Welland, M. E. (2007) Role of intermolecular forces in defining material properties of protein nano-fibrils. *Science*, 318, 1900–1903.
16. Makin, O. S. and Serpell, L. C. (2005) Structures for amyloid fibrils. *FEBS Journal*, 272, 5950–5961.
17. Tycko, R. and Wickner, R. B. (2013) Molecular structures of amyloid and prion fibrils: consensus versus controversy. *Acc. Chem. Res.*, 46, 1487–1496.
18. Jimenez, J. L., Nettleton, E. J., Bouchard, M., Robinson, C. V., Dobson, C. M. and Saibil, H. R. (2002) The protofilament structure of insulin amyloid fibrils. *Proc. Natl. Acad. Sci. U. S. A.*, 99, 9196–9201.
19. Jarrett, J. T. and Lansbury, P. T., Jr. (1993) Seeding "one-dimensional crystallization" of amyloid: a pathogenic mechanism in Alzheimer's disease and scrapie? *Cell*, 73, 1055–1058.
20. Morris, A. M., Watzky, M. A. and Finke, R. G. (2009) Protein aggregation kinetics, mechanism, and curve-fitting: A review of the literature. *Biochim. Biophys. Acta*, 1794, 375–397.
21. Andersen, C. B., Yagi, H., Manno, M., Martorana, V., Ban, T., Christiansen, G., Otzen, D. E., Goto, Y. and Rischel, C. (2009) Branching in amyloid fibril growth. *Biophys. J.*, 96, 1529–1536.
22. Knowles, T. P., Waudby, C. A., Devlin, G. L., Cohen, S. I., Aguzzi, A., Vendruscolo, M., Terentjev, E. M., Welland, M. E. and Dobson, C. M. (2009) An analytical solution to the kinetics of breakable filament assembly. *Science*, 326, 1533–1537.
23. Nilsson, M. R. (2004) Techniques to study amyloid fibril formation in vitro. *Methods*, 34, 151– 160.
24. Westermark, P., Benson, M. D., Buxbaum, J. N., Cohen, A. S., Frangione, B., Ikeda, S., Masters, C. L., Merlini, G., Saraiva, M. J. and Sipe, J. D. (2007) A primer of amyloid nomenclature. *Amyloid*, 14, 179–183.
25. Chiti, F. and Dobson, C. M. (2006) Protein misfolding, functional amyloid, and human disease. *Annu. Rev. Biochem*., 75, 333–366.
26. King H, Aubert R. E. and Herman W.H. (1998) Global burden of diabetes, prevalence, numerical estimates and projections. *Diabetes care*, 21, 1414-1431.
27. Definition, diagnosis and classification of diabetes mellitus and its complications. Part 1: Diagnosis and classification of diabetes mellitus. Geneva, World Health Organization, (1999) (WHO/NCD/NCS/99.2)
28. Spellman, C. W. (2010). Pathophysiology of type 2 diabetes: targeting islet cell dysfunction. *Journal of American Osteopathic Association.* 110 (3), S2-S7.
29. Chou K. (2004) Molecular therapeutic target for type-2 diabetes, *Journal of Proteome Research*, 3, 1284-1288.

30. IDF Diabetes Atlas, (2019), 9th ed., International Diabetes Federation, Brussels, Belgium.
31. Cho, N. H., Shaw, J. E., Karuranga, S., Huang, Y., Fernandes, J. D., Ohlrogge, A. W. and Malanda, B. (2018) IDF Diabetes global estimates of diabetes prevalence for 2017 and projections for 2045. *Diabetes Res. Clin. Pract*., 138, 271-281.
32. Abreu, J. R. F. and Roep, B. O. (2013). Immune monitoring of islet and pancreas transplant recipients. *Current Diabetes Report*, 13, 704-712.
33. Woerle, H. J., Albrecht, M., Linke, R., Zschau, S. Neumann, C., Nicolous, M., Gerich, J. E., Goke, B. and Schirra, J. (2008). Impaired hyperglycaemia induced delay in gastric emptying in patients with type 1 diabetes deficient for islet amyloid polypeptide. *Diabetes Care,* 31(12), 2325-2331.
34. Willcox, A. R., Bone, A. J., Foulis, A. K. and Morgan, N. G. (2009). Analysis of islet inflammation in human type 1 diabetes. *Clinical and Experimental Immunology*, 155(2), 173-181.
35. Westermark P, Andersson A, and Westermark T. (2011) Islet amyloid polypeptide, islet amyloid, and diabetes mellitus. *Physiol Rev.*, 91, 795-826.
36. Inkster, M. E., Fahey, T. P., Donnan, P. T. Leese, G. P., Mires, G. J. and Murphy, D. J. (2006). Poor glycated haemoglobin control and adverse pregnancy outcomes in type 1 and type 2 diabetes mellitus: systematic review of observational studies. *BMC Pregnancy and Childbirth*, 6, 30.
37. Hauner, H. (2010). Obesity and diabetes, textbook of diabetes, 4th edition (R. I. G. Holt, C. S. Cockram, A. Flyvbjerg and B. J. Goldstein), Wiley-Blackwell, Oxford, UK.
38. Vaxillaire, M. and Froguel, P. (2010). The genetics of Type 2 diabetes: from candidate gene biology to genome-wide studies, *Textbook of diabetes*, 4th editionf.
39. Sarwar, N., Gao, P., Seshasai, S. R. K, Gobin, R., Kaptoge, S., Angelantonio, E. D., Ingelsson, E., Lawlor, D. A., Selvin, E., Stampfer, E., Stehouwer, C. D. A., Lewington, S., Pannells, L, Thompson, A., Sattar, N., White, I. R., Ray, K. K. and Danesh, J. (2010). Emerging risk factors collaboration diabetes mellitus, fasting blood glucose concentration, and risk of vascular disease: a collaborative meta-analysis of 102 prospective studies. *Lancet*, 375 (9733), 2215- 2222.
40. Colhoun, H. M., Betteridge, D. J., Durrington, P. N., Hitman, G. A., Neil, H. A. W., Livingstone, S. J., Thomason, M. J., Mackness, M. I., Charlton-Menys, V. and Fuller, J. H. (2004). Primary prevention of cardiovascular disease with atorvastatin in Type 2 diabetes in the collaborative atorvastatin diabetes study (CARDS): multicentre randomised placebo-controlled trial. *Lancet*, 364 (9435), 685-696.
41. Morrish, N. J. Wang, S. L., Stevens, L. K. and Fuller, J. H. (2001). Mortality and causes of death in the WHO multinational study of vascular disease in diabetes. *Diabetologia*, 44(2), S14-S21.

42. Scherbaum, W. A. (1998) The role of amylin in the physiology of glycemic control. *Exp. Clin. Endocrinol. Diabetes*, 106(2), 97-102.
43. Brender, J. R., Salamekh, S. and Ramamoorthy A. (2012) Membrane disruption and early events in the aggregation of the diabetes related peptide IAPP from a molecular perspective. *Accounts of Chemical Research*, 45(3), 454-462.
44. Gedulin, B. R., Rink, T. J. and Young, A. A. (1997) Dose-response for glucagonostatic effect of amylin in rats. *Metabolism*, 46(1), 67-70.
45. Clementi, G., Caruso, A., Cutuli, V. M. C., Bernerdis, E., Prato, A. and Amico-Roxas, M. (1996) Amylin given by central or peripheral routes decreases gastric emptying and intestinal transit in the rat. *Experientia*, 52, 677-679.
46. Sanke, T., Bell, G.I., Sample, C., Rubenstein, A.H. and Steiner, D.F. (1988) An islet amyloid peptide is derived from an 89-amino acid precursor by proteolytic processing. *J. Biol. Chem*., 263, 17243–17246.
47. Marzban, L., Trigo-Gonzalez, G. and Verchere, C.B. (2005) Processing of pro islet amyloid polypeptide in the constitutive and regulated secretory pathways of beta cells. *Mol. Endocrinol*., 19, 2154–2163.
48. Jaikaran, E.T.A.S. and Clark, A. (2001) Islet amyloid and type 2 diabetes: from molecular misfolding to islet pathophysiology. *Biochim. Biophys. Acta, Mol. Basis Dis.*, 1537, 179–203.
49. Hull, R. L., Westermark, G. T., Westermark, P. and Kahn, S. E. (2004) Islet amyloid: a critical entity in the pathogenesis of type 2 diabetes. *J. Clin. Endocrinol. Metab*., 89, 3629–3643.
50. Janciauskiene, S., Eriksson, S., Carlemalm, E. and Ahren, B. (1997) β-cell granule peptides affect human islet amyloid polypeptide (IAPP) fibril formation in vitro. *Biochem. Biophys. Res. Commun.*, 236, 580–585.
51. Jaikaran, E.T.A.S., Nilsson, M.R. and Clark, A. (2004) Pancreatic β-cell granule peptides form heteromolecular complexes which inhibit islet amyloid polypeptide fibril formation. *Biochem. J*., 377, 709–716.
52. Williamson, J. A. and Miranker, A. D. (2007) Direct detection of transient alpha-helical states in islet amyloid polypeptide. *Protein Sci.*, 16, 110–117.
53. Breeze, A. L., Harvey, T. S., Bazzo, R. and Campbell, I. D. (1991) Solution structure of human calcitonin gene-related peptide by 1H-NMR and distance geometry with restrained molecular-dynamics. *Biochemistry*, 30, 575–582.
54. Westermark, P., Wernstedt, C., Wilander, E. and Sletten, K. (1986) A novel peptide in the calcitonin gene related peptide family as an amyloid fibril protein in the endocrine pancreas, *Biochem. Biophys. Res. Commun*., 140 827-831.

55. Johnson, K. H., O'Brien, T. D., Jordan, K., Betsholtz, C. and Westermark, P. (1990). The putative hormone islet amyloid polypeptide (IAPP) induces impaired glucose tolerance in cats. *Biochemical and Biophysical Research Communications*, 167(2), 507-513.
56. Betsholtz, C., Svensson, V., Rorsman, F., Engström, U. Westermark, G. T., Wilander, E., Johnson, K., Westermark, P. (1989). Islet amyloid polypeptide (IAPP): cDNA cloning and identification of an amyloidogenic region associated with species-specific occurrence of age-related diabetes mellitus. *Experimental Cell Research*, 183 (2), 484-493.
57. Westermark, P., Engstrom, U., Johnson, K.H., Westermark, G.T. and Betsholtz, C. (1990) Islet amyloid polypeptide – pinpointing amino-acid-residues linked to amyloid fibril formation. *Proc. Natl. Acad. Sci. U. S. A.*, 87, 5036–5040.
58. Abedini, A. and Raleigh,D.P. (2006) Destabilization of human IAPP amyloid fibrils by proline mutations outside of the putative amyloidogenic domain: Is there a critical amyloidogenic domain in human IAPP? *J. Mol. Biol.*, 355, 274–281.
59. Koo, B.W., Hebda, J.A. and Miranker, A.D. (2008) Amide inequivalence in the fibrillar assembly of islet amyloid polypeptide. *Protein Eng. Des. Sel*., 21, 147–154.
60. Westermark, P. and Wilander, E. (1978). The influence of amyloid deposits on the islet volume in maturity onset diabetes mellitus. *Diabetologia*, 15, 417-421.
61. Cao, P., Marek, P., Noor, H., Patsalo, V., Tu, L. H., Wang, H., Abedini, A. and Raleigh, D. P. (2013) Islet amyloid: From fundamental biophysics to mechanism of cytotoxicity. *FEBS Letters*, 587 (8), 1106-1118.
62. Jayasinghe, S. A. and Langen, R. (2007) Membrane interaction of islet amyloid polypeptide. *Biochim. Biophys. Acta.*, 1768, 2002-2009.
63. Goldsbury, C., Goldie, K., Pellaud, J., Seelig, J., Frey, P., Muller, S. A., Kistler, J., Cooper, G. J. and Aebi, U. (2000) Amyloid fibril formation from full-length and fragments of amylin, *J. Struct. Biol.*, 130, 352-362.
64. Engel, M. F., Yigittop, H., Elgersma, R., Risjkers, D., Liskamp, R., Kruijff, B., J. W. Höppener, J. W. and Antoinette, K. J. (2006) Islet amyloid polypeptide inserts into phospholipid monolayers as monomer, *J. Mol. Biol*., 356, 783-789.
65. Dunkelberger, E. B., Buchanan, L. E., Marek, P., Cao, P., Raleigh, D. P. and Zanni, M. T. (2012) Deamidation accelerates amyloid formation and alters amylin fiber structure. *J. Am. Chem. Soc*., 134, 12658–12667.
66. Azriel, R. and Gazit, E. (2001) Analysis of the structural and functional elements of the minimal active fragment of islet amyloid polypeptide (IAPP) – an experimental support for the key role of the phenylalanine residue in amyloid formation. *J. Biol. Chem*., 276, 34156–34161.
67. Marek, P., Abedini, A., Song, B. B., Kanungo, M., Johnson, M. E., Gupta, R., Zaman, W., Wong, S. S. and Raleigh, D. P. (2007) Aromatic interactions are not required for amyloid

fibril formation by islet amyloid polypeptide but do influence the rate of fibril formation and fibril morphology. *Biochemistry,* 46, 3255–3261.

68. Koo, B. W. and Miranker, A. D. (2005) Contribution of the intrinsic disulfide to the assembly mechanism of islet amyloid, *Protein Sci*., 14, 231-239.
69. Kahn, S. E., Verchere, C. B., Andrikopoulos, S., Asberry, P. J., Leonetti, D. L., Wahl, P. W., Boyko, E. J., Schwartz, R. S., Newll-Morris, L. and Fujimoto, W. Y. (1998). Reduced amylin release is a characteristic of impaired glucose tolerance and type 2 diabetes in Japanese Americans. *Diabetes*, 47, 640-645.
70. Knight, J. D. Hebda, J. A. and Miranker, A. D. (2006). Conserved and cooperative assembly of membrane-bound α-helical states of islet amyloid polypeptide. *Biochemistry*, 45(31), 9496-9508.
71. Landchild, M. J., Knowles, N. G. and Yao, Q. (2000). Increased β-cell secretory demand is not the simple explanation for inefficient proinsulin processing and islet amyloid formation in type 2 diabetes. *Journal of Investigative Medicine*, 48, 21A.
72. Cui, W., Ma, J., Lei, P. and Wu, W., Yu, Y., Xiang, Y., Tong, A., Zhao, Y. and Li, Y. (2009). Insulin is a kinetic but not a thermodynamic inhibitor of amylin aggregation. *FEBS Journal*, 276(12), 3365-3371.
73. Radovan, D., V. Smirnovas, V. and Winter, R. (2008) Effect of pressure on islet amyloid polypeptide aggregation: revealing the polymorphic nature of the fibrillation process. *Biochemistry,* 47 6352-6360.
74. Westermark, P., Wernstedt, C., Wilander, E., Hayden, D. W., O'Brien, T. D., and Johnson, K. H. (1987) Amyloid fibrils in human insulinoma and islets of langerhans of the diabetic cat are derived from a neuropeptide-like protein also present in normal islet cells. *Proc. Natl. Acad. Sci. U. S. A.*, 84, 3881-3885.
75. Wiltzius, J. J. W., Sievers, S. A., Sawaya, M. R., Cascio, D., Popov, D., Riekel, C. and Eisenberg, D. (2008) Atomic structure of the cross-β spine of islet amyloid polypeptide (amylin). *Protein Sci*., 17, 1467–1474.
76. Ahmad, E., Ahmad, A., Singh, S., Arshad, M., Khan, A. H. and Khan, R. H. (2011) A mechanistic approach for islet amyloid polypeptide aggregation to develop anti-amyloidogenic agents for type-2 diabetes. *Biochimie*, 93, 793-805.
77. Nilsson, M. and Raleigh, D. P. (1999) Analysis of amylin cleavage products provides new insights into the amyloidogenic region of human amylin, *J. Mol. Biol*., 294, 1375-1385.
78. Padrick, S. B. and Miranker, A. D. (2002) Islet amyloid: phase partitioning and secondary nucleation are central to the mechanism of fibrillogenesis, *Biochemistry*, 41, 4694-4703.
79. Green, J. D., Goldsbury, C., J. Kistler, J., Cooper, G. J. and Aebi, U. (2004) Human amylin oligomer growth and fibril elongation define two distinct phases in amyloid formation, *J. Biol. Chem.*, 279, 12206-12212.

80. Wilson**,** M. R., Yerbury, J. J. and Poon, S. (2008). Potential roles of abundant extracellular chaperones in the control of amyloid formation and toxicity. *Molecular BioSystems.*, 4, 42-52.
81. Brender, J. R., Lee, E. L., Cavitt, M. A., Gafni, A., Steel, D. G. and Ramamoorthy, A. (2008), Amyloid fibre formation and membrane disruption are separate processes localised in two distinct regions of IAPP, the Type-2 Diabetes related peptide. *J. Am. Chem. Soc*., 130, 6424-6429.
82. Janson, J., Ashley, R. H., Harrison, D., McIntyre, S. and Butler, P. C. (1999) The mechanism of islet amyloid polypeptide toxicity is membrane disruption by intermediate-sized toxic amyloid particles. *Diabetes*, 48, 491–498.
83. Mirzabekov, T. A., Lin, M. C. and Kagan, B. L. (1996) Pore formation by the cytotoxic islet amyloid peptide amylin. *J. Biol. Chem*., 271, 1988–1992.
84. Seeliger, J., Weise, K., Opitz, N. and Winter, R. (2012) The effect of Aβ on IAPP aggregation in the presence of an isolated beta-cell membrane. *J. Mol. Biol*., 421, 348–363.
85. (a) Westermark, G. T., Westermark, P., Berne, C. and Korsgren, O. (2008) Transplantation NNCI. widespread amyloid deposition in transplanted human pancreatic islets. *N. Engl. J. Med.*, 359, 977-979. (b) Potter, K. J., Abedini, A., Marek, P., Klimek, A. M., Butterworth, S., Driscoll, M., Baker, R., Nilsson, M. R., Warnock, G. L., Oberholzer, J., Bertera, M., Trucco, M., Korbutt, G. S., Fraser, P. E., Raleigh, D. P. and Verchere, C. B. (2010) Islet amyloid deposition limits the viability of human islet grafts but not porcine islet grafts. *Proc. Natl. Acad. Sci. U. S. A.*, 107, 4305-4310.
86. Kurkimilis, K. (2013) The role of amylin in type-2 diabetes. *Senior Honors Theses*, *Eastern Michigan University*.
87. (a) Ryan, G. J., Jobe, L. J. and Martin, R. (2005) Pramlintide in the treatment of type1 and type2 diabetes mellitus. *Clin. Ther*., 27, 1500-1512. (b) Kruger, D. F. and Gloster, M. A. (2004) Pramlintide for the treatment of insulin-requiring diabetes mellitus-rationale and review of clinical data. *Drugs*, 64, 1419-1432.
88. McClean, P. L and Hölscher, C. (2014). Lixisenatide, a drug developed to treat type 2 diabetes, shows neuroprotective effects in a mouse model of Alzheimer's disease. *Neuropharmacology*, 86, 241-258.
89. (a) Vilsboll, T., Christensen, M., Junker, A. E., Knop, F. K. and Gluud, L. L. (2012) Effects of glucagon-like peptide-1 receptor agonists on weight loss: systematic review and meta analysis of randomised control trials. *BMJ*, 344, d7771.(b) Drucker, D. J. and Nauck, M. A. (2006) The incretin system: glucagon-like peptide-1receptor agonists and dipeptidyl peptidase-4 inhibitors in type-2 diabetes. *Lancet*, 368, 1696-1705.
90. (a) Xu, F., Zhao, C., Huang, X. and Du, W. (2020) Tetracycline derivatives resist the assembly behavior of human islet amyloid polypeptide. *Biochimie*, 174, 95-106. (b) Meng, Q. Y., Wang, H., Cui, Z. B., Yu, W. G. and Lu, X. Z. (2020) Chitosan oligosaccharides attenuate

amyloid formation of hIAPP and protect pancreatic β-cells from cytotoxicity. *Molecules*, 25, 1314-1318. (c) Saravanan, M. S., Ryazanov, S., Leonov, A., Nicolai, J., Praest, P., Giese, A., Winter, R., Khemtemourian, L., Griesinger, C. and Killian, J. A. (2019) The small molecule inhibitor Anle145c thermodynamically traps human islet amyloid peptide in the form of non-cytotoxic oligomers. *Sci. Rep*., 9, 19023. (d) Xu, J., Zhao, C., Huang, X. and Du, W. (2019) Regulation of artemisinin and its derivatives on the assembly behaviour and cytotoxicity of amyloid polypeptides hIAPP and Aβ. *ACS Chem. Neurosci*., 10, 4522-4534. (e) Kumar, S., Vogel, M. C. and Hamilton, A. D. (2018) Teaching an old scaffold new recognition tricks: oligopyrrolamide antagonists of IAPP aggregation. *Org. Biomol. Chem*., 16, 733-741. (f) Zou, Y., Qian, Z., Sun, Y., Wei, G. and Zhang, Q. (2017) Orcein-related small molecule O4 destabilizes hIAPP protofibrils by interacting mostly with the amyloidogenic core region. *J. Phys. Chem*., B 121, 9203-9212. (g) Nath, A., Schlamadinger, D. E., Rhoades, E. and Miranker, A. D. (2015) Structure-based small molecule modulation of a pre-amyloid state: pharmacological enhancement of IAPP membrane-binding and toxicity. *Biochemistry*, 54, 3555-3564. (h) Mishra, R., Bulic, B., Sellin, D., Jha, S., Waldmann, H. and Winter, R. (2008) Small molecule inhibitors of islet amyloid polypeptide fibril formation. *Angew. Chem., Int. Ed*. 47, 4679-4682. (i) Zhang, Y., Zhang, D., Tang, Y., Ren, B., Liu, F., Xu, L., Chang, Y. and Zheng, J. (2020) Aromadendrin: a dual amyloid promoter to accelerate fibrillization and reduce cytotoxicity of both Amyloid-β and hIAPP. *Mater. Adv*., 1, 1241-1252.

91. (a) Bai, C., Lin, D., Mo, Y., Lei, J., Sun, Y., Xie, L., Yang, X. and Wei, G. (2019) Influence of fullerenol on hIAPP aggregation: amyloid inhibition and mechanistic aspects. *Phys. Chem. Chem. Phys*., 21, 4022-4031. (b) Wang, M., Sun, Y., Cao, X., Peng, G., Javed, I., Kakinen, A., Davis, T. P., Lin, S., Liu, J., Ding, F. and Ke, P. C. (2018) Graphene quantum dots against human IAPP aggregation and toxicity in vivo. *Nanoscale*, 10, 19995-20006. (c) Yousaf, M., Huang, H., Li, P., Wang, C. and Yang, Y. (2017) Fluorine functionalized graphene quantum dots as inhibitor against hIAPP amyloid aggregation. *ACS Chem. Neurosci*., 8, 1368-1377. (d) Zhao, L., Xin, Y., Li, Y., Yang, X., Luo, L. and Meng, F. (2019) Ultraeffective inhibition of amyloid fibril assembly by nano body gold nanoparticle conjugates. *Bioconjugate Chem*., 30, 29-33.
92. Mo, Y., Brahmachari, S., Lei, J., Gilead, S., Tang, Y., Gazit, E. and Wei, G. (2018) The inhibitory effect of hydroxylated carbon nanotubes on the aggregation of human islet amyloid polypeptide revealed by a combined computational and experimental study. *ACS Chem. Neurosci*. 9, 2741-2752.
93. Franko, A., Camargo, D. C. R., Boddrich, A., Garg, D. Camargo, A. R., Rathkolb, B., Janik, D. Aichler, M., Feuchtinger, A., Neff, A., Fuchs, H., Wanker, E. E., Reif, B., Haring, H., Peter, A. and Angelis, M. H. (2018) Epigallocatechin gallate (EGCG) reduces the intensity of

pancreatic amyloid fibrils in human islet amyloid polypeptide (hIAPP) transgenic mice. Sci. Rep., 8(1), 1-12.

94. (a) Armiento, V., Spanopoulou, A. and Kapurniotu, A. (2020) Peptide-based molecular strategies to interfere with protein misfolding, aggregation and cell degeneration. *Angew. Chem., Int. Ed*., 59, 3372-3384. (b) Henninot, A., Collins, J. C. and Nuss, J. M. (2018) The current state of peptide drug discovery: back to the future? *J. Med. Chem*., 61, 1382 1414. (c) Goyal, D., Shuaib, S., Mann, S. and Goyal, B. (2017) Rationally designed peptides and peptidomimetics as inhibitors of amyloid-β (Aβ) aggregation: potential therapeutics of Alzheimer's disease. *ACS Comb. Sci*., 19, 55-80.
95. Tenidis, K., Waldner, M., Bernhagen, J., Fischle, W., Bergmann, M., Weber, M., Merkle. M., Voelter, W., Brunner, H. and Kapurniotu, A. (2000) Identification of a penta- and hexapeptide of islet amyloid polypeptide (IAPP) with amyloidogenic and cytotoxic properties. *J. Mol. Biol*., 295(4), 1055-1071.
96. Scrocchi, L. A., Chen, Y., Waschuk, S., Wang, F., Cheung, S., Darabie, A. A., McLaurin, J. and Fraser, P. E. (2002) Design of peptide-based inhibitors of human islet amyloid polypeptide fibrillogenesis. *J. Mol. Biol*., 318, 697-706.
97. Porat, Y., Mazor, Y., Efrat, S. and Gazit, E. (2004) Inhibition of islet amyloid polypeptide fibril formation: a potential role for heteroaromatic interactions. *Biochemistry*, 43, 14454-14462.
98. Abedini, A., Meng, F., and Raleigh, D. P. (2007) A single point mutation convert the highly amyloidogenic human islet amyloid polypeptide into a potent fibrillization inhibitor. *J. Am. Chem. Soc*., 129, 11300-11301.
99. Cao, P., Meng, F., Abedini, A. and Raleigh, D. P. (2010) The ability of rodent islet amyloid polypeptide to inhibit amyloid formation by human islet amyloid polypeptide has important implications for the mechanism of amyloid formation and the design of inhibitors. *Biochemistry*, 49, 872-881.
100. Wang, H., Abedini, A., Ruzsicska, B. and Raleigh, D. P. (2014) Rationally designed, nontoxic, non-amyloidogenic analogues of human islet amyloid polypeptide with improved solubility. *Biochemistry*, 53, 5876-5884.
101. Khemtemourian, L., Guillemain, G., Foufelle, F. and Killian, J. A. (2017) Residue specific effects of human islet polypeptide amyloid on self-assembly and on cell toxicity. *Biochimie*, 142, 22-30.
102. Figueroa, H., Peddi, D., Osborne, J. M., Wilson, B. M., Pesaru, R. R., Kurva, B., Ramaraju, S., Milletti, M. C. and Heyl, D. L. (2012) Modelling the interface between islet amyloid polypeptide and insulin-based aggregation inhibitors: correlation to aggregation kinetics and membrane damage. *J. Chem. Inf. Model*., 52, 1298-1307.

103. Zhou, X., Cao, C., Chen, Q., Yu, Q., Liu, Y., Yin, T. and Liu, J. (2015) PEG modified graphene oxide loaded with EALYLV; peptides for inhibiting the aggregation of hIAPP associated with type-2 diabetes. *J. Mater. Chem*., B3, 7055-7067.
104. Ghosh, A., Pithadia, A. S., Bhat, J., Bera, S., Midya, A., Fierke, C. A., Ramamoorthy, A. and Bhunia, A. (2015) Self-assembly of a nine residue amyloid-forming peptide fragment of SARS corona virus E-protein: mechanism of self-aggregation and amyloid-inhibition of hIAPP. *Biochemistry*, 54, 2249-2261.
105. Shi, Y., Lv, W., Jiao, A., Zhang, C. and Zhang, J. (2019) A novel penta-peptide inhibitor reduces amyloid deposit formation by direct interaction with hIAPP. *Int. J. Endocrinol*., 2019, 9062032.
106. Kapurniotu, A., Schmauder, A. and Tenidis, K. (2002) Structure-based design and study of non-amyloidogenic, double N-methylated IAPP amyloid core sequences as inhibitors of IAPP amyloid formation and cytotoxicity. *J. Mol. Biol*., 315, 339-350.
107. Yan, L. M., Tatarek-Nossol, M., Velkova, A., Kazantzis, A. and Kapurniotu, A. (2006) Design of a mimic of non-amyloidogenic and bioactive human islet amyloid polypeptide (IAPP) as nano-molar affinity inhibitor of IAPP cytotoxic fibrillogenesis. *Proc. Natl. Acad. Sci. U. S. A.*, 103, 2046-2051.
108. Wang, L., Lei, L., Li, Y., Wang, L. and Li, F. (2014) A hIAPP derived all-D-amino acid inhibits hIAPP fibrillation efficiently at membrane surface by targeting α-helical oligomeric intermediates. *FEBS Lett*ers, 588, 884-891.
109. Huggins, K. N. L., Bisaglia, M., Bubacco, L., Tatarek-Nossol, M., Kapurniotu, A. and Andersen, N. H. (2011) Designed hairpin peptides interfere with amyloidogenesis pathways: fibril formation and cytotoxicity inhibition, interception of the pre-amyloid state. *Biochemistry*, 50, 8202-8212.
110. Gilead, S. and Gazit, E. (2004) Inhibition of amyloid fibril formation by peptide analogues modified with α-aminoisobutyric acid. *Angew. Chem., Int. Ed*., 43, 4041-4044.
111. Andreasen, M., Nielsen, S. B., Mittag, T., Bjerring, M., Nielsen, J. T., Zhang, S., Nielsen, E. H., Jeppesen, M., Christiansen, G., Besenbacher, F., Dong, M., Nielsen, N. C., Skrydstrup, T. and Otzen, D. E. (2012) Modulation of fibrillation of hIAPP core fragments by chemical modification of the peptide backbone. *Biochim. Biophys. Acta, Proteins Proteomics*, 1824, 274-285.
112. Mishra, A., Misra, A., Vaishnavi, T. S., Thota, C., Gupta, M., Ramakumar, S. and Chauhan, V. S. (2013) Conformationally restricted short peptides inhibit human islet amyloid polypeptide (hIAPP) fibrillization. *Chem. Commun*., 49, 2688-2690.
113. Sivanesam, K., Shu, I., Huggins, K. N. L., Tatarek-Nossol, M., Kapurniotu, A. and Andersen, N. H. (2016) Peptide inhibitors of the amyloidogenesis of IAPP: verification of the hairpin-binding geometry hypothesis. *FEBS Lett*ers, 590, 2575-2583.

114. Profit, A. A., Vedad, J. and Desamero, R. Z. B. (2017) Peptide conjugates of benzene carboxylic acids as agonists and antagonists of amylin aggregation. *Bioconjugate Chem.*, 28, 666-677.

115. Saini, R. K., Goyal, D. and Goyal, B. (2020) Targeting human islet amyloid polypeptide aggregation and toxicity in type-2 diabetes: An overview of peptide-based inhibitors. *Chem, Res. Toxicol*., 33(11), 2719-2738.

116. (a) Hamoro, Y., Geib, S. J. and Hamilton, A. D. (1996) Oligoanthranilamides: Non-peptide subunits that show formation of specific secondary structure. *J. Am. Chem. Soc*., 118, 7529-7541. (b) Katoh, T. and Suga, H. (2020) Ribosomal elongation of aminobenzoic acid derivatives. *J. Am. Chem. Soc*., 142, 16518-16522.

117. Ramesh, V. V. E., Priya, G., Kotmole, A. S., Gonnade, R. G., Rajamohanan, P. R. and Sanjayan, G. J. (2012) Multifaceted folding in a foldamer featuring highly cooperative folds. *Chem. Commun*., 48, 11205-11207.

118. Paul, A., Nadimpally, K. C., Mondal, T., Thalluri, K. and Mandal, B. (2015) Inhibition of Alzheimer's amyloid-β peptide aggregation and its disruption by a conformationally restricted α/β hybrid peptide. *Chem. Commun*., 51, 2245-2248.

119. (a) Pravakaran, P., Kale, S. S., Puranik, V. G., Rajamohanan, P. R., Chetina, O., Howard, J. A. K., Hofmann, H. J. and Sanjayan, G. J. (2008) Sequence specific unusual type helical turns in α/β hybrid peptides. *J. Am. Chem. Soc.* 130, 17743-17754. (b) Maity, S., Jana, P., Maity, S. K., Kumar, P. and Haldar, D. (2012) Conformational heterogeneity, self-assembly and gas adsorption studies of isomeric hybrid peptides. *Cryst. Growth Des*. 12, 422-428.

120. (a) Dalsgaard, P. W.; Larsen, T. O.; Christophersen, C. (2005) Bioactive cyclic peptides from the psychrotolerant fungus Penicillium algidum. *J. Antibiot*., 58, 141-144 (b) Haynes, S. W., Gao, X., Tang, Y. and Walsh, C. T. (2012) Assembly of asperlicin peptidyl alkaloids from anthranilate and tryptophan: A two enzyme pathway generates heptacyclic scaffold complexity in Asperlicin E. *J. Am. Chem. Soc*., 134, 17444-17447.

121. (a) Cheng, R. P., Gellman, S. H. and DeGrado, W. F. (2001) β-peptides: From structure to function. *Chem. Rev*., 101, 3219-3232. (b) Shen, Y., Hixson, K. K., Tolic, N., Camp, D. G., Purvine, S. O., Moore, R. J. and Smith, R. D. (2008) Mass spectrometry analysis of proteome-wide proteolytic post-translational degradation of proteins. *Anal. Chem*, 80, 5819-5828.

122. Soto, C., Sigurdsson, E. M., Morelli, L., Kumar, R. A., Castano, E. M. and Frangione, B. (1998) β-sheet breaker peptides inhibit fibrillogenesis in a rat brain model of amyloidosis: Implications for Alzheimer's therapy. *Nature Medicine, 4*, 822–826.

123. Nadimpally, K. C., Paul, A. and Mandal, B. (2014) Reversal of aggregation using β-breaker dipeptide containing peptide: Application to Aβ(1-40) self-assembly and its inhibition. *ACS Chem. Neurosci*., 5, 400-408.

124. Oza, V. B., Petrassi, H. M., Purkey, H. E. and Kelly, J. W. (1999) Synthesis and evaluation of anthranilic acid besed transthyretin amyloid fibril inhibitors. *Bioorg. Med. Chem. Lett*., 9, 1-6.
125. Simons, L. J., Caprathe, B. W., Callahan, M., Graham, J. M., Kimura, T., Lai, Y., LeVine, H., Lipinski, W., Sakkab, A. T., Tasaki, Y., Walker, L. C., Yasunaga, T., Ye, Y., Zhuang, N. and Augelli-Szafran, C. E. (2009) The synthesis and structure-activity relationship of substituted N-phenylanthranilic acid analogs as amyloid aggregation inhibitors. *Bioorg. Med. Chem. Lett.*, 19, 654-657.
126. Takahashi, T. and Mihara, H. (2008) Peptide and protein mimetics inhibiting amyloid beta peptide aggregation. *Acc. Chem. Res*. 41(10) 1309-1318.
127. Formaggio, F., Bettio, A., Moretto, V., Crisma, M., Toniolo, C. and Broxterman, Q. B. (2003) Disruption of the β-sheet structure of a protected pentapeptide, related to the β-amyloid sequence 17-21, induced by a single, helicogenic Cα-tetrasubstituted α-amino acid. *J. Peptide Sci*., 9, 461-466.
128. Moretto, V., Crisma, M., Bonora, G. M., Toniolo, C., Balaram, H. and Balaram, P. (1989) Comparison of the effect of five guest residues on the β-sheet conformation of host $(L\text{-}Val)_n$ oligopeptides. *Macromolecules*, 22, 2939-2944.
129. Stewart, J. M., and Young, J. D. (1984) *Solid Phase Peptide Synthesis*. 2nd ed.; Pierce Chemical, Rockford, IL.
130. (a) Coin, I., Beyermann, M., and Bienert, M. (2007) Solid-phase peptide synthesis: from standard procedures to the synthesis of difficult sequences. *Nat. Protoc. 2*, 3247–3256. (b) Amblard, M., Fehrentz, J. A., Martinez, J. and Subra, G. (2006) Methods and Protocols of Modern Solid Phase Peptide Synthesis. *Mol. Biotech*. *33*, 239-254.
131. Brender, J. R., Salamekh, S. and Ramamoorthy, A. (2012) Membrane disruption and early events in the aggregation of the diabetes related peptide IAPP from a molecular prospective. *Acc. Chem. Res*. 45, 454-462.
132. Anguiano, M., Nowak, R. J. and Lansburry, P. T. Jr. (2002) Protofibrillar islet amyloid polypeptide permeabilizes synthetic vesicles by a pore like mechanism that may be relevant to type II diabetes. *Biochemistry*, 41, 11338-11343.
133. Cao, P., Abedini, A., Wang, H., Tu, L. H., Zhang, X., Schmidt, A. M. and Raleigh, D. P. (2013) Islet amyloid polypeptide toxicity and membrane interactions. *Proc. Natl. Acad. Sci. U. S. A.*, 110, 19279-19284.
134. Sciacca, M. F. M., Kotler, S. A., Brender, J. R., Chen, J., Lee, D. K. and Ramamoorthy, A. (2012) Two-step mechanism of membrane disruption by Aβ through membrane fragmentation and pore formation. *Biophys. J*., 103, 702-710.
135. Brender, J. R., Lee, E. L., Cavitt, M. A., Gafni, A., Steel, D. G. and Ramamoorthy, A. (2008) Amyloid fiber formation and membrane disruption are separate processes localised in two

distinct regions of IAPP, the type-2-diabetes related peptide. *J. Am. Chem. Soc*., 130. 6424-6429.

136. Williams, T. L., Day, I. J. and Serpell, L. C. (2010) The effect of Alzheimer's Aβ aggregation state on the permeation of biomimetic lipid vesicles. *Langmuir*, 26, 17260-17268.
137. McLaurin, J. and Chakrabartty, A. (1996) Membrane disruption by Alzheimer beta-amyloid peptides mediated through specific binding to either phospholipids or gangliosides, implications for neurotoxicity. *J. Biol. Chem*, 271, 26482-26489.
138. Traikia, M., Warschawski, D. E., Recouvreur, M., Cartaud, J. and Devaux, P. F. (2000) Formation of unilamellar vesicles by repetitive freeze thaw cycles: characterisation by electron microscopy and 31P nuclear magnetic resonance. *Eur. Biophys. J*., 29, 184-195
139. Jenssen, H. and Aspmo, S. I. (2008) Serum stability of peptides. *Methods Mol. Biol*., 494, 177-186.
140. Frackepohl, J., Arvidsson, P. I., Schreiber, J. V. and Seebach, D. (2001) The outstanding biological stability of beta and gamma peptides toward proteolytic enzymes: an *in vitro* investigation with fifteen peptidases. *Chembiochem*, 2, 445-455.
141. Jones, M. C., (2007) Therapies for diabetes: pramlintide and exenatide. *Am. Fam. Physician*, 75, 1831-1835.
142. Ryan, G. J., Jobe, L. J. and Martin, R. (2005) Pramlintide in the treatment of type 1 and type 2 diabetes mellitus. *Clin. Ther*, 27, 1500-1512.
143. Hollander, P., Maggs, D. G., Ruggles, J. A., Finemann, M., Shen, L., Kolterman, O. G. and Weyer, C. (2004) Effect of pramlintide on weight in overweight and obese insulin-treated type-2 diabetes patients. *Obes Res*., 12, 661-668.
144. Paul, A., Kalita, S., Kalita, S., Sukumar, P. and Mandal, B. (2017) Disaggregation of amylin aggregate by novel conformationally restricted aminobenzoic acid containing α/β and α/γ hybrid peptidomimetics. *Sci. Rep.*, 7, 40095-40107.
145. Tendis, K., Waldner, M., Bernhagen, J., Fischle, W., Bergmann, M., Weber, M., Merkle, M. L., Voelter, W., Brunner, H. and Kapurniotu, A. (2000) Identification of a penta and hexapeptide of islet amyloid polypeptide (IAPP) with amyloidogenic and cytotoxic properties. *J. Mol. Biol*., 295, 1055-1071.
146. Kumar, J., Namsechi, R. and Sim, V. L. (2015) Structure based peptide design to modulate Amyloid-Beta aggregation and reduce cytotoxicity. *PLoS ONE*, 10 (6), 1-18.
147. Kalita, S., Kalita, S., Paul, A., Sarkar, A. and Mandal, B. (2020) Peptidomimetics prepared by tail-to-side chain one component peptide stapling inhibits Alzheimer's amyloid-β fibrillogenesis. *Chem. Sci.*, 11, 4171-4179.
148. Kalita, S. Kalita, S., Paul, A., Shah, M, Kumar, S. and Mandal, B. (2021) Site-specific single point mutation by anthranilic acid in $hIAPP_{8-37}$ enhances anti-amyloidogenic activity. *RSC Chem. Biol.*, 2, 266-273.

149. Verdine, G. L. and Hilinski, G. J. (2012) All hydrocarbon stapled peptides as synthetic cell accessible mini proteins. *Drug. Discov. Today Technol.*, 9, 41-47.
150. Bullock, B. N., Jochim, A. L. and Arora, P. S. (2011) Assessing helical protein interfaces for inhibitor design. *J. Am. Chem. Soc.*, 133, 14220-14223.
151. Long, Y. Q, Huang, S. X., Zawahir, Z., Xu, Z. L., Li, H., Sanchez, T. W., Zhi, Y., Houwer, S. D., Christ, F.m Debyser, Z and Neamati, N. (2013) Design of cell-permeable stapled peptides as HIV-1 integrase inhibitors. *J. Med. Chem*., 56 (13) 5601-5612.
152. Sinclair, J. K. L., Denton, E. V. and Schepartz, A. (2014) Inhibiting epidermal growth factor receptor at a distance. *J. Am. Chem. Soc.*, 136 (32), 11232-11235.
153. Lau, Y. H., Andrade, P. D., Wu, Y. and Spring, D. R. (2015) Peptide stapling technique based on different macrocyclisation chemistries. *Chem. Soc. Rev.*, 44, 91-102.
154. Tan, Y. H., Lane, D. P. and Verma, C. S. (2016) Stapled Peptide design: principles and roles of computation, *Drug Discovery Today*, 21, 1642-1653.
155. Felix, A. M., Heimer, E. P., Wang, C. T., Lambros, T. J., Fournier, A., Mowels, T. F., Maines, S., Campbell, R. M., Wegrzynski, B. B., Toome, V., Fry, D. and Madison, V. S. (1988) Synthesis, biological activity and conformational analysis of cyclic GRF analogs. *Int. J. Pept., protein Res.*, 32, 441-454.
156. Barthe, P., Rochette, S., Vita, C. and Roumestand, C. (2000) Synthesis and NMR solution structure of an alpha-helical hairpin stapled with two disulfide bridges. *Protein Sci*., 2000, 9 (5), 942-955.
157. Schafmeister, C. E., Po, J and Verdine, G. L. (2000) An all-hydrocarbon cross-linking system for enhancing the helicity and metabolic stability of peptides. *J. Am. Chem. Soc.*, 122(24) 5891-5892.
158. Giri, R. S., Manne, S. R., Dolai, G., Paul, A., Kalita, T. and Mandal, B. (2017) $FeCl_3$ mediated side chain modification of aspartic acid and glutamic acid containing peptides on a solid support. *ACS Omega*, 2(10) 6586-6597.
159. Sheynis, T., Friediger, A., Xue, W. F., Hellewell, A. L., Tipping, K. W., Hewitt, E. W., Radford, S. E. and Jelinek, R. (2013) Aggregation modulators interfere with membrane interactions of β2-microglobulin fibrils. *Biophys J*., 105(3) 745-755.
160. Chen, S., and Wetzel, R. (2001) Solubilization and disaggregation of polyglutamine peptides. *Protein Sci*. *10*, 887-891.
161. Khurana, R., Coleman, C., Zanetti-Ionescu, C., Carter, S. A., Krishna, V., Grover, R. K., Roy, R., and Singh, S. (2005) Mechanism of Thioflavin T binding to amyloid fibrils. *J. Struc. Biol*. *151*, 229-238. Kaiser, E., Colescot, R. L., Bossinge, C. D., and Cook, P. I. (1970) Color test for detection of free terminal amino groups in solid phase synthesis of peptides. *Anal. Biochem*. *34*, 595-598.

162. Kaiser, E., Colescot, R. L., Bossinge, C. D., and Cook, P. I. (1970) Color test for detection of free terminal amino groups in solid phase synthesis of peptides. *Anal. Biochem*. *34*, 595-598.

Publications:

1. Kalita, S., Kalita, S., Paul, A., Shah, M., Kumar, S. and Mandal, B., (2021) Site-specific single point mutation by anthranilic acid in $hIAPP_{8-37}$ enhances anti-amyloidogenic activity. *RSC Chem. Biol*., 2, 266-273.
2. Kalita, S., Kalita, S., Shill, S., Kawa, A. K. and Mandal, B., Side-chain to tail stapled peptides disrupts amyloid aggregation into non-toxic species. (manuscript under preparation)
3. Paul, A., Kumar, S., Kalita, S., Kalita, S., Sarkar, D., Bhunia, A., Bandyopadhyay, A., Mondal, A. C. and Mandal, B. (2021) An explicitly designed paratope of amyloid-β prevents neuronal apoptosis *in vitro* and hippocampal damage in rat brain. *Chem. Sci*., 12, 2853-2862.
4. Kalita, S., Kalita, S., Kawa, A. H., Shill, S. and Mandal, B. Copper chelating cyclic peptidomimetic inhibits Aβ fibrillogenesis in Alzheimer's disease. (Manuscript under revision).
5. Kalita, S., Kalita, S., Paul, A., Sarkar, A. and Mandal, B.; (2020) Peptidomimetics prepared by tail to side chain one component peptide stapling inhibit Alzheimer's amyloid-β fibrillogenesis. *Chem. Sci*., 11, 4171-4179.
6. Ratha, B. N., Kar, R. K., Kalita, S., Kalita, S., Raha, S., Singha, A., Garai, K., Mandal, B. and Bhunia, A.; (2019) Sequence specificity of amylin-insulin interaction: a fragment-based insulin
7. Paul, A., Kumar, S., Kalita, S., Ghosh, A. K., Mondal, A. C. and Mandal, B.; (2018) A Peptide-Based Pro-drug Disrupts Alzheimer's Amyloid into Non-toxic species and reduces Aβ induced toxicity in vitro. *Int J Pept Res Ther*, 24 (1), 201-211.
8. Kumar, S., Paul, A., Kalita, S., Kumar, A., Hazra, S., Ghosh, A. K., Mandal, B. and Mondal, A. C.; (2017) A peptide-based pro-drug ameliorates Amyloid-β induced neuronal apoptosis in vitro SH-SY5Y cells. *Current Alzheimer Research*. 14 (12) 1293.
9. Kumar, S., Paul, A., Kalita, S., Ghosh, A. K., Mandal, B. and Mondal, A.C.; (2017) Protective effects of β-sheet breaker α/β-hybrid peptide against amyloid β-induced neuronal apoptosis in vitro. *Chem Biol Drug Des*; 89 (6), 888-900.
10. Paul, A., Kalita, S., Kalita, S., Sukumar, P. and Mandal, B.; (2017) Disaggregation of Amylin Aggregate by Novel Conformationally Restricted Aminobenzoic Acid containing α/β and α/γ Hybrid Peptidomimetics. *Sci. Rep., 7*, 40095.
11. Sharma, B., Kalita, S., Paul, A., Mandal, B. and Paul, S.; (2016) The role of caffeine as an inhibitor in the aggregation of amyloid-forming peptides: a unified molecular dynamics simulation and experimental study. *RSC Adv*., 6, 78548.
12. Saha, A., Nadimpally, K.C., Paul, A., Kalita, S. and Mandal, B.; (2014) Phenolic Ester mediated oligopeptide synthesis promoted by HOBt. *Protein and Peptide Letters*, 21 (2) 188.

Conferences attended:

1. **Kalita, S**., Kalita, S. and Mandal, B.; (2020) Effective modulation against amyloid aggregation of hIAPP using modified stapled peptides. *SSD 2020*, 25th-26th September, 2020, B. Borooah College, Assam, India, PP16. (Poster presentation)
2. **Kalita, S**., Kalita, S., Paul, A. and Mandal, B.; (2019) Inhibition of amylin aggregation by single point mutant of hIAPP at different positions. *IPS 2019* 28th February–1st March, 2019, BITS Pilani, Hyderabad Campus, India, P41. (Poster presentation).
3. **Kalita, S**., Kalita, S., Paul, A. and Mandal, B.; (2019) Inhibition of toxic diabetic's amyloid aggregation by conformationally restricted hybrid Peptidomimetics. *SSD 2019*, 9th January, 2019, B. Borooah College, Assam, India, OP40, page 55. (Oral presentation)
4. Kalita, S., Paul, A., **Kalita, S**., and Mandal, B.; (2017) Disaggregation of amylin aggregation by novel conformationally restricted aminobenzoic acid containing α/β and α/γ hybrid Peptidomimetics. *ICSIMR 2017*, 30th June-1st July, 2017, IIT Guwahati, India, PP61, page 122. (Participation).
5. **Kalita, S**., Paul, A., Kalita, S. and Mandal, B.; (2017) A novel strategy for drug design against Diabetes Type II (T2D) by disaggregation of amylin aggregation by conformationally restricted hybrid Peptidomimetics. *Chem Convene 2017*, 25th July, 2017, IIT Guwahati, India, P40, page 84. (Poster presentation, recipient of best poster presentation award).
6. **Kalita, S**., Paul, A., Kalita, S. and Mandal, B.; (2016) Anti-diabetic activity of aminobenzoic acid containing α/β and α/γ but not α/δ hybrid peptide. *FICS 2016*, 8th -10th December 2016, IIT Guwahati, India, OP13, page 50. (Oral presentation)

Workshop attended:

1. National Workshop on Advanced Probing Techniques in TEM (APTTEM-2016) at IIT Guwahati, Assam, India, 15th-16th February, 2016.

Book Chapter:

1. Sourav Kalita, (2020) Diabetes: A striking correlation with amylin and strategic development against the disease. *Aspects of sustainable chemical sciences*, First edition, September-2020, Page no: 102-118, Purbayon Publication, Panbazar, Guwahati, Assam, India. Editors: Dr. Sanjeev Pran Mahanta and Dr. Dipjyoti Kalita, ISBN: 978-93-89940-82-4.

Curriculum Vitae

Personal Details

Name: Sourav Kalita

Date of Birth: 08th May, 1991

Nationality: Indian

Religion: Hinduism

Marital Status: Single

Contact No.: 9531106348/ 8638893361

Email: chemistrysourav91@gmail.com/ sourav.kalita@iitg.ac.in

Present Address:

Senior Research Fellow, Laboratory of Peptide and Amyloid Research, Department of Chemistry, IIT Guwahati, Guwahati-781039, Assam, India.

Permanent Address:

Vill: Pub Par Jatiya Bhangara, P.O.: Bardangeri Kuchi, Dist: Kamrup (R), Assam, India. PIN: 781366.

Qualifications

07/2014-Present

Ph.D. in Chemistry (CPI 8.25 out of 10)

Indian Institute of Technology Guwahati, Guwahati, Assam, India

Thesis title: Effect of Anthranilic Acid Insertion in β-sheet Breaker Hybrid Peptidomimetics on hIAPP Aggregation

Thesis advisor: Prof. Bhubaneswar Mandal

07/2012-06/2014

M.Sc. in Chemistry (CGPA 8.97 out of 10)

Gauhati University, Guwahati, Assam, India

Thesis title: Characterization and Catalytic Reactivity of Parent and Isomorphously Iron Substituted Mordenite Zeolite

Thesis advisor: Prof. Anup Kumar Talukdar

07/2009-06/2012

B.Sc. in Chemistry Honours (79.6%, First Class with Distinction) with Physics, Mathematics and English

B. Borooah College, Gauhati University, Guwahati, Assam, India

07/2007-05/2009

Higher Secondary (H.S.) (68.8%, First Division) with Physics, Chemistry, Mathematics, Biology, English and Assamese

Jigyas Academy, Guwahati, Assam, India

05/2007

Matriculation (HSLC) (78.16%, First Division, Star) with Social Science, General Science, General Maths, Advanced Maths, General English and Assamese

Adarsha Jatiya Vidyalaya, Bihdia, Kamrup (R), Assam, India

Honours / Awards

- Received Best Poster Presentation Award, *Chem Convene*, 2017, IIT Guwahati, Guwahati, 25th July, 2017.
- Received Graduate Aptitude Test in Engineering (GATE) in 2019 (rank 510) and in 2014 (rank 838) in Chemistry
- Received State Level Eligibility Test (SLET-NE) February-2014 in Chemical Science.

Research Experiences

- During my Ph.D. tenure, I have learned and gained experiences working on peptide synthesis including solution phase and solid phase peptide synthesis (SPPS), self-assembly of peptides, Alzheimer's disease and Type-II diabetes.
- I have expertise in various instrumental techniques including, HPLC, ESI-MS, Fluorescence, UV-Vis, CD, FTIR, TEM, DLS, Optical-polarizable microscope, *etc*.
- During my PhD tenure, I mainly focused on the design and synthesis of different peptide based molecules as inhibitors against Alzheimer's disease (AD) and type-2 Diabetes (T2D). I have developed three different peptide-based strategies for the design of therapeutic tools against T2D, including small BSBHps, long BSBHps, and stapled peptides via inserting anthranilic acid (Ant). All the designed peptidomimetics exhibited excellent anti-Diabetic activities, which were verified *in vitro* at physiological conditions using various biophysical tools like Thioflavin T fluorescence assay, TEM and Congo-red stained birefringence analyses.

- I have worked on the mechanism of amyloid inhibition by the designed peptidomimetics using dynamic light scattering technique, TEM analysis and LUV dye leakage assay.
- I also have worked on synthetic organic reactions such as Fmoc-protections, Boc-protections, fluorophore attachments, esterification reactions and solution phase synthesis of novel and recyclable coupling reagent, Ethyl 2-cyano-2-(2-nitrobenzenesulfonyloxyimino) acetate (o-NosylOXY) and its utilization in peptide synthesis.

Academic and Professional Skills

- **Laboratory and Instrumentation:** Familiar with Synthetic Organic Chemistry, peptide synthesis (solution phase and solid phase) and purification, Mass spectrometry (ESI), MALDI-TOF, HPLC, Fluorescence spectroscopy, UV-Visible spectroscopy, Circular Dichroism, Infrared spectroscopy, ESR spectroscopy, Optical Polarisable Microscopy, TEM, FESEM.
- **Software:** Familiar with Origin, Adobe Illustrator, MS-office, Chemdraw.
- **Teaching Experience:** Worked as Teaching Assistant (TA) in B.Tech and M.Sc Laboratory at IIT Guwahati, India.
- **Language:** English, Assamese, Bengali and Hindi.

Research Interests

- Protein and peptide chemistry
- Protein/peptide self-assembly
- Type II Diabetes and other protein aggregating diseases.